THEME 5: URBAN WATER MANAGEMENT

Editor: Sobri Harun

RAINFALL-RUNOFF PROCESSES AND MODELLING

MECHANISM MODEL OF URBAN WATER CONSUMPTION

JIAHONG LIU[1], JINJUN ZHOU[2], WEIWEI SHAO[3], HAO WANG[4] ,ZHENTAO CONG[5]

[1,3,4] State Key Laboratory of Simulation and Regulation of Water Cycle in River Basin, China Institute of Water Resources and Hydropower Research, Beijing 100038, China; Engineering and Technology Research Center for Water resources and Hydro-ecology of the Ministry of Water Resources, Beijing 100038, China
liujh@iwhr.com; shaoww@iwhr.com; wanghao@iwhr.com
[2,5] State Key Laboratory of Hydroscience and Engineering, Tsinghua University, Beijing 100084, China
zhoujj15@mails.tsinghua.edu.cn; congzt@ tsinghua.edu.cn

ABSTRACT

Water balance analysis showed that the intensity of water consumption in urban units was significantly higher than that in suburban areas. In this study, the city area is divided into different water consuming units based on the prototype observation of water consumption and the characteristics of the underlying surface of the city, and the mechanism of urban water consumption was analyzed. A mathematical model was built to simulate the water consumption processes in cities with complicated underlying surfaces. For example, the water consumption intensity (WCI) of each unit was calculated in Beijing city. Beijing's urban water consumption intensity was 850 mm in 2014, which was verified by water balance analysis based on observation datasets. The breakdown results show that the WCI of residential buildings depend on the residents living and work habits. The WCI of municipal square and road is determined by precipitation characteristics and runoff coefficients of the underlying surface. The WCI of water and green land depends on temperature, solar radiation, precipitation and other meteorological factors like wind speed, humidity, etc. The amount of water consumption for one kind of urban unit is the product of WCI and area of the urban unit. In the study area, the amount water consumption of residential buildings is the largest contributor for the urban water consumption, followed by that of green land. In urban areas, residential buildings, roads and municipal squares greatly enhance the water consumption intensity, and their contributions to total amount water consumption are greater than that of green land and water.

Keywords: Urban hydrology; water consumption; dualistic water cycle; mechanism model; evapotranspiration.

1 INTRODUCTION

There have been considerable urban developments in China and some other developing countries. As urbanization develops, urban hydrology process attains more and more concern. Comparing to natural surfaces, the urban surfaces change greatly, which result in large changes of hydrology process and energy balance (Collier, 2006). Urbanization has impact on hydrology process in many aspects, including energy budget (urban heat island, Gedzelman et al., 2003), water vapor variability (Champollion et al., 2009); precipitation changes (Rosenfeld, 2000), urban storm and flood (Jauregui & Romales, 1996), water supply and water resources consumption (Hof & Schmitt, 2011; Chen & Qian, 2006). Human activities also exert an impact on natural environment and urban microenvironment (Tian & Yang, 2011).

The process of urban water cycling can be generalized as water supply, water use, water consumption, drainage, recycling etc. The amounts of water supply, water use, drainage and water recycling are easy to measure except for water consumption. In other words, the statistical data of these aspects can be obtained from related reports and documents. Generally, water consumption involves evapotranspiration, groundwater recharge and water delivered in products, among which the groundwater recharge can be estimated by the change of groundwater table, and the water delivered in products can be negligible due to its tiny amount, therefore urban evapotranspiration is a key problem in the urban water cycle research. The traditional evapotranspiration estimation methods mainly focus on uniform underlying surface, and have little knowledge of the heterogeneity of the urban surface. The remote sensing evapotranspiration model starts with estimating sensible heat and then calculating the latent heat based on the energy balance, which draw a conclusion that the evapotranspiration of urban area is smaller to that of forests or farmlands. Meanwhile, high evapotranspiration in urban area is worldwide prevailing. Columbia University carried on the Global Rural-Urban Mapping Project in 2005, and this research shows that urban area occupies 3% of the total land area while the quantity of urban water use accounts for one third of the total amount of water supply.

In order to understand the high water-consumption of urban area, a mechanism model is needed. Liu et al. (2009) have put forward a framework to estimate regional evapotranspiration called objective ET calculation model. Based on the framework, a mechanism model of urban water consumption was built. The proposed model was used to estimate the evapotranspiration in Beijing.

2 PROJECT SITE

The mathematic model was applied in Beijing. Beijing is one of the most affected cities suffering from water shortage in the world. In the top fifteen populous cities in the world, Beijing is the only one whose annual average precipitation is less than 600mm. The water resources per capita is about 100 m³ in Beijing in 2014, which is far below the standard quantity of water resources per capita, 1000 m³, defined by the United Nations (Zhang, 2005). According to Beijing's Water Resources Bulletin (2003 to 2014), the average water resources in Beijing is about 2.63 billion m³/a, with overland runoff of 0.9 billion m³/a and groundwater resources of 1.73 billion m³/a. With rapid growth in urbanization, the urban area of Beijing increased significantly. According to data from the Chinese City Construction Statistical Yearbook, the urban area of Beijing increased nearly by 3 times from 366 km^2 in 1980 to 1261 km^2 in 2014, while the farming area decreased from 4130 km^2 (in 1980) to 2317 km^2 (in 2014). There has also been a great increase in Beijing's population from 9.04 million (in 1980) to 20.69 million (in 2014).

2.1 Underlying Surface Types

The terrain condition of Beijing is characterized in having a high elevation in the northwest and low elevation in the southeast, and the plain area in the southeast are surrounded by mountains on three sides. The land use of Beijing is shown in Figure 1, which is mapped based on the remote sensing images of Beijing in 2014. The underlying surface of mountain area mainly involves forests, shrub land, sparse woodland and grassland. The plain area is mainly covered by farmland and urban land, which are hardly influenced by human activities. The urban surface in the plain area includes roads, streets, rivers, lakes, and the building surface of both high and low density. Considering difference types of underlying surface, Beijing can be divided into a mountain zone of 10019km^2, and a plain zone of 6391km^2. The plain zone is divided into two parts, the urban zone and the suburban zone, which are changing over time with average of 1241km^2 and 5150km^2 respectively. Table 1 shows the area of different types of land use in Beijing in 2014.

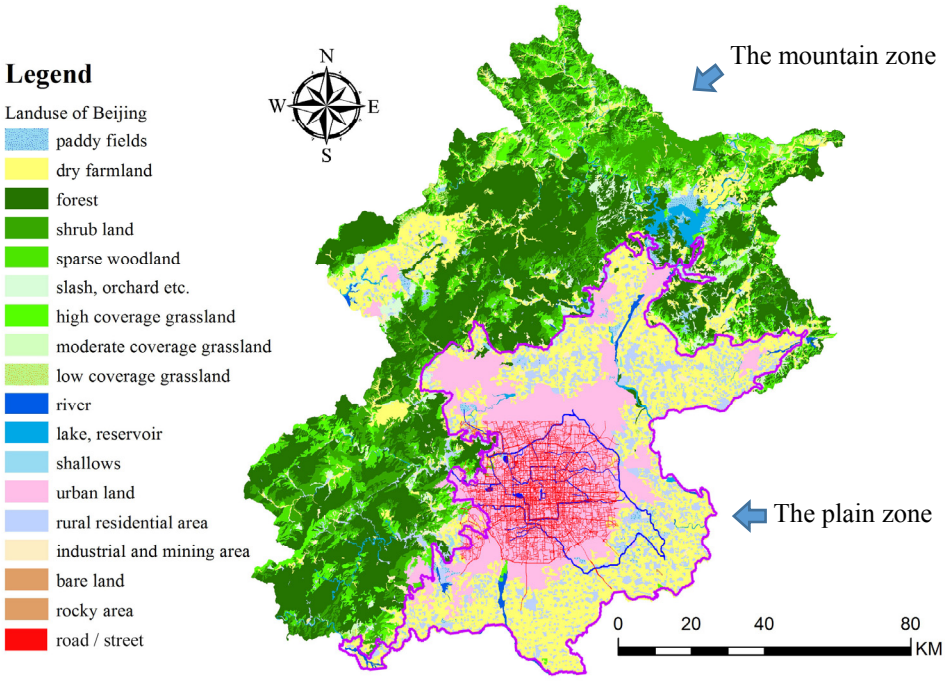

Figure 1. The Land Use of Beijing in 2014

2.2 Data

The data of this study consist of three kinds of dataset, which are the dataset of water, underlying surface, social / economic status. The dataset of water includes precipitation, water supply, drainage, etc., which were collected from the Beijing Water Resources Bulletin. In addition, the precipitation of divided zones was estimated based on the local precipitation contour map. The underlying surface data was obtained by interpreting the map of Beijing's land use in 2014, which is shown in table 1. The social / economic data needed in this study is mainly population distribution and building density. It was obtained by sample survey and spatial interpolation. The other data including different area zones in Beijing, population, industrial output originate from the Beijing Statistical Yearbook and China City Construction Statistical Yearbook.

Table 1. The area of different land use in Beijing (2014)

Classification	Index number	Type of land use	Area /hm^2
1 farmland	11	paddy fields	16026
	12	dry farmland	347750
2 woodland	21	forest	449763
	22	shrub land	161336
	23	sparse woodland	83445
	24	slash, orchard etc.	32822
3 grassland	31	high coverage grassland	88178
	32	moderate coverage grassland	16009
	33	low coverage grassland	6604
4 wetland	41	river	10864
	43	lake, reservoir	18809
	46	shallows	6048
5 habitation land	51	urban land (except roads/street)	224237
	52	rural residential area	123908
	53-1	industrial and mining area	16366
	53-2	road/street	38672
6 unused land	65	bare land	115
	66	rocky area	49

3 METHODOLOGY

In order to calculate the water consumption in urban area, this paper proposed a framework to integrate the soil moisture model (Pei et al., 2006), model for urban water dissipation (Zhou et al., 2017), distributed hydrology model, remote sensing methods and water budget method (Figure 2). The calculation of regional evapotranspiration (ET) includes two process of “from top to bottom, from bottom to top”. “From top to bottom” means to calculate the regional ET by water budget method. The input data includes precipitation, runoff, water supply, drainage, and groundwater recharge. The output is the regional ET, which could be calculated by equation of water budget illustrated in left of figure 2. Most of the data input in this step was measured, so the output of this step could be used to calibrate and validate the models on the right of figure 2. “From bottom to top” is the process to calculate the ET for different kinds of land use through the sub-item simulation models.

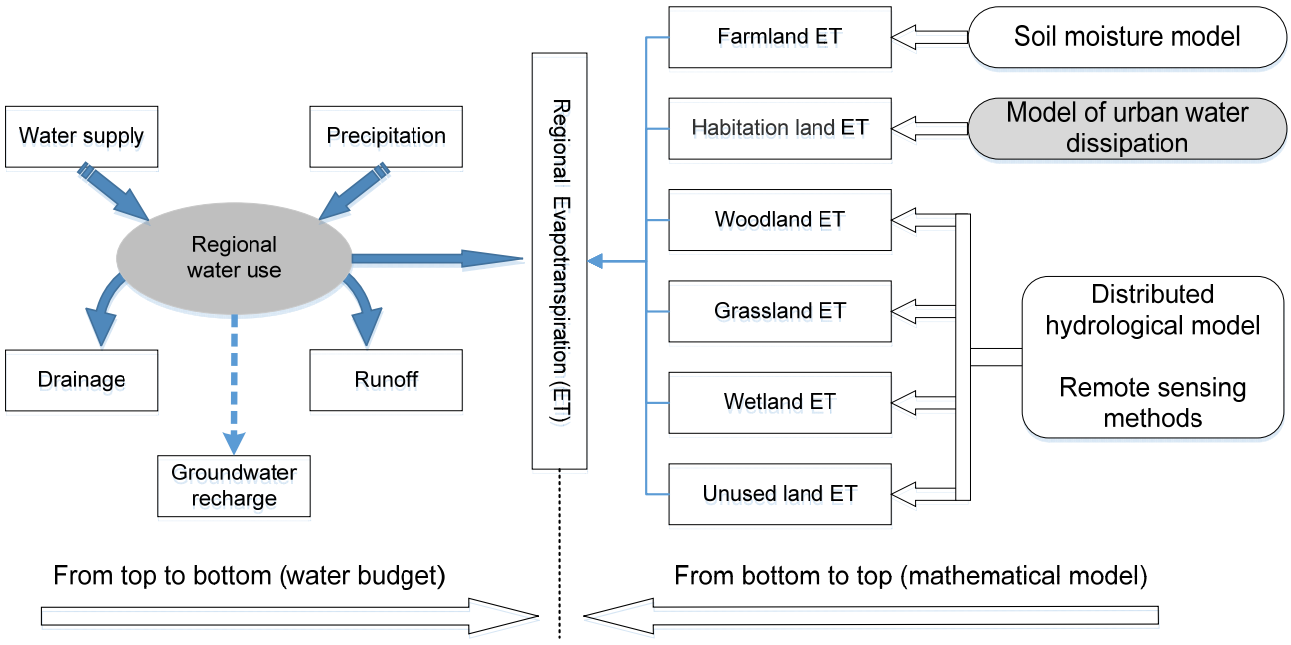

Figure 2. Framework of water consumption calculation method

Among the framework, the most important is to calculate the ET of habitation land, which includes the urban land, rural residential area, industrial/mining area and road/street. The parameters that influence ET of habitation land are population distribution, building density, types of buildings, economic development level, etc. In order to analyze the characteristics and intensity of water consumption in different types of habitation land, several types of buildings in Beijing were investigated. There is a total of 70 buildings that have been sampled,

of which 47 were residential buildings, 9 were office buildings, 6 were school buildings, and 8 were restaurants. All samples were located in independent locations with separate water supplies and in different drainage systems (Zhou et al., 2017). The sampled buildings covered an area of 712,000 m^2 and hosted a gross population of 64,886. This large sample size was chosen to ensure that the results of the study would be the representative of building's water consumption features. In addition, the ET on road /street was estimated based on precipitation dataset and the observed runoff on typical road. Table 2 shows the results of the sampling survey and the typical experiment. The results were used as key parameters to calculate the ET of habitation land. For example, the water consumption intensity on building's floor is 170.9 mm, if the building has 10 floors, the water consumption intensity per unit projected area would be 1709 mm. The higher the building, the more water it would consume, which is the reason that the habitation land usually has high water consumption intensity.

Table 2. The water consumption parameters in habitation land of Beijing

Index	Type of surface	Water consumption intensity /mm (water consumption / surface area)	Main water consumption behavior
1	Buildings	170.9	toilet flushing, washing, cooking, air humidification
2	road / street	189.9	evapotranspiration, wheel atomization, road spraying

4 RESULTS AND DISCUSSIONS

The proposed model was applied to estimate the evapotranspiration of different zones from 2003 to 2014 in Beijing. The results are shown in table 3. The average evapotranspiration in Beijing from 2003 to 2014 is 501mm, which is very close to the average precipitation of 514 mm. The results show that the potential water resources throughout Beijing have been greatly exploited; it also illustrates that Beijing makes limited contribution on water resources for the Haihe River Basin.

Table 3. Evapotranspiration of different underlying zones in Beijing (mm)

Year	Precipitation	Evapotranspiration				
		Beijing average	Mountain Zone	Plain Zone	Urban Zone	Suburban Zone
2014	439	461	403	550	850	478
2013	501	496	452	565	890	489
2012	708	604	551	674	1120	572
2011	552	521	480	581	927	502
2010	524	518	478	568	858	500
2009	448	462	406	554	812	491
2008	638	597	548	658	1010	572
2007	449	472	403	565	877	486
2006	448	471	421	543	847	470
2005	468	464	426	541	862	464
2004	539	512	490	540	859	472
2003	453	438	408	480	846	439
Average	514	501	456	568	897	495

The urban evapotranspiration is 897 mm/a, which has the highest evapotranspiration amongst all zones. In recent years, such as year 2008, 2011, and 2012, the evapotranspiration has exceeded 900 mm/a, which is near to the local water surface evaporation. This seemed to have violated the principles of conventional evaporation rates. The main reasons for this extraordinary phenomenon are the local high-density buildings and intensive human activities. On one hand, high-rise buildings form porous sponge-like structures, leading to increased evapotranspiration; on the other hand, urban heat islands effect, the car's wheel atomization effect and other human activities also contributed to the evapotranspiration enhancement. The adequate water supply will lead to an increase in the amount of evapotranspiration in urban area. For instance, a phenomenon called "fogging effect of car's wheel" on road surface will accelerate street surface evapotranspiration rate when it is raining. A lot of water-vapor increases when the car's wheels rotate on the road, resulting in a quick dry up of the carriageway after raining. The changing trends of evapotranspiration in different zones were analyzed based on the observed precipitation and simulated evapotranspiration. Since evapotranspiration and precipitation have

a close relationship, this paper carried out regression analysis of the evapotranspiration and precipitation in different zones, as shown in Figure 3.

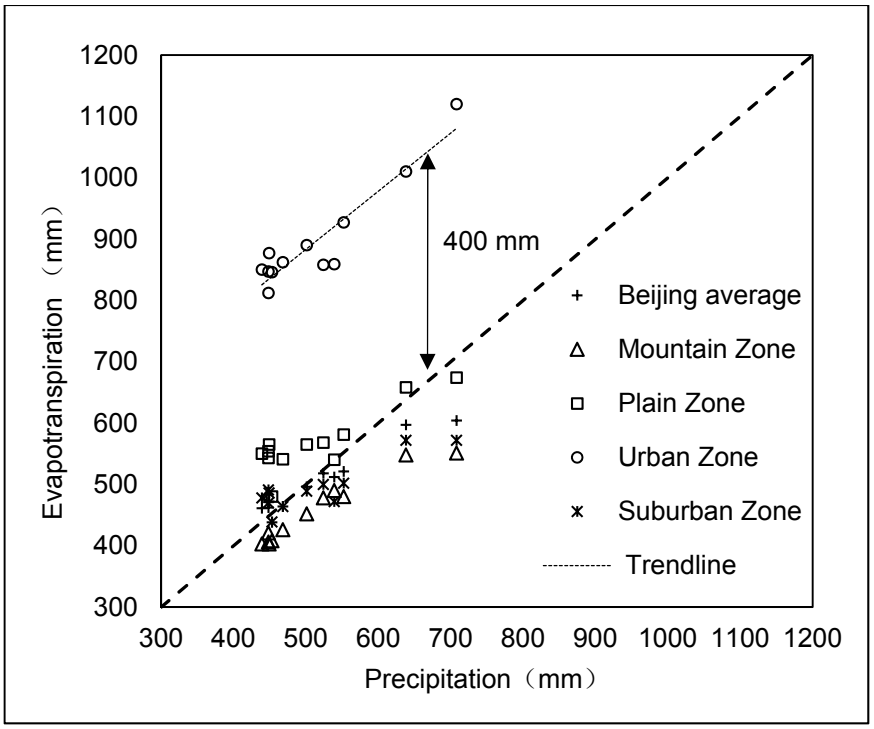

Figure 3. Regression analysis of evapotranspiration and precipitation of different zones

It can be seen in Figure 3 that ET in urban zone is significantly higher than ET in suburban zone, and even higher than the precipitation (above the "45-degree diagonal line"). There is a visible difference between evapotranspiration and precipitation. The ET in mountain zone is smaller than precipitation; while the ET in plain zone is higher than precipitation except for 2012, in which the precipitation is very high (708 mm). The plain zone evapotranspiration is slightly higher than precipitation, which is mainly because evapotranspiration is much higher than precipitation in the urban zone. The ET in urban zone is about 400mm higher than the precipitation.

This paper carried out linear regression analysis of evapotranspiration and precipitation in different underlying zones in Beijing. The square of correlation coefficient for Beijing-average and mountain zone is above 0.90, while the square of correlation coefficient for plain zone is 0.75. It can be explained by the fact that mountain zone is less affected by human activities, so evapotranspiration receives greater impact from precipitation. Whereas for plain areas, where evapotranspiration is more greatly influenced by human activities, and thus the correlation coefficient is smaller.

Figure 4 shows the city evapotranspiration volatility, and there is a small peak in 2008 and 2012. In the research period, the trends of evapotranspiration and precipitation are similar to each other. The precipitation of 2008 and 2012 are 638mm and 708mm respectively, far higher than the average annual precipitation of 514 mm in the recent twelve years, thus, the evapotranspiration in these two years were slightly higher than the other years. The figure shows that the change of evapotranspiration in plain zone in the past dozen years is small; while the mountainous and suburban evapotranspiration change with precipitation to a slightly larger extend. Further analyzing on Beijing's overall composition of evapotranspiration, it could be found that the mountainous area (covers 61% of the total area) has relative low evapotranspiration (55%), and urban zone area (8%) has relative high evapotranspiration proportion (14%), which indicates that the urban water consumption intensity is greater than that of other underlying surface types.

The ET in urban area can be classified into four categories: ET of buildings, ET of roads, ET of green land, ET of wetland (rivers and lakes). The average ET of buildings, roads, green land, wetland are 529 million m^3; 104 million m^3, 431 million m^3, and 49 million m^3, with the proportion of 47.6%, 9.3%, 38.7%, 4.4% respectively. In the urban area of Beijing, the residential building is the largest contributor for the urban water consumption, following by that of green land.

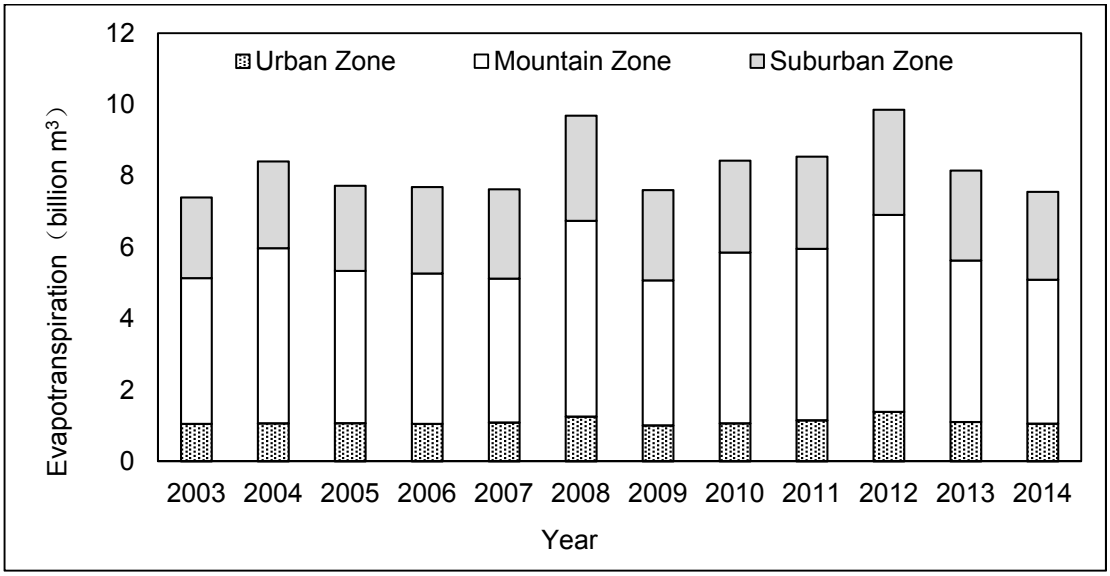

Figure 4. Change of evapotranspiration of different zones in Beijing

5 CONCLUSIONS

The urban area is very active for water use and consumption. This paper focused on the simulation of water dissipation process in urban area, and proposed a framework to calculate and validate the water consumption in regional scale. The proposed mathematical model was applied in Beijing and the water consumption in mountain zone, plain zone, urban zone and suburban zone from 2003 to 2014 were calculated. The results show that evapotranspiration vary widely in different zones of the same period in Beijing. The dozen-year average evapotranspiration of Beijing is 501mm/a, from 2003 to 2014. With high-density construction and human activities gathering in urban zone, the urban evapotranspiration is the highest, with an average of 897 mm/a, a maximum of 2012, reaching 1120mm/a; mountainous evapotranspiration is the minimum, with an average of 456mm/a; suburban evapotranspiration is the medium, with an average of 495 mm/a.

The relationship between evapotranspiration and precipitation varies according to different zones. Urban evapotranspiration is significantly greater than precipitation, and even higher than the local water evaporation for a few years. Plain evapotranspiration is slightly larger than precipitation except for year 2012, which had extremely high precipitation. Urban and suburban evapotranspiration in the plain zone are less affected by changes of precipitation, while the mountainous evapotranspiration is most influenced by precipitation. The evapotranspiration and precipitation correlation coefficient of Beijing is 0.94, that of mountainous zone is 0.91, and that of the plains zone is 0.75. The intensity of water consumption in urban area is about 400 mm higher than the precipitation. The largest contributor for the urban water consumption is residential buildings, which occupies 47.6% of the total evapotranspiration in the urban area of Beijing.

ACKNOWLEDGEMENTS

The researchers would like to extend thanks to the Chinese National Natural Science Foundation (No. 51522907, No. 51279208), the National Key Research and Development Program of China (2016YFC0401401), the Research Fund of the State Key Laboratory of Simulation and Regulation of Water Cycle in River Basin, China Institute of Water Resources and Hydropower Research (No. 2016ZY02). The study was also supported by Junior Fellowships for CAST Advanced Innovation Think-than Program (DXB-ZKQN-2016-035).

REFERENCES

Collier. C.G. (2006). The Impact of Urban Areas on Weather. *Quarterly Journal of the Royal Meteorological Society*, 132(614), 1-25.

Champollion, C., Drobinski, P., Haeffelin, M., Bock, O., Tarniewicz, J. & Bouin, M. N. (2009). Water Vapour Variability Induced by Urban/Rural Surface Heterogeneities during Convective Conditions. *Quarterly Journal of the Royal Meteorological Society*, 135(642), 1266-1276.

Chen, H.J. & Qian, H.S. (2006). Change of Water Consumption and Its Relationships to Economy and Climate: Cases from Beijing, Shanghai and Guangzhou. *Environment*, 15(6), 1331-1336. (In Chinese).

Gedzelman, S. D., Austin, S., Cermak, R., Stefano, N., Partridge, S. & Quesenberry, S. (2003). Mesoscale Aspects of the Urban Heat Island around New York City. *Theoretical and Applied Climatology*, 75(1), 29-42.

Global Rural-Urban Mapping Project. (2005). Urban Expansion. *Science*, 307(5716), 1718-1718.

Hof, A. & Schmitt, T. (2011). Urban and Tourist Land Use Patterns and Water Consumption: Evidence from Mallorca, Balearic Islands. *Land Use Policy*, 28(4), 792–804.

Jauregui, E. & Romales, E. (1996). Urban Effects on Convective Precipitation in Mexico City. *Atmospheric Environment*, 30(20), 3383-3389.

Liu, J.H., Qin, D.Y., Wang, M.N. & Zhang, R.M. (2009). Theories and Calculation Methods for Regional Objective ET (Evapotranspiration): Applications. *Science China in Technological Sciences*, 52(5), 1390-1396.

Pei, Y.S., Sun, S.Y. & Yu, F.L. (2006). Soil Moisture Prediction Model for Heihe River Basin. *Advances in Science and Technology of Water Resources*, 26(4), 5-8. (In Chinese).

Rosenfeld, D. (2000). Suppression of Rain and Snow by Urban and Industrial Air Pollution. *Science*, 287(5459), 1793.

Tian, Y.J. & Yang. (2011). Statistical Spectrum Model of Wind Velocity at Beijing Meteorological Tower. *Science China in Technological Sciences*, 54(11), 2869-2877.

Zhang, L.P. (2005). *Mechanism of Effects of Beijing Urbanization on Urban Water Use. Beijing*, Capital Normal University (In Chinese).

Zhou, J., Liu, J., Dong, Q., Wang, Z., Wang, H., Xiang, C. & Luan, Y. (2017). Simulation Model for Urban Water Dissipation. *Advances in Water Science*, 28(1), 67-75.

Proceedings of the 37th IAHR World Congress
August 13 – 18, 2017, Kuala Lumpur, Malaysia

A COARSE GRID APPROACH-BASED MODEL CHAIN FOR FAST RAINFALL-RUNOFF PREDICTIONS IN NATURAL AND URBAN AREAS

ILHAN ÖZGEN[(1)]

[(1)]Chair of Water Resources Management and Modeling of Hydrosystems, Technische Universität Berlin, Berlin, Germany
ilhan.oezgen@wahyd.tu-berlin.de

ABSTRACT

Flood events in urbanized areas are usually caused by localized rainfall events with very high intensity that occur in catchments located at the upstream of the city. The typical model chain for forecasting this type of event is a hydrological model that generates input for a two-dimensional hydraulic model. However, in recent years, the depth-averaged two-dimensional shallow water equations are applied to compute rainfall-runoff in natural catchments as well as inundation areas in city environment. The application is limited by computational constraints, which resulted from the high mesh resolution required to account for microtopography in natural and buildings in urban catchments. In this context, coarse grid approaches aim to reduce computational cost by enabling simulations on coarser meshes and introducing subgrid treatments to recover some of the information at subgrid-scale. This contribution presents a novel model chain that comprises two coarse grid approaches with specialized application domains: (1) friction law-based coarse grid approach and (2) anisotropic porosity-based coarse grid approach. The hydrological model that is usually used for these type of predictions was replaced by a shallow water model with a specialized friction law to account for microtopography. The urban flood inundation model was sped up by introducing anisotropic porosity terms to account for buildings. The model chain was applied to predict rainfall-runoff in an idealized city, based on a real rainfall event in a real natural catchment. An averaged behavior of a high-resolution model chain can be obtained with significantly lower computational cost such that the simulations run on average about 100 times faster than the high-resolution counterpart.

Keywords: Shallow water model; porosity; coarse grid approach; urban catchment; friction law.

1 INTRODUCTION

In most forecasting systems, a model chain that consists of a hydrological model and a two-dimensional hydraulic model is used to predict inundated areas for a rainfall event. Here, the hydrological model calculates a discharge at the outlet of the natural catchment that is then down-scaled and used as a boundary condition to drive the hydraulic model that computes inundation areas in city environment.

Using a hydraulic model instead of the hydrological model is currently hardly feasible due to high computational cost. In addition, the computational cost of conventional hydraulic finite-element and finite-volume codes typically prevents model discretization at a resolution that is achievable with airborne LIDAR technology (McMillan & Brasington, 2007). The computational constraint on the discretization scale can be illustrated by the fact that the computational cost of an explicit finite-volume code is quantified by Kim et al. (2014) as inversely proportional to the third power of the cell size. Codes that operate on the high-resolution data set scale to simulate flooding of large urban catchments are usually utilizing high-performance computing technology on supercomputers to achieve feasible computation time, e.g. (Hinkelmann, 2005; Smith and Liang, 2013; Lacasta et al., 2014; Abily et al., 2016).

Besides from high-performance computing, the issue can be approached in two ways, either by simplifying the mathematical model (McMillan & Brasington, 2007; Chen et al., 2012a; Chen et al., 2012b; Jahanbazi et al., 2017), or by reducing the cell number by means of a subgrid parameterization of the building or microtopography effects on the flow. Figure 1 shows an overview of the motivation for using coarse grid approaches in hydro- and environmental system modeling.

A very straight-forward subgrid approach is to artificially increase the roughness parameter in the shallow water model to account for head loss due to unresolved obstacles. This approach has been investigated for urban flood modeling in (Néelz and Pender, 2007), wherein it was noted that this approach may lead to errors in the modeled flow routes and in (Liang et al., 2007), wherein it was reported that finding suitable values for the roughness parameters was rather non-intuitive. For applications in natural catchments, Razafison et al. (2012) derived a friction approach to account for ridges and furrows and Jain & Kothyari (2004) presented a friction approach that accounts for vegetation. In this study, we used the friction law derived in (Özgen et al., 2015) to account for unresolved microtopography to enable an efficient shallow water equations-based computation of rainfall-runoff in natural catchments that replaces the hydrological model in the aforementioned model chain.

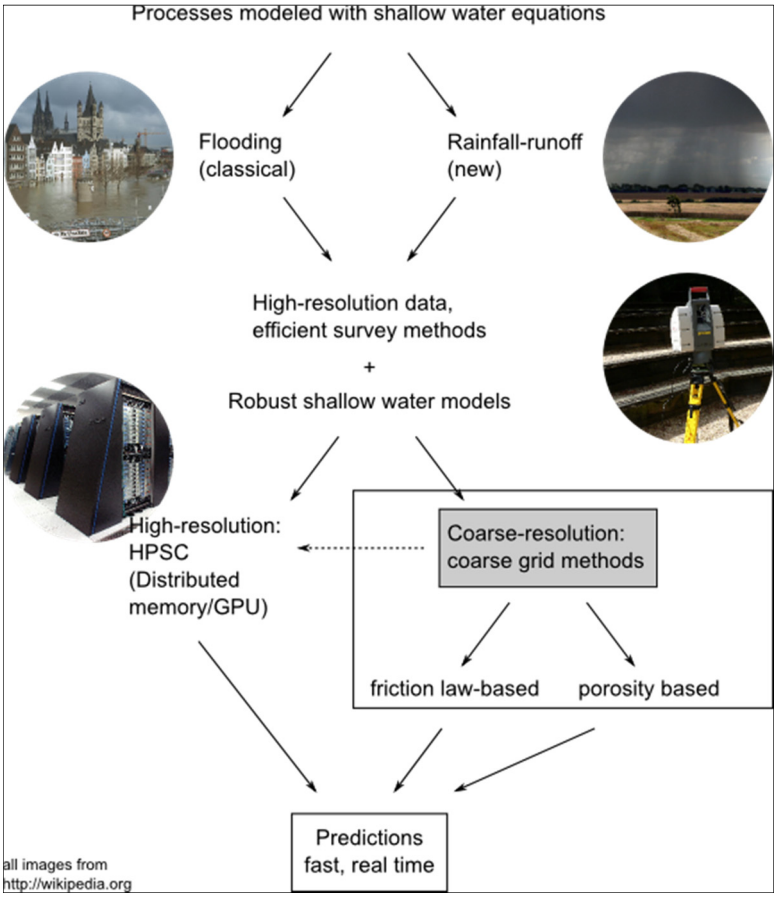

Figure 1. Motivation for using coarse grid methods

Another coarse grid approach is based on a porosity term. Essentially, in this approach the computational cell with unresolved buildings inside of it, is treated as a porous medium. Thus, a porosity term is introduced into the shallow water equations. Following the pioneering work by Defina (2000) and Hervouet et al. (2000), Guinot & Soares-Frazão (2006) and Soares-Frazão et al. (2008) presented the so-called isotropic porosity shallow water equations and provided a Godunov-type finite-volume method to solve them. The isotropic porosity shallow water equations were derived using a representative elementary area (REA) assumption. Guinot (2012) noted that the existence of an REA in urbanized areas is debatable. Assuming that a REA exists, Guinot (2012) then showed that the scale of the assumed REA exceeded the mesh resolution for several orders of magnitudes, but pointed out that from a numerical point of view, it is safe to choose a mesh resolution below the REA scale, as the numerical convergence requires the cell size to become infinitely small. We note that from an application point of view, the discussions about the REA scale are unimportant as satisfying results are obtained by using the isotropic porosity model (Guinot & Soares-Frazão, 2006; Soares-Frazão et al., 2008).

The anisotropic porosity shallow water equations have been derived in (Sanders et al., 2008), to overcome a limitation of the isotropic porosity shallow water model, that is, the impossibility for the isotropic porosity shallow water model to account for directional effects induced by local anisotropic structures. Sanders et al. (2008) derived the equations in integral form to remove the constraint of isotropy imposed by the REA assumption. In the anisotropic porosity model by Sanders et al. (2008), directionality was accounted for by means of additional porosity terms at the edges of the computational cell. A similar approach was later adopted in Chen et al. (2012a), where edge conveyance coefficients were defined at each edge. As pointed out by many researchers, e.g. Sanders et al., (2008), Guinot (2012) and Özgen et al. (2016a), the integral approach resulted in porosity terms which were heavily mesh-dependent. Currently, there is no treatment available to overcome the mesh-dependency of the anisotropic porosity shallow water model, although research in this direction is currently being carried out at the University of Liege (M. Bruwier, private communication). In this work, the anisotropic porosity shallow water equations, solved by the numerical model presented in Özgen et al. (2016a), were used to predict inundation heights in urban environment.

In this study, the anisotropic porosity shallow water model for urban environment was coupled with the friction-based coarse grid approach for natural catchments to obtain a novel model chain that can be applied for the fast prediction of urban runoff.

2 GOVERNING EQUATIONS

In this section, we give an overview of the mathematical model concepts that are used. For the sake of brevity, we omitted the derivation of the equations. The readers are referred to Özgen et al. (2015) and Özgen et al. (2016b) for a detailed discussion of the friction law-based coarse grid approach and the anisotropic porosity shallow water equations, respectively. We further note that in the following, turbulence and molecular viscosity as well as other momentum diffusion terms were neglected. This has the advantage that the governing equations become hyperbolic instead of being of mixed type. The physical justification is that in very shallow flows such as rainfall-runoff, turbulence is mainly produced by bed friction (Cea et al., 2007).

2.1 Classical shallow water equations with specialized friction law

The classical shallow water equations are written in differential form as

$$\frac{\partial \mathbf{q}}{\partial t} + \frac{\partial \mathbf{f}}{\partial x} + \frac{\partial \mathbf{g}}{\partial y} = \mathbf{s} \qquad [1]$$

where *t* is time, *x* and *y* denote the axes of the Cartesian coordinate system, **q** is the vector of conserved variables, **f** and **g** are the flux vectors in *x*- and *y*-direction, respectively, and **s** is the source term vector. The flux and storage vectors in Eq. [1] are defined as

$$q = \begin{bmatrix} h \\ hu \\ hv \end{bmatrix}, \qquad f = \begin{bmatrix} hu \\ hu^2 + gh^2/2 \\ huv \end{bmatrix}, \qquad g = \begin{bmatrix} hv \\ hvu \\ hv^2 + gh^2/2 \end{bmatrix}, \qquad [2]$$

with *h* standing for water depth, *u* and *v* standing for velocity in *x*- and *y*-direction, respectively, and *g* standing for the gravitational acceleration, usually set to 9.81 m/s^2. The source term vector is defined as

$$\mathbf{s} = \begin{bmatrix} i \\ -gh\dfrac{\partial z}{\partial x} - f_x \\ -gh\dfrac{\partial z}{\partial y} - f_y \end{bmatrix}. \qquad [3]$$

Here, *i* is the rainfall intensity, *z* is the bed elevation and f_x and f_y are the friction source terms in *x*- and *y*-direction, respectively. The definition of the friction source terms is according to the friction law in Özgen et al. (2015):

$$f_x = -\left(n\, g\, h^{-\frac{1}{3}} + K\right) |\mathbf{v}|\, u, \qquad f_y = -\left(n\, g\, h^{-\frac{1}{3}} + K\right) |\mathbf{v}|\, v, \qquad [4]$$

where $\mathbf{v} = [\, u,\, v\,]^T$ is the vector of velocity and | . | denotes the Euclidian norm of the vector, n is Manning's roughness coefficient and K is a geometrical parameter defined as

$$K = \alpha_0 \exp\left(-\alpha_1 \left(\Lambda - 1\right)\right), \qquad [5]$$

with α_0 and α_1 being calibration parameters and Λ being the inundation ratio (Lawrence, 1997):

$$\Lambda = \frac{h}{\left((1 - s_o)\, k\right)} \qquad [6]$$

Here, s_0 is the bottom slope and k is the characteristic roughness height, which is set equal to the standard deviation of the subgrid-scale structure. While in Özgen et al. (2015), a spatially uniform distribution of the roughness height was used, Özgen et al. (2016c) examined whether calculating the roughness height individually in each cell improves the model accuracy and report no significant improvement in natural catchments.

2.2 Anisotropic porosity-based shallow water equations

The anisotropic porosity shallow water equations are written in an integral-differential form as

$$\int_{\Omega} i \, \frac{\partial \mathbf{q}}{\partial t} d\Omega + \oint_{\partial\Omega} i \, \mathbf{F}\,\mathbf{n} \, dr = \int_{\Omega} i \, \mathbf{s} \, d\Omega, \qquad [7]$$

where *i(x,y)* is a phase function that returns 1 if *(x,y)* corresponds to a void or 0 if (x,y) corresponds to an obstruction. We note that **F n** = **f** n_x + **g** n_y, and that the flux and storage vectors correspond to Eq. [2], and the source term vector contains an additional source term that models the fluid-building interaction at subgrid scale. This reads

$$\int_{\Omega} i \, \mathbf{s} \, d\Omega = \int_{\Omega} i \, \mathbf{p} \, d\Omega + \oint_{\partial\Omega^*} g \, \frac{h^2|_{\eta_0}}{2} \, \mathbf{m} \, dr + \int_{\Omega} c \, \mathbf{v} \, |\mathbf{v}| d\Omega, \qquad [8]$$

where the term with **p** now corresponds to the source term of Eq. [3] and the second term on the right-hand side is the additional source term, calculated by a path integral along the fluid-building interface with **m** being the unit normal vector pointing outside of the fluid phase. The third term is a head loss term calculated via a drag force formulation with *c* being the drag force coefficient. A finite-volume type discretization of the equation then yields:

$$\left(1 + \kappa^{n^*}\right) (\phi q)^{n+1} = (\phi q)^n - \Delta t \sum_k (\psi_k \, F_k \, n_k)^{n^*} \Delta r_k, \qquad [9]$$

where κ represents an implicit treatment of friction and drag source terms (Bussing & Murman, 1988), ϕ is the cell porosity, ψ is the edge porosity, *n* stands for the time level and the choice of n^* determines the time-stepping method. If $n^*=n$, the method corresponds to an explicit forward Euler time-stepping, if $n^*=n+1/2$, the method corresponds to a two-step Runge-Kutta scheme.

3 NUMERICAL METHOD

The governing equations were solved in integral-differential form (Eq. [7]) with a cell-centered Godunov-type finite-volume method. Second order accuracy was achieved by means of a linear MUSCL reconstruction. Time was discretized by a second order accurate two-step TVD Runge-Kutta scheme, cf. Eq. [9]. More details about the numerical method can be found in Özgen et al. (2016a).

4 COMPUTATIONAL EXAMPLE

The two presented coarse grid approaches were coupled to obtain a model chain that is applied to model runoff in an urbanized environment caused by a heavy rainfall event in a natural catchment located at the upstream of the city. We considered an idealized city that is located at the outlet of the subcatchment and impose the discharge of the subcatchment as an inflow boundary condition of the model of the city. While there was measurement data available for the discharge of the subcatchment, no measurement data was available for the city.

4.1 Friction law-based coarse grid approach for rainfall-runoff in natural catchment

4.1.1 Initial and boundary conditions

The natural catchment is a real world subcatchment of the Heumöser slope in Vorarlberg, Austria, that spans about 100000 m^2. Bottom elevation was provided in 1 m by 1 m resolution by the Austrian Torrent and Avalanche Control department, cf. Figure 2 (left). The whole domain was initially dry. Discharge was generated by a spatially uniform rainfall according to a time series measured in July 2008 with a temporal resolution of 10 min, cf. Figure 2 (right). Here, the rainfall intensity was multiplied with the runoff coefficient ψ=0.3 to account for infiltration (Simons et al., 2014). In addition, following Simons et al. (2014), the interflow component was modeled by means of a linear storage model, with a storage coefficient of *K*=6 h, and added to the overland flow to obtain the total discharge at the outlet. All boundaries were open boundaries. The domain was discretized with a quadratic grid with cell size of 10 m. The model was calibrated as reported in (Özgen et al., 2015) with n = 0.035sm$^{-1/3}$, α_0 = 0.3 and α_1 = 0.87. The simulation run for 120 h, i.e. 5 days.

4.1.2 Results

Model results for the discharge at the outlet of the domain were compared with field measurement data and a high-resolution simulation (mesh resolution 1 m) by Simons et al. (2014) in Figure 3.

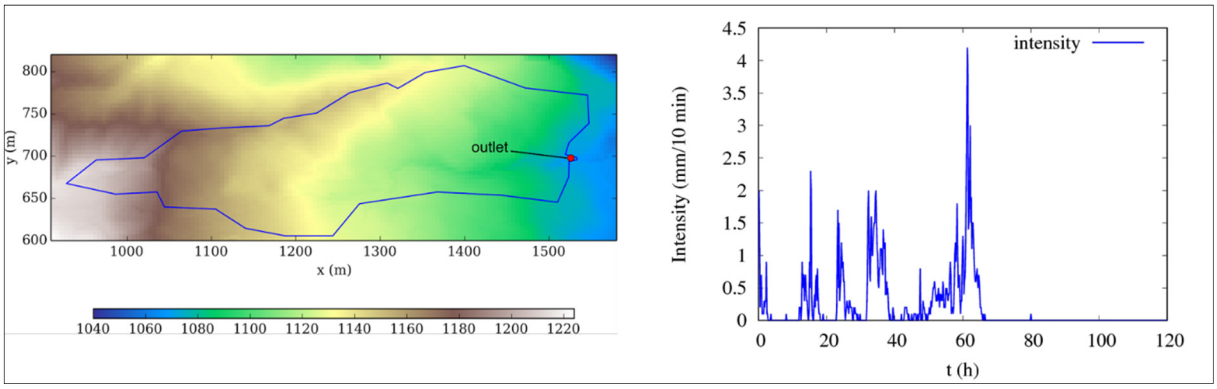

Figure 2. Catchment topography with position of measurement weir at the outlet (left); intensity of the rainfall event (right)

Both the high-resolution model and the coarse grid model overshot the measurement data at the beginning of the simulation. As discussed in (Cea et al., 2010), this might be due to shear effects on the thin water film in the real world that cannot be reproduced with the mathematical model of the shallow water equations. After t = 20 h, the deviation between the models and the measurement data diminished. The third and fourth peaks at about t = 40 h and t = 60 h, respectively, were captured fairly accurately.

The friction-law based coarse grid approach reduced the computational cost such that the simulation results were obtained 350 times faster than the high-resolution simulation of Simons et al. (2014).

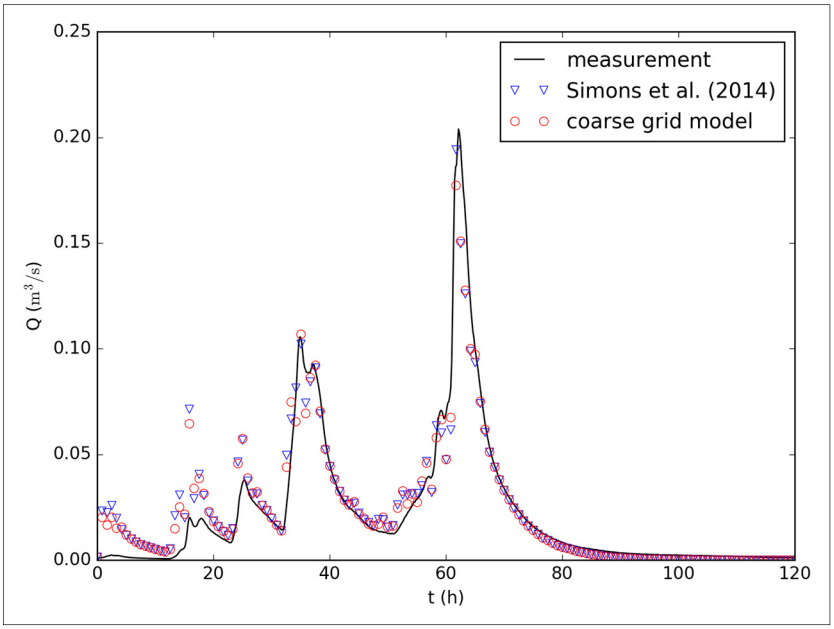

Figure 3. Comparison of coarse grid model results with measurement data and a high-resolution simulation by Simons et al. (2014)

4.2 Anisotropic porosity shallow water model for urban environment

We defined an idealized city geometry to complete the model chain. We assumed that the city, that represents the real city of Ebnit, Austria, in a very simplified way, is directly located at the outlet of the natural catchment, such that we can apply the model result obtained in the simulation above as an inflow boundary condition to drive the anisotropic urban flood model. In a second simulation run, we artificially increased the discharge at the boundary to produce a more hazardous flood event.

4.2.1 Initial and boundary conditions

The domain was a 500 m by 300 m large urban basin with flat bed, wherein the only topographical features were the buildings inside the domain, cf. Figure 4 (top). We constructed a building block with elements that were rectangles with dimensions 20 m by 30 m. Outside of the block, we positioned a C-shaped building that represented an important building with a high damage potential, e.g. school or university. We were interested in the arrival time of the flood wave and the resulting water depth at this location. Thus, a gauge was positioned at the front of this building. The domain was initially dry, the discharge calculated by the

previous model run was imposed at a 25 m wide inlet at the west boundary of the domain that shall represent a breach in the dam that protects the city. All other boundaries were open boundaries.

In Figure 4 (bottom), the coarse mesh used by the anisotropic porosity model is shown. Buildings were plotted only for illustration purposes and were actually accounted for by means of the porosity terms. We note that the mesh was constructed such that the outline of the building block aligns with cell edges. This discretization significantly enhanced the quality of the results (Özgen et al., in preparation).

The high-resolution mesh consisted of 8222 triangular cells with element size ranging between 10 m and 5 m, and the coarse-resolution mesh consisted of 698 triangular cells with cell size of 25 m. All meshes were generated with the software Gmsh (Geuzaine and Remacle, 2009).

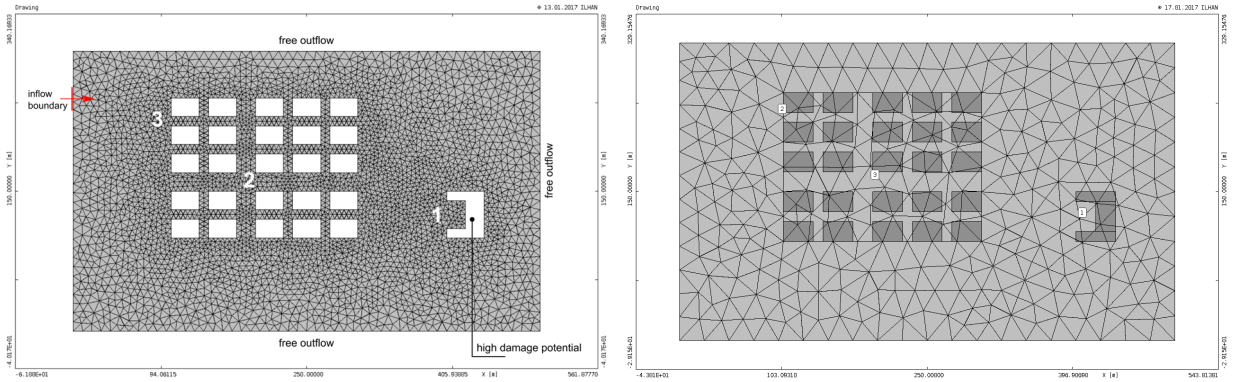

Figure 4. High-resolution mesh, building configuration and position of gauges and the inlet (left); coarse resolution mesh for the anisotropic porosity model with buildings plotted for illustration purposes (right)

4.2.2 Results

Model results for both the high resolution simulation and the anisotropic porosity approach are shown in Figure 5. The overall dynamics of the flood wave was captured well by the anisotropic porosity model. The hydrograph consisted of four peaks that corresponded to the peaks in the inflow (cf. Figure 3). For both models, the runoff arrived at gauge 1 (highest damage potential) at about t = 20 h, while gauge 2 at city center was inundated at about t = 15 h. We observed that gauge 3 was influenced more by fluctuations in the inflow than gauge 2 and gauge 3. The maximum water depth was measured at gauge 3 at about 62 h, which corresponded to the maximum peak in the inflow data. In comparison to the inflow hydrograph, the results at the gauges were damped and temporally delayed. This behavior was captured by both models, although we see that the maximum water depth in the anisotropic porosity approach results (about 1.6 cm) was smaller than in the high resolution results (about 1.8 cm).

The results of both model runs were compared in Figure 6. In the beginning, the results of the anisotropic porosity approach overall undershot the hydrograph produced by the high resolution model. In the late stage of the simulation, when the inflow began to decline (t = 80 h), the anisotropic porosity model results overshot the high resolution hydrograph. We reported an average deviation of about 3 mm in water depth at all gauges but an exact prediction of the arrival times of the runoff waved in all cases.

The forecast of this model chain predicted that fortunately the rainfall event in the natural catchment is not heavy enough to cause substantial damage in the city. The maximum water depth we observed was about 2 cm and located at the city border. The model chain was able to reproduce an averaged behavior of the high resolution simulation and was about 100 times faster than its high-resolution counterpart.

For illustration purposes, we artificially increased the discharge at the inlet boundary by factor 100. Results for the increased discharge are shown in Figure 7. We observed that the water level at all gauges increased significantly and the arrival time of the flood wave was significantly shorter. At gauge 3, a maximum water level of about 1.6 m at t=60 h was predicted by the high-resolution model (Figure 7 (top)) which was accurately captured by the anisotropic porosity shallow water model as well (Figure 7 (bottom)). As the flood wave propagated through the city environment, the amplitude of the water level was damped such that at gauge 2, the maximum water level calculated by the high-resolution model was about 0.8 m at about t=60 h. Here, the anisotropic porosity model underestimated the water level and yielded a maximum value of about 0.75 m. Finally, at gauge 1, which is located in the area with high damage potential, the anisotropic porosity model slightly overestimated the maximum water level.

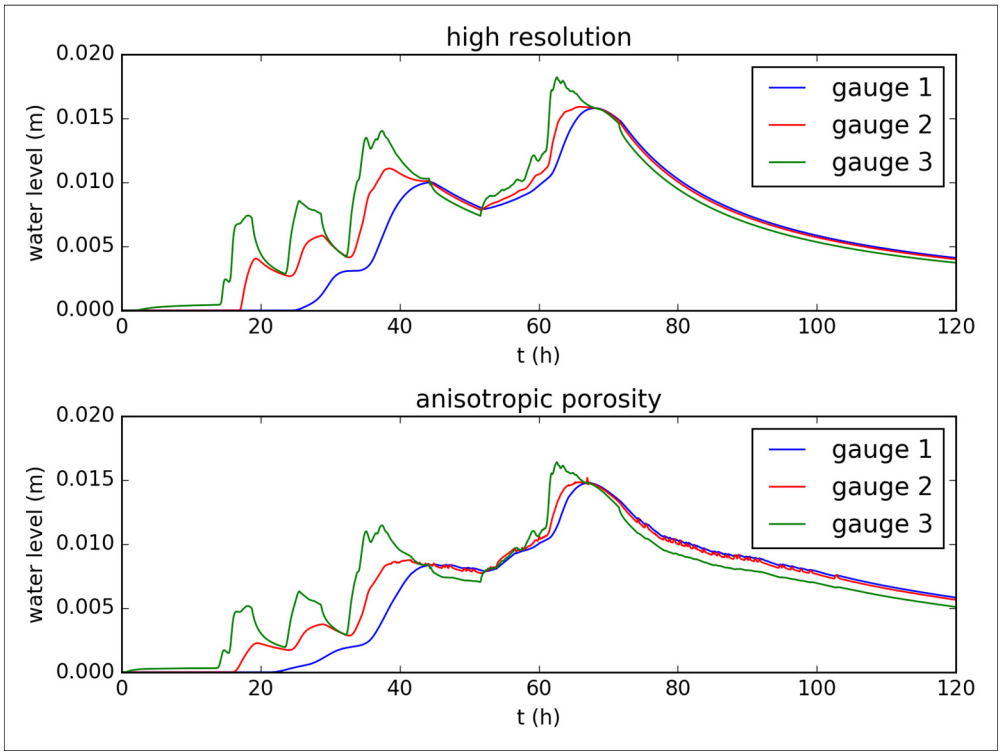

Figure 5. Model results for the high-resolution simulation (top) and the anisotropic porosity approach (bottom)

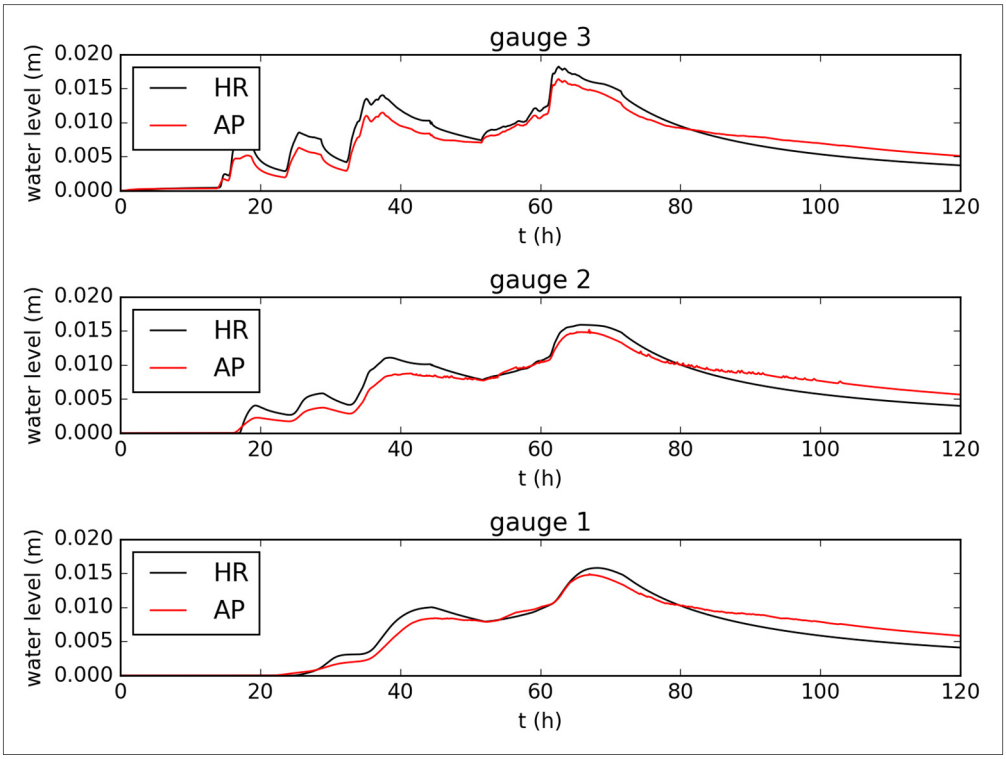

Figure 6. Comparison of high-resolution model results (HR) with anisotropic porosity model results (AP) at gauges 3 (top), 2 (center) and 1 (bottom)

Overall, the dynamic of the flood was reproduced accurately by the anisotropic porosity model. Figure 8 shows a comparison of the model results per gauge where the aforementioned discussions can be observed as well. Figure 9 shows water levels plotted at different time steps and good agreement between both models was observed. In both cases, the simulation with the anisotropic porosity model ran about 100 times faster.

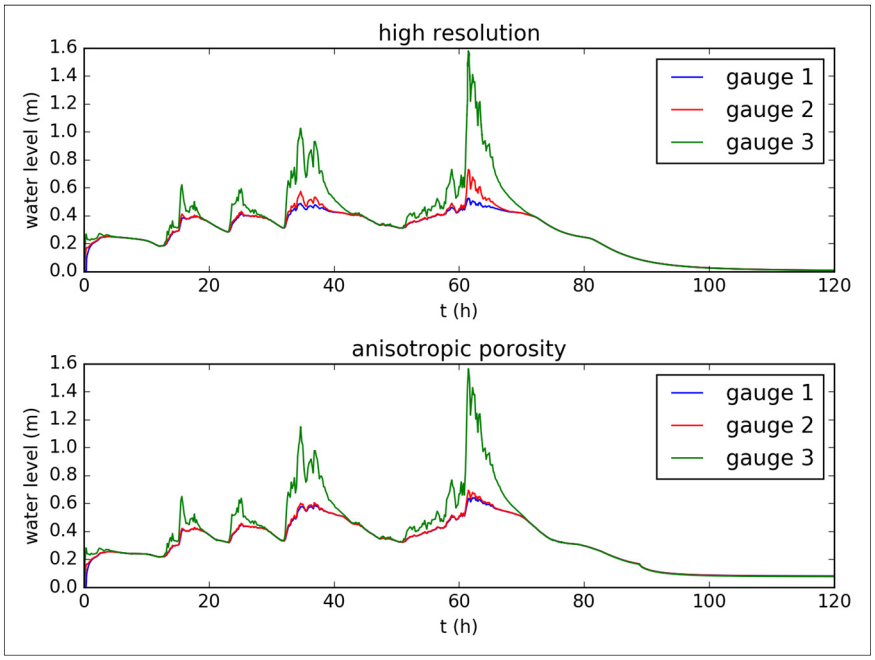

Figure 7. Model results for case with artificially increased discharge for the high-resolution simulation (top) and the anisotropic porosity approach (bottom)

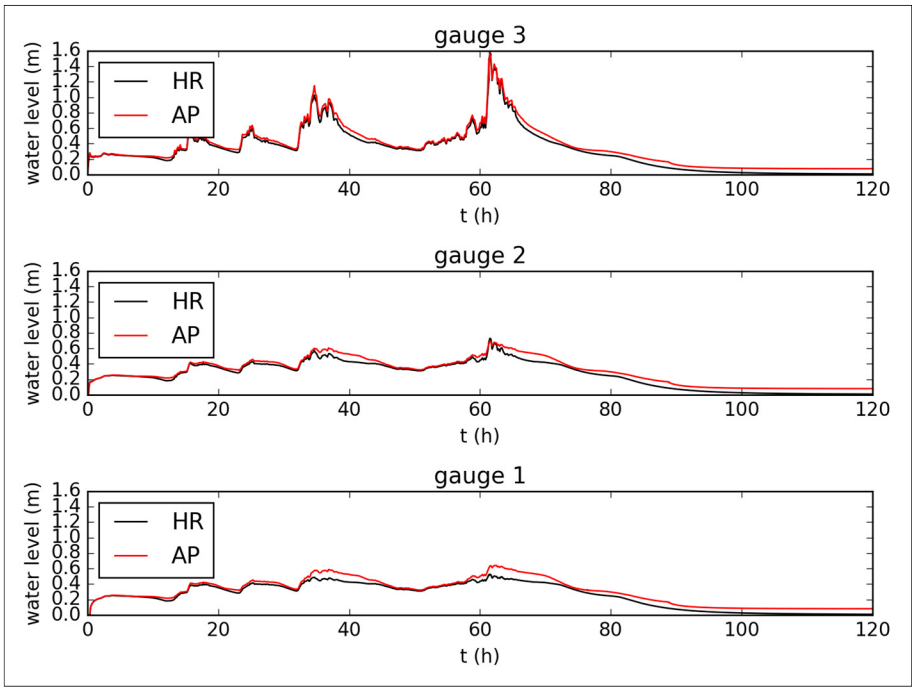

Figure 8. Comparison of high-resolution model results (HR) with anisotropic porosity model results (AP) at gauges 3 (top), 2 (center) and 1 (bottom) for case with artificially increased discharge

5 CONCLUSIONS

We presented and coupled two coarse-grid approaches, i.e. modified friction-law approach and anisotropic porosity approach, for application in urban runoff and urban flood modeling. The novelty of the presented approach is that the model chain contains two hydraulic models instead of the more common model chain hydrological model coupled with hydraulic model.

As a proof of concept, we simulated runoff and inundation in an idealized city using the suggested model chain. Model results were promising and indicated that this approach might indeed be used to forecast flood arrival times and flood inundation areas. The decrease in computational cost enables model results to be obtained in feasible time spans on a personal computer. On average, the models ran about two orders of magnitude faster than their high-resolution counterparts.

Future research may focus on studying the presented model approaches at even larger scales, e.g. large natural catchments and cities.

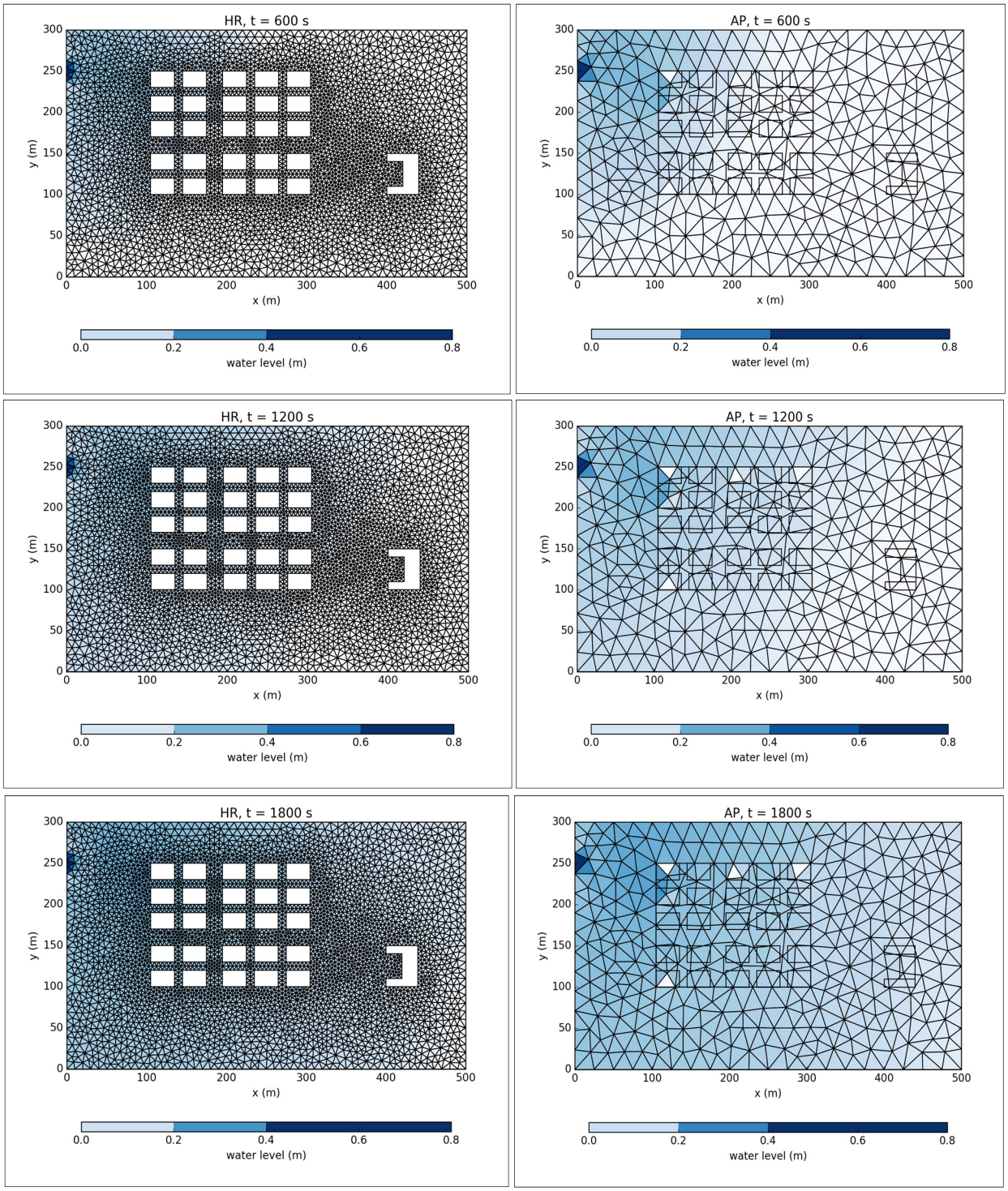

Figure 9. Water level plotted at different time steps for the artificially increased discharge for high-resolution model (left) and anisotropic porosity model (right)

ACKNOWLEDGEMENTS
This work was supported by the DFG Research Training Group 'Urban Water Interfaces' (DFG-GRK2032).

REFERENCES

Abily, M., Bertrand, N., Delestre, O., Gourbesville, P. & Duluc, C.-M. (2016). Spatial Global Sensitivity Analysis of High Resolution Classified Topographic Data Use in 2D Urban Flood Modelling. *Environmental Modelling & Software*, 77, 183-195.

Bussing, T.R.A. & Murman, E.M. (1988). Finite-Volume Method for the Calculation of Compressible Chemically Reacting Flows. *AIAA Journal*, 26(9), 1070-1078.

Cea, L., Garrido, M. & Puertas, J. (2010). Experimental Validation of Two-Dimensional Depth-Averaged Models for Forecasting Rainfall-Runoff from Precipitation Data in Urban Areas. *Journal of Hydrology*, 382, 88-102.

Cea, L., Puertas, J. & Vázquez-Cendón, M.E. (2007). Depth Averaged Modelling of Turbulent Shallow Water Flow with Wet-Dry Fronts. *Archives of Computational Methods in Engineering*, 14(3), 303-341.

Chen, A.S., Evans, B., Djordjević, S. & Savić, D.A. (2012a). A Coarse-Grid Approach to Representing Building Blockage Effects in 2D Urban Flood Modelling. *Journal of Hydrology*, 426-427, 1-16.

Chen, A.S., Evans, B., Djordjević, S. & Savić, D.A. (2012b). Multi-Layered Coarse Grid Modelling in 2D Urban Flood Simulations. *Journal of Hydrology*, 470-471, 1-11.

Defina, A. (2000). Two-Dimensional Shallow Flow Equations for Partially Dry Areas. *Water Resources Research*, 36(11), 3251-3264.

Guinot, V. & Soares-Frazão, S. (2006). Flux and Source Term Discretization in Two-Dimensional Shallow Water Models with Porosity on Unstructured Grids. *International Journal for Numerical Methods in Fluids*, 50, 309-345.

Guinot, V. (2012). Multiple Porosity Shallow Water Models for Macroscopic Modelling Of Urban Floods. *Advances in Water Resources*, 37, 40-72.

Hervouet, J.M., Samie, R. & Moreau, B. (2000). Modelling Urban Areas in Dam-Break Flood Wave Numerical Simulations. *Proceedings of the International Seminar and Workshop on Rescue Actions based on Dambreak Flood Analysis*, Seinâjoki, Finland.

Hinkelmann, R. (2005). *Efficient Numerical Methods and Information-Processing Techniques for Modeling Hydro- and Environmental Systems*. Springer-Verlag.

Geuzaine, C. & Remacle, J.F. (2009). Gmsh: A Three-D Finite Element Mesh Generator with Built-in Pre- and Post-Processing Facilities. *International Journal for Numerical Methods in Engineering*, 79, 1309-1331.

Jahanbazi, M., Özgen, I., Aleixo, R. & Hinkelmann, R. (2017). Development of a Diffusive Wave Shallow Water Model with A Novel Stability Condition and Other New Features. *Journal of Hydroinformatics*, 19(3), 108.

Jain, M.K. & Kothyari, U.C. (2004). A GIS Based Distributed Rainfall-Runoff Model. *Journal of Hydrology*, 299(1-2), 107-135.

Kim, B., Sanders, B.F., Schubert, J.E. & Famiglietti, J.S. (2014). Mesh Type Tradeoffs in 2D Hydrodynamic Modeling of Flooding with A Godunov-Based Flow Solver. *Advances in Water Resources*, 68, 42-61.

Lacasta, A., Morales-Hernández, M., Murillo, J. & García-Navarro, P. (2014). An Optimized GPU Implementation of A 2D Free Surface Simulation Model on Unstructured Meshes. *Advances in Engineering Software*, 78, 1-15.

Lawrence, D.S.L. (1997). Macroscale Surface Roughness and Frictional Resistance in Overland Flow. *Earth Surface Processes and Landforms*, 22, 365-382.

Liang, D., Falconer, R.A. & Lin, B. (2007). Coupling Surface and Subsurface Flows in a Depth Averaged Flood Wave Model. *Journal of Hydrology*, 337(1-2), 147-158.

McMillan, H. & Brasington, J. (2007). Reduced Complexity Strategies for Modelling Urban Floodplain Inundation. *Geomorphology*, 90, 226-243.

Néelz, S. & Pender, G. (2007). Sub-Grid Scale Parameterisation of 2D Hydrodynamic Models of Inundation in the Urban Area. *Acta Geophysica*, 56(3), 65-72.

Özgen, I., Teuber, K., Liang, D. & Hinkelmann R. (2015). Upscaling the Shallow Water Model with a Novel Roughness Formulation. *Environmental Earth Sciences*, 74(11), 7371-7386.

Özgen, I., Liang, D. & Hinkelmann, R. (2016b). Shallow Water Equations with Depth-Dependent Anisotropic Porosity for Subgrid-Scale Topography. *Applied Mathematical Modelling*, 40, 7447-7473.

Özgen, I., Serrano-Taslim, M., Zhao, J., Liang, D. & Hinkelmann, R. (2016c). Coarse Grid Shallow Water Simulations of Rainfall Runoff in Small Catchments with Modified Friction Law to Account for Unresolved Microtopography. *European Geosciences Union General Assembly 2016*, Vienna, Austria.

Özgen, I., Zhao, J., Liang, D. & Hinkelmann, R. (2016a). Urban Flood Modeling Using Shallow Water Equations with Depth-Dependent Anisotropic Porosity. *Journal of Hydrology*, 541, 1165-1184.

Razafison, U., Cordier, S., Delestre, O., Darboux, F., Lucas, C. & James, F. (2012). A Shallow Water Model for the Numerical Simulation of Overland Flow on Surfaces with Ridges and Furrows. *European Journal of Mechanics – B/Fluids*, 31, 44-52.

Sanders, B.F., Schubert, J.E. & Gallegos, H.A. (2008). Integral Formulation of Shallow-Water Equations with Anisotropic Porosity for Urban Flood Modeling. *Journal of Hydrology*, 362(1-2), 19-38.

Simons, F., Busse, T., Hou, J., Özgen, I. & Hinkelmann, R. (2014). A Model for Overland Flow and Associated Processes within the Hydroinformatics Modelling System. *Journal of Hydroinformatics*, 16, 375-391.

Soares-Frazão, S., Lhomme, J., Guinot, V. & Zech, Y. (2008). Two-Dimensional Shallow-Water Model with Porosity for Urban Flood Modelling. *Journal of Hydraulic Research*, 46, 45-64.

Smith, L.S. & Liang, Q. (2013). Towards a Generalised GPU/CPU Shallow-Flow Modelling Tool. *Computers & Fluids*, 88, 334-343.

Proceedings of the 37th IAHR World Congress
August 13 – 18, 2017, Kuala Lumpur, Malaysia

A DECISION SUPPORT TOOL FOR CONSTRUCTING RAINFALL INTENSITY-DURATION-FREQUENCY RELATIONS FOR URBAN HYDRAULIC STRUCTURE DESIGN IN A CHANGING CLIMATE

VAN-THANH-VAN NGUYEN[1], MYEONG-HO YEO[2] & TRUONG-HUY NGUYEN[3]

[1,2,3] Department of Civil Engineering and Applied Mechanics, McGill University, Montreal, Quebec, Canada H3A 0C3
van.tv.nguyen@mcgill.ca

ABSTRACT

The present study proposed a decision support tool (SDExRAIN) for constructing the rainfall intensity-duration-frequency (IDF) relations at a given site in the context of climate change. More specifically, the SDExRAIN consisted of two components: (i) a spatial statistical downscaling model to describe the linkage between large-scale global climate variables and daily annual maximum rainfalls at a given site; and (ii) a temporal statistical downscaling model to describe the relations between daily and sub-daily annual maximum rainfalls. Consequently, if the linkage between the large-scale climate variability to the historical observations of the extreme rainfall processes at a local site could be established, then the projected change of climate conditions provided by a GCM could be used to predict the resulting impact on the extreme rainfalls at the location of interest. The feasibility and accuracy of this tool was assessed based on the NCEP re-analysis data, the climate simulation outputs from two GCMs (the Canadian GCM3 and the UK HadCM3), and observed daily precipitation data available at two raingages with completely different climatic conditions: Seoul station in South Korea and Dorval Airport station in Canada. Results of this assessment have indicated that it is feasible to use the SDExRAIN for accurately describing the relations between climate predictors provided by GCMs under different climate change scenarios and daily and sub-daily annual maximum rainfalls at a given site. Therefore, the proposed decision support tool can be used for assessing the climate change impact on extreme rainfalls at a given location of interest.

Keywords: Design rainfall estimation; hydrologic frequency analysis; downscaling methods; climate change; urban hydraulic structure design.

1 INTRODUCTION

In recent years, climate change has been recognized as having a profound impact on extreme weather events. Many studies have been carried out to investigate this impact using outputs from Global Climate Models (GCMs) or Regional Climate Models (RCMs) and downscaling methods (Nguyen et al., 2006; Nguyen and Nguyen, 2008; Willems et al., 2012). The particular importance for water infrastructure design in small urban watersheds are those downscaling procedures dealing with the linkage of the large-scale climate variability to the historical observations of the sub-daily rainfall extremes at a local site (Nguyen et al., 2007; Arnbjerg-Nielsen et al., 2013). If this linkage could be established, then the projected change of climate conditions given by a GCM or RCM could be used to predict the resulting change of the local extreme precipitations and the corresponding urban runoff characteristics. Hence, in this study a decision support tool for statistical downscaling of extreme rainfall processes (hereafter called SDExRain) was developed to assess the climate change impact on the extreme rainfalls at a given location.

More specifically, the proposed tool SDExRain consisted of two components: (i) a spatial statistical downscaling model to describe the linkage between global climate variables and daily annual maximum rainfalls at a given site (Yeo and Nguyen, 2013); and (ii) a temporal statistical downscaling model to describe the relations between daily and sub-daily annual maximum rainfalls (Nguyen et al., 2002; Nguyen et al., 2007). Consequently, if the linkage between the large-scale climate variability to the historical observations of the extreme rainfall processes at a local site could be established, then the projected change of climate conditions provided by a GCM could be used to predict the resulting impact of the selected extreme rainfall variables.

The feasibility and accuracy of the SDExRain were assessed based on the NCEP re-analysis and observed daily precipitation data available at two raingages with completely different climatic conditions: Seoul station in South Korea and Dorval Airport station in Quebec (Canada). Results of this assessment have indicated that it is feasible to use this tool for accurately describing the relations between climate predictors provided by GCMs under different climate change scenarios and daily and sub-daily annual maximum rainfalls at a given site. Therefore, the proposed decision support tool can be used for assessing the climate change impacts on extreme rainfalls at a given location of interest.

2 SDEXRAIN: A DECISION SUPPORT TOOL FOR CLIMATE CHANGE IMPACT ASSESSMENT OF EXTREME RAINFALL PROCESSES

As mentioned in the previous section, the proposed decision support tool SDExRain was based on a combination of two statistical downscaling procedures: (1) a spatial downscaling method for linking the daily precipitation process at a local site to large-scale atmospheric variables given by a GCM under different climate change scenarios using the SDRain model (Yeo and Nguyen, 2013); and (2) a temporal downscaling approach for linking sub-daily annual maximum precipitations (AMPs) from daily AMP using the scaling-GEV method (Nguyen et al., 2002). More specifically, this integrated extreme rainfall modeling tool in the context of climate change can be used for the construction of the Intensity-Duration-Frequency (IDF) relations of extreme rainfalls at a given location. Hence, it can be used to assess the regional climate change impacts on the extreme rainfalls at a given site of interest.

2.1 A Statistical Model for Spatial Downscaling of Daily Precipitation Process (SDRain)

The proposed SDRain model for modeling the daily precipitation process consists of two components: the modeling of daily precipitation occurrences and the modeling of daily precipitation amounts. Daily time series of precipitation occurrence is defined by two values (O_i = 0 if dry, O_i = 1 if wet). The daily probability (π_i) of non-zero precipitation for a day i is formulated as follows:

$$ln\left(\frac{\pi_i}{1-\pi_i}\right) = a_0 + a_1X_1 + a_2X_2 + \cdots + a_mX_m \quad [1]$$

in which X_j, j = 1, 2, …, m, are the significant large-scale climate predictors, and the a_j's are the regression parameters. A uniformly distributed random number r_i ($0 \le r_i \le 1$) is used to determine whether it is a wet or dry day. In addition, similar to the SDSM method (Wilby et al., 2002), the relationship between the local daily precipitation amount (R_i) and the large-scale climate predictors (X_j's) is described by the following nonlinear expression:

$$R_i = exp(b_0 + b_1X_1 + b_2X_2 + \cdots + b_mX_m + SE \times \delta_i) \quad [2]$$

in which b's are the regression parameters, and SE is the standard error in non-linear regression model, and δ_i is a normal distributed random number with mean of 0 and standard deviation of Variance Inflation Factor (VIF). The VIF term is used to increase the accuracy in representing the variance of the observed daily precipitation amounts and will be empirically determined using the available data.

The daily annual maximum precipitations (AMPs) are extracted from the downscaled daily precipitation series given by the SDRain for different GCM-based climate scenarios. However, it is expected that these downscaled annual maximum precipitations are not comparable to the observed extreme values. Hence, a bias-correction procedure is required to improve the accuracy of the downscaled AMPs at a given site. The proposed procedure is described in the following (Nguyen et al., 2007).

Let

$$y_\tau = \hat{y_\tau} + e_\tau \quad [3]$$

in which y_τ is the adjusted daily AM precipitation at a probability level τ, $\hat{y_\tau}$ is the corresponding GCM-SDRain estimated daily AMP, and e_τ is the residual associated with y_τ . This residual is modelled by the second order polynomial regression as follows:

$$e_\tau = m_0 + m_1\hat{y}_\tau + m_2\hat{y}_\tau^2 + \epsilon \quad [4]$$

where m_0, m_1, and m_2 are regression parameters, $\hat{y}_\tau$ is the estimated AMP, and ϵ is the modelling error term.

2.2 A Statistical Model for Temporal Downscaling of Sub-Daily Precipitation Processes (SDExtreme)

The GEV distribution has been commonly used to describe the probability distribution of AMPs and for the construction of the IDF curves (Schaefer, 1990). The cumulative distribution function, F(x), of the GEV distribution is

$$F(x) = exp\left[-\left(1 - \frac{\kappa(x-\xi)^{1/\kappa}}{\alpha}\right)\right] \quad (\kappa \neq 0) \quad [5]$$

in which ξ, α, and κ are the location, scale, and shape parameter, respectively. The non-central moment (NCM) method can be used for estimation the GEV parameters in consideration of the scaling property of

these NCMs with the rainfall durations. The *k*-th order of NCM, μ_k, of the GEV distribution can be expressed as

$$\mu_k = \left(\xi + \frac{\alpha}{\kappa}\right)^k + (-1)^\kappa \left(\frac{\alpha}{\kappa}\right)^\kappa \Gamma(1+k\kappa) + k\sum_{i=1}^{k-1}(-1)^i \left(\frac{\alpha}{\kappa}\right)^i \left(\xi + \frac{\alpha}{\kappa}\right)^{k-1} \Gamma(1+ik) \quad [6]$$

in which $\Gamma(.)$ is the gamma function. Therefore, it is possible to estimate parameters (ξ, α, and κ) of GEV distribution using the first three NCMs. The quantile (X_T) corresponding to a return period *T* can be calculated using the following expression:

$$X_T = \xi + \frac{\alpha}{\kappa}\left\{1 - [1 - \ln(p)]^\kappa\right\} \quad [7]$$

where *p* is the exceedance probability of interest.

For a simple scaling process, it can be shown that (Nguyen et al., 2002)

$$\mu_k(x) = E\left\{f^k(x)\right\} = \alpha(k)x^{\beta(k)} \quad [8]$$

where $\beta(k) = \beta k$. Furthermore, for a simple scaling process, it can be shown that the statistical properties of the GEV distribution for two different time scales *t* and *λt* are related as follows:

$$\kappa(\lambda t) = \kappa(t) \quad [9]$$

$$\alpha(\lambda t) = \lambda^\beta \alpha(t) \quad [10]$$

$$\xi(\lambda t) = \lambda^\beta \xi(t) \quad [11]$$

$$X_T(\lambda t) = \lambda^\beta X_T(t) \quad [12]$$

Hence, based on these relationships, it is possible to derive the statistical properties of sub-daily AMPs using the properties of daily AMPs. Therefore, the proposed GEV distribution based on the scaling property of NCMs for different rainfall durations can be used to construct the IDF curves for a given site.

3 NUMERICAL APPLICATION

To assess the feasibility and accuracy of the proposed decision support tool SDExRain, a case study was carried out using NCEP re-analysis data, global GCM climate simulation outputs, and daily precipitation as well as at-site AMP data available at Seoul station in South Korea and Dorval Airport station in Quebec (Canada) for the 1961-1990 period. The selected global GCM predictors are based on the outputs from two GCMs (the Canadian CGCM3 and the UK HadCM3) for the current 1961-2000 period as well as for some future periods 2020s, 2050s, and 2080s under four different climate change scenarios (A1B and A2 for CGCM3 and A2 and B2 for HadCM3). The daily precipitation and at-site AMP series for durations ranging from 5 minutes to 1 day were used in this study, and the data for the 1961-1990 period were used for model calibration and the data for the remaining 1991-2000 period were used for validation purposes.

The proposed spatial downscaling method (SDRain) was used to generate 100 daily precipitation series and to provide the daily AMP amounts for a local site under the four selected climate scenarios. The generated daily precipitation series were used to performing the bias correction based on Equations [3] and [4]. The adjusted daily AMP values were then used for estimating the sub-daily AMPs using the proposed SDExtreme based on the scaling-GEV distribution. On the basis of these results, the IDF relations for the current and future periods for different climate change scenarios at a given site were constructed. For the purpose of illustration, Figure 1 shows the achievement of a very good agreement between the adjusted mean of GCM-downscaled AMP amounts and the observed at-site values given by HadCM3-A2 for Dorval and Seoul stations after making the bias-correction adjustment using the fitted second-order functions (Equation [4]). Hence, it can be seen that the derived bias-correction function from the data for the 1961-1990 calibration period could improve the accuracy of the GCM-based downscaled AMPs for other time periods in the future.

To examine the temporal scaling properties of the AMP series, the SDExtreme provides graphical analyses using the first three NCMs. For purposes of illustration, Figure 2 shows the scaling relationships between NCMs and rainfall durations for Dorval and Seoul stations. The log-linearity of NCMs shows two distinct scaling regimes: from 5 minutes to 30 minutes and from 30 minutes to 1 day for Dorval station; and

from 10 minutes to 1 hour and from 1hour to 1 day for Seoul station. In addition, the linearity of the scaling exponents *β(k)* against the order of NCMs of AMPs for both Dorval and Seoul as shown in Figure 3 has indicated the simple scaling behaviour of the AMPs at these two stations. Hence, it is possible to estimate the NCMs (and the corresponding GEV parameters) of AMPs for shorter durations using the NCMs of AMPs for longer time scales within the same scaling regime.

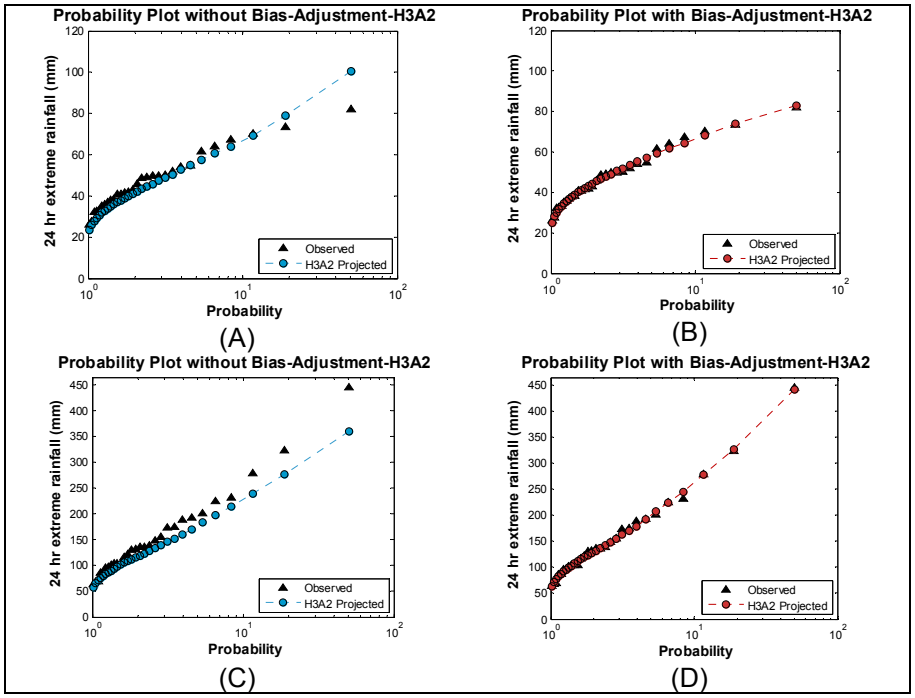

Figure 1. Probability Plots of Observed Daily AMPs and Simulated Values given by HadCM3-A2 for the Calibration 1961-1990 Period with and without Bias Correction for Dorval Airport (A and B) and Seoul (C and D) Stations

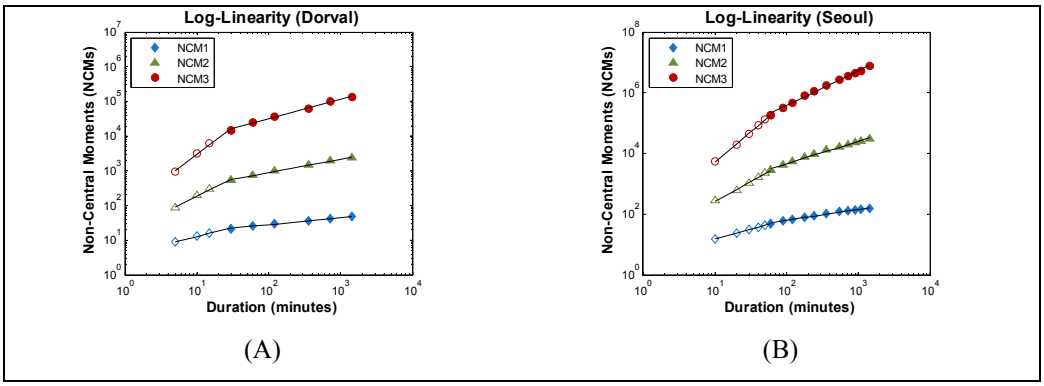

Figure 2. Log-log Plots of the Non-Central Moments (NCMs) of the First Three Orders against Durations for Dorval Airport and Seoul Stations

.

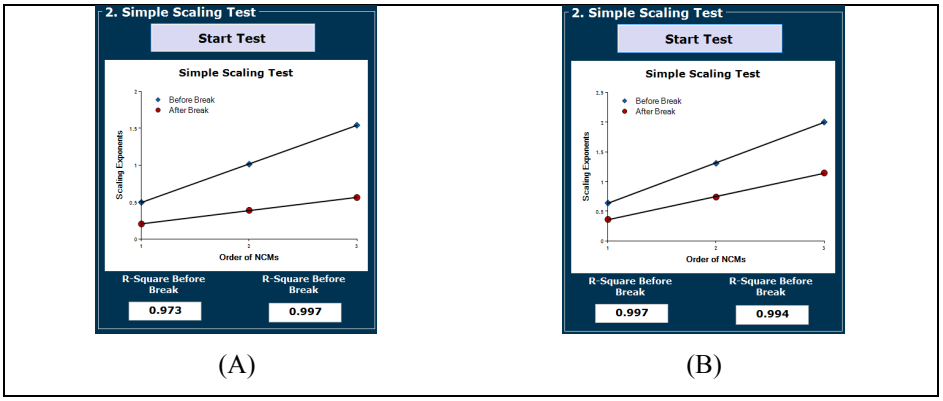

Figure 3. Plots of the Scaling Exponents β(k) against the Order of NCMs of AMPs for Dorval Airport (A) and Seoul (B) Stations.

Figure 4 shows the comparison between the observed and estimated AMPs by traditional and scaling GEV distributions for 1-hour AMPs for Dorval and Seoul stations. It can be seen that the quantiles derived from the daily AMPs using the established scaling relationships agree very well with those values given by the traditional fitted GEV distribution as well as with the observed values. Similar results were found for other duration and stations. The proposed SDExRain was used to construct IDF curves for Dorval and Seoul stations under four different climate change scenarios (HadCM3 A2 & B2 and CGCM3 A1B & A2) for the current (1961-1990) and future periods (2020s, 2050s, and 2080s). For illustration purpose, Figure 5 shows the probability plots of AMDPs at Dorval station for the 1961-1990 period and future periods (2020s, 2050s, and 2080s) using the proposed decision support tool. It can be seen that both CGCM3 and HadCM3 suggested increasing trends of AMPs for future periods under the four selected climate change scenarios. In addition, the climate simulations given by two different GCMs produced two different changes in the maximum rainfalls in the future.

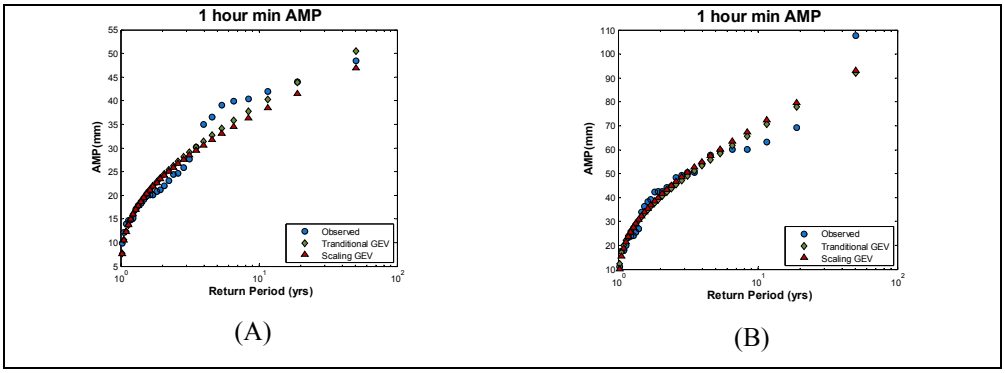

Figure 4. Probability Plots of 1-hour Observed and Estimated AMPs using Traditional and Scaling GEV Distributions for the 1961-1990 for Dorval Airport station (A) and Seoul station (B).

4 CONCLUSIONS

A decision support tool was proposed in this study to describe the linkages between large-scale climate variables at the daily scale to AMPs for daily and sub-daily scales at a given local site. The feasibility and accuracy of this modeling tool have been tested using climate simulation outputs from two GCMs (CGCM3 and HadCM3) under four different climate scenarios and using available AMP data for durations ranging from 5 minutes to 1 day at two stations located in completely different climatic regions: Dorval Airport station in Quebec (Canada) and Seoul station in South Korea for the 1961-2000 period. Results of this numerical application have indicated the feasibility and accuracy of the proposed modeling tool. More specifically, it was found that the AMP series in Quebec (Canada) and in South Korea displayed a simple scaling behaviour. Based on this scaling property, the scaling GEV distribution has been shown to be able to provide accurate estimates of sub-daily AM precipitations from GCM-downscaled daily AMP amounts. Therefore, it can be concluded that it is feasible to use the proposed SDExRain tool to describe the relationship between large-scale climate predictors for daily scale given by GCM simulation outputs and the daily and sub-daily AMPs at a local site. This relationship would be useful for various climate-related impact assessment studies for a given region.

Finally, the proposed decision-support tool SDExRAIN was used to construct the IDF relations for a given site for the 1961-1990 period and for future periods (2020s, 2050s, and 2080s) using climate predictors given

by the CGCM3 and HadCM3 simulations. In general, it was found that AM precipitations at a local site downscaled from the HadCM3 displayed a smaller change in the future, while those values estimated from the CGCM3 indicated a large increasing trend for future periods. This result has demonstrated the presence of high uncertainty in climate simulations provided by different GCMs.

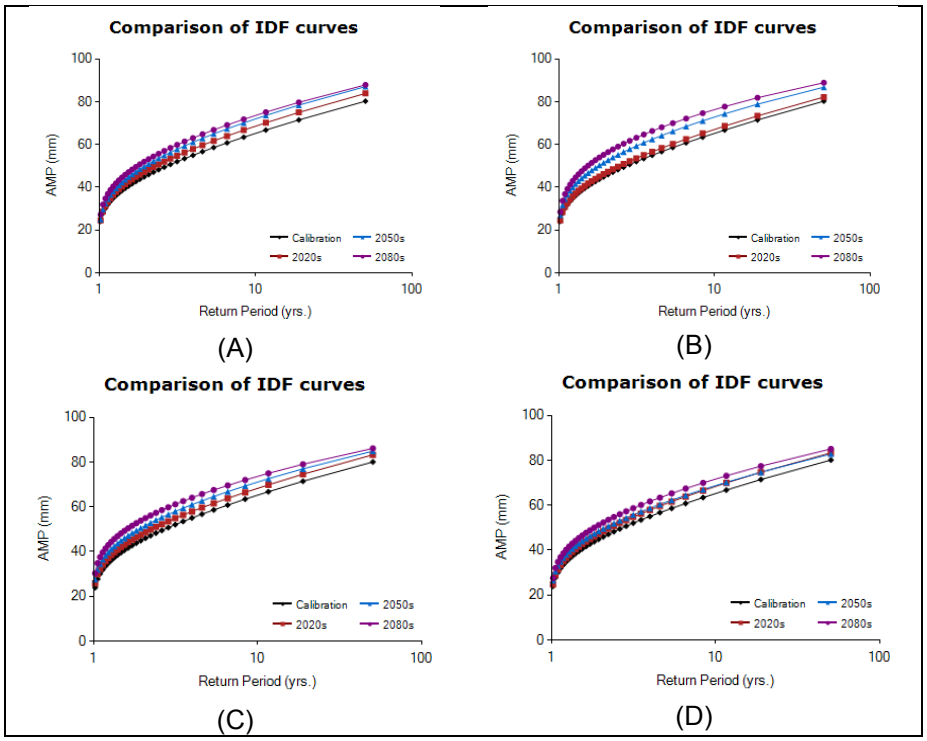

Figure 5. Probability Plots of daily AMPs Projected (A) from CGCM3A1B, (B) from CGCM3A2, (C) from HadCM3A2 and (D) from HadCM3B2 Scenarios for the 1961-1990 Period and for Future Periods (2020s, 2050s, and 2080s) for Dorval Airport Station.

REFERENCES

Arnbjerg-Nielsen, K., Willems, P., Olsson, J., Beecham, S., Athirana, A., Gregersen, I.B., Madsen, H. & Nguyen, V-T-V. (2013). Impacts of Climate Change on Rainfall Extremes and Urban Drainage Systems: A Review. *Water Science and Technology,* 68(1), 16-28.

Nguyen V.T.V., Nguyen T.D. & Ashkar F. (2002). Regional Frequency Analysis of Extreme Rainfalls. *Water Science and Technology*, 45(2), 75–81.

Nguyen, V-T-V., Nguyen, T-D. & Gachon, P. (2006). On the Linkage of Large-Scale Climate Variability with Local Characteristics of Daily Precipitation and Temperature Extremes: An Evaluation of Statistical Downscaling Methods. *Advances in Geosciences*, 4, 1-9

Nguyen V.T.V., Nguyen T.D. & Cung A. (2007). *A Statistical Approach to Downscaling Of Sub-Daily Extreme Rainfall Processes for Climate-Related Impact Studies in Urban Areas*. *Water Science and Technology*: *Water Supply*, 7(2), 183-192.

Nguyen, V-T-V. & Nguyen, T-D. (2008). *Statistical Downscaling of Daily Precipitation Process for Climate-Related Impact Studies*. Chapter 16 in Hydrology and Hydraulics, V.P. Singh (Ed.), Water Resources Publications, 12 pages.

Schaefer M. (1990). Regional Analyses of Precipitation Annual Maxima in Washington State. *Water Resources Research*, 26(1), 119–131.

Willems, P., Arnbjerg-Nielsen, K., Olsson, J. & Nguyen, V-T-V. (2012). Climate Change Impact Assessment on Urban Rainfall Extremes and Urban Drainage: Methods and Shortcomings. *Atmospheric Research*, 103,106-118.

Yeo, M-H. & Nguyen, V-T-V. (2013). Statistical Modeling of Daily Rainfall Process in the Context of Climate Change, *Proc. of the CSCE Annual Conference, May 29-June 1*, Montreal, Quebec, 6 pages.

Proceedings of the 37th IAHR World Congress
August 13 – 18, 2017, Kuala Lumpur, Malaysia

RAINFALL-RUNOFF MODEL ANALYSIS USING RADAR-BASED QUANTITATIVE PRECIPITATION ESTIMATION (QPE) AND GAUGE RAINFALL AT UPPER KLANG AMPANG RIVER BASIN

SALWA RAMLY[1], WARDAH TAHIR[2], ASMADI AHMAD[3] & NOOR HISHAM MOHD GHAZALI[4]

[1,3,4] Department of Irrigation and Drainage, Kuala Lumpur, Malaysia
salwaramly@yahoo.com
asmadi_ahmad@water.gov.my
hisham@water.gov.my
[2] Faculty of Civil Engineering, Universiti Teknologi MARA, Shah Alam, Malaysia
wardah_tahir@yahoo.com
[3,4] Department of Irrigation and Drainage, Malaysia

ABSTRACT

Rainfall-runoff model is a model to simulate the hydrologic processes of the watershed system. Streamflow, which is the result from the rainfall-runoff model, is essential for flood analysis especially for high risk flooded area such as Upper Klang Ampang River basin due to rapid development. One of the main input components in the rainfall-runoff model is a precipitation data. Radar-based Quantitative Precipitation Estimation (QPE) is a method to estimate the distribution of precipitation amount or rainfall by using weather radar data. Gauge rainfall data is commonly used in the rainfall-runoff model as a precipitation input. Gauge rainfall data provide accurate rainfall data yet it has less spatial distribution. However, Radar-based QPE offer high temporal and spatial distribution of rainfall data yet limited accuracy of the rainfall data compare to gauge rainfall data. The objective of the analysis is to analyze the streamflow result from the HEC-HMS rainfall runoff model using gauge rainfall and radar-based QPE rainfall data. In the HEC-HMS model, SCS CN method was applied as loss model and SCS CN Unit Hydrograph as transform method. Two significant events were selected to analyze the streamflow results using two different precipitation input, radar-based QPE and gauge rainfall data. Calibration factor for radar-based QPE will be discussed to improve the quality of the accuracy for radar-based QPE. From the analysis, radar-based QPE showed positive results and is applicable to be use in the flood analysis at Upper Klang Ampang River Basin.

Keywords: Rainfall-runoff model; Quantitative Precipitation Estimation (QPE); weather radar; HEC-HMS; streamflow.

1 INTRODUCTION

Hydrological cycle is a natural process and describes the continuous movement of water in the earth. The water experienced physical processes which changes from evaporation, condensation, precipitation, infiltration, surface runoff and sub-surface flow. Precipitation or known as rainfall is the most frequent measured in the hydrological cycle since the impact of the rainfall is significant to human life (Ward & Robinson, 2000). People are interested to know when and where the precipitation would happen, amount of rainfall and the impact of rainfall to the river basin either flood or drought in their area. Therefore, the measurement of the amount of rainfall is vital especially in the hydrological analysis for the purpose of water resources planning and design. Enhancement of the rainfall measurement method by researchers is continuous to improve the quality of estimation and the measurement of the rainfall. (Sun et al., 2000; Smith et al., 2007; Wardah et al., 2008).

The relationship between rainfall and runoff in the hydrological cycle could be described through rainfall-runoff model. The rainfall runoff model will estimate the surface runoff in the channel or river system as response to rainfall input data for the target catchment. Numerous rainfall-runoff model software's are available and each of it has its own advantages and disadvantages. One of the widely used rainfall-runoff model software is the HEC-Hydrologic Modelling System or known as HEC-HMS. This model shall predict runoff, stage, and timing for giving rainfall input into the basin (USACE-HEC, 2000). The model shall produce the hydrographs, which are useful for water resources studies such as for flood forecasting, water availability, urban drainage design or reservoir design.

A rainfall-runoff model requires mean areal rainfall estimation to do the computation of the runoff. Commonly, rainfall is measured by using a rain gauge instrument, which measures the actual amount of rain that falls over in the gauge. The rain gauge instrument provides a point based rainfall data and less spatial distribution due to the topography of the catchment area. Another option for better spatial distribution of rainfall data is by using weather radar that covers much larger areas that may be impossible for rain gauge installation. Radar-based Quantitative Precipitation Estimation (QPE) is able to provide high spatial and temporal rainfall data for better usage and analysis (Nagata, 2011). However, weather radar do not directly measure the rainfall but they measure variables related to the electromagnetic properties of hydrometeors (Berne & Krajewski,

2013). The weather radar is a remote sensing instrument that emits electromagnetic pulses into the surroundings to determine the range, movement's direction, speed of objects and altitude and gives the reflectivity values. (Marshall & Palmer, 1950) developed a power law equation of the relationship between reflectivity, Z and the rain rate, R to calculate the value of the rainfall. However, few factors contributing to the error of the weather radar data including conversion from reflectivity to rain rate, beam blockage, ground clutter and hardware calibration error. Hence, the radar rainfall product needs to be examined before it could be used as radar-based QPE in the hydrological modeling (Pedersen et al., 2010; Wüest et al., 2010). The accuracy of the radar rainfall data could be improved through calibration of the radar rainfall data with the radar rainfall adjustment factor (AF) (Vanaja et al., 2013; Versini, 2012).

The objective of the study is to analyze the streamflow results from the HEC-HMS rainfall-runoff model using gauge rainfall and radar-based QPE rainfall data. Therefore, the rainfall-runoff model was developed using HEC-HMS model. In this rainfall-runoff model, SCS CN method was applied as loss model and SCS CN Unit Hydrograph was selected to be used in the transform method. The rainfall-runoff model was calibrated and validated using the gauge rainfall data. The radar rainfall data was calibrated with the radar rainfall adjustment factor before it could be used as a radar-based QPE. Then, the calibrated model was tested with the radar-based QPE input data and the results were analyzed.

2 STUDY AREA, DATASETS AND SOFTWARES

2.1 Study Area

Upper Klang Ampang river basin is situated at the east part of the state of Selangor and Federal Territory of Kuala Lumpur between 101°.30' to 101°.55' E longitudes and 3° to 3°.30' N latitude. The river named Klang River is flowing through the city centre of Kuala Lumpur, which is the capital city of Malaysia. Kuala Lumpur is subjected to flood during heavy rain since the city is situated at the low laying area at the confluence of two main river systems, Klang River and Gombak River. At the upper part of Klang River, there is a confluence of the Ampang River and Klang River and the catchment named as Upper Klang Ampang river basin (Figure 1). Upper Klang Ampang river basin is a main watershed for Klang river system to control the amount of runoff flow to the downstream to avoid flooding at the Kuala Lumpur city centre during heavy rainfall. The total area for Upper Klang Ampang river basin is 171km^2. Approximately 10 km from the confluence of Klang Ampang River, the Klang Gate Dam is situated at the upstream of Klang River. This dam is surrounded with forest as a water catchment for the dam. This dam is used for water supply purposes and also as flood mitigation structure for Klang Valley by controlling the release of water to downstream from the dam. Upper Klang Ampang catchment has a big differences land use group between urban area and forest area. Immediately after the dam, there are many residential areas being developed and caused upper Klang river watershed experience land use change. There are high demands of residential area on the hillside of Upper Klang. According to (Kabiri et al., 2013), approximately 50% of Klang watershed is urban area and prone to flooding. Mean annual rainfall for upper Klang Ampang river basin is 2600mm.

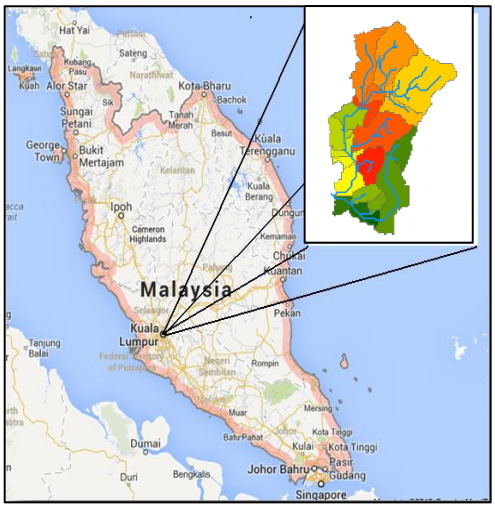

Figure 1. Location of study area: Upper Klang Ampang river basin

2.1 Data sources

Various data were used in this study. The land use data was obtained from Federal Department of Town and Country Planning Peninsular Malaysia (JPBD). Soil data was obtained from Department of Agriculture, Malaysia. The digital contour survey data was obtained from Department of Survey and Mapping Malaysia (JUPEM) and converted to Digital Elevation Model (DEM) using GIS software to delineate the basin and sub basin of the study area. Figure 2 and 3 illustrate the land use and soil type series in the study area. Hydrologic

Soil Group (HSG) for Upper Klang Ampang catchment is shown in table 1. Rainfall and flow data were obtained from Department of Irrigation and Drainage (DID), Malaysia. Radar data was obtained from Malaysian Meteorology Department (MMD) in the CAPPI file format.

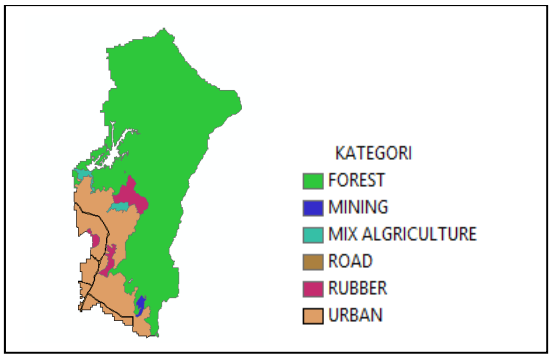

Figure 2. Land use for Upper Klang Ampang river basin

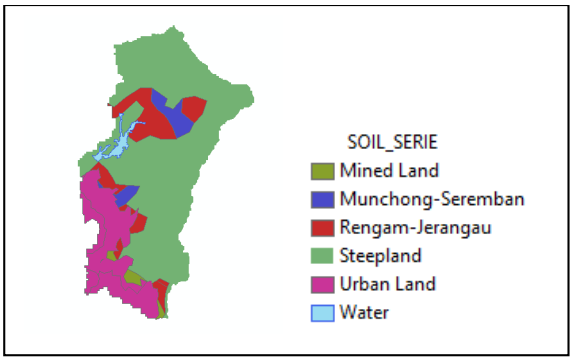

Figure 3. Soil type series for Upper Klang Ampang river basin

Table 1. HSG for Upper Klang Ampang Catchment

Soil Series	Area (km^2)	HSG	Texture
Steepland	99.21	B	Silt loam
Munchong-Seremban	6.06	C	Sandy clay
Rengam-Jerangau	17.07	C	Clay
Mined Land	1.89	D	Silty clay loam
Urban Land	44.69	D	Clay loam
Water	2.20	-	Water
TOTAL	171.12		

3 SOFTWARE USED FOR DATA PROCESSING

3.1 ArcGIS 10.2.1

Geographical Information system (GIS) was use intensively in this study to delineate the catchment of the study area from DEM. ArcGIS 10.2.1 was use together with HEC-GeoHMS extension to create the hydrological map and used in the rainfall-runoff model. HEC-GeoHMS extension is a hydrological tool developed by US Army Corps of Engineer, Hydrologic Engineering Centre.

3.2 Hydrologic Modeling System (HEC-HMS)

Flood peak or runoff hydrograph was simulated using the Hydrologic Engineering Centre-Hydrologic Modelling System (HEC-HMS) model. This model is developed by the United States Army Corps of Engineers (USACE). This model is semi-distributed, event-scale or continuous model and is designed to simulate the precipitation-runoff process of dendritic watershed systems (Feldman, 2000). The model takes into account all relevant hydrological processes such as surface runoff, infiltration evaporation and groundwater recharge. HEC-HMS has three main components, which are basin model, meteorologic model and control specifications. Basin model contains the element of the basin, the connectivity, and runoff parameters. Meteorologic model contains the rainfall and evapotranspiration data, while control specifications contain the start/stop timing and calculation intervals for the run. The basin elements consist of four main elements to be created, which are sub-basin, junction, reach and reservoir depends on the basin characteristics. The basin is divided into sub-basins based on the terrain condition and also homogenous of soil and land use types. Accuracy of the sub-basin characteristics is essential to produce good simulation results. Spatial data for sub-basin characteristics can be prepared in GIS platform using HEC-GeoHMS and can be directly imported into HEC-HMS. The Soil Conservation Service (SCS) Curve Number (CN) model was used to estimate the runoff.

3.3 Productx

The radar data provided by MMD need a specific software, Productx as an examiner program for radar data. Productx is a utility program under Interactive Radar Information System (IRIS) software developed by VAISALA. This program was used to check, process and compiled the CAPPI file of the weather radar data in the LINUX operating system.

3.4 RAINRATE AUTO V2 program

RAINRATE AUTO V2 program was developed to generate the gridded radar-based QPE from the CAPPI file. RAINRATE AUTO V2 is built in Linux environment using Shell Script program. It is a scripts collection of commands that are stored in a file. The shell can read this file and act on the commands as if they were typed

at the keyboard. The program compute the rainrate from the binary CAPPI file using the DB_RAINRATE2 calculator. This rainrate values will be corrected with radar rainfall adjustment factor and finally produce the radar-based QPE in the grid format.

4 METHODOLOGY

4.1 Basin model HEC-HMS

Basin model in HEC-HMS requires information on the basin characteristic. The total area for Upper Klang Ampang basin is 171km^2 derived from the DEM using ArcGIS 10.2.1. The basin was divided into 22 sub-basins based on flow path and the basin properties according to land use and soil type. Figure 4 shows the schematic diagram of basin model for the study area.

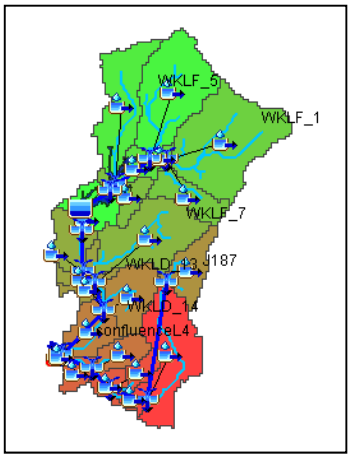

Figure 4. The schematic diagram of the basin model of the Upper Klang Ampang watershed.

Volume of runoff was estimated by loss model by calculating the losses for the given the rainfall and properties of the catchment. In this study, the Soil Conservation Service (SCS) Curve Number (CN) was used as a loss method to estimate the loss in the Upper Klang Ampang basin. The CN was determined from the value related to the land use and the hydrologic soil group data. For this study, the value of the CN was referred from the Guidelines for erosion and sediment Control in Malaysia (USAINS HOLDING SDN BHD, 2010). The HSGs consist of four types A, B, C, D. HSG type A is the highest infiltration rate, whereas, HSG type D is the and the lowest infiltration rate. The CN values range from 100 for water bodies and to approximately 30 for permeable soils with high rate of infiltration. The infiltration loss method or runoff is derived from a set of empirical equations define the process for rainfall change into infiltration and runoff;

$$P_e = (P - I_a)^2 / (P - I_a) + S \quad [1]$$

$$I_a = 0.2S \quad [2]$$

$$S = (25400 - 254CN) / CN \quad [3]$$

Substituting Eq. [2] into Eq. [1] gives

$$Pe = (P - 0.2S)^2 / (P + 0.8S) \quad [4]$$

where,

P_e= accumulated rainfall excess at time t;
P = accumulated rainfall depth at time t;
I_a = the initial abstraction (initial loss);
S = potential maximum retention

In HEC-HMS translation of excess rainfall to runoff on a basin is called the transform method. An empirical equation using unit hydrograph is commonly used in the transform method. In this study, SCS Unit Hydrograph (SCS UH) was used to generate the unit hydrograph. SCS UH model is a dimensionless, single-peak UH for event based rainfall analysis. SCS UH is based on the converting time and flow axis to dimensionless hydrograph for single-peak UH for event-based rainfall analysis. The basin lag time was estimated and calibrated during calibration process. The UH peak discharge and time of UH are related based on following equations.

$$Up = C (A / T_p) \quad [5]$$

$$Tp = (\Delta t / 2) + t_{lag} \quad [6]$$

where,

U_p = UH peak discharge
T_p = Time of UH peak
C = Conversion constant (2.08)
A = Area of watershed
Δt = the excess precipitation duration
T_{lag} = the basin lag

4.2 Meteorologic model

4.2.1 Rain gauge rainfall data

Rain gauge data represents a point rainfall data at specific location. Hence, it is not sufficient to represent the volume of the rainfall over a basin. Network of the gauge station could provide a better representation of the volume of rainfall over a basin. From the network of the rain gauges, mean areal precipitation for the basin could be establish. Nine rain gauges were used in this study for meteorologic model in HEC-HMS. Table 2 gives the geographical coordinate of nine rain gauge stations located in the study area. Gage weight was selected as precipitation input type for meteorologic model for Upper Klang Ampang River basin.

Table 2. Rain gauge station used in the study

No	Station Name	Station ID	Latitude	Longitude
1	Seleh	3217110	3.248	101.768
2	Klang Gate	3217111	3.235	101.75
3	Kg Melayu	3117113	3.153	101.761
4	L4	3117115	3.166	101.743
5	AU3	3117114	3.18	101.757
6	AU5	3217113	3.202	101.759
7	Bkt Belacan	3117111	3.143	101.787
8	IBMBS Kemensah	3217112	3.216	101.79
9	The Peak	3117110	3.178	101.783

4.2.2 Radar rainfall data

Radar data was obtained from Malaysian Meteorology Department (MMD). The Doppler weather radar station is situated at Bukit Subang, Selangor with latitude 3 8.7'N, longitude 101 33.5'E. The distance of radar station to study area is 50 km. The Doppler weather radar with S band type was set up with 250Hz frequency and 10.64 cm wavelength and has a maximum horizontal coverage of 300 km. The Doppler weather radar measures the reflectivity of the raindrop but does not measure the rainfall directly. Therefore, a conversion of the reflectivity into rainfall using an empirical power equation, the radar reflectivity (Z) and the rainfall rate (R) or known as Z-R relationship. The Subang radar station is using Marshall-Palmer equation, $Z = 200R^{1.6}$, where Z is radar reflectivity (mm^6/m^3) and R is rainrate R (mm/hr) to calculate the rainrate. Radar data was collected from year 2014 to 2015 and the data were archived every 10 minutes. The radar data was using CAPPI product type and the product data type is R (13) means DB_RAINRATE product. This product data type gives the value of rainfall rate by using Z/R Marshall-Palmer Equation. This weather radar data can only be read in LINUX operating system and a utility program named Productx was used to utilize the radar data.

The quality of radar data was examined using the Productx program and the radar rainfall adjustment factor needs to be determined. The value of radar rainfall adjustment factor was determined by using equation 7. The radar rainfall adjustment factor is an average total gauge rainfall over radar rainfall at the gauge rainfall station. The point radar data were matched with the point gauge rainfall data at each gauge stations. RAINRATE AUTO V2 program calculated the value of rainrate in the study area and generated the output in the grid format.

$$\text{Radar rainfall AF} = \sum \text{Gauge rainfall} / \sum \text{Radar rainfall} \quad [7]$$

5 RESULT AND ANALYSIS

5.1 Radar rainfall adjustment factor (AF)

Analysis on the weather radar data was done for event on 27 April 2015. The correlation between the radar rainfall data and the rain gauge data were tested. Figure 6 shows there is a strong correlation between the radar

rainfall and the rain gauge data with R^2 is 0.7738. Thus, the radar rainfall is able to be used as QPE for the rainfall runoff model. The accuracy of the radar rainfall data was assessed by using the comparison of radar rainfall data with observation rainfall data by rain gauges. Radar rainfall data computed from IRIS program was compared with the point rainfall data from rain gauges in the study area. Nine rain gauge stations were involved in the calibration and validation to determine the radar rainfall adjustment factor (AF). Figure 7 shows the one hour rainfall data between radar rainfall and gauge rainfall data for event on 27 April 2015. It shows the radar rainfall has low values compared to gauge rainfall data. Radar rainfall adjustment factor was determined from the calculation using equation 7 and the value of the radar rainfall adjustment factor was 7.77. Then, the radar rainfall was calibrated by multiplying with this radar rainfall AF to improve the radar rainfall data value. The improved radar-based QPE is shown in figure 8.

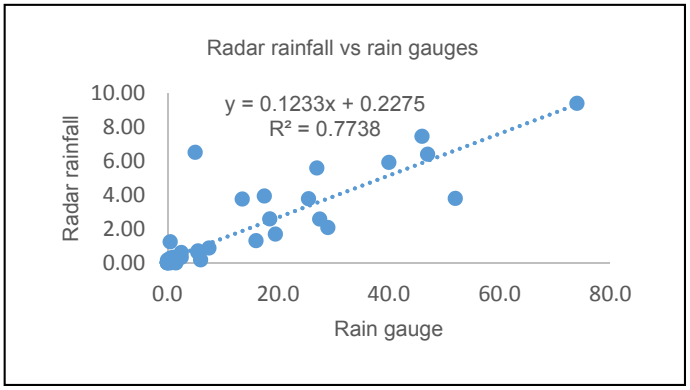

Figure 6. Correlation coefficient between radar rainfall and rain gauges rainfall data

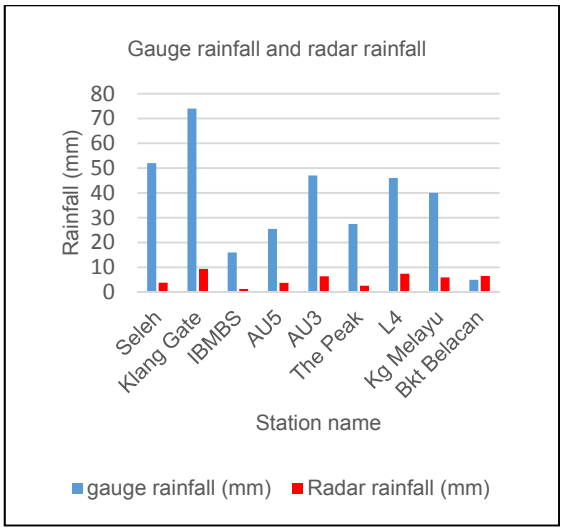

Figure 7: Comparison for gauge rainfall and radar rainfall for event 27 April 2007 at time 1500

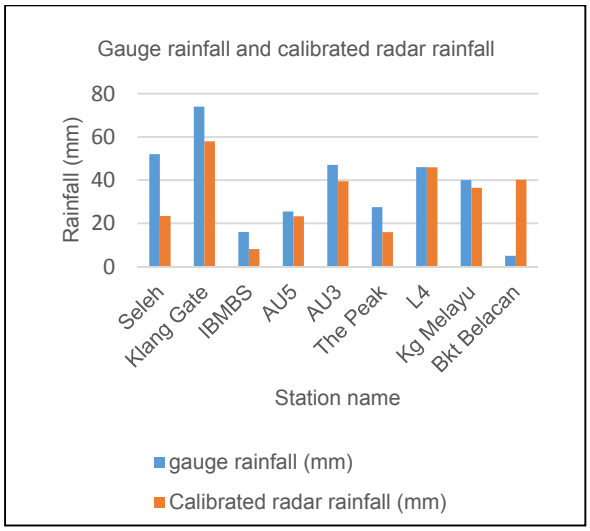

Figure 8: Comparison for gauge rainfall and calibrated radar rainfall after applying the radar adjustment factor for event 27 April 2007 at 1500.

5.2 Rainfall runoff model results using gauge rainfall data

The rainfall runoff model was calibrated and validated using the gauge rainfall data. Calibration was carried out for the event on 1 July 2014 and validation for the event on 16 April 2014 and the results are shown in the figure 9 and 10. Nash-Sutcliffe for calibration was 0.625 with RMS error 17.2 m^3/s, while Nash-Sutcliffe for validation was 0.580 with RMS error was 22.2 m^3/s.

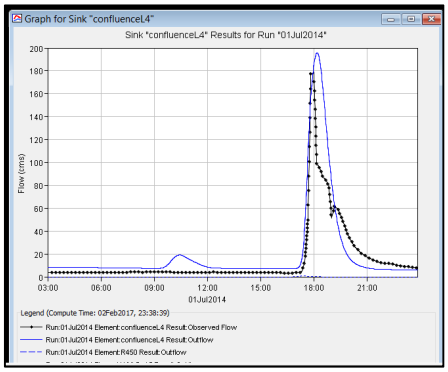

Figure 9: Simulation for calibration of the rainfall-runoff model using gauge rainfall data for event 1 July 2014.

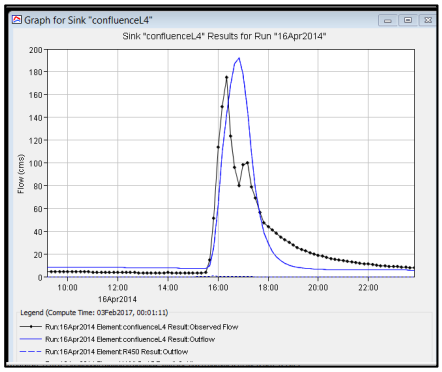

Figure 10: Simulation for validation of the rainfall-runoff model using gauge rainfall data for event 16 April 2014

5.3 Rainfall runoff model results using radar-based QPE

In order to test the radar-based QPE, one simulation using the radar-based QPE for the event on 27 April 2015 was done using the calibrated and validated rainfall-runoff model prepared beforehand. Figure 11 shows the hydrograph of the simulation peak of the radar-based QPE and the observed discharge value. The result shows that the peak discharge for radar based QPE is slightly lower than the observed discharge with acceptable Nash-Sutcliffe value, 0.655. Further refine analysis of the radar rainfall adjustment factor is needed to improve the result for the peak discharge in the rainfall-runoff model. However, it clearly shows that, there is an option to use radar-based QPE in the rainfall-runoff model.

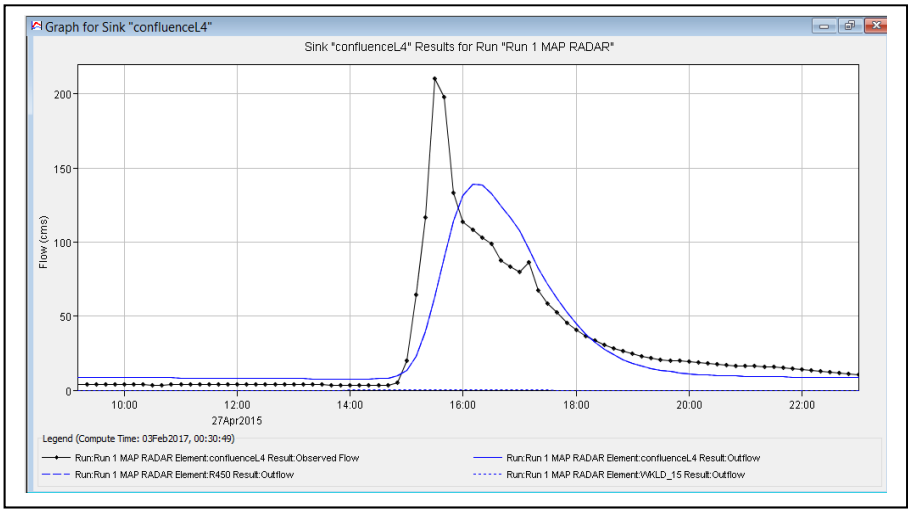

Figure 11: Simulation the rainfall-runoff model using radar-based QPE for event 27 April 2015.

6 CONCLUSIONS

This study investigates the availability of radar-based QPE as a precipitation input in the rainfall-runoff model. The rainfall-runoff model was successfully developed by using HEC-HMS software and was calibrated and validated using gauge rainfall data. The radar rainfall data was calibrated using radar rainfall adjustment factor to improve the quality of the radar-based QPE. The rainfall-runoff model was tested with the radar-based QPE to simulate the hydrograph. From the results of the rainfall runoff model for the gauge rainfall data and the radar-based QPE, it can be concluded that the radar-based QPE is available to be used as precipitation input in the rainfall runoff model to predict the peak discharge of the flood event. However, radar rainfall adjustment factor needs to improve and re-test to get better results of the peak discharge in the rainfall runoff model.

ACKNOWLEDGEMENTS

The authors gratefully acknowledge the help from Malaysian Meteorological Department and Department of Irrigation and Drainage in providing the data that was used in this study.

REFERENCES

Berne, A. & Krajewski, W. F. (2013). Radar for Hydrology: Unfulfilled Promise or Unrecognized Potential? *Advances in Water Resources*, 51, 357–366.

Feldman, A. D. (2000). *Hydrologic Modeling System HEC-HMS Technical Reference Manual*, US Army Corps. of Engineers Hydrologic Engineering Center. (March), 155 pp.

Kabiri, R., Chan, A. & Bai, R. (2013). Comparison of SCS and Green-Ampt Methods in Surface Runoff-Flooding Simulation for Klang Watershed in Malaysia. *Open Journal of Modern Hydrology*, *3*(3), 102–114.

Marshall, J. S. & Palmer, W. M. (1950). The Size Distribution of Raindrops. *Quarterly Journal of the Royal Meteorological Society*, *76*(327), 16–36.

Nagata, K. (2011). *Quantitative Precipitation Estimation and Quantitative Precipitation Forecasting,* The Japan Meteorological Agency.

Pedersen, L., Jensen, N. E. & Madsen, H. (2010). Calibration of Local Area Weather Radar-Identifying Significant Factors Affecting the Calibration. *Atmospheric Research*, 97(1–2), 129–143.

Smith, J. A., Baeck, M. L., Meierdiercks, K. L., Miller, A. J. & Krajewski, W. F. (2007). Radar Rainfall Estimation for Flash Flood Forecasting in Small Urban Watersheds. *Advances in Water Resources*, 30(10), 2087–2097.

Sun, X., Mein, R. G., Keenan, T. D. & Elliott, J. F. (2000). Flood Estimation Using Radar and Raingauge Data. *Journal of Hydrology*, 239(1–4), 4–18.

USACE-HEC. (2000). Hydrologic Modeling System HEC-HMS Technical Reference Manual, US Army Corps. of Engineers Hydrologic Engineering Center (March).

USAINS HOLDING SDN BHD. (2010). *Guideline for Erosion and Sediment Control in Malaysia*. Department of Irrigation And Drainage.

Vanaja, S. J., Mudgal, B. V, & Thampi, S. B. (2013). *Rainfall-Runoff Modeling Using Doppler Weather Radar Data*, Center for Water Resources Anna University Chennai.

Versini, P. A. (2012). Use of Radar Rainfall Estimates and Forecasts to Prevent Flash Flood in Real Time by Using a Road Inundation Warning System. *Journal of Hydrology*, 416–417, 157–170.

Ward, R. C. & Robinson, M. (2000). *Principle of Hydrology*. (E. Robinson, Ed.) (Fourth Esi). Alfred Waller.

Wardah, T., Abu Bakar, S. H., Bardossy, A. & Maznorizan, M. (2008). Use of Geostationary Meteorological Satellite Images in Convective Rain Estimation for Flash-Flood Forecasting. *Journal of Hydrology*, 356(3–4), 283–298.

Wüest, M., Frei, C., Altenhoff, A., Hagen, M., Litschi, M. & Schär, C. (2010). A Gridded Hourly Precipitation Dataset For Switzerland Using Rain-Gauge Analysis and Radar-Based Disaggregation. *International Journal of Climatology*, 30(12), 1764–1775.

Proceedings of the 37th IAHR World Congress
August 13 – 18, 2017, Kuala Lumpur, Malaysia

VARIABILITY OF RAINFALL DURING THE PAST CENTURY AT YOM RIVER BASIN

RUETAITIP MAMA[1], BUTSAWAN BIBORN[2], KWAN SUE JUNG[3], MATHARIT NAMSAI[4] & METHAT YUENPRAPHAN [5]

[1,3] Chungnam National University, Deajeon, Korea,
bluewater_june@hotmail.com; butsawan.p@chula.ac.th
[2] Chulalongkorn University, Bangkok, Thailand,
ksjung@cnu.ac.kr
[4,5] Royal Irrigation Department, Bangkok,Thailand,
matharit_mns@hotmail.com; methatjaipinta@gmail.com

ABSTRACT

Climate change is a global issue and is one of the major concerns in water resources planning and management during the past decades. Changing rainfall pattern can directly affect an occurrence of an extreme event on floods and droughts, which will cause future conflicts especially on water supply and flood management. The purpose of this study is to examine the variability of rainfall in the Yom River basin, Thailand, over the past 90 years (1921–2015). This study evaluates long-term trends in rainfall and various rainfall-related extreme events, which consist of the annual precipitation (PRCTPOP), consecutive dry days (CDD), consecutive wet days (CWD), number of heavy rainfall days (R_{10}), number of very heavy rainfall days (R_{20}), daily maximum rainfall (R_{max1}), five-day maximum rainfall (R_{max5}), and annual total rainy day (R_{day}) in the Yom River basin, Thailand. Rainfall dataset from 13 hydrological stations across the basin are analyzed using the Mann-Kendall method at 95 percent confident level. Analyses of these data showed that the average annual rainfall of the whole basin varies between 1,018 and 1,179 mm with the minimum and maximum annual rainfall of 480 and 4,047 mm/y, respectively. The results from this study reveals that an increasing trend are dominating in 3 indices as Rmax1, CWD and Rday, while the decreasing trend are dominating in the remaining in 5 indices as PRCPTOT, Rmax5, CDD, R10, and R20 during the past century. Results of this study indicate that the Yom River basin is highly vulnerable to droughts and floods driven by the variability in rainfall. The impacts of changes in rainfall pattern in the Yom River basin should be considered in the future water resources planning and management of the country.

Keywords: Long-term rainfall trend; rainfall indices; Mann-Kendall test; extreme rainfall events; climate change.

1 INTRODUCTION

Precipitation is one of the most important parameters in the design and planning of water resources management (Adamowski and Bougadis, 2003). Rainfall is the key factor in rainfall-runoff relationship, which is a crucial component in flood/drought assessment (Chattopadhyay and Edwards, 2016). Changes in daily rainfall pattern have been reported in many areas such as the Mediterarnean region (Philandras et al., 2011), United States (Karl and Knight, 1998; Pagán et al., 2016), Canada (Aziz and Burn, 2006), Pakistan (Ahmad et al., 2015), Australia (Barua et al., 2013). Furthermore, it was also suggested that extreme precipitation events have been increasing in intensity and frequency. For example, the elevated frequencies of extreme precipitation events were found in the central, western, and northern United States possibly resulting in hydrological flood events in some areas of the United States (Kunkel and Andsager,1999; Kunkel et al., 2003). In contrast, the dry areas become drier and the wet areas become wetter in some regions of the world (Beule et al., 2016). In the Maghreb countries (Algeria, Morocco and Tunisia) located in northern Africa, for instance, have significant decrease trends of total precipitation and wet days, whereas the duration of dry periods of the region tends to increase (Tramblay et al., 2013; Di Baldassarre et al., 2010).

For Thailand, rainfall pattern trend was conducted by several studies. Based on analyses long-term trends of rainfall indices over the Indochina Peninsula using Asian Precipitation-Highly-Resolved Observational Data Integration towards Evaluation of Water Resources (APHRODITE) data (1960-2007) with a spatial resolution of 0.5°×0.5°, Yazid and Humphries (2015) suggested that Thailand's annual rainfall pattern over the past five decades is mainly dominated by non-significant negative trend, and the country experienced a negative trend in number of dry days (CDD), and a positive trend in the number of wet days (CWD). Meanwhile, Beule et al. (2016) found an increasing trend in CDD and a decreasing trend of CWD the rainfall data from 48 stations across the country during the period 1964-2012. With different dataset and number of rainfall stations, it possibly resulted a different trend in a regional and national scale of existing studies. Therefore, analyses of long-term rainfall trend in local scale may be needed for better understanding of changes in hydrological processes which plays a major role for effective water supply and demand

management.

The objective of this study is to analyze long-term trends of daily rainfall indices over the Yom River basin where floods and droughts occur in common using rainfall data observed at 13 hydrological stations during the period 1921-2015. The non-parametric statistical method, Mann-Kendall test, was used to determine the long-term trend in 8 rainfall indices recommended by Expect Term on Climate Change Detection and Indices (ETCCDI). The selected indices, which provide information on the wetness and dryness, consist of thenumber of heavy rainfall days, (R_{10}≥10 mm), number of very heavy rainfall days, (R_{20}≥20 mm), consecutive wet days (CWD ≥1 mm), daily maximum rainfall (R_{x1}), five-day maximum rainfall (R_{x5}), annualrainy day total ($R_{rainyday}$), consecutive dry days, (CDD <1 mm).The results of this study will contribute information on trend and variability of rainfall extremes that are useful for an effective water resources planning and management in the Yom River basin.

2 STUDY AREA AND DATA SET

2.1 Study area

The Yom River basin originates in the northern part of Thailand. The basin is situated roughly between 14° 50’ and 18° 25’ northern latitudes, and 99° 16’ - 100° 40’ eastern (Apichichat, 2014). The Yom River basin is a part of the Great Chao Phraya River Basin, which is the largest drainage basin in Thailand located at the heart of the country. The drainage area of the Yom River basin is approximately 24,074 km^2 (Figure 1). The elevation of the basin broadly ranges between 20 and 360 m above mean sea level (MSL) (Phetchprayoon et al., 2010). The main channel of the river is 735 km in length with the river gradient varying from 1:700 to 1:35,000 (Bidorn et al., 2015). The river flows from north to south through eleven provinces before merge into the Nan River forming the Chao Phraya River at Nakhon Sawan Province (RID, 2004).

The Yom River basin can be divided into two districts terrain systems: the upper and lower Yom River basins. The upper Yom River sub-basin is characterized by a mountainous feature with the elevation varying between 280 and 360 m MSL. About 51 percent of upper Yom River sup-basin is a forest area, and the remaining consists of agricultural and urban areas (Phetchprayoon et al., 2010). The lower Yom River basin is defined by floodplain with the geographic relief ranging from 20 to 180 m MSL. Approximately 74 percent of the lower Yom River basin is occupied by farming and residential areas, while the rest of the basin (26 percent) is a forest area (Geo-Informatics and Space Technology Development Agency (GISTDA), 2005). The climate of the Yom River basin is under the influence of the southwest and northeast monsoons. The mean annual rainfall is about 1,250 mm (Bidorn et al., 2015) with the minimum and maximum of 800 and 1,600 mm, respectively. Almost 90 percent of the annual rainfall occurs during rainy season (May to October) caused by the southwest monsoon. The mean annual discharge of the basin widely varies from 200 to 2,000 m^3/s (Sriariyawat et al., 2013).

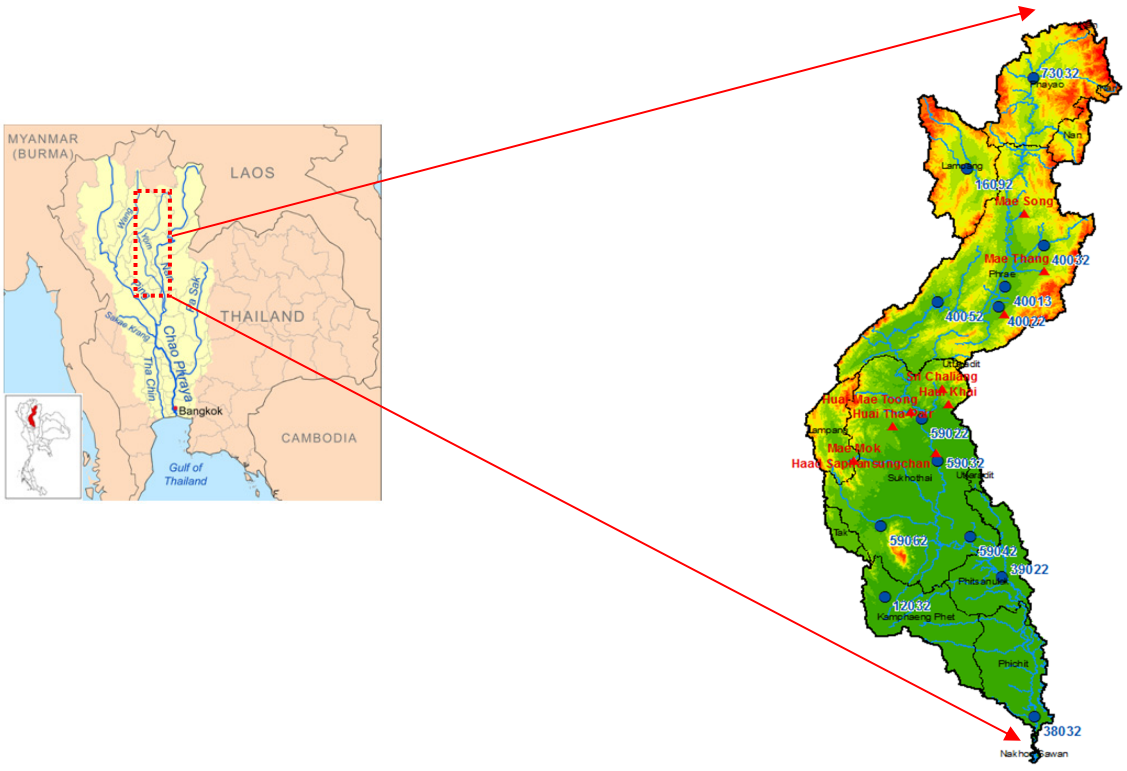

Figure1. Location map of the Yom River basin and the location of hydrological stations.

2.2 Rainfall data and quality control

In this study, daily rainfall data from 13 hydrological stations across the Yom River basin during the period 1921-2015 were collected from the Royal Irrigation Department (RID) and Thai Meteorology Department (TMD). The location of the stations is depicted in Figure 2, and the basic information of the rainfall data from each station is summarized in Table 1. Of the 13 hydrological stations, 6 stations situated in the upper Yom River basin (73032, 16092, and 40032 station are located in the mountainous areas and 40052, 40013, and 40022 stations are in the agricultural areas). It was found that the rate of missing data at these stations ranged between 5 and 12 percent. Meanwhile, the rainfall datasets from the remaining stations located in the lower Yom River basin (59032, 59042, 12032, 38032, and 39022 station are located in the mountainous areas and 59062 and 59022 stations are in the agricultural areas) have missing data rate of 17-45 percent. Because rainfall record length of those 13 stations are more than 25 years, these rainfall datasets are statistically valid for analyzing the trend. However, if more than 5 percent of data during the rainy season (May-September) for a year is found, that year is discarded from the trend analysis.

Table1. Detail of rainfall stations.

Name	Upper Yom						Lower Yom						
	73032	16092	40022	40013	40032	40052	12032	38032	59022	59032	59042	59062	39022
Latitude (E)	19° 8' 31.1"	18° 42' 25.2"	18° 2' 56.3"	18° 8' 45.6"	18° 20' 20.3"	18° 4' 26.4"	16° 39' 46.8"	16° 5' 27.6"	17° 30' 54"	17° 18' 54"	16° 57' 3.6"	17° 0' 14.4"	16° 45' 21.6"
Longtitude (N)	100° 16' 40.8"	99° 58' 19.1"	100° 6' 53.9"	100° 15' 57"	100° 19' 11.9"	99° 50' 9.5"	99° 35' 31.2"	100° 15' 54"	99° 45' 50.3"	99° 50' 9.5"	99° 58' 44.3"	99° 34' 37.1"	100° 7' 19.2"
Open Year - 2015	1952	1921	1921	1921	1921	1921	1921	1923	1921	1921	1922	1922	1921
Missing Year	3	5	16	7	9	9	19	41	26	18	17	35	16
Period Year	60	89	78	87	85	85	75	51	68	76	76	58	78
% of missing data	5	5	17	7	10	10	20	45	28	19	18	38	17
average rainfall (mm.)	1154	1100	1075	1151	1229	1115	1221	1018	1112	1116	1242	1054	1088
max (mm.)	1622	1823	1695	1746	2443	2021	3695	1730	1798	3039	2551	1626	4048
min (mm.)	650	655	615	728	613	481	615	570	603	604	804	575	621

3 METHODS

3.1 Extreme rainfall indices

To investigate long–term patterns in annual rainfall and extreme rainfall events in the Yom River basin, the rainfall data series observed during the past nine decades were used. The original of rainfall event analysis was adapted from World Meteorological Organization, (WMO, 2009) and established by several indices that has been widely used to determine trends including frequency and intensity of extreme weather events. In this study, 8 rainfall indices that represent frequency and intensity of rainfall pattern and rainfall extremes were selected as detailed in Table 2. Frequency indices compose of CDD, CWD, R_{10}, R_{20}, and R_{day} whereas PRCPTOT, R_{max1}, R_{max5} are intensity indices. Trends of these eight rainfall indices were analyzed to assess the climate dynamic occurred in the Yom River basin.

Table2. Definition of rainfall indices.

Name	Indices	Difinition	Unit
annual precipitation total	PRCPTOT	The annual precipitation total	mm
Consecutive dry days	CDD	The Maximum length of consecutive dry days with R < 1 mm	Days
Consecutive wet days	CWD	The Maximum legth of consecutive wet days with R $\geq$ 1 mm	Days
Daily maximum rainfall	R_{max1}	The daily annual maximum rainfall	mm
5-day maximum rainfall	R_{max5}	The 5-day annual maximum rainfall	mm
Number of heavy rainfall days	R_{10}	The annual count of days when days rainfall $\geq$ 10 mm	Days
Number of very heavy rainfall days	R_{20}	The annual count of days when days rainfall $\geq$ 20 mm	Days
Annual rainy day total	R_{day}	The annual total rainfall in wet day (R > 1 mm)	Days

*** R = Daily rainfall**

3.2 Trend Analysis

Many different techniques have been proposed for statistical analyzing trend of time series data. Those techniques can be categorized as parametric and non-parametric methods. Parametric method is normally used to detect trends in data with independent and normal distribution (Gocic and Trajkovic, 2013). For non-parametric method, it can be used to identify trend in independent data with skewness. The Mann-Kendall (MK) test is one of the most effective non-parametric method to test for randomness against trend in hydrologic and climatic time series (Partal and Kahya, 2006; Gajbhiye et al., 2016), and the MK test is low sensitive to missing data (Yazid and Humphries, 2015). Onaz and Bayazit (2003) suggested that the parametric method, t-test, has less accuracy than non- parametric test for detecting trend in data with skewness. During the last decade, the Mann-Kendall test has been widely used in trend analyses in many studies (Chattopadhyay and Edwards, 2016; Salami et al., 2014; Antonnia and Paolo, 2009).

The Mann-Kendall test is based on statistics (S) for a time series of the length. The S is defined as Eq. [1]:

$$s = \sum_{k=1}^{n-1} \sum_{j=k-1}^{n} \mathrm{sgn}(x_j - x_k) \quad [1]$$

where x_j and x_k are and the time series observations in chronological order, n is the length of time series, and sgn can be obtained from Eq. [2]:

$$\mathrm{sgn}(x_j - x_k) = \begin{cases} 1, \text{ if } x_j\text{-}x_k > 0 \\ 0, \text{ if } x_j\text{-}x_k = 0 \\ -1, \text{ if } x_j\text{-}x_k < 0 \end{cases} \quad [2]$$

The standardized Mann-Kendall test statistics (Z), which is used to evaluate the statistical significant of trend, is calculated using Eq. [3]:

$$Z = \begin{cases} \dfrac{s - 1}{\sqrt{v(s)}}, \text{ if } s > 0 \\ 0, \text{ if } s = 0 \\ \dfrac{s + 1}{\sqrt{v(s)}}, \text{ if } s < 0 \end{cases} \quad [3]$$

where v(s) is variance of S calculated from Eq. [4]:

$$v(s) = \left[\frac{n(n - 1)(2n - 5)}{18} \right] \quad [4]$$

A positive Z value indicates an increasing trend in the time series. Meanwhile, a negative Z value indicates that the time series have a decreasing trend. To test for upward or downward trends at αlevel of significance (ρ - value), the null hypothesis (H_0) is rejected when the absolute value of Z is greater than $Z_{1-\alpha/2}$ where $Z_{1-\alpha/2}$ and α are the standard normal deviates and significant level for the test, respectively. If the null hypothesis in invalid, the trend is significant meaning that the trend did not occur by chance. In this study, the 5 % significance level ($Z_{0.025}$=1.96) was used to.

In addition, Sen non-parametric test (Sen, 1968) is can be used to calculate the magnitude of trends in the time series data. The test proceeds by calculating the slope of a change in observation values to the change of the corresponding times. According to Sen's test, the overall estimator b_{se_n} is the median of the data slopes, and it can be calculated from Eq. [5]:

$$b_{se_n} = \text{Median} \left[\frac{X_i - X_j}{i - j} \right] \quad [5]$$

where X_i and X_j are data values at time i and j, respectively.

4. RESULT AND DISCUSSIONS

In this study, the significant and magnitude of trend in the selected rainfall indices were analyzed based on the long-and short-terms dataset of each hydrologic station. The long-term trend was calculated using rainfall time series more than 50 years to investigate the impact of climate change in the river basin. The short-term trend, which probably provide an information of current rainfall situations and frequency extreme events of the basin, was analyzed based on 15-years rainfall dataset (2000-2015). Results from trend analyses of the rainfall and rainfall-related extremes in the Yom River basin are discussed below.

4.1 Trend in rainfall

Long-term and short-term trends of annual rainfall (PRCPTOT) at 13 stations over the Yom River basin are listed in Table 3, and the variation of the annual rainfall of each station is plotted as shown in Figure 2. It appears that about 62% of the Yom River basin area, which mainly is located in the upper Yom River basin, had an insignificant decrease trend over the long-term period. About 18% of the basin area had an insignificant increase long-term trend. The significant increase trend in annual rainfall during the past 50 years

was found at two locations (Stations 16092 and 59062) situated at the western part of the upper and lower Yom River basins (Figure 1), and the trend is likely to continue. Results from short-term rainfall data analysis indicate that the annual rainfall of about 69% of the basin area was an insignificant decrease during the period 2000-2015 and the annual rainfall reduction occurred mainly in the upper Yom River basin. However only 17% of the basin area (mainly located in the lower Yom River basin) had an increase in annual rainfall with an insignificant trend during the past 15 years. However, a significant reduction in annual rainfall between 2000 and 2015 was found at Station 40052 located at the mid of the Yom River basin covering approximately 8% of the basin.

Even through only a few stationsshow statistical significance in their long-term trends, Sen's slopes of those stationsvarid from 17.36 to – 84.36, meaning that the abruptly changes in annual rainfall occurred during the past decade have a higher degree than those occurred during the past century.

Table 3. The detail of PRCPTOT index.

station	73032	16092	40032	40013	40022	40052	59022	59032	59062	59042	12032	38032	39022
Long term data set during 1921 - 2015													
Trend nature	-	+	-	-	-	-	-	-	+	+	+	+	-
Trend signifcant	No	**Yes**	No	No	No	No	No	No	**Yes**	No	No	No	No
Sen's slope:	-1.06	2.50	-1.83	-1.14	-1.46	-0.63	-3.64	-1.69	5.87	0.68	3.49	2.62	0.35
Available years	61	87	86	88	79	86	68	76	60	78	76	54	79
Min (mm)	650	655	613	728	615	481	603	604	575	804	615	570	621
Max (mm)	1622	1823	2443	1746	1695	2021	1798	3039	1626	2551	3695	1730	4048
Short term data set during 2000 - 2015													
Trend nature	-	-	-	-	+	-	-	+	+	-	+	NA	-
Trend signifcant	No	No	No	No	No	**Yes**	No	No	No	No	No	No	No
Sen's slope:	-23.47	-15.44	-30.30	-9.86	25.30	-40.26	-84.06	17.36	22.26	-21.48	-5.33	55.84	-32.37
Available years	15	13	15	16	11	16	8	10	12	12	11	5	9
Min (mm)	650	827	774	814	661	664	713	672	575	806	795	681	745
Max (mm)	1511	1715	1672	1513	1469	1743	1600	1409	1601	1523	1754	1202	1489

*** + = Increasing Trend, - = Decreasing Trend**

4.2 Trend in extreme rainfall events

Trends in extreme rainfall indices were analyzed at each hydrological station to assess changes in frequency and intensity of rainfall-related extreme events. Results from extreme rainfall indices in the Yom River basin are discussed below.

4.2.1 Rainfall intensity

The daily annual maximum rainfall (R_{max1}) and the 5-daily annual maximum rainfall(R_{max5}) indices give an indication of the trends in rainfall amounts, which usually come from extreme weather events. Any significant changes in these indices may cause severe damages in the Yom River basin due to insufficient facilities dealing with water-related extreme events in this area. Results from trend analyses for R_{max1} and R_{max5} are shown in Tables 4 and 5, respectively. It appears that the R_{max1} in the study area varied from 63.1 to 96.0 mm/year for the long-term period and from 61.2 to 104.7 mm/year for the short-term period.The average of 5 daily annual maximum rainfall ranged from 112.9 to 175.0 mm/year and 113.7 to 185.2 mm/year during the long- and short-term periods respectively.

Based on trend significance values of R_{max1} in Table 4, it appears that a significant increasing trend in rainfall intensity or extreme events during the past century was found along the western part of the Yom River basin covering about 28% of the total basin area. Meanwhile, about 32% of the basin area located along the eastern part of the basin has an increasing rainfall intensity during the same period. During the past decade, it was found that approximately 86% of the basin area has experienced an insignificant decline of rainfall intensity due to extreme events.

The majority R_{max5} trend found in Table 5 is similar to trend of R_{max1}. However, the significance of either increase or decrease trends in rainfall intensity analyzed from R_{max5} covers less areas than from $R_{max1}$for the long-term period. Only 16% of the basin area has a significant decrease trend in rainfall intensity over the recent years.

4.2.2 Wet, dry and rainy days

The maximum consecutive dry days (CDD) and maximum consecutive wet days (CWD) indices describe the duration of dry and wet period, respectively. In general, the CDD and CWD always show an opposite trend. Results of trend test of CDD and CWD indices for the Yom River basin are presented in Tables 6 and 7, respectively.

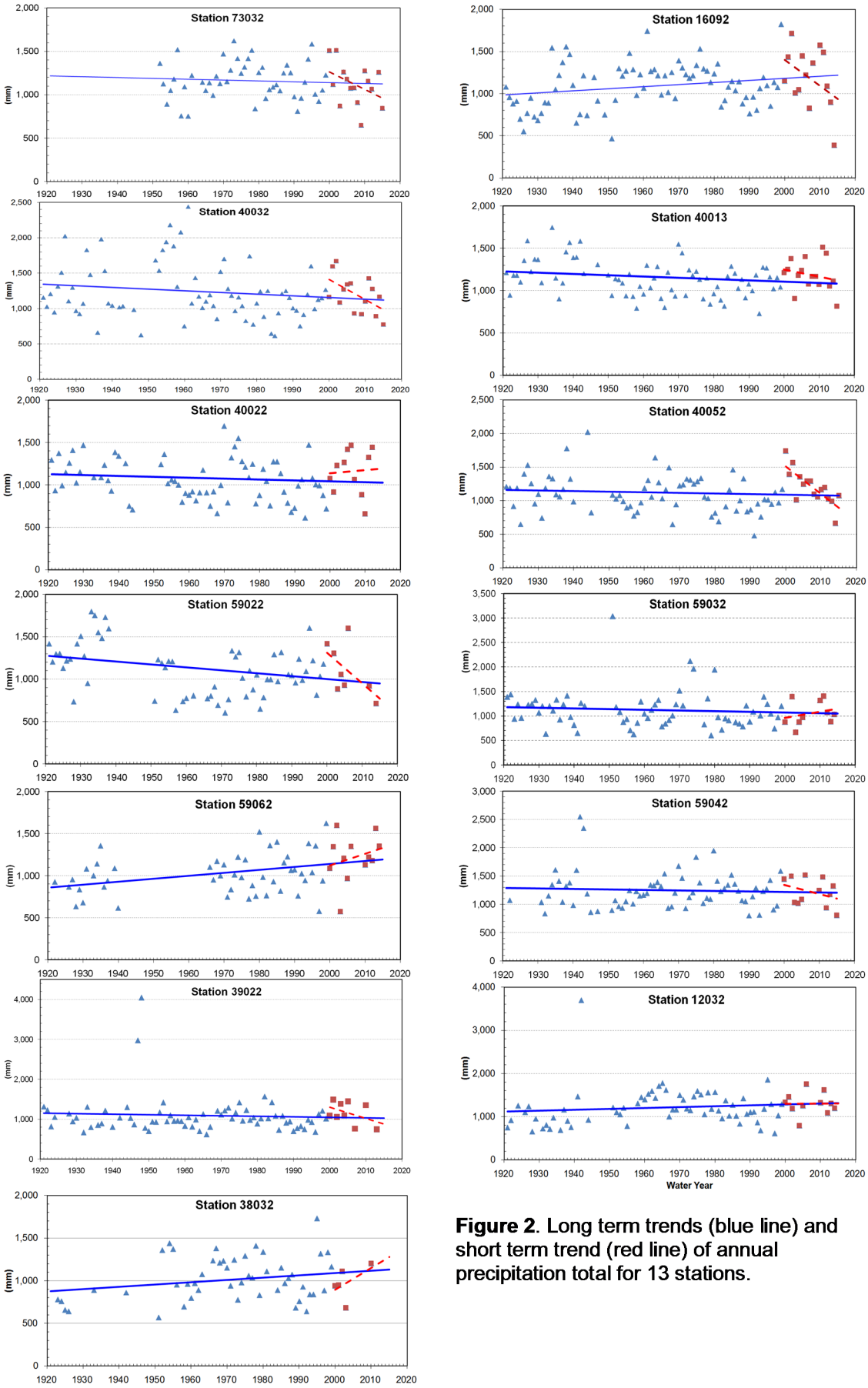

Figure 2. Long term trends (blue line) and short term trend (red line) of annual precipitation total for 13 stations.

Table 4. The detail of Rmax1 indices.

station	73032	16092	40032	40013	40022	40052	59022	59032	59062	59042	12032	38032	39022
Long term data set during 1921 - 2015													
Trend nature	-	+	-	+	-	+	-	-	+	+	+	+	+
Trend signifcant	**Yes**	**Yes**	No	No	No	**Yes**	**Yes**	**Yes**	**Yes**	No	No	No	No
Sen's slope:	-0.49	0.38	-0.26	0.03	-0.20	0.21	-0.32	-0.25	0.29	0.11	0.25	0.82	0.12
Available years	61	92	90	90	83	88	85	85	69	85	86	73	90
Min (mm)	42	34	36	37	19	35	8	14	30	10	14	6	20
Max (mm)	181	216	267	218	212	157	181	230	163	213	205	129	500
Short term data set during 2000 - 2015													
Trend nature	-	-	-	-	-	-	-	+	-	+	+	NA	-
Trend signifcant	No	**Yes**	No	**Yes**	No	No	No	No	No	No	No	No	**Yes**
Sen's slope:	-1.30	-6.45	-0.54	-3.01	-4.43	-1.53	-2.82	-0.35	-0.65	3.43	0.72	-1.87	-3.71
Available years	15	15	16	16	15	16	16	14	16	16	15	8	15
Min (mm)	43	45	37	49	19	37	8	14	33	10	25	49	20
Max (mm)	140	216	144	218	171	153	141	92	163	213	191	86	401

*** + = Increasing Trend, - = Decreasing Trend**

Table 5. The detail of Rmax5 indices.

station	73032	16092	40032	40013	40022	40052	59022	59032	59062	59042	12032	38032	39022
Long term data set during 1921 - 2015													
Trend nature	-	+	-	-	-	+	-	-	+	-	+	+	+
Trend signifcant	No	**Yes**	**Yes**	No	No	No	No	**Yes**	No	No	No	**Yes**	No
Sen's slope:	-0.40	0.80	-0.51	-0.16	-0.44	0.30	-0.37	-0.46	0.31	-0.03	0.45	0.96	0.15
Available years	62	92	90	90	83	88	83	85	69	85	86	73	89
Min (mm)	80	59	75	45	19	84	14	27	40	10	20	11	22
Max (mm)	336	347	518	253	394	281	355	833	269	303	562	281	770
Short term data set during 2000 - 2015													
Trend nature	-	-	-	-	-	-	-	+	-	-	-	NA	-
Trend signifcant	No	No	No	No	No	**Yes**	No	No	No	No	No	No	**Yes**
Sen's slope:	-2.61	-2.60	-2.98	-4.46	-5.93	-5.58	-6.30	0.10	-1.98	-1.94	-0.49	-8.77	-5.69
Available years	15	15	16	16	15	16	15	14	16	16	15	8	15
Min (mm)	80	70	75	76	19	96	14	27	77	10	38	52	22
Max (mm)	256	347	260	252	262	240	355	185	269	300	562	155	408

*** + = Increasing Trend, - = Decreasing Trend**

Regarding the Table 6, the decreasing trend in dry duration was found in 56% of total basin scattered across the Yom River basin over the period 1921-2015. However, only 13% of the basin area has a statistically significant reduction of dry period. However, during the past 15 years, the insignificant increase of dry duration was found in the Yom River basin up to 70% of the total area, and about 20% of the basin has a significantly increase trend in dry period.

For the wet duration, Table 7 shows that the increasing trend in wet duration was found in 77% of the basin area over the past century, whereas the decrease trend in wet period was mainly found in the lower Yom River basin. However, the change in wet duration over the long-term period is not statistical significant. During the past decade, insignificant decline trend in wet duration was found in most of the whole basin. However, only 15% of the total area located in the upper Yom River basin has a significant reduction in wet duration.

The number of total annual rainy day (R_{day}, rainfall > 1 mm) indices provide information of the wetness of the area. Results of trend analysis on R_{day} is summarized in Table 8. The results indicate that the whole area of the upper Yom river basin has an increasing trend of annual rainy days during the period 1921-2015, but only 4% of the area has a statistically significant increase trend. In the lower Yom River basin, the annual rainy days is statistically significant reducing in 44% of the lower Yom River basin area over the last century.However, most of the whole area of the Yom River basin has experiencing the reduction of rainy day during the period 2000-2015 with a statistical significant decrease trend found at the mid of the basin.

Table 6. The detail of CDD indices.

station	73032	16092	40032	40013	40022	40052	59022	59032	59062	59042	12032	38032	39022
Long term data set during 1921 - 2015													
Trend nature	-	+	+	-	-	+	+	-	-	-	-	+	-
Trend signifcant	No	No	No	**Yes**	No	No	**Yes**	No	**Yes**	No	No	No	No
Sen's slope:	-0.21	0.28	0.00	-0.26	-0.26	0.11	0.51	-0.08	-0.75	-0.08	-0.04	0.07	-0.15
Available years	61	92	88	90	80	88	83	84	69	91	85	64	88
Min (mm)	30	48	37	36	40	49	38	48	47	35	26	55	32
Max (mm)	197	212	212	168	218	214	267	191	190	184	181	236	247
Short term data set during 2000 - 2015													
Trend nature	+	+	+	-	+	-	+	-	+	+	-	NA	+
Trend signifcant	No	**Yes**	No	No	No	No	No	No	No	No	No	No	**Yes**
Sen's slope:	3.40	8.00	1.58	0.16	1.00	-0.08	2.23	-2.80	0.81	0.50	-3.00	22.60	7.46
Available years	15	15	16	16	12	16	14	13	16	15	15	6	12
Min (mm)	38	67	37	38	48	61	54	48	50	41	49	68	63
Max (mm)	164	212	159	111	218	180	267	184	190	171	181	222	215

*** + = Increasing Trend, - = Decreasing Trend**

Table 7. The detail of CWD indices.

station	73032	16092	40032	40013	40022	40052	59022	59032	59062	59042	12032	38032	39022
Long term data set during 1921 - 2015													
Trend nature	+	+	+	-	+	-	+	-	+	+	+	-	+
Trend signifcant	No	No	No	No	No	No	No	No	No	No	No	No	No
Sen's slope:	0.00	0.00	0.00	0.00	0.00	0.00	0.00	0.00	0.00	0.00	0.02	0.00	0.02
Available years	63	92	90	90	80	88	82	84	69	91	89	72	88
Min (mm)	1	2	3	4	3	3	2	3	2	2	1	2	2
Max (mm)	15	16	23	14	16	28	22	16	15	22	21	19	21
Short term data set during 2000 - 2015													
Trend nature	-	-	-	-	-	-	-	-	+	-	-	NA	-
Trend signifcant	No	**Yes**	No	No	**Yes**	No	No	No	No	No	No	No	No
Sen's slope:	-0.07	-0.30	-0.05	-0.08	-0.63	0.00	-0.25	0.00	0.00	-0.20	-0.27	-0.23	-0.12
Available years	15	15	16	16	13	16	13	13	16	15	13	8	12
Min (mm)	3	3	5	4	4	3	3	3	3	3	1	3	3
Max (mm)	13	12	17	11	13	11	12	7	9	9	10	11	10

*** + = Increasing Trend, - = Decreasing Trend**

Table 8. The detail of R_{day} indices.

station	73032	16092	40032	40013	40022	40052	59022	59032	59062	59042	12032	38032	39022
Long term data set during 1921 - 2015													
Trend nature	+	+	+	+	+	+	-	-	+	-	+	-	+
Trend signifcant	No	No	No	**Yes**	No	No	**Yes**	No	No	**Yes**	No	**Yes**	**Yes**
Sen's slope:	0.37	0.17	0.08	0.53	0.21	0.03	-0.20	-0.02	0.11	-0.22	0.02	-0.35	0.23
Available years	62	75	74	85	71	75	73	71	57	80	81	65	75
Min (mm)	28	32	39	37	31	37	18	18	15	19	21	19	22
Max (mm)	133	102	111	150	115	110	91	94	104	124	112	101	109
Short term data set during 2000 - 2015													
Trend nature	-	-	-	-	-	-	-	-	+	-	-	NA	-
Trend signifcant	No	No	No	No	**Yes**	No	No	No	No	No	No	No	No
Sen's slope:	-1.50	-1.11	-1.00	-0.91	-4.25	-2.06	-1.00	-2.93	0.33	-1.44	-1.05	-3.13	-3.13
Available years	15	10	12	14	9	13	12	9	14	14	12	5	12
Min (mm)	41	45	64	93	55	42	18	18	15	19	22	19	22
Max (mm)	133	92	106	136	97	86	80	78	92	92	84	71	96

*** + = Increasing Trend, - = Decreasing Trend**

4.2.3 Heavy and extreme rainfall days

The number of heavy rainfall day (R_{10}, Rainfall>10 mm) and the number of very heavy rainfall days (R_{20}, Rainfall>20 mm) is define by the number of maximum consecutive day that rainfall greater than 10 mm/day and rainfall greater than 20 mm/day during a year. The spatial trends of the R_{10} and R_{20} indicesare presented in Tables 9 and 10 respectively. The results in Table 9 indicate that about 62% of the basin mainly located in the upper Yom River basin has a decreasing trend in number of the days with heavy rainfall, and the extreme events are found to decrease significantly in 17% of the whole basin area over the period 1921-2015. Meanwhile, the rainfall extreme events seem to insignificantly increase in the lower Yom River basin during the same period. From 2000 to 2015, the rainfall extreme events decreased insignificantly for the whole river basin.

Based on trend analysis of the R_{20} in Table 10, the occurrence of rainfall extreme events seems to decrease over the upper Yom River basin during the past century. However, the rainfall extremes increase significantly at the southmost part of the lower Yom River basin during the same period. Similar to the trends in R_{10}, more than 90% of the basin area has a reduction in rainfall extreme events, especially in the lower Yom river basin over the past 15 years.

Table 9. The detail of R_{10}indices.

station	73032	16092	40032	40013	40022	40052	59022	59032	59062	59042	12032	38032	39022
Long term data set during 1921 - 2015													
Trend nature	-	+	-	-	-	-	-	-	+	+	+	+	-
Trend signifcant	No	No	No	**Yes**	No	No	**Yes**	No	No	No	No	No	No
Sen's slope:	-0.06	0.02	-0.05	-0.06	-0.06	-0.03	-0.14	-0.07	0.12	0	0	0	-0.03
Available years	62	92	81	89	90	88	84	69	81	84	84	69	87
Min (mm)	11	8	8	16	10	9	8	7	8	6	7	9	9
Max (mm)	52	75	66	54	68	85	69	72	51	56	62	56	81
Short term data set during 2000 - 2015													
Trend nature	-	-	-	-	-	-	-	-	-	-	-	NA	-
Trend signifcant	No	No	No	No	No	No	**Yes**	No	No	No	No	No	No
Sen's slope:	-0.50	-0.33	-0.71	-0.05	-0.61	-0.50	-1.86	-0.27	-0.54	-0.92	-0.50	-3.53	-1.73
Available years	15	15	13	16	16	16	14	8	14	13	15	16	12
Min (mm)	25	15	8	25	22	31	8	9	8	6	7	10	12
Max (mm)	47	50	46	50	54	63	52	40	42	44	48	56	54

*** + = Increasing Trend, - = Decreasing Trend**

Table 10. The detail of R_{20}indices.

station	73032	16092	40032	40013	40022	40052	59022	59032	59062	59042	12032	38032	39022
Long term data set during 1921 - 2015													
Trend nature	-	+	-	-	-	-	-	-	+	-	+	+	-
Trend signifcant	No	No	**Yes**	**Yes**	No	No	**Yes**	**Yes**	No	No	**Yes**	**Yes**	No
Sen's slope:	-0.02	0.04	-0.10	-0.04	-0.03	-0.05	-0.10	-0.06	0.06	0.00	0.08	0.17	0.00
Available years	62	92	81	90	90	88	84	67	80	84	84	69	88
Min (mm)	5	4	3	3	7	6	1	2	2	2	2	2	2
Max (mm)	29	43	35	31	44	40	44	36	35	36	50	33	46
Short term data set during 2000 - 2015													
Trend nature	-	+	-	+	+	-	-	-	-	-	-	NA	-
Trend signifcant	No	No	No	No	No	**Yes**	**Yes**	No	No	No	No	No	No
Sen's slope:	-0.40	0.64	-0.50	0.04	0.58	-0.88	-1.43	-0.75	-0.05	-0.40	-0.33	-1.75	-1.22
Available years	15	15	13	16	16	16	14	8	14	13	15	16	12
Min (mm)	11	9	3	8	10	8	1	2	5	3	4	6	3
Max (mm)	25	43	31	27	31	31	33	24	26	24	29	31	26

*** + = Increasing Trend, - = Decreasing Trend**

5. CONCLUSIONS

This study was to determine long-term (1921-2015) and short-term (2000-2015) trends in rainfall indices for 13 rainfall stations covered the Yom River basin. The non-parametric statistics test,Mann-Kendall method, was applied to detect eight rainfall indices event, which are the annual precipitation (PRCTPOP), consecutive dry days (CDD), consecutive wet days (CWD), number of heavy rainfall days (R_{10}), number of very heavy rainfall days (R_{20}), daily maximum rainfall (R_{max1}), five-day maximum rainfall (R_{max5}), and annual total rainy day (R_{day}).

The PRCTPOP indicator shows that increasing trend of annual rainfall mainly occurred in the lower part of the Yom River basin. Meanwhile, decreasing trend of the annual rainfall was found in the upper part of the basin. The analyses of R_{max1} and R_{max5} indices reveal that approximately 28% of the total area of the Yom River basin located in the western part of the basin has a significant increasing trend in rainfall intensity or extreme events during the past century. Meanwhile, decrease of rainfall intensity or extreme events was found along the eastern part of the basin covering 32% of the Yom River watershed. The results also indicate that rainfall intensity due to extreme events is insignificantly decreasing in more than 80% of the total basin area during the past 15 years.

Based on the analyses of CDD, CWD, and R_{day} indices, which define duration of wet and dry periods, it appears that the dry duration of more than 55% of the Yom River basin is seemly decreasing over the period 1921-2015. However, during the past 15 years, about 70% of the river basin has experienced an insignificant increase of dry duration. The results also show that increasing trend in wet duration was found in 77% of the basin area during the past century except in the lower Yom River basin where the decrease trend in wet period was found. Nevertheless, wet duration of the whole basin is insignificantly decreasing during the past decades. Results of trend analysis on R_{day} indicate that the annual rainy days of the areas located in the upper Yom river basin has insignificantly increased during the period 1921-2015, but the significant decrease of annual rainy days was found in 44% of the lower Yom River basin area. It was also found that during the period 2000-2015 a statistical significant decrease trend was found only at the mid of the basin.

The results from the analyses of number of heavy rainfall (R_{10} and R_{20}) suggest that the occurrence of rainfall extreme events is likely decreasing over the upper Yom River basin during the past century. Meanwhile, the significantly increasing of rainfall extremes was found at the south most part of the lower Yom River basin. It also found that rainfall extreme events have decreased in more than 90% of the basin area, especially in the lower Yom river basin over the past 15 years.

Based on the results analyzed from the eight rainfall indices, it can be implied that a significantly increasing tendency of flooding was found along the western part of the Yom River basin where the effective drainage capacity is limited. Furthermore, the results also suggest that the occurrence of drought trends to increase in middle portion of the Yom river basin. The information from this study may be helpful for improving water resources planning including flood/drought management in the Yom River basin.

ACKNOWLEDGEMENTS

This research was supported by a grant (16AWMP-B079625-03) from Water Management Research Program funded by Ministry of Land, Infrastructure and Transport of Korean government.

REFERENCES

Antonia, L. & Paolo, V. (2009). Trend Analysis of Annual and Seasonal Rainfall Time Series in The Mediterranean Area. *International journal of Climatology*, 30(10), 1538-1546.

Ahmad, I., Tang, D., Wang, T., Wang, M. & Wagan, B. (2015). Precipitation Trends over Time using Mann-Kendall and Spearman's Rho Tests in Swat River Basin, Pakistan. *Advances in Meteorology,* 2015(2015), 1-15.

Apichitchat, S. (2014). Hydrological Simulation for Impact Assessment of Kaeng Sue Ten Dam in Thailand, *MSc Thesis*. Changnam National University.

Aziz, O.I.A. & Burn, D.H. (2006). Trends and Variability in the Hydrological Regime of the Mackenzie River Basin. *Journal of hydrology,* 319, 282-294.

Barua, S., Muttil, N., Ng, A.W.M. & Perera, B. (2013). Rainfall Trend and its Implications for Water Resource Management within the Yarra River catchment, Australia. *Hydrological Processes,* 27, 1727-1738.

Beule, L., Lanhenke, J.K. & Tantanee, M. (2016). Trends in Precipitation in Thailand from 1964 to 2012. *Asia - Pasicfic Journal of Science and Technology*, 21(4), 11-15.

Bidorn, B., Chanyotha, S., Kish, S.A., Donoghue, J.F., Bidorn, K. & Mama, R. (2015). The Effect of Thailand's Great Flood of 2001 on River Sediment Discharge in The Upper Chao Phraya River Basin, Thailand. *International Journal of Sediment Research*, 30(4), 328-337.

Di Baldassarre, G., Montanari, A., Lins, H., Koutsoyiannis, D., Brandimarte, L. & Blöschl, G. (2010). Flood Fatalities in Africa: from Diagnosis to Mitigation. *Geophysical Research Letters*, 37(22), 1-5.

Gajbhiye, S., Meshram, C., Singh, S.K., Srivastava, P.K. & Islam, T. (2016). Precipitation Trend Analysis of Sindh River Basin, India, from 102-Year Record (1901–2002). *Atmospheric Science Letters*, 17(1), 71-77.

Gocic, M. & Trajkovic, S. (2013). Analysis of Changes in Meteorological Variables using Mann-Kendall and Sen's Slope Estimator Statistical Tests in Serbia. *Global and Planetary Change,* 100*,* 172-182.

Karl, T.R. & Knight, R.W. (1998). Secular Trends of Precipitation Amount, Frequency, and Intensity in the United States. *Bulletin of the American Meteorological society*, 79(2), 231-241.

Kunkel, K.E., Easterling, D.R., Redmond, K. & Hubbard, K. (2003). Temporal Variations of Extreme Precipitation Events in the United States: 1895–2000. *Geophysical research letters*, 30(17), 5-4.

Pagán, B.R., Ashfaq, M., Rastogi, D., Kendall, D.R., Kao, S., Naz, B.S., Mei, R. & Pal, J.S. (2016). Extreme Hydrological Changes in the Southwestern US Drive Reductions in Water Supply to Southern California by Mid Century. *Environmental Research Letters,* 11(9)*,* 1-12.

Partal, T. & Kahya, E. (2006). Trend Analysis in Turkish Precipitation Data. *Hydrological processes,* 20, 2011-2026.

Petchprayoon, P., Blanken, P.D., Ekkawatpanit, C. & Hussein, K. (2010). Hydrological Impacts of Land Use/Land Cover Change in a Large River Basin in Central–Northern Thailand. *International Journal of Climatology*, 30(13), 1917-1930.

Philandras, C.M., Nastos, P.T., Kapsomenakis, J., Douvis, K.C., Tselioudis, C.S. & Zerefos, C.S. (2011). Long Termprecipitation Trends and Variability within the Mediterranean Region. *Natural Hazards and Earth System Sciences*, 11(12), 3235.

Salami, A.W., Mohammed, A.A., Abdulmalik, Z. H. & Olanlokun, O.K. (2014). Trend Analysis of Hydro-Meteorological Variables using the Mann-Kendall Trend Test: Application to the Niger River and the Benue Sub-Basins in Nigeria. *International Journal of Technology,* 5(2), 100-110.

Sen, P.K. (1968). Estimates of the Regression Coefficient Based on Kendall's Tau. *Journal of the American Statistical Association,* 63(324), 1379–1389.

Sriariyawat, A., Pakoksung, K., Sayama, T., Tanaka, S. & Koontanakulvong, S. (2013). Approach to Estimate the Flood Damage in Sukhothai Province Using Flood Simulation. *Journal of Disaster Research,* 8(3), 406-414.

Tramblay, Y., Adlouni, S.E. & Servat, E. (2013). Trends and Variability in Extreme Precipitation Indices over Maghreb Countries. *Nature Hazards and Earth System Sciences*, 13(12), 3235-3248.

Yazid, M. & Humphries, U. (2015). Regional Observed Trends in Daily Rainfall Indices of Extremes Over Indochina Peninsula from 1960 to 2007. *Climate*, 3(1), 168-192.

Proceedings of the 37th IAHR World Congress
August 13 – 18, 2017, Kuala Lumpur, Malaysia

INTEGRATED ONE-DIMENSIONAL AND TWO-DIMENSIONAL FLOOD MODELLING FOR THE URBAN DRAINAGE STUDY ALONG JALAN SIBIYU, BINTULU SARAWAK

JUDY JOO KHENG KUEH [1] & SIN POH LIM[2]

[1,2] G&P Water & Maritime Sdn Bhd, Wisma G&P, 41-2, Jalan Tasik Selatan 3, Bandar Tasik Selatan, 57000 Kuala Lumpur, Malaysia
pisces.jk@gmail.com; limsinpoh@gmail.com

ABSTRACT

Flash flooding is the rapid flooding caused by the stormwater of intense rainfall associated with thunderstorms. Flash flooding in urban area has always been a nightmare as it can happen anytime and cause severe damage and sometimes can even lead to loss of lives. Flooding reveals the deficiencies in existing stormwater facilities and management practices. The development of effective design requires comprehensive understanding of flooding together with the stormwater infrastructure and system. Although one-dimensional (1-D) hydraulic modelling has been extensively used and proven to be useful for flood management but the capability is basically limited to water profiles and some hydraulic variables. For specific analyses such as overland flow in floodplains, determining direction and flood propagation rate, inundation extent, depths and duration requires a more sophisticated two-dimensional (2-D) modelling techniques. With the advent of geographic information system (GIS), digital terrain model (DTM), and advancement in hydraulic modelling software, 2-D modelling have begun to be adopted for analyses that require flood plain mapping and the analysis of overland flows. Besides, recent developments in flood modelling have led to the concept of coupled hydraulic model. With the availability of DTM for an urban drainage study, this paper illustrates the successful application of a coupled XP SWMM 1D and XP-2D model. The study is conducted for urban drainage along Jalan Sibiyu, Bintulu. Simulation results show that the coupled model is capable of providing crucial information such as direction and rate of flood propagation, flood inundation extent, flood depth as well as duration which in turn provides a better understanding of the actual flood behavior at the study area. The study illustrate that 2-D modelling results provide a better representation of the actual flood phenomenon to the designers in order to derive the optimum and cost-effective flood mitigation solutions.

Keywords: One-dimensional (1-D); two-dimensional (2-D); flood, XP SWMM.

1 INTRODUCTION

Flash flooding is the rapid flooding caused by the stormwater of intense rainfall associated with thunderstorms. Flash flooding in urban area has always been a nightmare as it can happen anytime and cause severe damage and sometimes can even lead to loss of lives. Flooding reveals the deficiencies in existing stormwater facilities and management practices. The development of effective design requires a comprehensive understanding of flooding together with the stormwater infrastructure and system. Although one-dimensional (1-D) hydraulic modelling has been extensively used and proven to be useful for flood management but the capability is basically limited to water profiles and some hydraulic variables. For specific analyses such as overland flow in floodplains, determining direction and rate of flood propagation, flood inundation extent, flood depths and duration requires a more sophisticated two-dimensional (2-D) model and modelling techniques. With the advent of geographic information system (GIS), digital terrain model (DTM), and advancement in hydraulic modelling software, 2-D modelling have begun to be adopted for analyses requiring flood plain mapping and the analysis of overland flows. Besides, recent developments in flood modelling have led to the concept of coupled hydraulic model (Barnard et al, 2007).

The study area is at Jalan Sibiyu areas, located at southeastern of Bintulu town. The drainage at certain stretches of Jalan Sibiyu is subject to flash flooding. The flooding caused traffic disruption, damages to properties and relocation of people. Considering the frequent occurrence of flash flooding, a study had been initiated by agency to investigate the flooding phenomenon along Jalan Sibiyu and proposed mitigation measures.

The purpose of this paper is to illustrate the successful application of a coupled XP SWMM 1D and XP-2D model using XP software in modelling the flood plain, which in turn provides a better understanding of the actual flood behaviour at the Study area.

2 STUDY AREA

Jalan Sibiyu is located at the southeastern side of Bintulu, extending from the junction of Jabatan Pengangkutan Jalan (JPJ) area and Jalan AH150, until the junction of Kg Baru and Jalan Kemena for about 5.5 km. Drainage system can be found along both sides of Jalan Sibiyu ('Study area') (refer Figure 1). At certain stretches, the drainage is subjected to flash flooding after a storm. The study area falls within the southern portion of the Sg Sibiyu catchment. Sg Sibiyu drains into Btg Kemena, where the confluence between Sg Sibiyu and Btg Kemena is just 3 km from the Btg Kemena river mouth with South China Sea.

The study area is having a catchment area of 783 ha, with left and right side of Jalan Sibiyu having catchment area of 432.4 ha and 350.6 ha respectively. As shown in Figure 1, right side of Jalan Sibiyu (looking towards downstream) is mostly developed; about 50% of the areas have been developed into residential areas, followed by 40% of the areas being opened up and the remaining areas are still covered by bush. On the other hand, left side of Jalan Sibiyu is still not yet developed; about 40% of the areas are opened up and the remaining areas are still covered by bush. Figure 2 shows the terrain of the Study Area.

There are a total of 9 major drainage outlets along Jalan Sibiyu (refer Figure 3). The urban drainage network along Jalan Sibiyu comprises an estimated total of 77 main and secondary drains. As the study area is semi-developed, 50% of the drains are concrete lined while the remaining is earth lined.

Outlet 1 is the most upstream outlet discharging into Sg Sibiyu, about 9.2 km from the confluence between Sg Sibiyu and Btg Kemena. While Outlet 9 is the most downstream outlet discharging into Sg Sibiyu, about 870 m from the confluence between Sg Sibiyu and Btg Kemena. As Outlet 8, 9 and 10 are located quite near to the confluence between Sg Sibiyu and Btg Kemena, backflow from Btg Kemena due to fluctuation of tide can be felt at these locations.

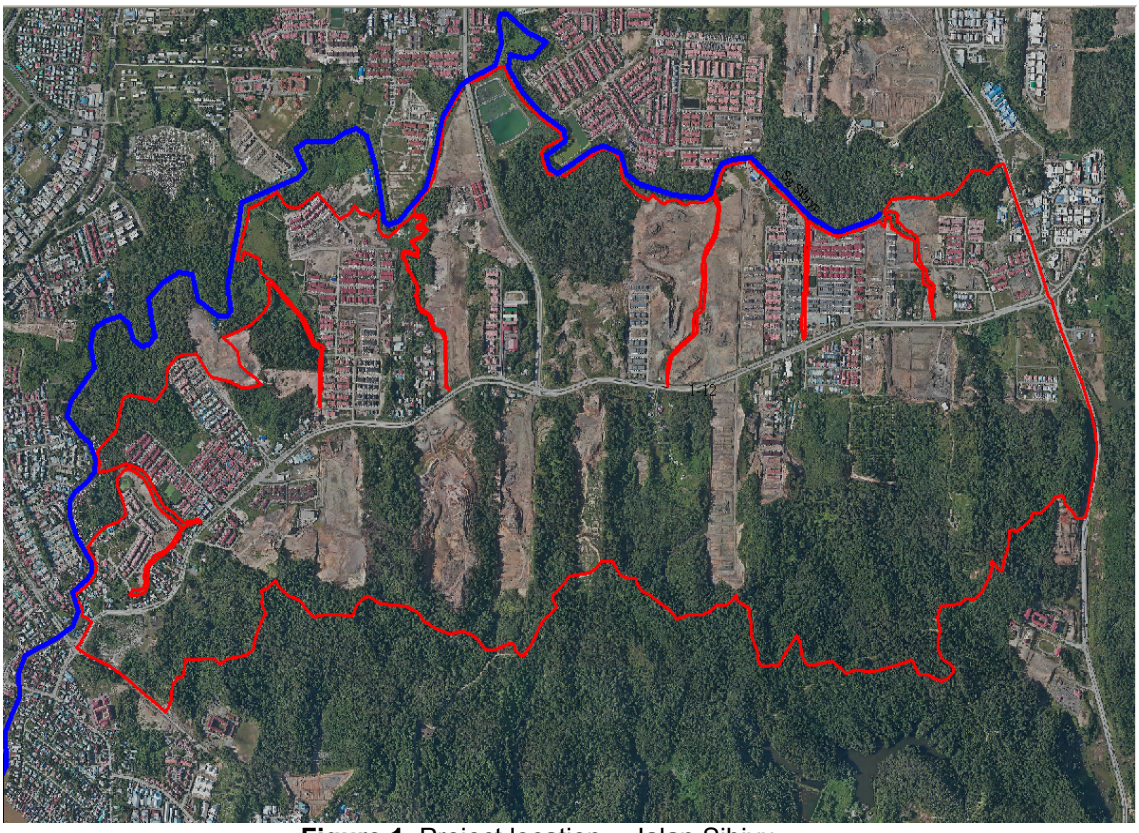

Figure 1. Project location – Jalan Sibiyu.

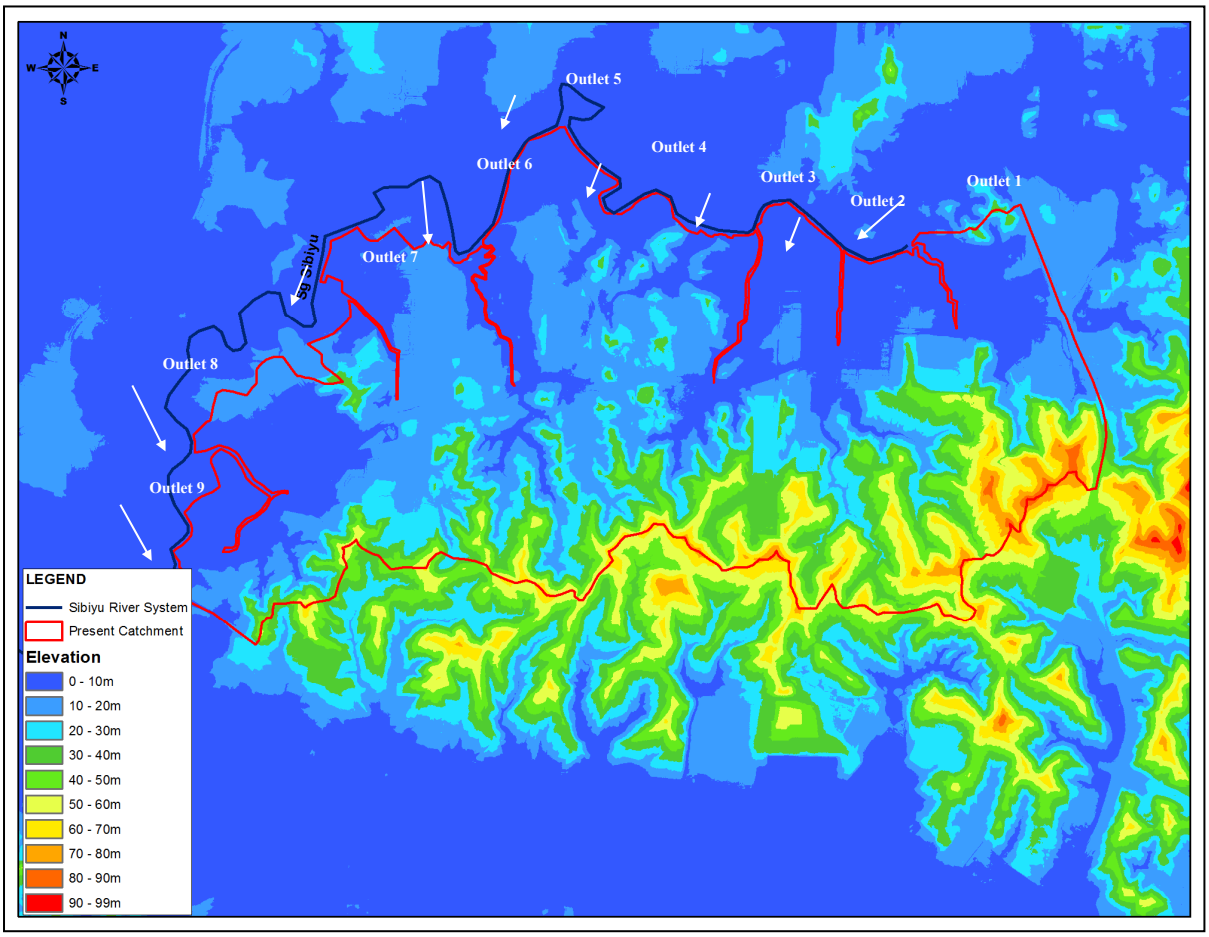

Figure 2. Terrain of study area.

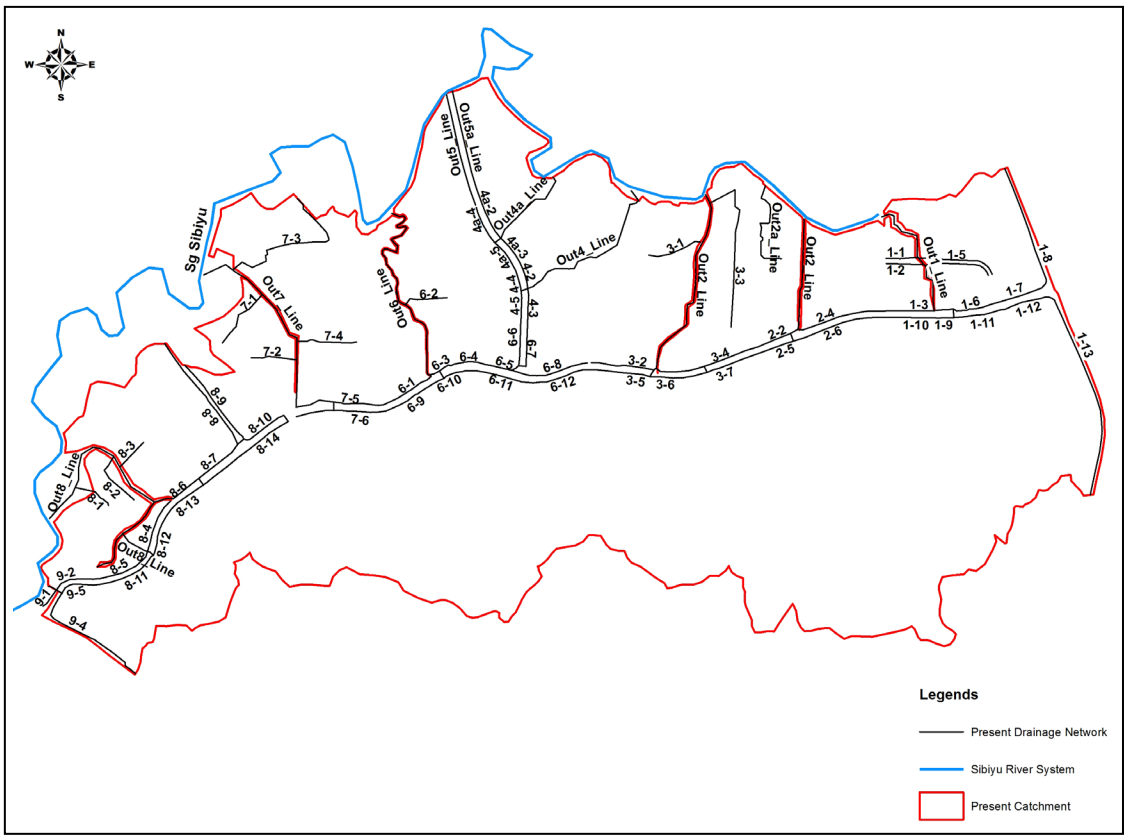

Figure 3. Present drainage network along Jalan Sibiyu.

3 WHY TWO-DIMENSIONAL MODELLING

In Malaysia, most stormwater studies are carried out using the traditional method that is 1-D modelling technique. In 1-D hydraulic modelling, floodplain are usually modelled as wide uniform sections that are linked to nodes of the network. Although the results seem to be practicable, this traditional technique is still unable to model accurately the phenomenon of overspilling as well as the magnitude, extent and rate of flood wave propagation over the flood plain. Even though engineers are aware of the advantages of 2-D hydraulic modelling in simulating flood plains, owing to the lack of reliable survey information, 2-D hydraulic modelling is still not commonly being adopted (Lim and Cheok, 2009).

With the advent of GIS, survey technologies such as Light Detection and Ranging (LiDAR), availability of DTM data, and advancement in hydraulic modelling software, 2-D modelling have begun to be adopted for analyses requiring flood plain mapping and the analysis of overland flows. The combination of all these factors has enabled the present study to be carried out using 2-D hydraulic modelling approaches (Shen et al, 2015).

4 METHODOLOGY

The study was carried out using XP SWMM software. XP SWMM is a one-dimensional link-node model that performs hydrological and hydraulic analysis suitable for urban stormwater systems. XP 2D is an overland flow module, of which coupled with the 1-D capability of XP SWMM, allows simulation of flows in and out of urban drainage networks and river systems. It provides a useful tool to predict the extent, depth, velocity and duration of flooding. The model was setup as a combination of 1-D network domains linked to 2-D domains as a single model.

Under this study, 12 models were setup according to the numbers of outlets exist in the study area. Each model comprised a 2-D overland flow model and a 1-D drainage model. They are coupled together to form a complete 1-D / 2-D overland flow model. Each outlet has its own sub-catchments. The sub-catchments were defined and entered into a rainfall runoff model. Time Area method embedded in XP SWMM 1-D model was adopted to derive the design hydrographs. The model was run to estimate the 50-year Annual Return Interval (ARI) design flows under future land use and developed condition.

Topographic data is required for 2-D modelling. Thus, LiDAR data with a vertical accuracy of about 0.15 m was procured in this Study. XPSWMM uses a triangulated irregular networks (TIN) for obtaining elevation data for the 2-D grid. Various grid sizes were attempted during model setup to arrive at an optimum resolution. Smaller grid resolution requires much longer computation duration whereas coarser grid resolution would produce inaccurate inundation simulation results (Barnard et al, 2007). Thus, grid spacing of 20 m x 20 m was adopted in this Study after considering the computation duration, result accuracies as well as capability of the XP2D software.

The model parameters and values adopted for the 2-D modelling in this Study are tabulated in Table 1 below.

Table 1. XP2D Model Parameters and Adopted Values.

Parameter and Criteria	Value
Manning's Roughness for channel (earth)	0.03
Manning's Roughness for channel (concrete)	0.015
Manning's Roughness for floodplain	0.05
Eddy viscosity (m^2/s)	Use Smagorinsky formulation
XP2D flooding depth (m)	0.002
XP2D drying depth (m)	0.002

5 RESULT AND DISCUSSIONS

Upon successful completion of all the model simulations, the outputs from the simulations in term of flood extent and depth were extracted and discussed.

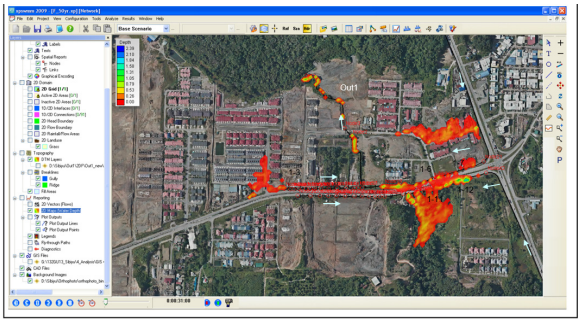

Outlet 1

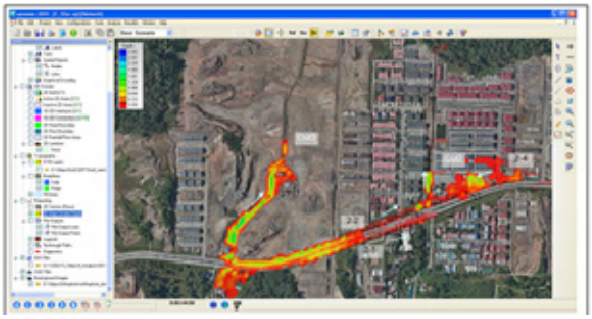

Outlet 2

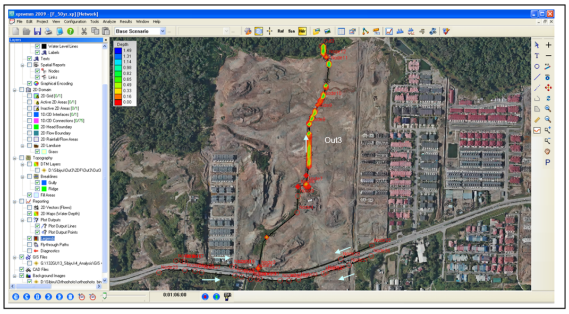

Outlet 3

Outlet 4

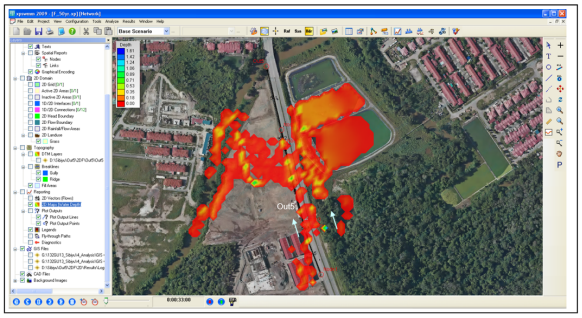

Outlet 5

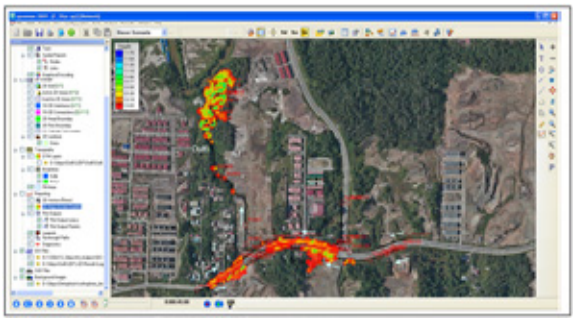

Outlet 6

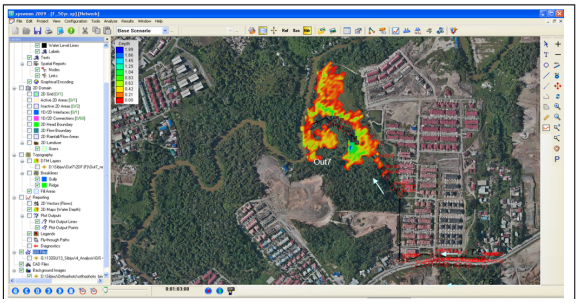

Outlet 7

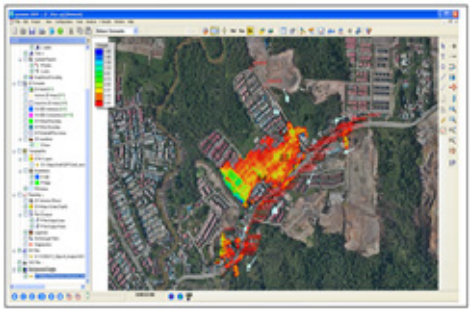

Outlet 8

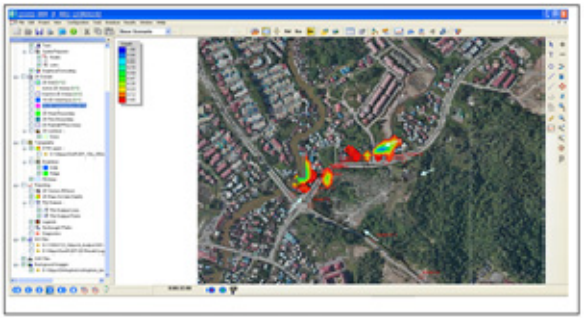

Outlet 9

Figure 4. Inundation extent and depth for each outlet.

Figure 4 shows the inundation extent and depth at each outlet under 50-year ARI flow of future and developed condition. Sizable areas are inundated under 50-year ARI flooding condition. Despite the sizeable inundated areas, the flooding depth is less than 1 m at most of the areas. The model results also revealed the

deficiencies and interconnection of drainage system along Jalan Sibiyu. During flooding, certain stretches of Jalan Sibiyu will be cut off due to overspilling of floodwater.

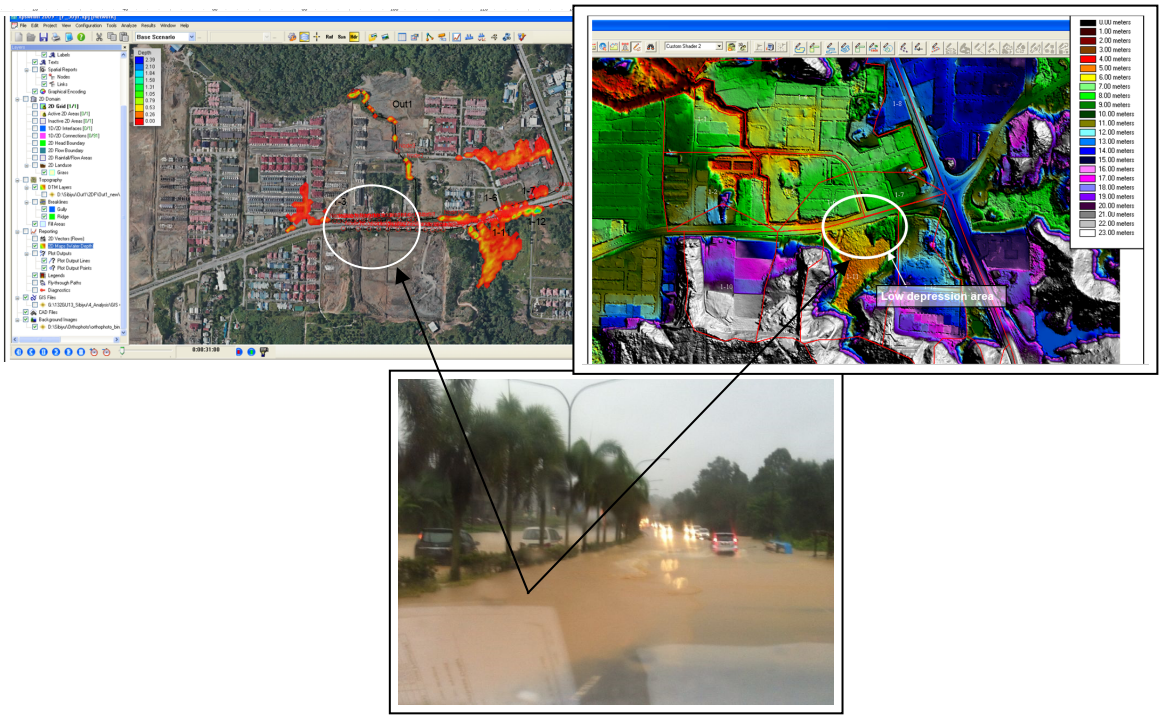

Figure 5. Flooding extent within outlet 1 catchment and its terrain.

Figure 5 shows the flooding extent within the outlet 1 catchment as well as its topography. From the figure, Jalan Sibiyu junction is lower and depressed towards the middle stretch of the road. As the culvert crossings across Jalan Sibiyu are inadequate to convey the stormwater, stormwater will overspill and flood Jalan Sibiyu.

The flood photo taken during the flash flood on Jan 2014 could well indicate that this stretch of road is depressed and compounded by inadequate conveyance capacity, floodwater overspilled to the surrounding area.

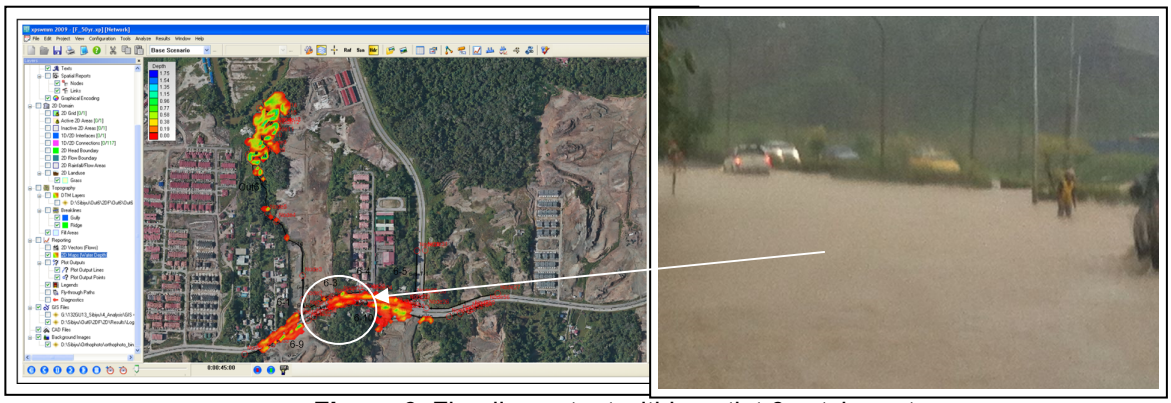

Figure 6. Flooding extent within outlet 6 catchment.

Figure 6 shows the flooding extent within the outlet 6 catchment. Similar to Outlet 1, Jalan Sibiyu junction is lower and the existing crossings are unable to convey the stormwater effectively. During the occurrence of flash flood on Jan 2014, this location had been flooded. This is consistent with the model prediction where this area is the overspilling points.

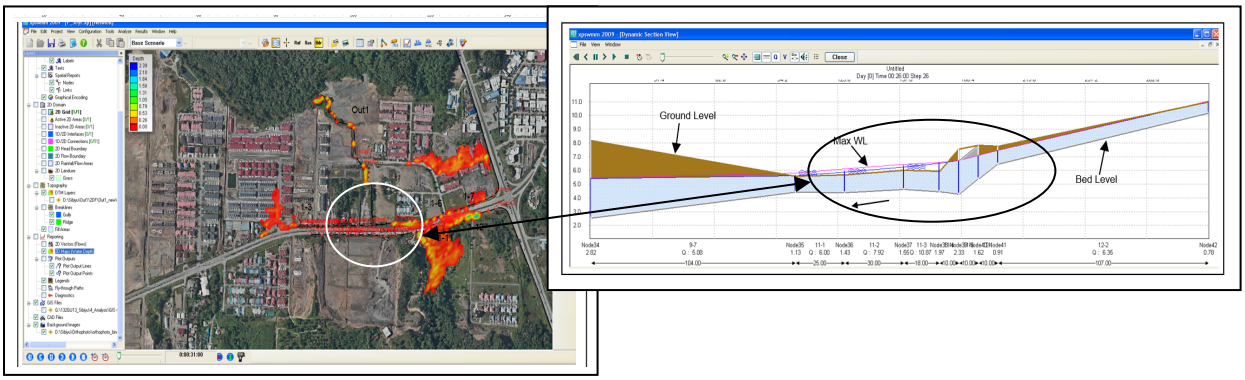

Figure 7. Maximum water level profile under present condition with 50 year ari future landuse flow.

Figure 7 shows the results of model simulation using 1D hydraulic model. The maximum water level is as presented in longitudinal profile. From the profile, overspilling locations where maximum water level exceeded the ground level could be identified. On the other hand, the 2D model results not only show the overspilling point, but also show the flooding extent, flow direction and flood propagation rate.

From this study, it is truly shown that pertinent flood info like maximum water level, discharge, flooding depth as well as duration can be obtained via 1D hydraulic model. However, such flood info could not be insufficient to illustrate the flooding phenomenon graphically. In contrast, 2D hydraulic model can provide additional info to the flooding phenomenon in term of flood inundation extent, flow direction as well as flood propagation rate which could not be performed by 1D hydraulic model capability only.

The combined 1-D / 2-D modelling capabilities in the XP SWMM 2D package allow this study to undertake more detailed investigations of the flooding phenomenon of the drainage system along Jalan Sibiyu and identify areas of over flows before arriving at mitigation measures to resolve the flash flooding.

6 CONCLUSIONS

Due to the advancement of technologies, the use of 2-D modelling is expected to become a normal engineering practice for flood assessment in the future. 2-D modelling is capable of providing crucial information such as direction and rate of flood propagation, flood inundation extent and depths as well as inundation time across the studied flood plains.

Based on the analysis and results presented in this paper, it is concluded that although 1-D steady and unsteady flow models are the dominant tools for the design and analysis of drainage systems, for flood mapping, 2-D models are a better option to model complex flow patterns on floodplains. The presentation of modelling results in 2-D allow a more detailed investigations of the flooding phenomenon.

Although the results of this study presented here have not been verified with flood events, the work demonstrates the features and powers of 1-D / 2-D linked hydrodynamic modelling capabilities.

ACKNOWLEDGEMENTS

A debt of gratitude is owed to Bintulu Development Authority (BDA) Malaysia for their supports during the project. This paper would not have been possible without expertise and contributions from Ir. Chong Sun Fatt and Ir. Lim Sin Poh.

REFERENCES

Barnard, T., Barnard, T.E., Kuch, A.W., Thompson, G.R., Mudaliar, S. & Phillips, B.C. (2007). Evolution of an Integrated 1D/2D Modeling Package for Urban Drainage. *Computational Hydraulics International*, 18, 343-365.

Lim, S.P. & Cheok, H.S. (2009, February). Two-Dimensional Flood Modelling of the Damansara River. In *Proceedings of the Institution of Civil Engineers-Water Management,* 162(1), 13-24).

Shen, D., Wang, J., Cheng, X., Rui, Y. & Ye, S. (2015). Integration of 2-D Hydraulic Model and High-Resolution Lidar-Derived DEM For Floodplain Flow Modeling. *Hydrology and Earth System Sciences*, 19(8), 3605-3616.

RUNOFF ANALYSIS MODEL WITH A DEEP LEARNING

TOMOKI IZUMI [(1)] & NORIYUKI KOBAYASHI [(2)]

[(1,2)] Graduate School of Agriculture, Matsuyama, Japan,
t_izumi@agr.ehime-u.ac.jp

ABSTRACT

A deep neural network (DNN) model for runoff analysis was developed. The model consists of one input layer, three middle layers, and one output layer. In order to avoid the gradient vanishing, the layer-wise pre-training by the auto-encoder was employed. For the problem of overfitting, the number of training run is limited based on the early-stopping technique. The model validity was examined through runoff analysis. The model predicted the daily river discharge from the daily rainfall. The study area was at Shigenobu River watershed, Ehime prefecture, Japan. The daily discharge and rainfall data were obtained at the observatory of Deai and Matsuyama, respectively. The training (calibration) period was from 2001 to 2010, and prediction (verification) period was from 2011 to 2013. To assess effectiveness of the model, calibration and verification results were compared with those of a hierarchical neural network (HNN) model, which consisted of the same number of layers without employing the layer-wise pre-training by the auto-encoder. From the results, it was found that the statistical performance indices of DNN model in verification period is better than that of HNN model.

Keywords: Runoff analysis; neural network; deep learning.

1 INTRODUCTION

Runoff analysis is a crucial technique for the use and management of water resources, and has been implemented by use of a runoff model like a conceptual model or physical model. However, it is difficult to represent the relation between rainfall and discharge because of its high nonlinearity.

For the representation of nonlinearity, models using artificial neural network (ANN) are useful. Hsu et al. (1995) applied a hierarchical neural network (HNN) model to runoff analysis and demonstrated its effectiveness by comparing with the linear ARMAX (autoregressive moving average with exogenous inputs) time series approach or the conceptual SAC-SMA (Sacramento soil moisture accounting) model. Minns and Hall (1996) implemented runoff analysis using HNNs in a hypothetical catchment and evaluated the performance of ANNs. Dawson and Wilby (1998) developed an HNN model and applied it to flow forecasting in two rivers. Sajikumar and Thandaveswara (1999) developed a monthly rainfall-runoff model using an HNN and investigated its performance by comparing with functional series models. Abe et al. (2000) developed an HNN model and applied to long-term (10 years) daily runoff analysis. Kiyama et al. (2003) developed an HNN model to predict flood discharge and discussed its predictability or applicability.

Previous works showed applicability or effectiveness of HNN models for runoff analysis. To obtain more accurate representation of the relation between rainfall and discharge, there are some improvements such as increase of layers and computational nodes (neurons), and so on. However, increase of layers and/or nodes causes problems such as "vanishing gradient" and "overfitting" in the typical ANN such as HNN. Recently, deep learning methods were proposed to overcome those problems (LeCun et al., 2015; Schmidhuber, 2015). Izumi et al. (2016) developed a deep neural network (DNN) model for runoff analysis. The model consists of one input layer, two middle layers, and one output layer. In order to avoid the vanishing of the gradient, the layer-wise pre-training by the auto-encoder was employed (Bengio, 2006). For the problem of overfitting, the number of training run is limited based on the early-stopping technique (Kamishima et al., 2015). The model effectiveness was shown by comparing the DNN and HNN model output in terms of the reproducibility and predictability for observed data.

In this study, DNN model developed by Izumi et al. (2016) was extended to the model with deeper layers and its performance or effectiveness was assessed from the comparison of a HNN model with the same number of layers and nodes.

2 DNN MODEL

ANN is a nonlinear mathematical model which imitates biological nervous systems. A representative neural network model is HNN model, which is a three-layer feed forward neural network model consisting of input, hidden and output layers. DNN is an HNN which has more than two hidden layers. Generally, increase of layers leads to not only acquisition of more complicated representation but also problems of “vanishing gradient" and "overfitting”. DNN is also designed to avoid these problems by incorporated the layer-wise pre-training by the

auto-encoder and the early-stopping technique (LeCun et al., 2015; Schmidhuber, 2015; Kamishima et al., 2015).

In this study, a DNN model for daily runoff analysis was developed. The model is an extended one developed by Izumi et al. (2016) and consists of one input layer, three middle layers, and one output layer (Figure 1). The output in *j*-th layer (Middle Layer 1 in Figure 1) is described as follows:

$$f(u_j) = \frac{1}{1+\exp(-u_j)} \quad [1]$$

$$u_j = \sum_{i=1}^{n} w_{ij} x_i - \theta_j \quad [2]$$

where, $f(u_j)$ is output value in *j*-th layer, x_i is input in *j*-th layer, w_{ij} is weight coefficient, θ is threshold value, n is the number of node in *i*-th layer. The training procedure is used the error backpropagation algorithm (Rumelhart et al., 1986). In the algorithm, the weight coefficients and threshold values are adjusted based on errors between resultant outputs from the network and expected outputs (teacher signals).

In order to avoid the gradient vanishing, the layer-wise pre-training by the auto-encoder is employed (Bengio, 2006). The auto-encoder consists of three layers, i.e. input, middle, and output layers. The number of node in output layer was set as same as that in input layer. The auto-encoder learns to output or reproduce the input signals. The weight coefficients and threshold values after learning were used as initial values of those in DNN model. Examples of the auto-encoder are shown in Figure 2. Figure 2(a) shows the auto-encoder based on the Input Layer and Middle Layer 1, in which initial values of w_{ij} was determined. Figure 2(b) also shows the one for determining initial values of w_{jk}. For the problem of overfitting, the number of training run is limited based on the early-stopping technique (Kamishima et al., 2015).

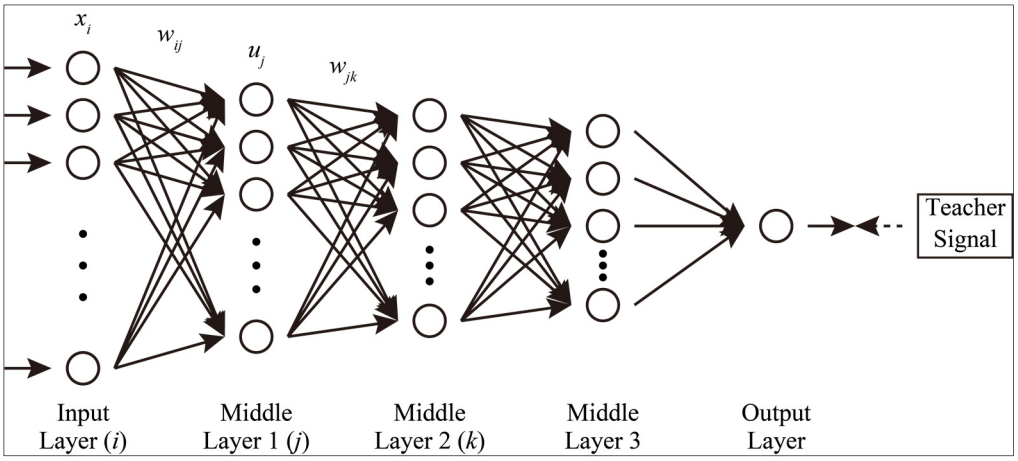

Figure 1. DNN model

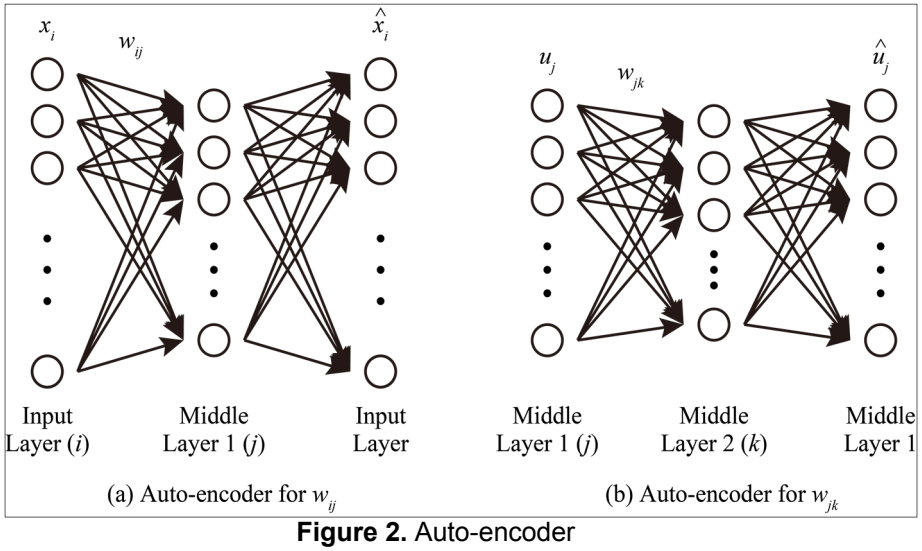

Figure 2. Auto-encoder

3 MODEL ASSESSMENT

3.1 Study area

The study area was at Shigenobu River basin, Ehime prefecture, Japan as shown in Figure 3. Shigenobu River is 36 km length and flows into Seto Inland Sea. The basin area is 445 km^2 and 70% of the basin is covered by forest. The alluvial fan, Dogo Plain, is formed in the downstream basin. The average annual rainfall in the plain is approximately 1,300 mm/year, which is less than that of Japan (1,700 mm/year).

The daily discharge and rainfall were observed at the observatory of Deai (N33° 48' 21'', E132° 43' 31'') and Matsuyama (N33° 49' 18'', E132° 44' 22''), respectively. Those data can be obtained from Water Information System (Ministry of Land, Infrastructure, Transport and Tourism). The observed data of daily discharge and rainfall were used for teacher signal and input signal, respectively.

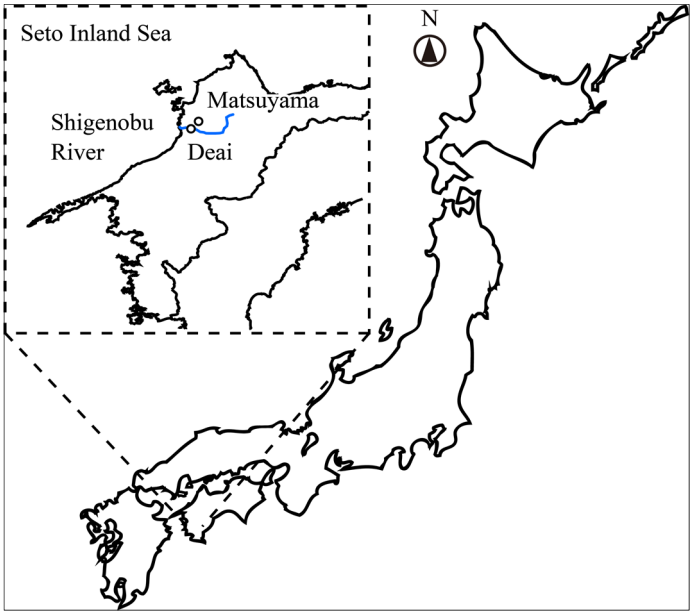

Figure 3. Study area

3.2 Conditions of runoff analysis

Runoff analysis outputs (reproduces or predicts) daily discharge from daily rainfall. The daily discharge data was used as the teacher signal. Generally, daily discharge depends on daily rainfall before several days. Thus, daily rainfall before 10 and 15 days were used as input data based on the hyeto and hydro graph at the observatory of Matsuyama and Deai. While the number of computational nodes in three middle layers can be arbitrary determined, those are set as two cases: (1) seven, five and three, and (2) five, five and five because it is beyond the scope of this study.

In order to assess effectiveness of the DNN model, the calibration and verification results were compared with those of a HNN model which has the same number of layers as the DNN model. The training (calibration) period was set from 2001 to 2010, and thus the number of datasets were 3,640 for the model that has 10 input nodes and 3,635 for 15 nodes. The prediction (verification) period was from 2011 to 2013. The parameter of learning rate was set to be a constant value of 0.75. The number of learning run of DNN and HNN model was set to be 10,000. In DNN model, the number of the pre-training by the auto-encoder was set to be 5,000.

3.3 Statistical performance indices

In this study, the model performance was assessed by three statistical indices: the correlation coefficient (*R*), the coefficient of efficiency (*E*) proposed by Nash and Sutcliff (1970), and the normalized root mean square error (*NRMSE*).

$$R = \frac{\sum_t \left(Q^{obs}(t) - Q_m^{obs}\right)\left(Q^{com}(t) - Q_m^{com}\right)}{\sqrt{\sum_t \left(Q^{obs}(t) - Q_m^{obs}\right)^2 \sum_t \left(Q^{com}(t) - Q_m^{com}\right)^2}} \quad [3]$$

$$E = \frac{\sum_t \left(Q^{obs}(t) - Q_m^{obs}\right)^2 - \sum_t \left(Q^{com}(t) - Q_m^{com}\right)^2}{\sum_t \left(Q^{obs}(t) - Q_m^{obs}\right)^2} \quad [4]$$

$$NRMSE = \frac{\sqrt{\frac{1}{N}\sum_t \left(Q^{com}(t) - Q^{obs}(t)\right)^2}}{\frac{1}{N}\sum_t Q^{obs}(t)} \quad [5]$$

where $Q^{obs}(t)$ is the observed discharge at time t, $Q^{com}(t)$ the reproduced or predicted discharge at time t, N the total number of discharge data, Q_m^{obs} the mean observed discharge, Q_m^{com} the mean reproduced or predicted discharge.

4 RESULTS AND DISCUSSIONS

4.1 Calibration results

Scatter diagrams of the calibration results are shown in Figure 4, and three statistical indices are summarized in Table 1. The correlation coefficients (*R*-values) and coefficient of efficiencies (*E*-values) are more than 0.870 and 0.754, respectively. The normalized root mean square errors (*NRMSE*-values) are less than two.

4.2 Verification results

As verification results, time-series of predicted and observed discharge are shown in Figure 5, and three statistical indices are summarized in Table 2. *R*-values and *E*-values are smaller than those of calibration results. It can be seen that *R*-values are 0.717 at most, *E*-values include negative ones and *NRMSE*-values are more than two.

Table 1. Statistical performance indices of DNN and HNN model in calibration results

Model	*R*	*E*	*NRMSE*
DNN 10-7-5-3-1	0.880	0.766	1.574
HNN 10-7-5-3-1	0.923	0.837	1.315
DNN 10-5-5-5-1	0.910	0.816	1.394
HNN 10-5-5-5-1	0.920	0.833	1.329
DNN 15-7-5-3-1	0.921	0.838	1.310
HNN 15-7-5-3-1	0.937	0.865	1.194
DNN 15-5-5-5-1	0.870	0.754	1.614
HNN 15-5-5-5-1	0.939	0.870	1.173

Table 2. Statistical performance indices of DNN and HNN model in verification results

Model	*R*	*E*	*NRMSE*
DNN 10-7-5-3-1	0.717	0.390	2.115
HNN 10-7-5-3-1	0.591	0.283	2.845
DNN 10-5-5-5-1	0.611	-0.082	2.696
HNN 10-5-5-5-1	0.622	0.182	2.709
DNN 15-7-5-3-1	0.621	0.036	2.520
HNN 15-7-5-3-1	0.610	-0.150	2.320
DNN 15-5-5-5-1	0.687	0.091	2.414
HNN 15-5-5-5-1	0.432	-0.386	2.862

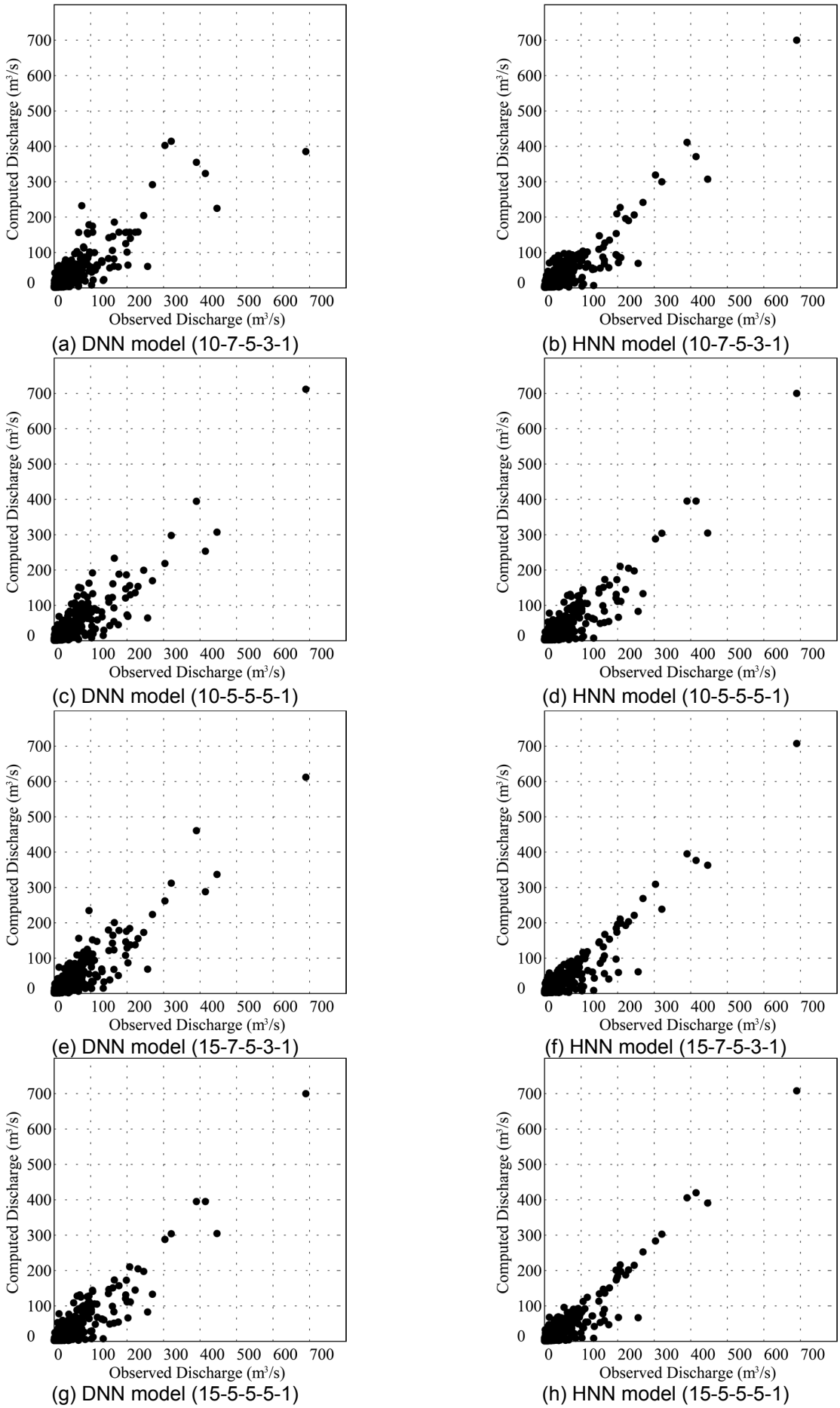

(a) DNN model (10-7-5-3-1)
(b) HNN model (10-7-5-3-1)
(c) DNN model (10-5-5-5-1)
(d) HNN model (10-5-5-5-1)
(e) DNN model (15-7-5-3-1)
(f) HNN model (15-7-5-3-1)
(g) DNN model (15-5-5-5-1)
(h) HNN model (15-5-5-5-1)

Figure 4. Scatter diagrams of calibration result

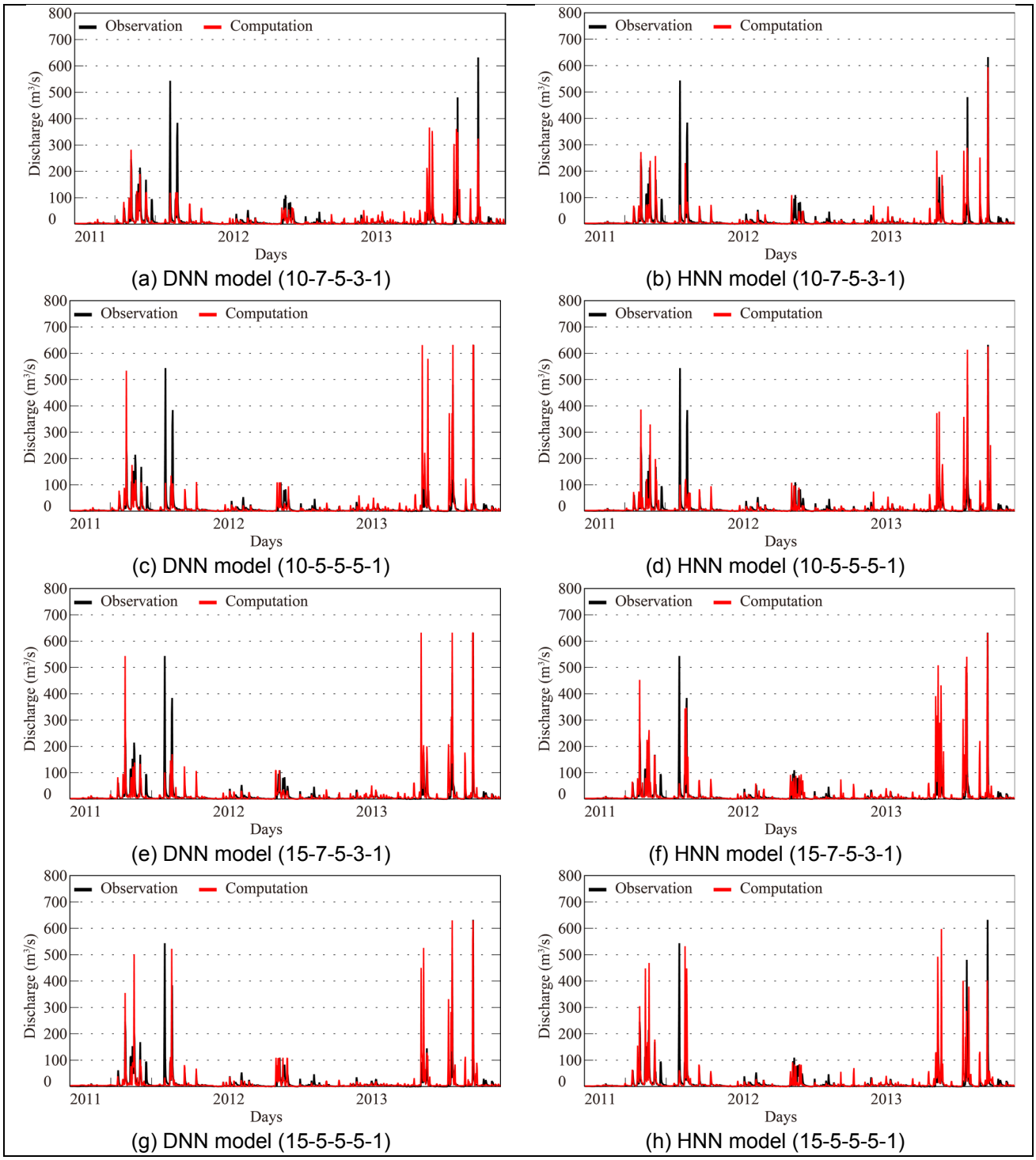

Figure 5. Verification results

4.3 Discussions

From the calibration results, we can see the linear relationship between the observed and computed values in Figure 4 and *R*-values. *E*-values were more than 0.754 and it means that the runoff analysis models have high reproducibility. All performance indices showed that the reproducibility of HNN model is higher than that of DNN model.

From the verification results, predictability of both DNN and HNN model is low. Specifically, there are failures in prediction of peak discharge (Figure 5). The performance indices showed that the predictability of DNN model is higher than that of HNN model expect for the model of 10-5-5-5-1.

The comparison results that reproducibility of DNN model is lower than that of HNN model and predictability of DNN model is inversely higher indicate that DNN model is prevented from falling into the overfitting. There is no clear tendency in network structure such as the number of computational nodes in each layer.

5 CONCLUSIONS

A DNN model for runoff analysis was developed. Comparing with the application results of HNN model, performance or effectiveness of DNN model was assessed. To clarify the reproducibility and predictability, three statistical indices are shown. From the results, it was found that the reproducibility of DNN model is lower than that of HNN model and the predictability of DNN model is inversely higher, and it indicates that DNN model is prevented from falling into the overfitting.

ACKNOWLEDGEMENTS

This study was supported by JSPS 16H04997.

REFERENCES

Abe, K., Kikuchi, H., Furukawa, K. & Shiotsuki, Y. (2000). Study on a System of Runoff (Daily) Analysis Using Neural Network. *Journal of Japan Society Civil Engineering*, 656(II-52), 1-13. (In Japanese with English abstract).

Bengio, Y., Lamblin, P., Popovici D. & Larochelle, H. (2006). Greedy Layer-Wise Training of Deep Networks. *In Proc. Advances in Neural Information Processing Systems*, 19, 153-160.

Dawson C.W. & Wilby R. (1998). An Artificial Neural Network Approach to Rainfall-Runoff Modelling. *Hydrological Sciences*, 43(1), 47-66.

Hsu K., Gupta H.V. & Sorooshian S. (1995). Artificial Neural Network Modeling of the Rainfall-Runoff Process. *Water Resources Research*, 31(10), 2517-2530.

Izumi T., Miyoshi M. & Kobayashi N. (2016). Runoff Analysis Using a Deep Neural Network. *Proceedings of 12th International Conference on Hydroscience & Engineering*, 04-0002.

Kamishima, T., Asho, H., Yasuda M., Maeda S., Okanohara D., Okatani T., Kubo Y. & Bollegala D. (2015). *Deep Leaning*. Kindaikagaku-sha, 267pp.

Kiyama, T., Toyama, H., Sasahara, K., Mama S., Seki M. & Takemura H. (2003). Basic Study of the Use of a Neural Network to Predict Flooding on the Abukuma River. *Advances in River Engineering*, 9, 173-178. (In Japanese with English abstract)

LeCun, Y., Bengio, Y. & Hinton G. (2015). Deep Learning. *Nature*, 521, 436-444.

Minns, A.W. & Hall, M.J. (1996). Artificial Neural Networks as Rainfall-Runoff Models. *Hydrological Sciences*, 41(3), 399-417.

Rumelhart, D.E., Hinton, G.E. & Williams, R.J. (1986). Learning Representations by Back-Propagating Errors. *Nature*, 323, 533-536.

Sajikumar, N. & Thandaveswara, B.S. (1999). A Non-Linear Rainfall-Runoff Model Using an Artificial Neural Network. *Journal of Hydrology*, 216, 32-55.

Schmidfuber, J. (2015). Deep Learning in Neural Networks: An overview. *Neural Networks*, 61, 85-117.

Proceedings of the 37th IAHR World Congress
August 13 – 18, 2017, Kuala Lumpur, Malaysia

MODELING OF TOTAL MAXIMUM DAILY LOAD FOR AN URBAN CATCHMENT

NAZIRUL MUBIN ZAHARI[1], LARIYAH MOHD SIDEK [2], MING FAI CHOW[3], SITI HUMAIRA HARON[4]
NUR ALIA NIZA[5] & HIDAYAH BASRI[6]

[1,2,3,4,5,6] Sustainable Technology & Environment Group, Institute for Energy Infrastructure, Universiti Tenaga Nasional, Selangor, Malaysia
mubinzahari@gmail.com[1]; drlariyah66@gmail.com[2]; Chowmf@uniten.edu.my, sthumaira@yahoo.com[4]; nuralia.niza@gmail.com[5]; hidayahbasri@gmail.com[6]

ABSTRACT

Penchala River is one of the longest rivers in Selangor, Malaysia and is under threat due to effluent disposals mainly from commercial and industrial sector near Petaling Jaya area. As per the DOE water quality index classification, the river is not acceptable as Class II River and has since surpassed as Class IV river at some parts of the river. Due to the outcome of effluent disposition in this river, modelling of one dimensional steady state water quality model is carried out by adapting QUAL2Kw. In order to minimize the watershed load, simulation of model involves simulating water quality data, temperature and hydraulics data to calculate the required reduction of pollutant loads to achieve or maintain the river at Class II. Several BMPs are then proposed for pollutant loads reduction. Analysis of the water quality model and manual calculation of TMDL indicated that NH4, TP, TN, COD, NO3, and TSS loads should be reduced by 80%, 70%, 70%, 60%, 89%, 52% respectively.

Keywords: TMDL; pollutant load; BMP; penchala river.

1 INTRODUCTION

Based on the recent Malaysia Environmental Quality Report (2014), Biochemical Oxygen Demand (BOD), Ammonical Nitrogen (NH3-N) and Suspended Solids contributes prominently in terms of river pollution. From the report, incompetency of the treatment of effluent from agricultural and industrial sectors mainly attributes to a high BOD. The report also stated that the main causes of NH_3-N are derived from livestock farming and domestic sewage while inadmissible earthworks and site clearing activities primarily contributed to an increasing Suspended Solid in domestic rivers.

Malaysia's River Quality Trend is characterized; "out of the 43 polluted rivers, 25 rivers were classified as Class III, 18 rivers as Class IV. In terms of BOD, 10 rivers were classified as Class IV and 33 rivers as Class V. In terms of NH3-N, three rivers were classified as Class II, two as Class III, 14 rivers as Class IV and 24 rivers as Class V. In terms of SS, 24 rivers were classified as Class I, 14 rivers as Class II, and five rivers as Class III (Department of Environment, 2014). To improve the conditions of most rivers in Malaysia, a few actions are needed to be taken. The first action needed to be done is to determine the different types of pollutant loads in the river. Based on this study, in order to execute this is by developing a water quality model. A steady state flow modeling software called QUAL2Kw is used. Parameters such as total nitrogen, total phosphorus, Biochemical Oxygen Demand (BOD) and Dissolved Oxygen is used as input data for the modeling based on observation data acquired from UNITEN's database.

This study also proposes the most suitable BMPs which act as an alternative to improve the water quality of the river (Lung, 1993). Several BMPs were introduced and the ability of several different types of BMPs is regulated based on their ability to reduce the amount of pollutant loads. To make sure that the study area receives the most suitable BMP, an analysis of the percentage reduction must be executed.

2 METHODOLOGY

2.1 Introduction

In order to perform the water quality modeling, some of the default system ID needed to be changed. Components such as the river name, the file location of the output should be modified. For the simulation and output options, an Euler integration method was used, while the pH solution method was Brent method. In order to simulate hyporheic exchange and pore water quality, the simulation and output option was modified to be on level.

2.2 Configuration on ID system

Figure 1 show the input data of headwaters which consist of parameters such as temperature, pH, DO, TN, and CBOD. Several of the parameters were collected from a prehistoric observation data from UNITEN's

database of Penchala River from the year 1995 to 2010. The input data shown in Figure 2 was inserted for every one hour of observation data every day for 7 days. Headwaters input data was needed in order to execute the water quality model. Some of the data parameters such as conductivity, inorganic solids, organic phosphorus, and pathogen were default data that was specified in the QUAL2Kw model. These default data were eventually modified until the output data, which was in the form of a graph is in sync with the line graph of maximum and minimum output data of several parameters.

Headwater Flow	0.713	m3/s											
Prescribed downstream boundary?	No												
Headwater Water Quality	*Units*	*12:00 AM*	*1:00 AM*	*2:00 AM*	*3:00 AM*	*4:00 AM*	*5:00 AM*	*6:00 AM*	*7:00 AM*	*8:00 AM*	*9:00 AM*	*10:00 AM*	*11:00 AM*	*12:00 PM*
Temperature	C	25.00	27.00	25.80	26.80	25.80	25.20	23.20	24.80	25.80	25.20	24.80	23.50	30.00
Conductivity	umhos	276.42	277.23	279.22	282.26	286.14	290.60	295.33	300.02	304.33	307.98	310.72	312.36	312.80
Inorganic Solids	mgD/L	11.94	12.13	12.07	11.78	11.27	10.58	9.76	8.86	7.94	7.06	6.30	5.69	5.28
Dissolved Oxygen	mg/L	6.98	6.98	7.08	7.25	7.49	7.79	8.12	8.46	8.79	9.09	9.33	9.49	9.58
CBODslow	mgO2/L	1.34	1.34	1.34	1.34	1.34	1.34	1.34	1.34	1.34	1.34	1.34	1.34	1.34
CBODfast	mgO2/L	1.34	1.34	1.34	1.34	1.34	1.34	1.34	1.34	1.34	1.34	1.34	1.34	1.34
Organic Nitrogen	ugN/L	1561.00	1560.27	1565.73	1577.01	1593.33	1613.59	1636.40	1660.21	1683.40	1704.38	1721.73	1734.27	1741.13
NH4-Nitrogen	ugN/L	87.59	87.59	87.59	87.59	87.59	87.59	87.59	87.59	87.59	87.59	87.59	87.59	87.59
NO3-Nitrogen	ugN/L	165.56	165.56	165.56	165.56	165.56	165.56	165.56	165.56	165.56	165.56	165.56	165.56	165.56
Organic Phosphorus	ugP/L	18.15	25.31	33.43	41.96	50.32	57.93	64.29	68.95	71.60	72.05	70.29	66.42	60.71
Inorganic Phosphorus (SRP)	ugP/L	73.46	69.42	64.07	57.80	51.01	44.18	37.78	32.23	27.92	25.14	24.07	24.80	27.28
Phytoplankton	ugA/L	0.00	0.00	0.00	0.00	0.00	0.00	0.00	0.00	0.00	0.00	0.00	0.00	0.00
Detritus (POM)	mgD/L	1.29	1.43	1.54	1.61	1.65	1.63	1.58	1.48	1.36	1.21	1.04	0.87	0.72
Pathogen	cfu/100 mL	100.00	100.00	100.00	100.00	100.00	100.00	100.00	100.00	100.00	100.00	100.00	100.00	100.00
Generic constituent	user defined	100.00	100.00	100.00	100.00	100.00	100.00	100.00	100.00	100.00	100.00	100.00	100.00	100.00
Alkalinity	mgCaCO3/L	90.91	91.18	91.93	93.09	94.60	96.35	98.22	100.09	101.82	103.30	104.43	105.12	105.35
pH	s.u.	7.33	7.21	7.13	7.10	7.12	7.19	7.30	7.44	7.61	7.80	7.98	8.16	8.31

Figure 1. The regulated headwaters data obtained from one week observation data for every one hour.

2.3 Input water quality data

Figure 2 shows the input data of minimum and maximum water quality data, which consists of parameters such as DO, CBOD, NH_4, NO_3, Phosphorus and pH. These data were collected from the observation data. There were different input data based on the different distance of the river. Minimum and maximum water quality data were input based on different parts of distance of the river. From many data of water quality obtained from the prehistoric observation data, the least amount of load of each parameters were chosen to be input for water quality minimum data while the highest amount of load of each parameters were chosen as the input for maximum data.

	Minimum	*Minimum*	*Minimum*	*Minimum*	*Minimum*	*Minimum*	*Minimum*	*Minimum*	*Minimum*
Distance (km)	*cond-data*	*ISS-data*	*DO-data*	*CBODs-data*	*No-data*	*NH4-data*	*NO3-data*	*Po-data*	*Inorg P-data*
9.60	279.00	5.00	7.10	52.00	1468.00	40.00	120.00	14.00	30.00
6.39	468.00	6.40	3.70	62.00	2490.00	2720.00	1350.00	128.00	1660.00
5.08	448.00	1.60	1.50	63.00	2192.80	2380.00	1260.00	44.00	1400.00
2.83	465.00	0.40	2.60	85.00	2559.20	410.00	2240.00	26.00	1250.00
0.42	525.00	1.60	3.80	78.00	2250.40	80.00	2820.00	70.00	1020.00

	Maximum	*Maximum*	*Maximum*	*Maximum*	*Maximum*	*Maximum*	*Maximum*	*Maximum*	*Maximum*
Distance (km)	*cond-data*	*ISS-data*	*DO-data*	*CBODs-data*	*No-data*	*NH4-data*	*NO3-data*	*Po-data*	*Inorg P-data*
9.60	312.00	13.80	9.80	20.00	2051.20	220.00	200.00	96.00	30.00
6.39	536.00	10.20	5.90	15.00	3666.80	7060.00	2520.00	260.00	2290.00
5.08	536.00	5.40	8.40	12.50	3902.80	5140.00	3020.00	156.00	2170.00
2.83	536.00	2.20	12.20	10.50	4122.40	3020.00	4060.00	96.00	1910.00
0.42	557.00	36.20	12.00	15.30	4488.00	1600.00	4200.00	242.00	1400.00

Figure 2. Water quality minimum and maximum input data.

2.4 Configuration on temperature data

Figure 3 shows the distances of first modified model to suit the distance of the total 10 km length of Penchala River that was used in this study area. From observation data at a distance of 0.42 km, the mean temperature data was at 14.9 °C. At distance of 2.83km, the mean temperature data was at 16.13 °C. At distances of 5.08 km, 6.39 km and 9.6 km of the river the mean temperature data was 15.66, 17.2, and 14.9°C respectively. The temperature data had to be changed and modified from the default data to the observation data. The observation data collected from UNITEN's database were basically the data used as most of the input data in this model.

Distance x(km)	Mean Temp-data	Minimum Temp-data	Maximum Temp-data
9.60	14.90	12.00	18.60
6.39	17.20	14.60	20.10
5.08	15.66	13.50	19.00
2.83	16.13	13.00	20.00
0.42	15.69	12.10	21.00

Figure 3. Modified temperature data.

3 RESULTS

The maximum amount of pollutant loads were considered for each output parameter, in order to calculate the amount of percentage of reduction and determine the TMDL. As seen in Table 1, NH_4 has the maximum amount of 5 mg/l load after simulation of the model. For BOD, TSS and DO, the maximum simulated pollutant loads were 23 mg/l, 14 mg/l and 12.5 mg/l respectively. In terms of total phosphorus and total nitrogen, the loads were at 100 mg/l and 23 mg/l respectively. The last two parameters simulated in this model were pH and NO_3. Maximum NO_3 load was at 25 mg/l and pH was 9 respectively.

Table 1. Simulated Result From QUAL2K.

Parameters	Simulated Pollutant Loads From Qual2k Modelling
NH4	5 mg/l
Biochemical Oxygen Demand (BOD)	23 mg/l
Total Suspended Solids (TSS)	14mg/l
Dissolved Oxygen (DO)	12.5 mg/l
Total Nitrogen (TN)	100 mg/l
Total Phosphorus (TP)	23 mg/l
pH	9
NO3	25 mg/l

3.1 Dissolved Oxygen

The simulated graph of the maximum load was 6.2 mg/l when located at 5-kilometre mark of the study area. DO load was progressively decreasing as the distance of the river increases. Chin (2006) states that the increase of BOD from the river affects the decrease of DO because DO is consumed by bacteria when large amounts of organic matter from sewage or other discharges were present in the water. The observed DO or pH may be expected to be somewhat higher than the daily average that the model predicts for the data collected in the afternoon (Chin, 2006). Pelletier and Chapra (2005) states that the DO levels decreases during the night hours because of lower rates of photosynthesis by river plants. The decrease of dissolved oxygen was apparent during low flow periods. The impacts of low dissolved oxygen concentrations will eventually lead to an unbalanced ecosystem in the river.

3.2 Ammonia

From Table 4, the maximum simulated load was 5 mg/l and at the 6 km mark. The amount of NH_4 load increases as the distance increases. When ammonia reaches the soil surface, it usually reacts with water in the soil. From this reaction, it will converted into its ionic form, ammonium (NH4+) and will be absorbed in to the soil (Kunwar, 2004). Ammonia usually comes from domestic, industrial or agricultural pollution, primarily from fertilizers, organic matter or fecal matter (Kunwar, 2004). Ammonia levels in excess from the recommended limits may harm aquatic life. Ammonia toxicity is thought to be one of the main causes of unexplained losses in fish hatcheries. Although the ammonia molecule is a nutrient required for life, excess ammonia may accumulate in the organism and cause alteration of metabolism or increases in body pH.

3.3 Nitrate

The simulated graph of the maximum load was at 25 mg/l and located from the start point of the river to 5.8 kilometer mark of the study area. Nitrates also come from the earth. Soil that contains organic matter will contain nitrogen compounds. Just like the ammonia in water, these nitrogen compounds in the soil are converted by bacteria into nitrates (Owens et al., 1964). In this study, sources of excess nitrates come from human activity. The source of excess nitrates can usually be traced to agricultural activities, human wastes, or industrial pollution near the study area.

3.4 Total Nitrogen

At distance of 6 km of the study area, the maximum pollutant load after the simulation of the graph was at a load of 100 mg/l. The increase of Nitrogen can lead to overstimulation of growth of aquatic plants and algae. Excessive growth of these organisms, in turn, can clog water intakes, use up dissolved oxygen as they decompose, and block light to deeper waters (Chin, 2006). Porcella and Soresson (1980) suggested that the drop in respiration efficiency of fish and aquatic invertebrates can occur, leading to a decrease in animal and plant diversity, and affects our use of the water for fishing, swimming, and boating.

3.5 Total Phosphorus

At distance of 6.2 km of the study area, the maximum pollutant load after running the model was at 23 mg/l. Phosphorus starts to increase at distance 6 km of the total length of study area of Penchala River. Phosphorus gets into water due to urban and agricultural settings. At 4 to 8 km distance of river, the present of residential areas was distinct. The highest load of TP was at the point distance of 6 km to 8 km. Phosphorus tends to attach to soil particles and, thus, moves into surface-water bodies from runoff. Phosphorus can also migrate with groundwater flows.

3.6 Total Suspended Solids

At distance of 6.2 km of the study area, the maximum pollutant load after the simulation of the graph was at a load of 14 mg/l. The presence of car and machinery factories along the distance of 6 km to 10 km give rise to higher loading of TSS at these distances. The largest amounts of solids were usually generated from construction activities, agriculture, unpaved surfaces, and waste management (Chin, 2006).

3.7 Biochemical Oxygen Demand

The maximum pollutant load after the simulation of the graph was at a load of 12 mg/l due to which the dissolved oxygen level along the river was less than minimum permissible limit. Due to the increment of pollutant loads such as TP, NH_4, TN and TSS, the loads instantly effects the BOD of the river making the load to also gradually increase. In such circumstances, it is because the sewerage from commercial and residential areas along the river has poor waste management (Owens et. al., 1964). The increament of BOD may due to urban runoff that carries wastes from streets and sidewalks; nutrients from lawn fertilizers; leaves, grass clippings, and paper from residential areas, which increase oxygen demand (Liu et al., 2008).

3.8 pH

The input pH was at its maximum at pH 9. At distance of 6 km of the study area, the maximum pH recorded after the simulation of the graph was at a pH of 8. The results start decreasing at 6.2 km distance. The decreasing in pattern may be due to constant human activity and a large portion of industrial area in the geographical scope. Liu et al. (2008) suggested that the level of pH decreases due to release of CO2 in water column.

3.9 Pollutant Load Allowable

To determine whether the pollutant load reached the target goal, the pollutant loads were compared between the maximum allowable load and the loads after reduction. The maximum allowable load for different pollutant parameters were obtained from WQI table (DOE). This means that the amount pollutant load achieved must be less than the maximum allowable load and also attain the required water quality standard of Class II. Before the pollutant load meets its target goal, the maximum allowable load must be determined. Different BMPs have different pollutants load reduction capabilities. After determining the amount of pollutant load reduction, different BMPs can contribute. The pollutant loads derived from the water quality model was multiplied with the percentage of the reduction. The total was considered to be the pollutant load after reduction. The pollutant load was achieved the target goal when the pollutant load obtained after going through a BMP reduction was less than the maximum allowable load.

Table 2. The summary of BMPs types and the total number of the pollutant loads that attain a required WQS after load reduction.

Four staged wetland		Floating Constructed wetland		Bio retention System	
Type of pollutant load	Achieve required Water Quality Standard (YES/NO)	Type of pollutant load	Achieve required Water Quality Standard (YES/NO)	Type of pollutant load	Achieve required Water Quality Standard (YES/NO)
NH_4	NO	NH_4	NO	TSS	YES
NO_3	YES	NO_3	YES	TP	NO
TN	YES	BOD	NO	TN	NO
TP	NO	COD	YES	NO_3	NO
CBOD	YES	TSS	YES	CBOD	NO
Total number of pollutant loads that attain a required WQS	3		3		1

Table 2 represents the summary of four staged constructed wetland, floating constructed wetland and bio retention system with the type of pollutant loads from the different BMPs from this study. It also summarizes whether the pollutant load parameters achieved the target goal or not. The pollutant load that does not achieve the target goal is the ones that still exceed the maximum allowable load of the river even after reduction has been done. The pollutant loads that do meet the target goal had successfully been reduced to the amount of load without exceeding the maximum allowable load.

4 CONCLUSION

Based on the observation data and the results of the simulation of water quality modeling using QUAL2Kw, most of the pollutant loads in the Penchala River exceeded the maximum allowable load or also known as the total maximum daily load. To mitigate this situation, a storm water treatment facility can be introduced near the river. Three types of storm water treatment facilities are also proposed in this study. The uses and benefits of each and every storm water treatment facility are evaluated in reducing the amount of pollutants. From the observations and analysis, the four stage wetland is the best at reducing the pollutant loads. Most of the pollutant loads achieved reduction even when there was some load that still exceeds the allowable load. Comparing to the floating constructed wetland, the reduction efficiency of the four stage wetland is similar. In a situation where land or space is limited near the river, floating constructed wetland is used as the next best option.

ACKNOWLEDGEMENTS

The authors like to acknowledge Centre for Sustainable Technology and Environment, Universiti Tenaga Nasional (CSTEN), UNITEN Internal Grant (UNIIG) and Department of Irrigation & Drainage Malaysia (DID) for their support and collaboration in making this project successful.

REFERENCES

Chin, D.A. (2006). *Water Quality Engineering in Natural Systems.* Hoboken, New Jersey: John Wiley & Sons, Inc, 454.

Department of Environment, M.O.E. (2014). *Malaysia Environment Quality Report,* DOE.

Kunwar, P.S. (2004). Multivariate Stastical Techniques for the Evaluation of Special and Temporal Variation in Water Quality of Gomtiriver (India). *Water Research,* 38(18), 3980-3992.

Liu, Y., Yang, P.J., Hu, C. & Guo, H.C. (2008). Water Quality Modeling for Load Reduction under Uncertainty: a Bayesian Approach. *Water Research,* 42(13), 3305-3314.

Lung, W.S. (1993). *Water Quality Modelling: Application to Estuaries*. CRC Press, 208.

Owens, M., Edwards, R.W. & Gibbs, J.W. (1964). Some Reaeration Studies in Streams. *Air Water Pollution,* 8, 469-486.

Pelletier, G.J. & Chapra, S.C. (2005). QUAL2Kw Theory and Documentation (version 5.1), a Modeling Framework for Simulating River and Stream Water Quality. Available: www.ecy.wa.gov/programs/eap/models [Accessed 10/05/2016].

Porcella, D.B. & Sorenson, D.L. (1980). *Characteristics of Nonpoint Source Urban Runoff and its Effect on Stream Ecosystems*. Corvallis Environmental Research Laboratory, Office of Research and Development, U.S. Environmental Protection Agency, EPA, 100.

COMPARISON AND ANALYSIS OF DIFFERENT METHODS FOR THE PEAK DISCHARGE ESTIMATION FROM DRAINAGE BASINS RUNOFF IN SAUDI ARABIA

MATTEO VENTURA[1], FABRIZIO CABAS[2], GIOVANNI COSTANTINI[3] & CHIARA CESALI[4]

[1,2] Hydraulics and Hydrology Specialist, Italferr Spa, Rome, Italy
m.ventura@italferr.it; f.cabas@italferr.it
[3] Hydraulics and Hydrology Consultant, Italferr Spa, Rome, Italy
acq2304@gmail.com
[4] Ph.D. Student, Dept. of Civil and Information Engineering, University of Rome 'Tor Vergata', Rome, Italy
chiara.boz@tiscali.it

ABSTRACT

The lack of hydrological data records, and in particular of discharge measurements, represents, in the arid and semi-arid regions, a critical aspect that many authors, engineering firms and organizations have faced in the last few years, in order to define reliable methods and equations for the estimation of the peak discharge from drainage basins, applicable to infrastructures, flood defense and groundwater management projects. The present article shows the main results of a study conducted during the design of *The Saudi Landbridge Railway Project* (client: S.A.R.) for an elevated number of watersheds in the Central Regions of the Kingdom of Saudi Arabia. In these areas, the only available rainfall data with acceptable time interval of records and an adequate spatial distribution, are the daily cumulative rainfall depths. Suitable peak discharge estimation methodologies with this type of data were investigated; particularly, three different methods for the Peak Discharge Estimation related to a Return Period of 1 in 100 year ARI (Average Recurrence Interval) were considered: *Regression Equation* (Saudi Ministry of Transportation), *Talbot Equation*, and *HEC-HMS software* (using SCS method). Since it is the only method that takes into account both the actual rainfall phenomenon and the ground features through the so-called Curve Number (CN), HEC-HMS method has been considered as a base reference in comparison with the other methods. The suitability of this method for the territory of the KSA has been verified through a calibration analysis, using available local information and existing studies. The comparison between the different methodologies, for different drainage basin dimensions and for different locations within the area of study, showed that the Talbot and the Regression Equations are affected by a considerable error in the estimation of peak discharge; conversely, the HEC-HMS method provides reliable estimations of the Peak Discharge for engineering purposes in these zones.

Keywords: Kingdom of Saudi Arabia; hydrologic analysis; peak discharge; arid zones hydrology.

1 INTRODUCTION

The estimation of peak discharge of hydrographic basins is a primary element for the hydraulic design of drainage and flood protection structures. For the transport infrastructures, such as railroads and highways, generally crossing a relevant amount of watersheds with different geological, morphological and pluviographic characteristics, the choice of the method that has to be applied for the peak flow calculation of each basin, could constitute an important challenge. It has been widely stated that the major limitation of the development of arid zone hydrology is the lack of high quality observations (Wheater, 2002), where suitable recordings are not available along the alignment, especially in desert non-urban areas, it is hence necessary to investigate the most appropriate method that optimizes the collected data and leads to the best performance in terms of safety and economic sustainability of the project.

For this study that was performed for the *Saudi Landbridge Railway Project (Section 2)*, the only data obtained for a suitable spatial and temporal distribution were the 24-hours cumulated rainfall depths. In fact, especially for the gauging stations located in remote areas, the new generation pluviographs allowing the measurement of short rainfall durations were recently installed and, in most cases, need maintenance. Thus, due to their short operation period, these pluviographs with difficulty in providing rainfall data for an adequate statistical analysis.

As a consequence of the above mentioned considerations, the method to estimate the peak discharge should meet the following requirements:

- Reliable results with the available data.
- Not excessive overestimations of the peak discharge (to limit the dimensions and hence the costs of the structures)
- Easy application (because of the huge number of basins to study)

Different methods can be adopted to estimate the peak discharge, and can be divided into two following main categories:

- Methods that do not require rainfall data analysis;
- Methods that require rainfall data analysis;

The first group includes the Modified Talbot Formula (Wilson Murrow Consultant, 1971) and the Regression Equations that have been widely used for ungauged basins in the Kingdom of Saudi Arabia. The second group includes the SCS-DUH (Dimensionless Unit Hydrograph) Method (Mc Cuen, 1982) and the Rational Method (Mc Cuen, 2002). The SCS method has been implemented using the HEC-HMS software (U.S. Army Corps of Engineers, 2000).

The main purpose of this paper is to compare the design peak discharge values (1 in 100 year ARI) for 62 large watersheds (sized between 1,258 and 35,944 hectares) within the Riyadh Region by using different methods, i.e. the Modified Talbot empirical approach; the Regression Method, and the SCS Unit Hydrograph (HEC-HMS modeling with Type 2 distribution) method. The SCS method is considered to be the most reliable, since it is based on actual rainfall data; however, a calibration analysis was performed to verify the suitability of this approach for the study area.

2 DESCRIPTION OF STUDY AREA

The study area is located in the central part of Saudi Arabia, in the Riyadh Region (Figure 1). The Saudi Arabian regions are typically characterized by the *wadis*; a wadi is an ephemeral stream in which runoff is present for only a limited time, mostly during and after a rainstorm event. In some seasons, wadis become conveyors of runoff, flood or flash floods that carry away large amounts of sediment, leaving a marked imprint on the landscape. Permanently flowing water often exists in the gravels below the surface of a large wadi subsurface terrain. As all arid and semi-arid regions of the Kingdom of Saudi Arabia, the selected basins are characterized by short-lived and often very intense rainfalls. As a result of the thin top soils cover, most of the rainfall runs directly off the surface and the downslope infiltration in deep soils is limited.

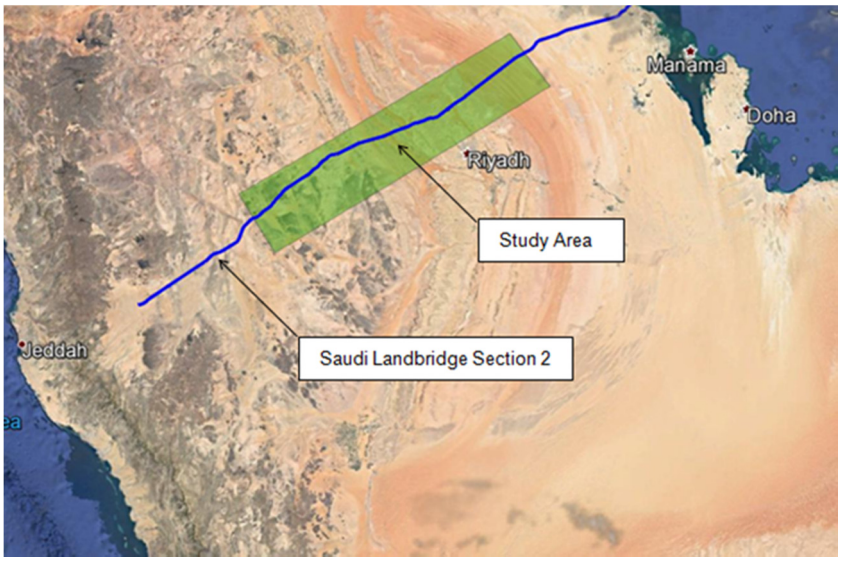

Figure 1.Location of the study area.

3 HYDROLOGICAL MODELLING

3.1 Basic assumptions

The computed design flood estimates (peak discharge) according to historical rainstorm records are based on certain assumptions and are subject to some restrictions. The basic assumptions related to computation of peak discharge are:

- regional daily rainfall data of good quality with reasonable representation of the 24-hour precipitation pattern in the area;
- rainfall intensity is uniformly distributed over the entire drainage area which contributes to the peak discharge when the time of concentration has elapsed;
- rainfall intensities assumed as uniform spatially and temporally during a storm and storm cells are relatively significant enough that extreme rainfall intensities for a given rainstorm are uniform;
- the frequency of peak discharge is the same as the rate of the rainfall intensity for the given time of concentration;

- watershed comprises similar characteristics throughout the area, and the Coefficient of Runoff (C) value is assumed as constant and uniform;
- the run-off is directly related to rainfall and rainfall excess for a given return period will produce the run-off of the same return period;
- Time of Concentration is equal to duration time to get the maximum peak flow discharge;
- runoff characteristics of drainage basins are assumed as constant during design period with no change in land use and surface conditions;
- Curve Number (CN) values have been evaluated through geological and land use maps;
- the boundaries and other physiographical parameters of catchment areas of wadis (stream channel) were determined by DSM maps (30x30 mesh) and spot elevations given on published topographic maps (scale 1:50,000).

3.2 Available rainfall data and statistical analysis

Adequacy of recorded rainfall data is required to perform a reliable statistical analysis of the rainfall distribution, and that is one of the basic input design parameters for railway drainage structures.

The KSA territory, in general, has a lack of information regarding the rainfall measures both in terms of spatial distribution of gauging stations and event recording data (Pluvio), as well as the daily rainfall recording series data (years).

However, a comprehensive set of data for a considerable number of gauging stations were collected and analyzed. The obtained rainfall data represents the daily (24-hour) cumulative measurements recorded with different recording periods and variable time frames of operation.

In flood frequency analysis, the Gumbel distribution were adopted to estimate the 1 in 100 year 24h rainfall depth.

3.3 Methods to estimate the peak discharge

3.3.1 HEC-HMS modelling

The Hydrologic Modelling System HEC-HMS is a product of the Hydrologic Engineering Center of the U.S. Army Corps of Engineers (http://www.hec.usace.army.mil/ software/hec-hms/).

It is designed to simulate the complete hydrologic processes of watershed systems. The program includes many traditional hydrologic analysis procedures such as event infiltration (e.g. Green Ampt, Smith Parlange.), unit hydrographs (e.g. Clark, Snyder, and SCS) and hydrologic routing (e.g. Muskingum and modified Puls methods).

HEC-HMS also includes procedures necessary for continuous simulation including evapotranspiration, snowmelt, and soil moisture accounting. The program features a completely integrated work environment including a database, data entry utilities, computation engine, and results reporting tools. The program allows selecting from a variety of precipitation meteorology models, loss methods and transform methods.

First of all, for the estimation of the peak-runoff, HEC-HMS requires the choice of an input hyetograph. Different methods to simulate a storm event are provided; when specific recordings of storms are not available, it is possible to choose a user specified SCS time distribution (Type 1, 1a, 2 or 3) entering a 24h total storm depth. The most conservative hyetograph curve *Type 2* were chosen. This rainfall distribution were developed for the arid zones of U.S.A. and encompassed a huge number of severe thunderstorms of different durations (Mc Cuen, 1982; 2002; Ponce, 1989). For the use of the SCS unit hydrographs, the software requires to digit a Lag Time and the Curve Number of the watershed. A Curve Number of 90 were considered, since it corresponds to the most conservative soils encountered. The Lag Time of the basins were estimated equal to 0.6 Tc (Time of Concentration) (Mc Cuen, 2002).

3.3.2 Modified Talbot Formula

The empirical “Modified Talbot Formula” was developed in Saudi Arabia by the MOT (Quraishi and Al Hassoun, 1996) in order to estimate the amount of floods for different areas, particularly for catchments areas where actual flood records are not available. This method was used to estimate the amount of runoff generated from all drainage areas.

Flow estimation in the “Modified Talbot Formula” depends upon the catchment areas as follows *(Large Watersheds 1,258 ha < S < 35,944 ha)*:

$$Q_{100} = K \cdot \varphi \cdot S^{n} \cdot R_{f} \cdot 1.4 \qquad [1]$$

Q_{100} being the peak discharge for the 1 in 100 years storm (in m^3/s); the constant K assumes the values 3.561 for large watersheds; S, the catchments area (in ha); φ, the coefficient of discharge depending on terrain condition, slope of drainage area and shape factor: φ = C1+C2+C3 (C1 is the coefficient of terrain condition,

C2 is the coefficient of slope of drainage area and C3 is the coefficient of shape of drainage area). The exponent *n* assumes the values 0.5, R_f is the rainfall factor which was suggested to be 1.4.

3.3.3 Regression Method

The Regression method were developed for use in the arid and desert-like regions of the southwest part of the United States; the M.O.C. (Kingdom of Saudi Arabia Ministry of Communication) proposed an adjustment of the equation for their use in Saudi Arabia.
The method considered different equations depending on the Hydrologic Region of reference; for the region related to the study area, the equation assumes the following form:

$$Q_{100} = 0.0969 \cdot S^{0.610} \cdot E^{-1.30} \cdot P^{0.915} \qquad [2]$$

where Q_{100} is the design flood discharge [m^3/sec] for 100 years ARI (adopted for railway works); S is the drainage area (in km^2); E is the mean basin elevation (in 10^3 m a.s.l.); P is the mean annual precipitation (in mm).The value of the mean annual precipitation can be obtained from Figure 2 (Alazba, 2004).

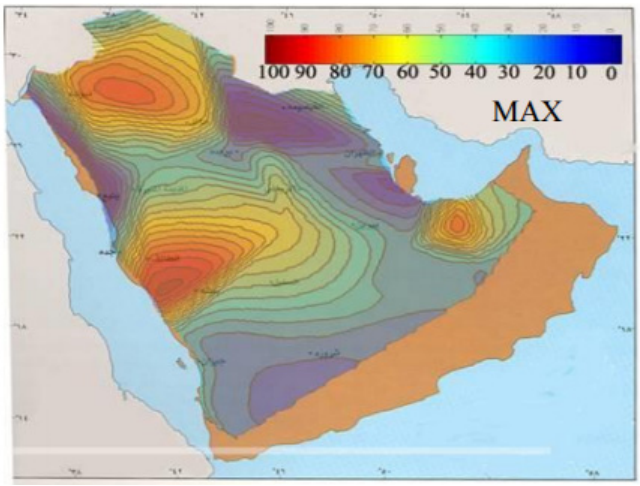

Figure 2. Regression Method: maximum annual rainfall depth distribution.

4 PEAK DISCHARGE CALCULATIONS AND DISCUSSIONS

The results obtained with the three methods and for the selected basins are shown in Figure 3.

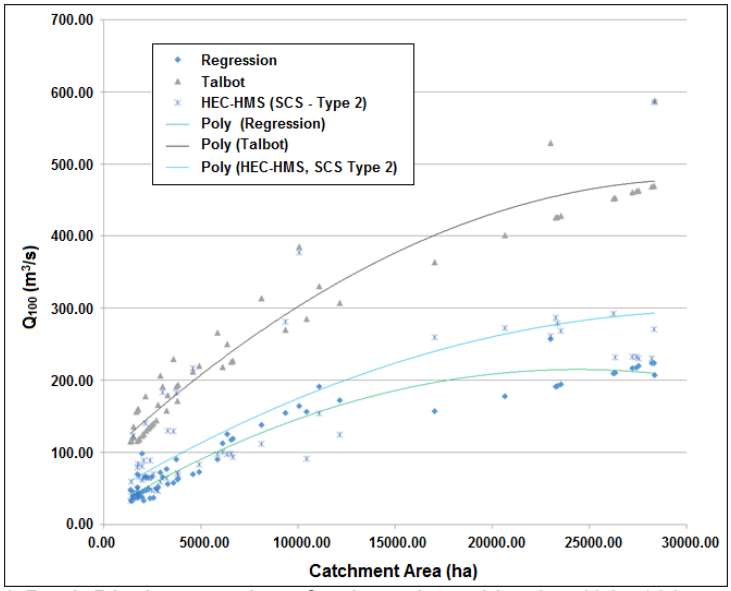

Figure 3.Peak Discharge values for the selected basins (1 in 100 years ARI).

Basically, the Talbot formula provides the higher values of the peak discharge, confirming the results obtained by previous studies (Fouli et al., 2016; Quraishi and Al Hassoun, 1996). The Regression method, included in the M.O.C. Highway Design Manual, leads to the lower values. HEC-HMS calculations, computed

with 24-hr rainfall and SCS Type 2 distribution, gave an intermediate value that is allegedly to be considered more reliable, since it is based on more accurate modeling and actual rainfall data.

However, the results were obtained through cumulative daily rainfall depths adapted to dimensionless hyetographs (Type 2 curves) that are not representative of the actual time distribution of the storms typical of the study area. For this reason, an additional effort of calibration had to be made to validate the results obtained with this method and to justify its use in the peak discharge estimations for engineering purposes. In fact, the main aim of the present paper is not to model the exact hydrograph shape that could be produced by a given storm, but to find an easy and reliable method to estimate the design peak discharge of different watersheds in the study area, when only 24-hr rainfall data are available.

5 CALIBRATION AND COMPARISON OF THE RESULTS

5.1 Calibration Methodology

Since no official discharge measurements are available, the following steps were followed to carry out the calibration of the results computed with HEC-HMS (SCS Type 2 distribution):

i. Selection of a representative watershed within the study area
ii. Peak discharge estimation of an actual past storm event, through the collaboration of information obtained by the interviews of local eye-witnesses
iii. Peak discharge estimation of the above mentioned storm event, by modeling the runoff with HEC-HMS software and using specific dimensionless rainfall hyetographs valid for the Riyadh Region (Elfeki et al., 2013), re-scaled on the actual 24-hr rainfall that produced the observed runoff, and for a duration equal to the Time of Concentration of the studied watershed.
iv. Peak discharge estimation of the selected basin, for the above mentioned storm event, applying the Rational Method and using the rainfall intensity derived from specific IDF curves for the Riyadh Region (Al Hassoun, 2011) for a Time of Return derived by the frequency analysis performed for the closer gauge station (Figure 5).
v. Comparison of the results.

5.1.1 Selection of the watershed (Step I)

The following criteria for the choice of the basin are adopted:

- The selected watershed should be as close as possible to a gauging station
- Size between 1,258 and 35,944 ha (Large watersheds by the Talbot method classification), consistently with the range considered in the current study
- Conservative geological features in terms of soil type (low infiltration capacity)
- The selected watershed should be as close as possible to areas where other studies were performed and where it is possible to obtain IDF curves and specific hyetographs
- An adequate presence of local inhabitants or resident shepherds along the wadi

The selected watershed that fulfills all the above mentioned requirements is shown in Figure 4.

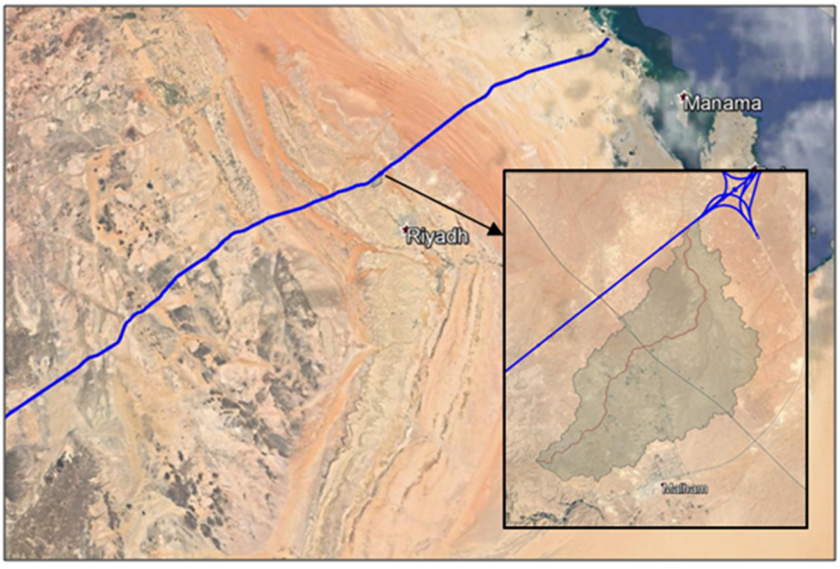

Figure 4. Calibration analysis: location of the selected watershed.

The main morphological features of the selected drainage basin are reported in Table 1.

Table 1.Morphological parameters of considered basin.

Catchment Area (ha)	Main stream length (km)	Difference in Elevation (m)	Mean slope (m/m)	Maximum Elevation (m a.s.l.)	Minimum Elevation (m a.s.l.)	Time of Concentration (hours)
11067.1	24	120	0.005	731	611	6

5.1.2 Rainfall data and frequency analysis results

Table 2 lists the gauging station that was considered for the analysis of the selected watershed; Figure 5 shows the locations on the territory and the results of the frequency analysis using the Gumbel distribution.

Table 2.Rainfall gauging station considered in the calibration analysis.

ID	Lat	Long	Elevation (ma.s.l.)	Recording start year	Recording end year	Total years
00462	25.217	46.283	645	1964	2015	51

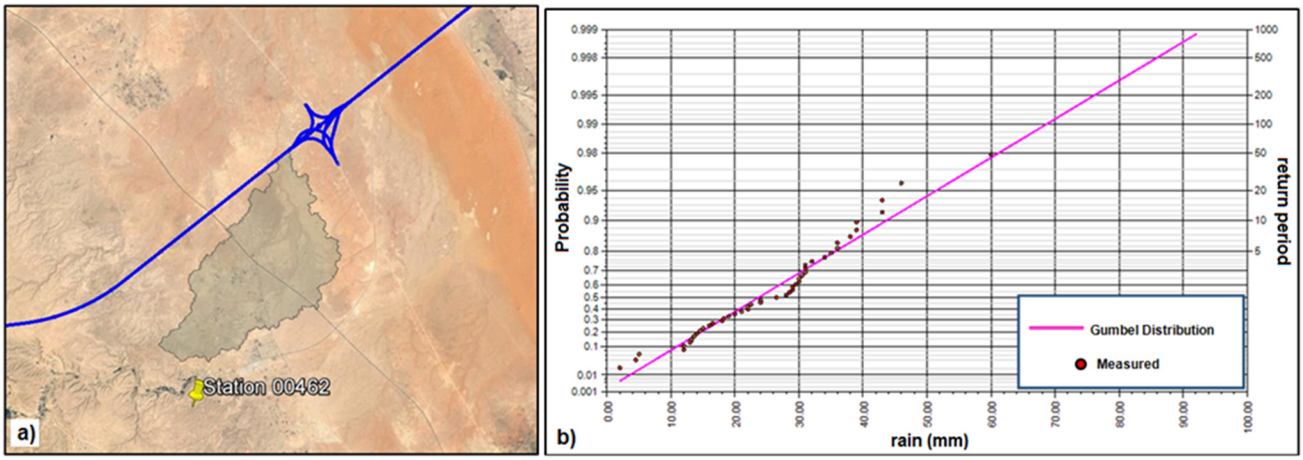

Figure 5. a) Location of considered rainfall station; b) Results of the frequency analysis.

5.1.3 Curve Number estimation

The Curve Number is the index that represents the combination of a hydrologic soil group and a land use and treatment class (Mc Cuen, 2002).

The soils of the studied areas are constituted primarily by shallow layers of limestones (Figure 6) which are mainly impervious and hence characterized by a low infiltration capacity, especially if the design storm event is preceded by another event that can saturate the superficial pervious layers.

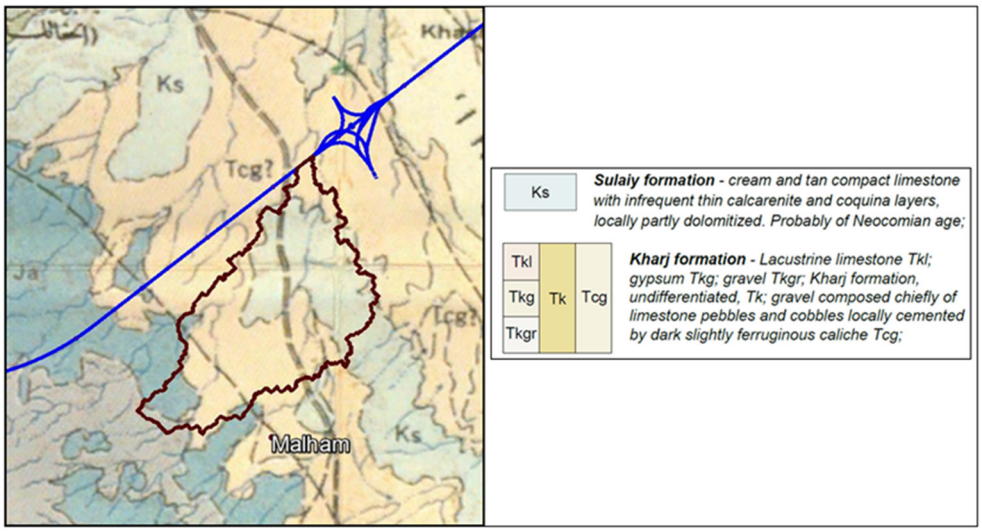

Figure 6. Geological Map of the study area.

The land is mainly featured by unpaved and desert surfaces, with pastures and rare crops. For these reasons, Group D soils were assumed, and desert shrub cover type, in poor hydrologic conditions were considered.

The corresponding CN value of these types of soils and land use is usually 88, however a CN = 90 was used as recommended by some authors for limestone soils (Sen, 2008).

The Modified Talbot Method and the Regression Equation do not take into account this parameter, that plays a key role in the rainfall-runoff processes and hence in the peak discharge estimations.

5.1.4 Indirect Peak Discharge Estimation by eye-witnesses information (Step II)

A relevant number of inhabitants, shepherds and Bedouins were interviewed to request information about the past flooding events they viewed, specifying the date of the observation, the maximum water level in the wadi and an idea of the velocity of the flow. The data and the location where the most reliable and accurate information have been obtained are shown in Figure 7.

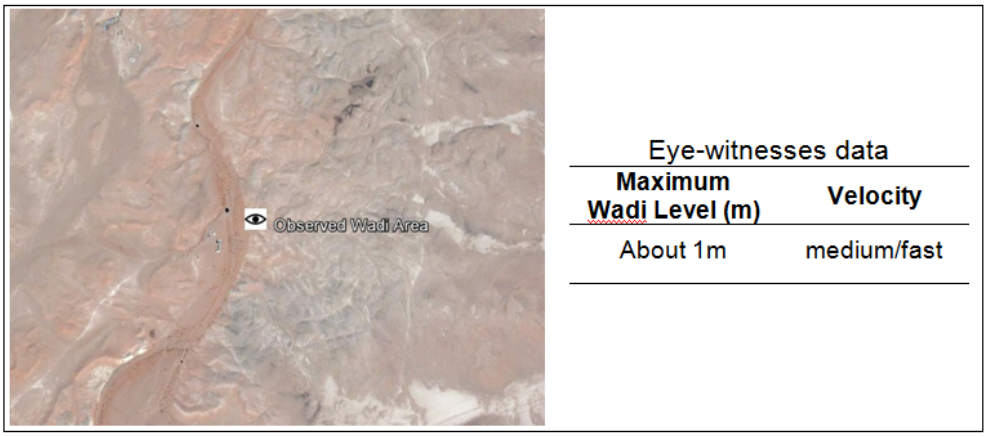

Figure 7. Eye-witnesses location map and data.

All the respondents referred their observations to a storm event that occurred between the 27th and the 28th of November 2016. Information collected on the web weather archives reported a 24-hr rainfall depth of roughly 20 mm in those two days (font: www.meteoblue.com). According to the performed frequency analysis (Figure 5), this event can be associated to Time of Return of 3 years.

To complete the analysis, a stretch of the wadi was modeled using a detailed DSM (Digital Surface Model). The flow rate of the observed event was then derived with an iterative process with the HEC-RAS software (Figure 8), trying different input discharge values and Manning's roughness coefficients, until the observed water levels in steady flow conditions were obtained.

For a wadi stretch of about 300 meters across the observation point, the HEC-RAS results led to water depths varying from 0.9 to 1.3 meters and maximum flow velocities of 1.16 m/s, matching with the collected information.

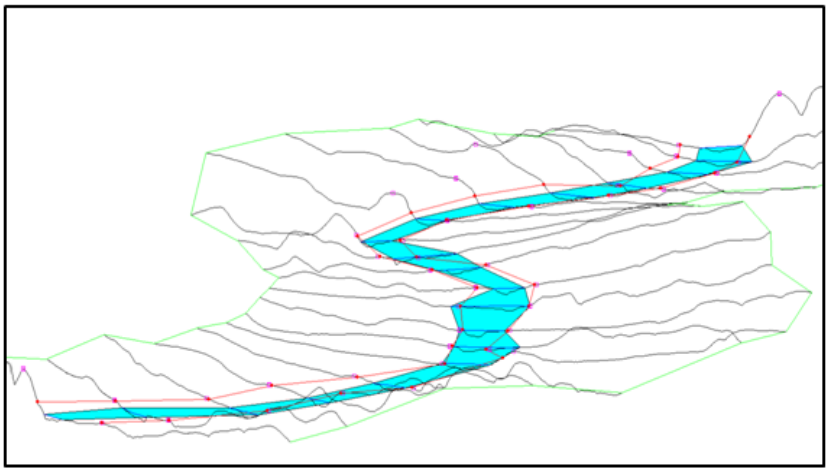

Figure 8. HEC-RAS modelling for the selected wadi.

5.1.5 Peak Discharge Estimation with specific hyetographs (Step III)

Several dimensionless hyetographs for some regions of KSA are available in literature (Elfeki et al., 2013). The Hyetographs obtained for the Riyadh Region was used in the present study, rescaling the 24-hr

rainfall depth of 20 mm (observed event) for a fixed duration event of 6 hr (with the assumption that the event duration time is equal to time of concentration to get the maximum peak flow discharge).

The discharge was then calculated with HEC-HMS software by applying the *Specified Hyetograph precipitation method* option.

5.1.6 Peak Discharge Estimation with Rational Method (Step IV)

The Rational Method for peak discharge estimation is usually applied for basins with areas smaller than 50-80 ha. However, to have an additional parameter for comparison and validation, it was applied to the studied watershed, considering an Areal Reduction Factor (ARF) to reduce the over-estimation effect due to the features of this method, which assumes the rainfall intensity homogenous for all the catchment area.

The peak discharge was derived using the following equation:

$$Q_p = \frac{C \cdot S \cdot i \cdot ARF}{360} \quad [3]$$

where *C* is the Runoff Coefficient which is assumed to be equal to 0.45; *S* is the area of the watershed in hectares; *i*, the Rainfall Intensity (mm/h); ARF is the Areal Reduction Factor equal to 0.95 (Mc Cuen, 2002). The rainfall intensity was derived using the following equation (Al Hassoun, 2011):

$$i_T = \frac{153 \cdot T_r^{0.35}}{t_d^{0.82}} \quad [4]$$

where i_T is Rainfall Intensity for a given Time of Return and storm duration (mm/h); T_r is the Time of Return (years); t_d is storm event duration (minutes). For large basins (catchment area > 50 ha), the following relationship can be applied to compute t_d (Almeida et al., 2014):

$$t_d = 0.191 \cdot L^{0.76} \cdot i^{-0.19} \quad [5]$$

where *L* is the main stream length (in km); *i* (m/m), the main slope.

5.2 Results of calibration and discussions

The results obtained through the above methods are shown in Table 3 together with the value of the peak discharge calculated with HEC-HMS (Type 2 distribution).

Table 3.Values of peak discharge Q_3, computed through different methods, for the considered basin.

Q_3 (m^3/s)			
HEC-HMS (SCS Type 2)	**Indirect Eye-Witness (Step II)**	**HEC-HMS (Step III)**	**Rational Method (Step IV)**
20	19	20	23

As shown in Table 3, the discharge values estimated with the different methods are very close to the value calculated with HEC-HMS (Type 2 distribution).

A further verification were performed by comparing the HEC-HMS (SCS Type 2) results with the results obtained from HEC-HMS (Step III) and Rational Method, including further 7 basins in the study area (with Time of Concentration equal to 3, 6 and 12 hours) and considering a Time of Return of 100 years.

The rainfall depths for the different durations were derived by DDF curves (Duration – Depth - Frequency) related to the IDF curve of Riyadh (Equation 4). The obtained results are shown in Table 4 and in Figure 9.

Since the observations related to actual storm events of 1 in 100 years ARI (Average Recurrence Interval) are not available, it is not possible to calibrate the method with recorded flow data. However, the following comparison is useful to confirm, with a certain level of accuracy, the reliability of the proposed method.

Moreover, it is worth to observe that the use of the IDF and DDF curves for deriving the 24-hour rainfall depths should ensure a consistency between the input data of the different methods and hence to validate the approach rather than the obtained values. For the design applications, the 24-hour rainfall data derived from the statistical analysis of the gaging stations should be used.

Figure 9 and Table 4 confirm that, even for a higher Time of Return, the use of the HEC-HMS SCS-Type 2 distribution for the peak discharge estimation leads to values comparable to the flow rates calculated with other methods, based on local IDF curves and rainfall distribution hyetographs.

Table 4.Values of peak discharge Q_{100} computed through different methods, for considered basins.

Catchment Area (ha)	Tc (hours)	DDF 24-hr Rain Depth (mm)	DDF Tc Rain Depth (mm)	Rainfall Intensity (mm/hour)	HEC-HMS SCS Type 2 Q_1 (m^3/s)	HEC-HMS Method (III) Q_2 (m^3/s)	Rational Method Q_3(m^3/s)
513	3	47	33	10.78	8.3	5.7	7.4
718.9	3	47	33	10.78	11.7	8.1	10.3
1,721.8	3	47	33	10.84	28.1	19.5	24.4
1,797	3	47	33	10.55	28.1	19.5	24.7
6,542	6	47	37	5.94	52.1	43.6	49.6
9,353	6	47	37	6.16	88.7	65.7	72.1
11,067	6	47	37	6.33	111	85.0	88.0
26,321	12	47	42	3.55	151	125.0	116.8

Furthermore, the peak discharge values computed with the proposed method and for the 1 in 100 year ARI (Average Recurrence Interval), are always slightly higher than the values obtained with the methods considered in the comparison.

This aspect is positive in a design context, since it leads to more conservative dimensioning and avoids excessive over sizing as this could occur using the Talbot Equation.

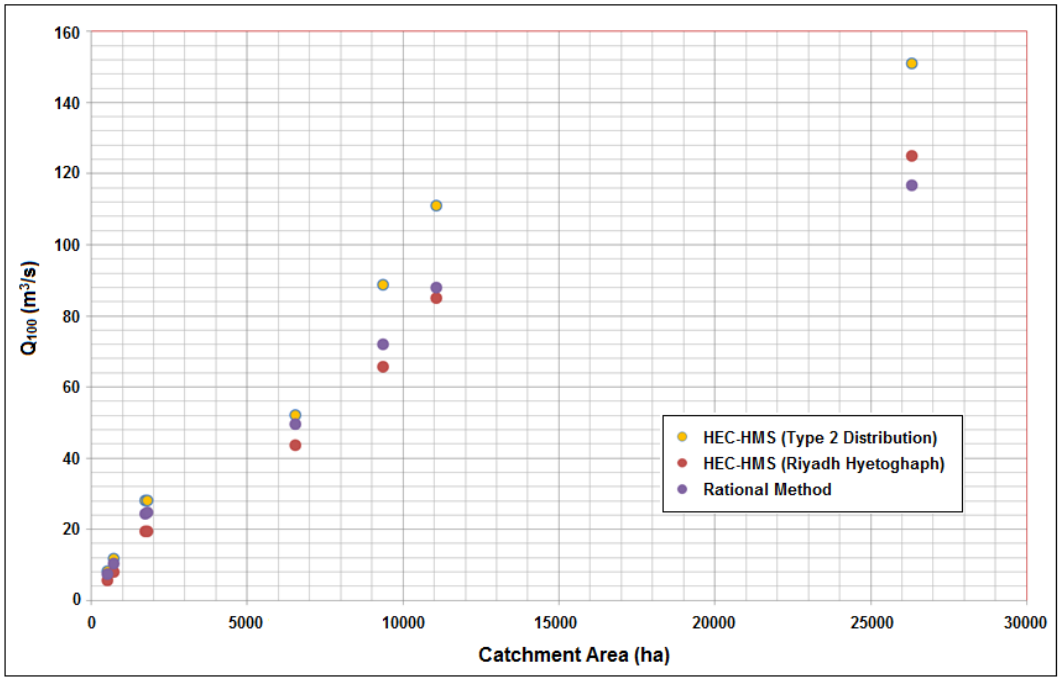

Figure 9. Peak discharge Q_{100} vs Catchment Area, for considered basins.

6 CONCLUDING REMARKS

The performed hydrological study has highlighted the need for a methodological approach for the peak discharge estimation to meet the requirements with the easy application and reliability of the results.

The performed study has shown that, for a relevant amount of watersheds, the Modified Talbot equation, in spite of its practical use, leads to excessive values of peak discharge consistently with other studies conclusions (Fouli et al., 2016; Quraishi and Al Hassoun, 1996). Conversely, the Regression Equation underestimates the peak flow rate, confirming substantially the error declared in the Highway Design Manual of the M.O.C. (Kingdom of Saudi Ministry of Communications). The reason for these inconsistencies can be found in the fact that both methods do not take into account actual rainfall data, the soil type and land use features (Curve Number). Even if the territory of the Kingdom of Saudi Arabia is affected by a lack of rainfall measurements, there is a relevant number of 24-hour cumulative rainfall recordings, with good spatial and temporal distribution.

The use of a method suitable with these types of data has been investigated, and subsequently the SCS method has been applied, processing the input data through the HEC-HMS software and considering a

Type 2 rainfall distribution. The results obtained for this approach have been compared with other methods, performing a calibration based on indirect peak discharge estimation of a recent actual storm event and using information available in the literature. The calibration outputs show a good fit for the HEC-HMS/SCS method that could be considered a reliable instrument in the peak discharge estimation for detail engineering purposes in the study area. However, the use of the Modified Talbot Method and the Regression Equations, is recommended where no information is available or in the feasibility studies where minor accuracy in the results is justified by a reduced level of detail and simplified calculations.

Finally, it is recommended in the future to carry on the research with additional efforts in the calibration process, obtaining official discharge measures of different wadis, together with adequate rainfall recordings of actual storm events.

AKNOWLEDGEMENT

The authors would like to thank Eng. Khanh Nguyen for the stimulating and inspiring debates held on the topic, and Eng. Emiliano Pacitti for the help in the computations.

REFERENCES

Alazba A.A. (2004). Contour Maps for Hydrologic and Climatic Parameters in Saudi Arabia. *ASAE/CSAE Annual International Meeting.*

Al Hassoun S.A. (2011). Developing Empirical Formulae to Estimate Rainfall Intensity in Riyadh region. *Journal of King Saud University – Engineering Science,* 23, 81–88.

Almeida I.K.(2014). Estimation on Time of Concentration of Overland Flow in Watersheds: A Review. *São Paulo, UNESP, Geociências,* 33(4), 661-671.

Elfeki A.M., Ewea H. & Alamri N. (2013). Development of Storm Hyetograph for Flood Forecasting in the Kingdom of Saudi Arabia. *Arabian Journal of Geosciences*, 7(10), 4387–4398.

Fouli H., AL-Turbak A.S., Bashir B. & Loni O.A. (2016). Assessment of a Water-Harvesting Site in Riyadh Region Kingdom of Saudi Arabia Using Hydrological Analysis. *Arabian Journal of Geosciences*, 9, 387-397

Mc Cuen, R.H. (2002). *Hydraulic Design Series No.2, Second Edition-Highway Hydrology*, U.S. Department of Transportation, Federal Highway Administration, National Highway Institute, Publication No. FHWA-NHI-02-001.

Mc Cuen R.H. (1982). *A Guide to Hydrologic Analysis Using Scs Methods*. Prentice-Hall.

Ponce V.M. (1989). *Engineering hydrology: Principles and practices*. Prentice-Hall.

Quraishi A.A & Al Hassoun S.A. (1996). Use of Talbot Formula for Estimating Peak Discharge in Saudi Arabia. Civil Engineering Department, College of Engineering, King Saud University, Riyadh, Saudi Arabia. *JKAU: Engineering Science,* 8, 73-85.

Sen Z. (2008). *Wadi Hydrology*. Taylor Francis Group, Boca Raton, 347.

U.S. Army Corps of Engineers (2000). *Hydrologic Modeling System HEC-HMS*: *Technical Reference Manual*, Hydrological Engineering Center.

Weather H.S. (2002*). Hydrological Processes in Arid and Semi-Arid Areas. Hydrology of Wadi System, IHP Regional Network on Wadi Hydrology in The Arab Region*, International Hydrological Programme, Technical Documents in Hydrology No.55, UNESCO, 5-22.

Wilson Murrow Consultant (1971). *Drainage Report 1971*, A Report Submitted to the Ministry of Communications, Riyadh, Saudi Arabia, 217.

SENSITIVITY ANALYSIS OF SPATIAL INPUT PARAMETER IN DISTRIBUTED HYDROLOGICAL MODEL

SITI HUMAIRA HARON[1], ISMAIL SAHID[2] NOR FAIZA ABD RAHMAN[3], KHAIRI KHALID[4], MUHAMMAD RADZALI MISPAN[5] & LARIYAH MOHD SIDEK[6]

[1, 2] Faculty of Science and Technology, Universiti Kebangsaan Malaysia, Bangi, Malaysia,
sthumaira10@gmail.com; ismail@ukm.edu.my
[3] Faculty of Engineering and the Built Environment, SEGi University, Malaysia,
doctor_cute84@yahoo.com
[4] Faculty of Civil Engineering, Universiti Teknologi MARA Pahang, Jengka, Pahang, Malaysia,
khairikh2011@gmail.com
[5] Malaysian Agricultural Research and Development Institute (MARDI),
radzali@mardi.gov.my
[6] Centre For Sustainable Technology and Environment, Universiti Tenaga Nasional (UNITEN), Putrajaya, Malaysia
drlariyah66@gmail.com

ABSTRACT

Hydrological model is an important tool in enabling the researchers to predict the runoff in the catchment areas and assess the water resources management practices. Distributed models must undergo calibration procedures before it is used to help in making decisions in the planning and management of water resources. Generally, manual calibration is performed repeatedly which is time-consuming and needs experienced staffs. This paper describes a semi-automatic approach for calibrating long term monthly streamflow periods estimated by the Soil and Water Assessment Tool (SWAT) hydrological model. After 26 repetitions, 9 SWAT input parameters reflect the sensitivity on the streamflow simulation. For Cameron Highlands river basin, the Runoff Curve Number (CN2.mgt), Base flow recession constant (ALPHA_BF.gw) and Groundwater delay time (GW_DELAY.gw) is found to be the most sensitive input parameters. CN2.mgt is established to be the most sensitive to surface respond parameter and followed by ALPHA_BF.gw and GW_DELAY.gw for subsurface response. Therefore, the next step needed is a long-term continuous hydrological modeling which is to be conducted into the SWAT 2012 model with all the selected sensitive SWAT input parameters in order to finalize the objective functions for the watershed.

Keywords: Hydrological modeling; monthly streamflow; SWAT input parameter; SUFI-2 algorithms.

1 INTRODUCTION

Water that is the end result of interactions between the atmosphere, land surface and the ocean will flow into the catchment area acting as a hydrological unit. River flow reflects the amount of water moving from the watershed to the channel and the number of discharges from the river. Flow can be influenced by several factors. River flow can be affected by natural and human factors. It can also respond to changes in the flow parameters. Evaporation and water consumption by plants significantly affect the flow of the river. Vegetation greatly affects the flow in the dry season. This is because when the temperature rises, the plants that grow on the banks of the river will use the most water. In addition, the flow is also affected by the water under the surface, but at a slower rate. Seasonal conditions, addition with increasing population pressure on water resources management. This applies particularly in the dry season, when water demand is high and supply from stream flow is low. Adequate stream flow can cause erosion, transport and deposition of sediments. Strong current will keep sediment longer in the riverbed. Therefore, prediction and assessment of river flow is important for watershed management, agriculture and sustainable development in the water resources sector.

Cameron Highlands catchment receives good amount of rainfall during the year and has ecological and economic diversity. It is located in the northern state of Pahang, Peninsular Malaysia. Apart from the hilly topography, highly intensive farming practices and deforestation in the basin causing great loss of productive land and water runoff. Thus, watershed management plans integrated based on hydrological simulation study using an appropriate model approach is required to evaluate this issue. The use of mathematical models for assessing the hydrological watershed is the current trend and extraction watersheds using hydrologic model based on parameter-in high-speed computer assisted tools and techniques for it. Therefore, the current study was conducted with the use of ground water assessment tool (SWAT) and SWAT CUP (calibration and program uncertainty) in the integration of remote sensing and GIS environment to estimate surface runoff trend in a long time. Watershed model calibration is a challenging task because of the uncertainty of input data, model structure and algorithm, parameterization and output obscurity. Sources of uncertainty structure model including processes are not taken into account in the model, such as activities that are not known in the catchment area and not just because of over-simplification of the process considered in model it. Input

uncertainty may be related to the improper size or determining the spatial model input parameters such as elevation data, land use data, rainfall, temperature and other data.

2 STUDY AREA

The study area is located in Cameron Highlands watershed, sub-basin Jelai in Pahang, Malaysia and is between the longitude 101°20”0’- 101°60”0’ E and latitude 4°50”0’-4°0”0’N, which covers approximately 25890.04 km^2 catchment area. The gauge station, Sungai Jelai, Kuala Nam (Kuala Lipis District) was selected as the outlet of the catchment (Figure 1). A brief description of the river basin is summarized in Table 1.

Table 1. Background Cameron Highlands watershed.

	Description
Catchment area	2 5890.04 km^2
Longitude / latitude	N04°30'17.0" - N04°25'52.70"
	E101°23'14.7" -E101°23'16.40"
Major river	Bertam River and Telum River
Gauge Station (river discharge)	4218416 Sg. Jelai at Kuala Medang
Rainfall station	4414037Ldg. Boh (Bhg. Boh)
	4414038 Ldg. Boh (Bhg. Selatan)
	4414040 Mardi C Highlands
	4513033 Gunung Brinchang C. Higlands
	4514031 Ldg. Teh Blue Valley
	4514032 Ldg. Teh Sg. Palas C. Higlands

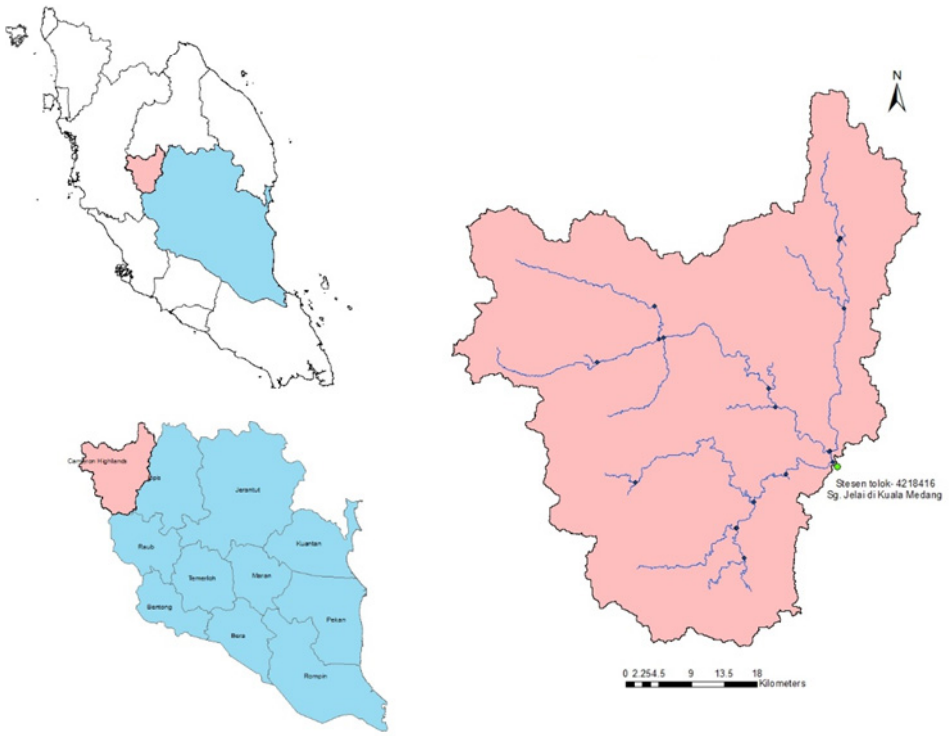

Figure 1. Index map of the study area.

3 MATERIALS AND METHODS

3.1 Model setup and simulation

The major geospatial input data includes Digital Elevation Model (DEM), soil data, land use and stream network layers. SWAT requires daily meteorological data that can either be read from a measured data set or generated by a weather generator model. The weather variables used in this study are daily precipitation, minimum and maximum air temperature for the period 1998 to 2006. A weather generator developed by (Schuol and Abbaspour, 2007) was used to fill the gaps due to missing data. Daily river discharge values for Kajang streamflow station were obtained from the Department of Irrigation and Drainage (DID) Malaysia. The model setup involved five steps: (1) data preparation; (2) sub-basin discretization; (3) Hydrologic Response

Unit (HRU) definition; (4) parameter sensitivity analysis; (5) calibration and uncertainty. The sub-basin discretization only focused on the 331.36 km^2 upper part of the Langat River basin as in Figure 1 . The watershed was divided into 33 sub-basins and 116 numbers of HRUs after completing the first three processes in the model setup.

In SWAT model, input parameters can be either manually adjusted in the SWAT model or can be accessed in the SWAT-CUP. SWAT-CUP is a semi-automatic approach to a computer program for the calibration of SWAT models, and the programs link SUFI-2 algorithms to SWAT. It enables sensitivity analysis, calibration, validation, and uncertainty analysis of SWAT models (Abbaspour et al, 2004; Abbaspour, 2012). Optimization of three different sets of spatial input parameters were tested, in order of, firstly focusing on the sets of groundwater inputs parameter, secondly for the soil input parameters and finally for the set consisting of 21 SWAT input parameters (Table 1) which reflects the sensitivity on the streamflow simulation. After setting up the model, the default simulation of streamflow was conducted in the Cameron Highlands basin for the calibration period and, after that, compared with the observed streamflow. A period of 9 years (1998 to 2006) daily rainfall data was utilized in the calibration periods with the first four years used for the model warm-up.

Table 2. Selected input parameter of SWAT model.

Nama Parameter	Huraian	Range	
		Min	Max
CN2.mgt	SCS runoff curve number	35	98
ESCO.hru	Soil evaporation compensation factor	0	1.00
SOL_AWC.sol	Available water capacity of the soil layer (mm H2O /mm soil)	0	1.00
ALPHA_BF.gw	Base flow recession constant	0	1.00
GW_DELAY.gw	Groundwater delay (days)	0	500
GWQMN.gw	Threshold depth of water in the shallow aquifer required for return flow to occur (mm)	0	5000
GW_REVAP.gw	Groundwater "revap" coefficient	0.02	0.2
REVAPMN.gw	Threshold depth of water in the shallow aquifer for "revap" to occur (mm)	0	500
SURLAG.bsn	Surface runoff lag coefficient	0.05	24

4 RESULTS

4.1 Model calibration on monthly basis using SUFI-2

In SUFI-2 program parameter uncertainties include all sources of uncertainty, such as uncertainty in input variables (variable climate), the concept model, the parameters and the observed data. The extent to which all the uncertainties taken into account assessed by measurement known as factor P, in which the measured data in brackets (bracketed) by 95PPU or 95% prediction uncertainty (Abbaspour 2015). Therefore, it measures the power of uncertainty analysis and calibration.

R Factor is another measure to measure the power of uncertainty analysis and calibration. R factor is the average thickness 95PPU band divided by the standard deviation of the observed data (Abbaspour 2015). The range of parameters used in the final repetition SUFI-2 provided adequate value for both the P and R factors ().

Table 3). Repetition rivals became less optimal when considering the two criteria (factor P and factor R). The parameters are then used for authentication purposes.

The results of last iteration in SUFI-2, produced acceptable results are displayed graphically in Figure 2. It provides Factor R = 1.63 (out of a perfect score of 0). Factor R which is under the value of one indicates that a small band 95PPU (Schuol et al., 2007). A total of 85% (95PPU) of the observed value of the monthly runoff can be captured by a band 95PPU (from a perfect score of 100%). In this figure, the upper and lower bands 95PPU shown between the two lines and describe 95PPU R factor (1.63). The extent to which data fall between the upper and 95PPU the lower line depicts 95PPU factor P = 0.85 (Figure 2).

Table 3. Various parameters for repeating last term during calibration with SUFI-2.

Parameters	Range	
	Minimum	Maximum
CN2.mgt	38.589	42.268
GW_DELAY.gw	638.865	682.239
ESCO.hru	-0.004	0.013
GWQMN.gw	0.891	0.942
ALPHA_BF.gw	-0.003	0.007
SURLAG.bsn	-21.654	-19.899

Parameters	Range	
	Minimum	Maximum
SOL_AWC.sol	1.749	1.793
GW_REVAP.gw	0.182	0.183
REVAPMN.gw	-225.385	-200.652

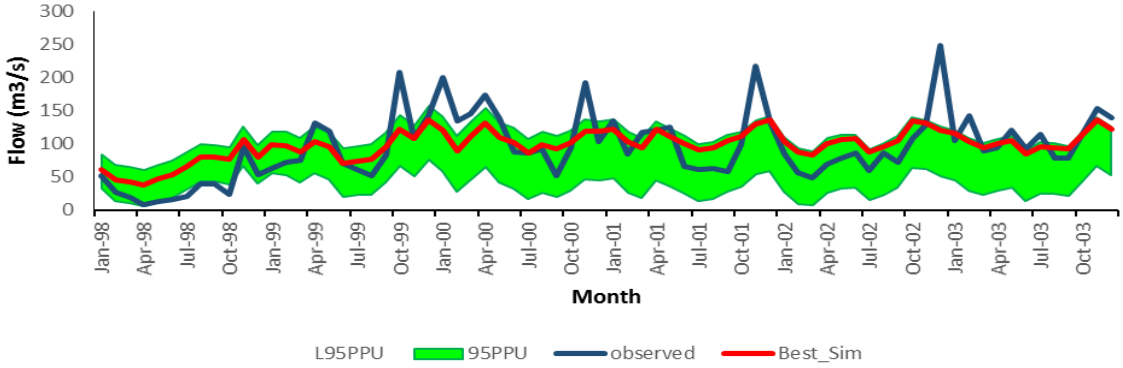

Figure 2. The results of the calibration of SUFI-2 compared to the measured flow (m3 / s) of the gauge 4218416, 1998-2006.

For the performance evaluation model in terms of quantitative statistics that measure the compatibility between the values of flow simulations and observations, NSE, PBIAS and R^2 were used as criteria. The objective function defined was NSE = 0.5 and this has been achieved during calibration, where NSE is 0.5. Performance evaluation is considered as satisfactory for 0.5 <NSE (Morias et al., 2007; Saleh and Du, 2004). NSE, as well as measures that other statistics to compare data in the observatory with the calibration data of simulation in SUFI-2. These include the percentage of bias (PBIAS) and correlation (R^2). PBIAS optimum value is zero, a low value indicates that the simulation model is accurate. The results of the calibration process SUFI-2, showing a good performance with PBIAS value of -7.5% (Table 4). R^2 = 0.61 indicated good correlation between the values of the observed and simulated (Table 4).

Table 4. Results of statistical analysis have been quantitative model to evaluate the performance of the observed and simulated data comparison monthly water flow during calibration (1998-2003) and validation (2004-2006).

	Nash-Sutcliffe coefficient	PBIAS	correlation (R^2)
Calibration	0.5	-7.5	0.61
Validation	0.1	-8.0	0.01

Global sensitivity analysis results conducted in SUFI-2 are shown in Table 5 and Figure 3. The statistics provide a measure of the sensitivity of the parameter t, where larger absolute value is more sensitive. P value indicates the importance of sensitivity, where the p-value is closer to zero is more important.

Table 5. Global decision 26x sensitivity analysis after repeated use SUFI-2.

Nama Parameter	t-stat	P-value
1:V__CN2.mgt	-2.02366	0.043547
2:V__ALPHA_BF.gw	31.41096	0
3:V__GW_DELAY.gw	0.672259	0.501736
4:V__GWQMN.gw	-0.45998	0.645734
5:V__GW_REVAP.gw	1.80829	0.071174
6:V__SURLAG.bsn	-0.25676	0.797474
7:V__REVAPMN.gw	-0.70421	0.481634
8:R__SOL_AWC(..).sol	-2.03032	0.042864
9:V__ESCO.hru	-0.21914	0.826633

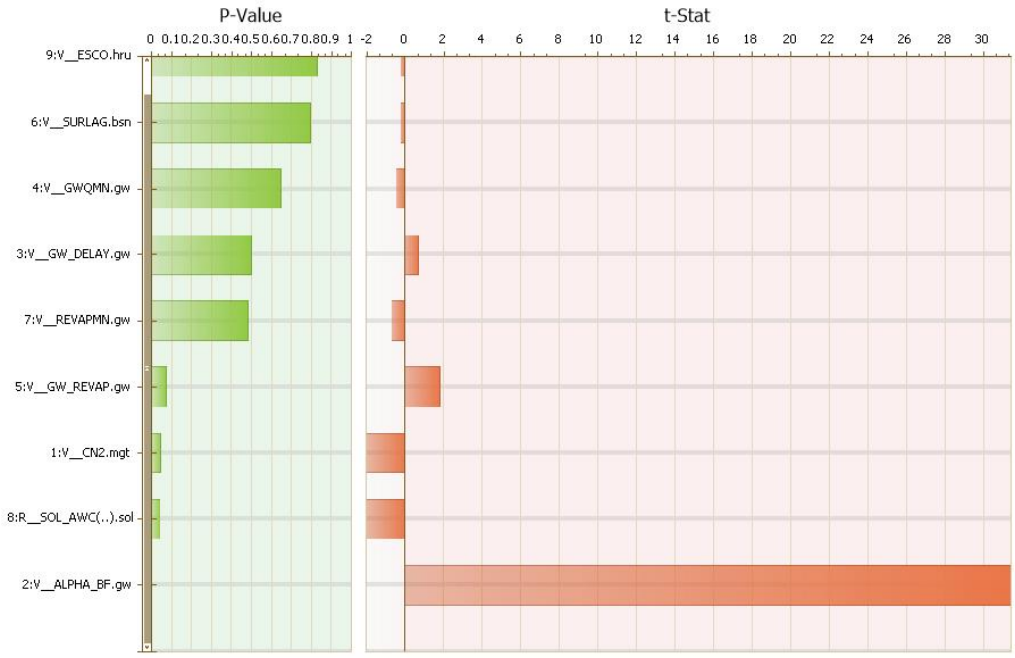

Figure 3. The results of the sensitivity analysis of global calibration.

The verification period is from 2004 to 2006. For verification, calibration of various parameters used in the repetition of the same amount of simulation as used in the calibration process, as much as 500 times the simulation. Results confirmation calibrated using various parameters are shown in Figure 4. For the confirmation, 56% of the observed data fall within the calibration band 95PPU corresponding period. (Factor R = 1.81 versus factor R = 1.63 for the calibration). R factor of 1.81 is acceptable, because it is approaching 1.0 (Schuol et al., 2007).

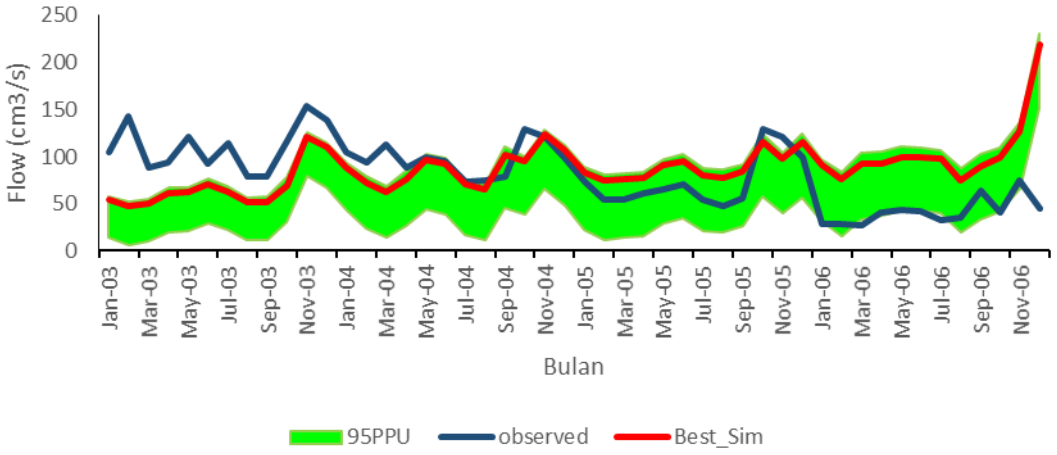

Figure 4. Results confirm the SUFI-2 compares the flow of gauge 4218416 was observed for 2003-2006.

NSE value for verification is 0.1 (Table 5). Although this does not meet the objective function> 0.5 expressed in Sufi-2, Morias et al. (2007) stated that values between 0.0 and 1.0 is generally viewed as an acceptable level of performance. NSE values <0, show that the average of the observed values is better than the simulations, show unacceptable performance. PBIAS for confirmation is -8.0%, is acceptable. R^2 = 0.01 is acceptable.

5 DISCUSSIONS

The results of this study are appropriate for the calibration model. This includes a comparison chart that takes into account all forms of uncertainty by SUFI-2 program (factor P and factor R), as well as quantitative statistical analysis. The model is calibrated and validated, still produces a poor value, especially for quantitative analysis. This model is still able to embrace most of the observed data within a small uncertainty band, as shown in the chart. NSE also still acceptable. The results show that this model can simulate peak and low flows satisfactorily, as demonstrated by statistical methods R^2 (R^2> 0.5), for calibration and

verification. Statistics PBIAS considered unacceptable during authentication. PBIAS negative value indicates that the model has a tendency to increase the flow direction (Moriasi et al., 2007). Abbaspour et al. (2014) explains that the choice of objective function in SUFI-2 can affect the obtained results. The best solution is to check the results, focusing on the statistical set as an objective function (in this case NSE). It also may be caused by a condition within the confirmation differ significantly from the last calibration. Although there is doubt, evaluation for confirmation can still be accepted. Generally, Morias et al. (2007) noted that appraisals are needed during the calibration model compared with confirmation.

Use of NSE for the objective function needs to be discussed. Although it has been widely used and accepted many literature (Moriasi et al., 2007; Fadil et al., 2011; Mango et al., 2011). There are also some negative issues that need to be considered. McCabe (1999) emphasized that because of the difference between the values of the observed and simulated is squared, the values the larger series will be wasted and the values of the lower will be ignored. This means for the calibration and verification of flow, NSE focused on peak efficiency and high flow and cause less focus on forecasting low flows (Krause et al., 2005; Qi and Grunwald, 2005). However, these measures have been in this research because preliminary results before calibration, simulation shows the trend of relatively high peak flow. NSE concentration to peak values can also help during the process of calibration and verification. It also explains the PBIAS during the confirmation, indicating that this model to underestimation bias NSE focused on correction of peak flow, that means it is important during the model calibration.

In this study, we have only one gauge in the catchment area of the river flow. Qi and Grunwald (2005) states "... more stations available for calibration and verification of models such as SWAT adapt to the characteristics of the local and regional watershed, water flow simulation prospects will be better and reliable". It will also lead to increased confidence when using the model to predict different scenarios and to predict trends in the stations that do not have gauges. Similarly, input data table, in addition to rainfall data, obtained from JPS stations that do not have sufficient data and questionable. However, due to rainfall data available in the catchment area and the weather station located in the watershed, this data is used together with data station to input data DID rain.

Among the limitations of the use of SWAT model to others is in the mountains of Cameron Highlands. It causes soil data and streams data to be limited. Although, the local soil data obtained, but the characteristics of the soil are quite difficult to identify. Therefore, in this study general data of FAO adopted and cause uncertainty in the modeling process. In addition, the database SWAT for land use parameters were used based on the type of vegetation cover from the United States. Although sufficient data, it can still cause some uncertainty in the model. For model calibration, the river flow (streamflow) emphasized. This is because there is no data flow (base flow) and surface runoff (runoff) can be found.

The overall results of this study indicate when the SWAT model calibration parameters are within the appropriate range, it can simulate a reasonable monthly streamflow in catchment areas in Cameron Highlands. Similar findings were also carried out in Africa, which also found that the SWAT model can generate a reasonable hydrological data between the observed data with simulation (Mango et al., 2004; Govender and Everson, 2005; Birhanu et al., 2007; Mutenyo et al., 2013; Noor, H., et al., 2014; Ridwansyah et al., 2014). Meanwhile, a study by Birhanu et al. (2007) studied the suitability of SWAT model in mountainous catchment in Northern Tanzania and got good results by stating that '... the SWAT model by monitoring the potential to become a tool in the water catchment area in the catchment area of the mountains. Mutenyo et al. (2013) used the SWAT model in a mountainous area in eastern Uganda and found that the model can simulate the monthly hydrological data successfully in the watershed. Hydrology estuary area in the catchment area of the mountains in Indonesia has successfully modeled using SWAT (Ridwansyah et al., 2014). Noor et al. (2014) found that SWAT model can predict accurately the hydrological watershed in the semi-arid mountainous Taleghan.

In order to parametrization and SWAT model adaptation to local stakeholders, researchers must have access to more data, or data that is of better quality. Limited data identified as an important issue in hydrological modeling, particularly in Malaysia and in the mountains (Mango et al., 2004; Mutenyo et al., 2013; Alford, 1985; Jayakrishnan et al., 2005; Messerli et al., 2004; Abbaspour, 2015). Mutenyo et al. (2013) found that for certain catchment areas of the mountains, to achieve results sufficient to enable researchers to simulate the daily river flow, more weather stations to 'catch microclimate' needs in the study area. Jayakrishnan et al. (2005) used the model SWAT River basin Bosque in Texas (USA), as well as in River basin sonde in Kenya, and said that this model has a good potential to be used worldwide and can be used to save time and money while catchment management water and make a decision. In the study, found the need to develop a dataset input variables in Africa (Mutenyo et al., 2013). Abbaspour, et al. (2007) used the SWAT model throughout Africa. Although the model is generally good, but there is considerable uncertainty in the forecast for several cases due to lack of database input (Schuol and Abbaspour, 2007).

The use of semi-automatic program like SUFI-2 in SWAT-CUP, combine all the uncertainties in the modeling process, as well as manual calibration coupled with the knowledge of hydrology in catchment areas, allowing adequate modeling. Ridwansyah et al. (2014) using the procedure SUFI-2 and found that it has managed to reduce the difference between observed and simulated data. Schuol et al. (2007) successful

calibration and validation of the SWAT model throughout Africa using SUFI-2 program. Forecast uncertainty also in quantity by using the program (Abbaspour, 2015).

6 CONCLUSIONS

This study focused on the hydrological model mountains in Cameron Highlands. Brincang Mountain is one of the highest mountains in Pahang. Catchment areas in Cameron Highlands, including Mount Brincang, is a natural mountainous area. The catchment area has a gauge stations that provide existing data, as well as precipitation data from weather stations located in the watershed. The catchment area of the forest reserve. A larger part of the catchment area was forested. This means the runoff coming from the mountain has relatively good quality. SWAT model was applied in the catchment area of Cameron Highlands. The model was successfully conducted using GIS interface that provides user-friendly methods in putting data into SWAT program. SWAT model successfully simulates the flow of data from the catchment area of the river.

ACKNOWLEDGEMENTS

The project was supported by MyBrain15, Ministry of Education, Universiti Kebangsaan Malaysia (UKM), SWAT Networks of Malaysia.

REFERENCES

Abbaspour, K.C., Johnson, C.A. & Van Genuchten, M.T. (2004). Estimating Uncertain Flow and Transport Parameters Using a Sequential Uncertainty Fitting Procedure. *Vadose Zone Journal*, 3(4), 1340-1352.

Abbaspour, K.C. (2012). *User Manual for SWAT-CUP, SWAT Calibration and Uncertainty Analysis Programs*, Swiss Federal Institute of Aquatic Science and Technology, Eawag, Duebendorf, Switzerland pp 93.

Abbaspour, K.C., Johnson, C.A. & Van, M.T. (2014). Genuchten, Estimating Uncertain Flow and Transport Parameters Using a Sequential Uncertainty Fitting Procedure. *Vadose Zone Journal*, 3(4), 1340-1352.

Abbaspour, K.C. (2015). *SWAT-Calibration and Uncertainty Programs*, SWAT.

Alford, D. (1985), *Mountain Hydrologic Systems*. Mountain Research and Development pp. 349-363.

Birhanu, B., Ndomba, P. & Mtalo, F. (2007). *Application of SWAT Model for Mountainous Catchment*. Catchment and Lake Research. pp. 182-187.

Chaponnière, A., Boulet, G., Chehbouni, A. & Aresmouk, M. (2008). Understanding Hydrological Processes with Scarce Data in a Mountain Environment. *Hydrological Processes*, *22*(12), 1908-1921.

Fadil, A., Rhinane, H., Kaoukaya, A., Kharchaf, Y. & Bachir, O.A. (2011). Hydrologic Modeling of the Bouregreg Watershed (Morocco) Using GIS and SWAT Model. *Journal of Geographic Information System*, 3(04), 279.

Govender, M. & Everson, C.S., (2005). Modelling Streamflow from Two Small South African Experimental Catchments Using the SWAT Model. *Hydrological Processes*, 19(3), 683-692.

Jayakrishnan, R.S.R.S., Srinivasan, R., Santhi, C. & Arnold, J.G., (2005). Advances in the Application of the SWAT Model for Water Resources Management. *Hydrological Processes,* 19(3), 749-762.

Krause, P., Boyle, D.P. & Bäse, F., 2005. Comparison of Different Efficiency Criteria for Hydrological Model Assessment. *Advances in Geosciences*, *5*, 89-97.

Legates, D.R. & Mccabe, G.J. (1999). Evaluating the Use of "Goodness-Of-Fit" Measures in Hydrologic and Hydroclimatic Model Validation. *Water Resources Research*, 35(1), 233-241.

Mango, L.M., Melesse, A.M., Mcclain, M.E., Gann, D. & Setegn, S.G. (2011). Land Use and Climate Change Impacts on the Hydrology of the Upper Mara River Basin, Kenya: Results of a Modeling Study to Support Better Resource Management. *Hydrology and Earth System Sciences*, 15(7), 2245.

Messerli, B., Viviroli, D. & Weingartner, R. (2004). *Mountains of the World: Vulnerable Water Towers for the 21st Century*. Ambio, pp.29-34.

Moriasi, D.N., Arnold, J.G., Van Liew, M.W., Bingner, R.L., Harmel, R.D. & Veith, T.L. (2007). Model Evaluation Guidelines for Systematic Quantification of Accuracy in Watershed Simulations. *Trans. Asabe*, 50(3), pp.885-900.

Moriasi, D.N., Arnold, J.G., Van Liew, M.W., Bingner, R.L., Harmel, R.D. & Veith, T.L., (2007). Model Evaluation Guidelines for Systematic Quantification of Accuracy in Watershed Simulations. *Trans. Asabe*, 50(3), pp.885-900.

Mutenyo, I., Nejadhashemi, A.P., Woznicki, S.A. & Giri, S. (2015). Evaluation of SWAT Performance on a Mountainous Watershed in Tropical Africa. *Hydrology: Current Research*, (S3), P.1.

Noor, H., Vafakhah, M., Taheriyoun, M & Moghadasi, M. (2014). Hydrology Modelling in Taleghan Mountainous Watershed Using SWAT. *Journal of Water and Land Development*, 20(1), pp.11-18.

Qi, C. & Grunwald, S. (2005). GIS-Based Hydrologic Modeling in the Sandusky Watershed Using SWAT. *Transactions of the ASAE*, 48(1), pp.169-180.

Ridwansyah, I., Pawitan, H., Sinukaban, N. & Hidayat, Y. (2014). Watershed Modeling with Arcswat and SUFI2 in Cisadane Catchment Area: Calibration and Validation of River Flow Prediction. *International Journal of Science and Engineering*, 6(2), 92-101.

Saleh, A. & Du, B., 2004. Evaluation of SWAT and HSPF within BASINS Program for the Upper North Bosque River Watershed in Central Texas. *Transactions of the ASAE*, 47(4), pp.1039-1049.
Schuol, J. And Abbaspour, K.C.(2007). Using Monthly Weather Statistics To Generate Daily Data In A SWAT Model Application To West Africa. *Ecological Modelling*, 201(3), 301-311.

A GPU BASED NUMERICAL MODEL EVALUATING SPONGE EFFECTS ON URBAN FLOOD FOR SPONGE CITY CONSTRUCTION IN CHINA

RUN WANG[1], JINGMING HOU[2], ZHANBIN LI[3], JIAN ZHOU[4], QUAN QUAN[5], GUODONG LI[6], BINGQIAN WEI[7], WEN WANG[8] & YUE MA[9]

[1,2,3,5,6,7,8] School of Water Resources and Hydro-electric Engineering, Xi'an University of Technology, Xi'an, China, jingming.hou@xaut.edu.cn
[4] The Cold and Arid Regions Environmental and Engineering Research Institute of The Chinese Academy of Sciences，Lanzhou, China,
[9] Technical Center of The Sponge City in Fengxi New Town, Xi'an, China

ABSTRACT

After 'Technical Guides of Sponge City Development-Low Impact Development of Rainwater System' has been issued by Ministry of Housing and Urban-Rural Development of the People's Republic of China (MOHURD), the construction of sponge city has gradually been implemented nationwide. In order to solve the flood, water shortage and water quality problems resulting from the high urbanization rate in China, 30 pilot cities have joined the urban development plan of sponge city in recent two years. However, no consensus is reached to plan, design, construct and manage the sponge city which results in more practical problems as the program goes by. For example, optimizing the distribution of the LID (Low Impact Development) techniques and evaluating the overall sponge effects of the sponge city. To address the problems, a GPU based hydrodynamic model is developed in this work which couples the hydrological and hydrodynamic to simulate the net rainfall, surface water runoff, flood propagation and inundation, etc.. The model is able to evaluate the sponge effect caused by the LID measures through changing the hydrological, hydrodynamic and biological processes in urban area. GPU technique is employed to accelerate the computation to implement the large scale high-resolution simulation in a very efficient way. The model is applied in Xi-Xian New Area Sponge City Project to quantitatively predict the sponge effect on urban flood.

Keywords: Low impact development (LID); sponge city; hydrodynamic model; GPU; storm water management.

1 INTRODUCTION

Over last decades, urban expansions have fast developed all over the world, especially in China. Due to the rapid urbanization, the infiltration capacity of underlying surface in cities have significantly decreased. The global climate change and the fast urbanization in China have greatly raised the risk of the urban floods which occurs more frequently and spreading across coastal cities to inland cities. For example, the urban flood in Wuhan lead to massive losses of properties and lives in 2016. In order to mitigate the urban flood damage, water shortage and water quality problems, Ministry of Housing and Urban-Rural Development of the People's Republic of China (MOHURD) issued 'Technical Guides of Sponge City Development-Low Impact Development of Rainwater System' and the construction of sponge city has gradually been implemented nationwide. Mitigation of urban flood has become an important duty of the Chinese government.

Reliable simulation for urban flood which is characterized by complex flow patterns on complex terrain demands a robust hydrodynamic model with high resolution grid (Chen et al., 2012), generally beyond the capabilities of hydrological model. To address the problem, lots of flood forecasting models have been proposed, such as SWMM model (Cole and Shutt, 1976), Inforworks model (Koudelak and West, 2008) and MIKE-Urban. However, high resolution grid induces high computation burden. Most of the existing hydrodynamic models are not able to provide high-resolution and efficient simulations for large-scale rainfall runoff and flood propagation events. Besides, the lack of high accurate and robust numerical scheme also restricted the application. This paper therefore employs a stable 2D well-balanced shallow flow model proposed by a physically based dynamic wave model, which couples the hydrological and hydrodynamic processes to simulate the surface water runoff, flood propagation and inundation, drainage of sewer networks, etc.. The model uses the finite volume method to keep conservation. Aiming at enabling the large scale high-resolution simulation, the computation is accelerated by the high-performance Graphic Processing Units (GPUs) parallel computing technique. The model's reliability and efficiency for evaluating the sponge effects on urban flood are demonstrated by an application in Xi-Xian New Area Sponge City in Shaanxi Province, China.

2 GOVERNING EQUATIONS AND NUMERICAL SCHEMES

The shallow water equations (SWEs) are derived from depth-integrating the Navier-Stokes equations and assuming hydrostatic pressure distribution. If the kinetic and turbulent viscous terms, wind stresses and

Coriolis effects are neglected, a conservation law of the two-dimensional non-linear shallow water equations can be written in the vector form as:

$$\frac{\partial \boldsymbol{q}}{\partial t} + \frac{\partial \boldsymbol{f}}{\partial x} + \frac{\partial \boldsymbol{g}}{\partial y} = \boldsymbol{S} \qquad [1]$$

$$\boldsymbol{q} = \begin{bmatrix} h \\ q_x \\ q_y \end{bmatrix}, \boldsymbol{f} = \begin{bmatrix} uh \\ uq_x \\ uq_y \end{bmatrix}, \boldsymbol{g} = \begin{bmatrix} vh \\ vq_x \\ vq_y \end{bmatrix}, \qquad [2]$$

$$\boldsymbol{S} = \begin{bmatrix} i \\ -\frac{gh\partial z_b}{\partial x} - C_f u\sqrt{u^2+v^2} \\ -\frac{gh\partial z_b}{\partial y} - C_f v\sqrt{u^2+v^2} \end{bmatrix}. \qquad [3]$$

where, t represents the time; x and y are the Cartesian coordinates; q denotes the vector of conserved flow variables consisting of the water depth h, unit-width discharges in x- and y-directions $\mathrm{q_x}$ and $\mathrm{q_y}$; $\mathrm{q_x} = \mathrm{uh}$ and $\mathrm{q_y} = \mathrm{vh}$. And u and v are depth-averaged velocities in x- and y-directions; f and g are the flux vectors in x- and y-directions; S is the source vector that can be further subdivided into net rainfall source terms, slope source terms and friction source terms.$\mathrm{z_b}$ represents the bed elevation;$\mathrm{C_f}$ is the bed roughness coefficient that is generally computed by $\mathrm{gn^2/h^{1/3}}$ with n being the Manning coefficient. Moreover, rainfall, infiltration and drainage processes are also considered in this study.

The governing equations above are numerically solved by a Godunov-type finite volume scheme as presented in other papers of the authors, e.g. Hou et al. (2013a; 2013b). In this model, the Harten, Lax and van Leer approximate Riemann solver with the contact wave restored (HLLC) is applied to compute the numerical fluxes of water, momentum and sediment across cell interfaces. The values of variable at the midpoints of cell edges are extrapolated by the MUSCL method. The extrapolated values are then modified locally by a non-negative water depth reconstruction proposed in Audusee and Bristeau (2005) to preserve the C-property (Bermudez and Vazquez, 1994; Crnkovic et al., 2009). The slope source terms are computed by a slope flux method which converts the slope source at a cell into fluxes through its edge, so as to comfort to any complex unstructured grids (Hou et al., 2013). The friction source terms are solved through utilizing a splitting point-implicit method presented in Liang and Marche (2009). Moreover, a two-stage explicit Runge-Kutta scheme is adopted to update the values to the new time level (Zia and Qamar, 2014). The infiltration process is evaluated by using Green-Ampt model and the drainage of sewer-network is computed by solving the one-dimension diffusive wave equations. The proposed model is programmed by applying the C++ and CUDA code which could considerably accelerate the computation on GPUs.

3 GPU ACCELERATION

Dynamic wave method and Godunov-type scheme have successfully been applied in a wide range of literature, but computational power has limited their applications for extremely large domains with high-resolution representation. Graphic Processing Units (GPU) parallel computing technique offers a new approach to achieve such simulation. GPUs are designed to rapidly manipulate and alter memory to accelerate the creation of images in a frame buffer intended for output to a display device. GPUs are very efficient at manipulating computer graphics and image processing, and their highly parallel structure makes them more efficient than CPUs for algorithms where the processing of large volumes of data by performing the same calculation numerous times, typically on vectors and matrices. Since new programming language CUDA have developed, this hardware has been used in general-purpose applications. There are a number of attempts have been made for GPU computing in highly resolution large-scale flood simulations, such as Brodtkorb et al. (2011) with a finite-volume scheme implementation of the full SWEs. Smith and Liang (2013) demonstrated the potential for generalized approaches applicable to both CPU and GPU co-processors. Successful and efficient implementation for GPUs computing technique requires rational consideration of the six elements shown in Figure 1.

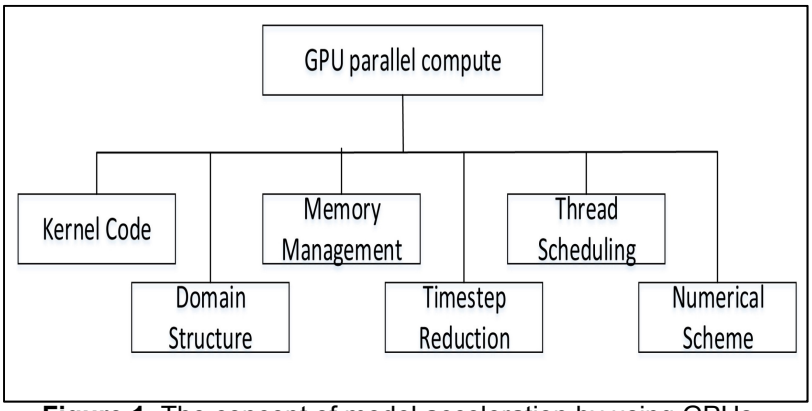

Figure 1. The concept of model acceleration by using GPUs.

4 MODEL APPLICATION

In this section, a real urban flood case with measured data is applied to verify the capability of the model and a desktop with a NVIDIA GeForce GTX 980Ti GPU is used to run all simulations. The 8h-flood event costed about 22h and 21h computational time for the two test cases, respectively.

4.1 Project introduction and data collection

Xi-Xian New Area is located between Xi'an city and Xianyang city in Shaanxi province. It is one of the 30 pilot cities that have joined the urban development plan of sponge city in China and the Sponge City Project has started since 2015. The planned sponge area is an independent drainage area and the area is 368 ha, including 25 ha roads, 93 ha school lands, 63 ha green fields and 187 ha residential and commercial land. The average annual precipitation is about 520 mm, with the July to September rainfall accounts for more than 50 %. The average annual evaporation is about 1065 mm as shown in Figure 2.

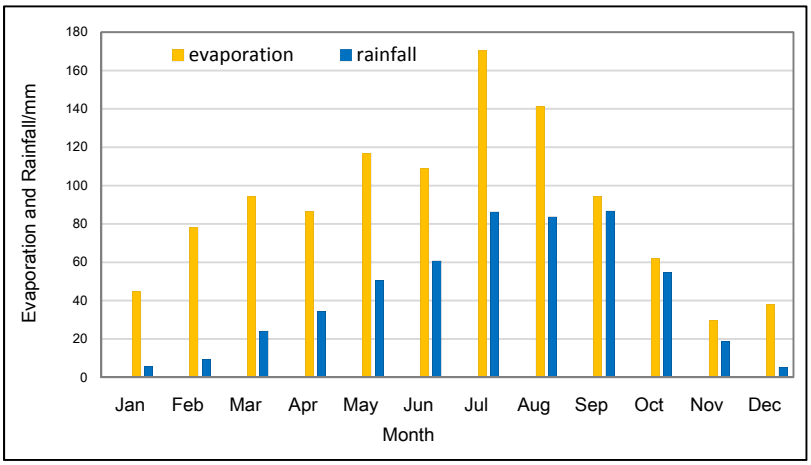

Figure 2. Averaged monthly rainfall and evaporation in Xi-Xian New Area.

Data collected for this work includes the underground pipeline data, the 1 m-resolution DEM and DOM of the study area and the observed precipitation. The measured precipitation of 114.4 mm lasting 8.5 h on August 25, 2016 is used as the input data in this work. It is double-peak one and the highest peak showed at 2.6 h (Figure 3(a)).

DEM is obtained by using the UAV and DOM survey techniques and data were supplied at 1 m resolution as shown in Figure 3(b). The computational domain contains 3,681,167 cells. For the parameters such as water storage facilities in city, soil type and the infiltration rate, surface roughness etc. were provided by the Technical Center of The Sponge City in Fengxi New Town.

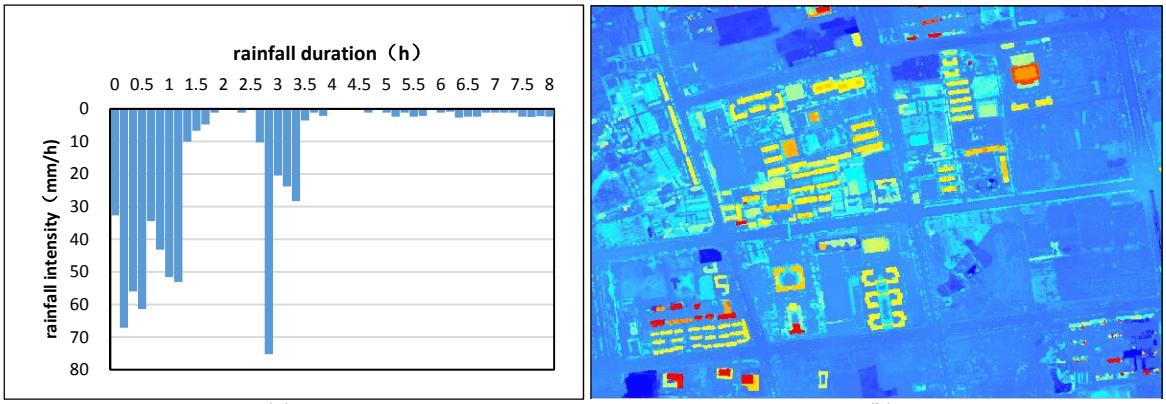

Figure 3. (a) Measured precipitation; (b)the DEM of the study area.

4.2 Results and discussions

Open boundary conditions are applied around the extremity of the domain. According to the real situation, the pump station at the outlet of the main pipelines has not yet been completed and the water could inject to the river in that event. That means the sewer network just worked as underground reservoirs with the total volume of approximately 11413 m^3. The models run for 8 h with a Courant number of 0.5 s to simulate the inundation process for the study area with current and future LID measures.

Figure 4 plots the computed flood inundation for the area with current LID measures after 20 mins when the inundation beginning to appear. The flood depths at 3.5 h reached to about 45 cm and the biggest area of inundation is up to around 2000 m^2.

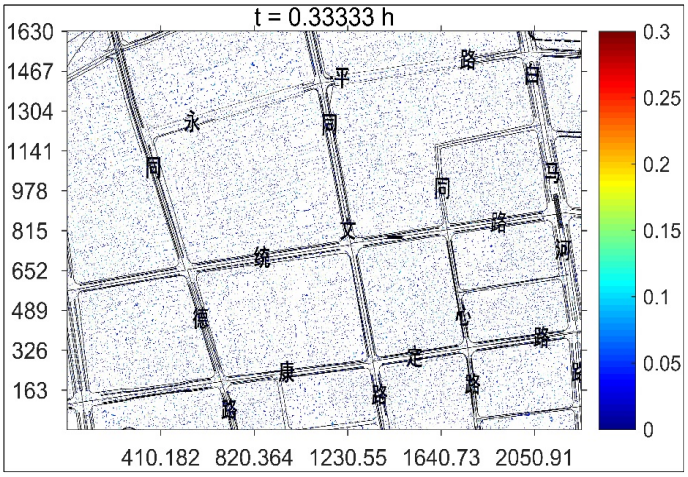

Figure 4. Computed flood inundation for the area with current LID measures at 20 mins. (Unit: m).

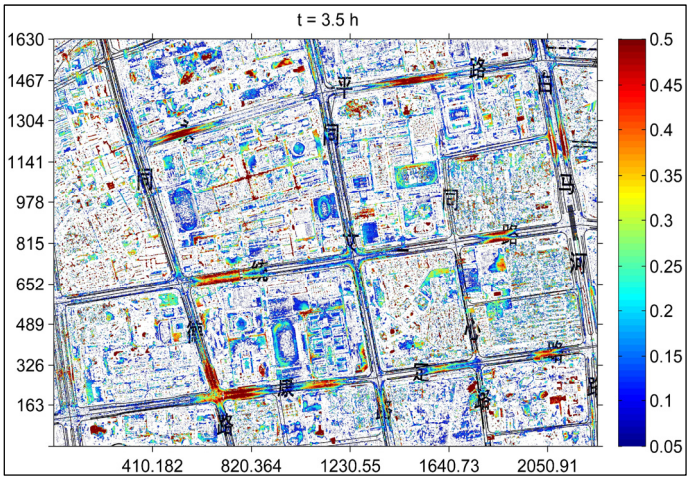

Figure 5. Computed flood inundation for the area with current LID measures at 3.5 h. (Unit: m).

The maximum depths of inundation are consistent with the measurement, and the inundation area is also close to the measured values as shown in Table 1. Figure 6 depicts the comparison between the computed and measured inundation locations. It is found that results of simulation again agree well with the measurements, proving the model is an accurate and robust one for urban flood modeling.

Then the proposed model is used to investigate the sponge effect on the flood inundations by assuming all the LID measures are completed (the reality is the construction is under way, so this case is termed as future LID measures). The LID measures are taken into account by change the infiltration rate and the storage volume and so on. We are running the model under the same initial and boundary conditions and the computed results are plotted in Figure 7 and 8. They sketch the comparison between two simulations. It is clearly observed that the future LID measures have greater effects on water quantity of urban rainfall runoff, significantly decreasing the flood inundation by mitigating the peak and the amount the surface runoff.

Table 1. Computed and measured inundations for the flood event on 2016/08/25.

	THE LARGESTINUNDATIONAREA (MEASURED/SIMULATED)	THE MAXIMUM DEPTHS (MEASURED/SIMULATED)
POINT 1	663m^2/700 m^2	15.1cm/20cm
POINT 2	567m^2/900 m^2	16.7cm/20cm
POINT 3	1378m^2/2000 m^2	17.7cm/21cm
POINT 4	675m^2/500 m^2	18,8cm/22cm
POINT 5	981m^2/1100 m^2	25.6cm/30cm

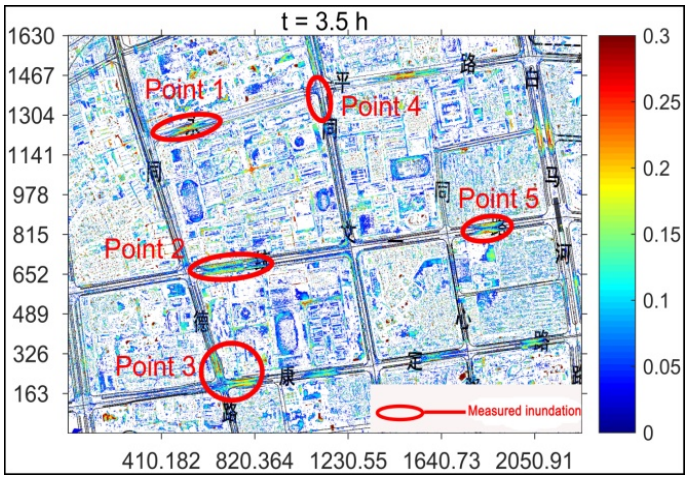

Figure 6. Comparison between the modelled and measured inundation for the area with future LID measures at 3.5 h. (Unit: m).

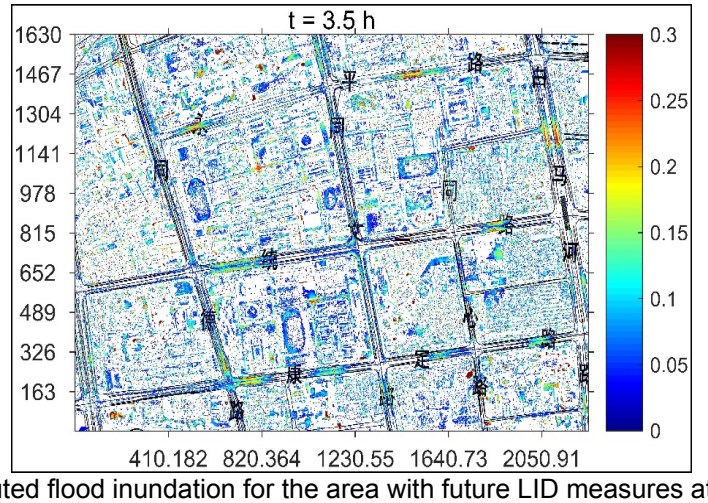

Figure 7. Computed flood inundation for the area with future LID measures at 3.5 h. (Unit: m)

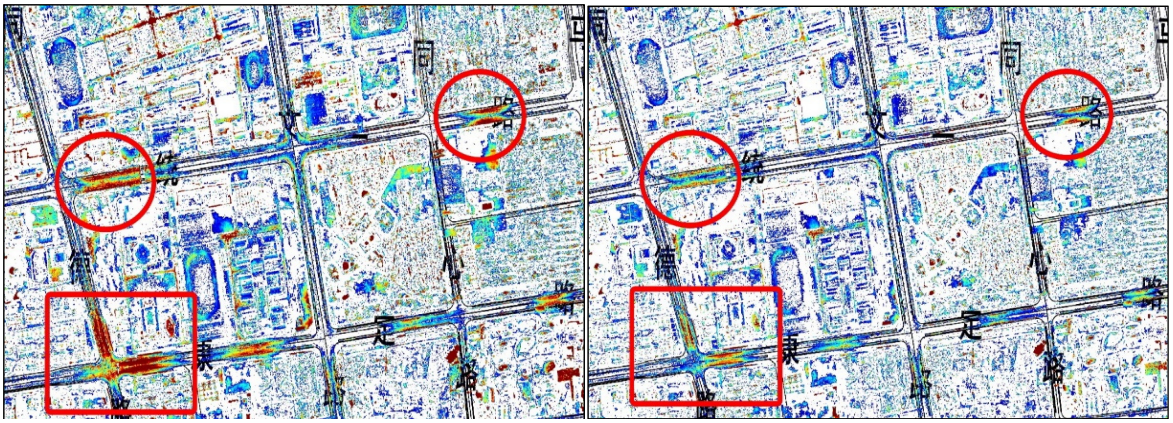

(a) (b)

Figure 8. Comparison of the modelled flood inundations between the area with (a) current and (b) future LID measures at 3.5 h.

5 CONCLUSIONS

In this work, a GPU-accelerated urban flood inundation model is developed and applied in a practical project to evaluate the sponge effect on for The Sponge City Project in China. The simulated results in terms of inundation area and depths are compared with the measured ones, indicating the model is able to compute the urban flood process in a reliable and efficient way. In addition, the model can be run on a desktop computer to predict the 1 m-resolution flood inundation, showing the GPU technique is an ideal approach to accelerate the computation. The sponge effect on the urban flood caused by the LID measures can also be reflected reasonably by the model. It therefore proposed an applicable and useful tool for planning, designing, constructing and managing the effects of the Sponge City Projects in China on the aspect of urban flood.

REFERENCES

Audusse, E. & Bristeau, M.O. (2005). A Well-Balanced Positivity Preserving “Second-Order” Scheme for Shallow Water Flows on Unstructured Meshes. *Journal of Computational Physics,* 206(1), 311-333.

Bermudez, A. & Vazquez, M.E. (1994). Upwind Methods for Hyperbolic Conservation Laws with Source Terms. *Computers and Fluids,* 23(8), 1049-1071.

Brodtkorb, A.R., Sætra, M.L. & Altinakar, M. (2011). Efficient Shallow Water Simulations on Gpus: Implementation, Visualization, Verification, and Validation. *Computers and Fluids,* 55(4), 1–12.

Chen, A.S., Evans, B., Djordjević, S. & Savić, D.A. (2012). A Coarse-Grid Approach to Representing Building Blockage Effects in 2D Urban Flood Modelling. *Journal of Hydrology*, 426-427(21), 1-16.

Cole, G.D. & Shutt, J.W. (1976). SWMM as a Predictive Model for Runoff. *National Symposium on Urban Hydrology, Hydraulics and Sediment Control*. University of Kentucky, Lexington, KY, USA, 193−201.

Crnkovic, B., Crnjaric-Zic, N. & Kranjcevic, L. (2009). Improvements of Semi-Implicit Schemes for Hyperbolic Balance Laws Applied on Open Channel Flow Equations. *Computers and Mathematics with Applications*, 58(2), 292–309.

Hou, J., Liang, Q., Simons, F. & Hinkelmann, R. (2013a). A 2D Well-Balanced Shallow Flow Model for Unstructured Grids with Novel Slope Source Term Treatment. *Advances in Water Resources*, 52(2), 107-131.

Hou, J., Liang, Q., Simons, F. & Hinkelmann, R. (2013b). A Stable 2D Unstructured Shallow Flow Model for Simulations of Wetting and Drying over Rough Terrains. *Computers and Fluids, 82*(17), 132–147.

Koudelak, P. & West, S. (2008). Sewerage Networkmodelling in Latvia, use of Infoworks CS and Storm Water Management Model 5 in Liepaja City. *Water and Environment Journal*, 22(2), 81−87.

Liang, Q. & Marche, F. (2009). Numerical Resolution of Well-Balanced Shallow Water Equations with Complex Source Terms. *Advances in Water Resources,* 32(6), 873–884.

Smith, L.S. & Liang, Q. (2013). Towards a Generalised GPU/CPU Shallow-Flow Modelling Tool. *Computers and Fluids,* 88(12), 334-343.

Zia, S. & Qamar, S. (2014). A Kinetic Flux-Vector Splitting Method for Single-Phase and Two-Phase Shallow Flows. *Computers and Mathematics with Applications,* 67(6), 1271-1288.

APPLICATION OF SWMM AND MIKE11 COUPLING MODEL IN URBAN TIDAL RIVER NETWORK

YUAN YUAN[1], MIN WANG[2] & YI HU[3]

[1,2] Changjiang River Scientific Research Institute of Changjiang Water Resources Commission, Wuhan, China, yuanht1020@foxmail.com
[3] State Key Laboratory of Water Resources and Hydropower Engineering Science, Wuhan University, Wuhan, China

ABSTRACT

Recently, as the economy develops rapidly and the urbanization process increases, the loss caused by waterlogging disaster has been more and more prominent and the urban flood has become a major issue that concerns the world. In this paper, SWMM hydrological model and MIKE11 hydrodynamic model are used in combination to simulate the rainfall runoff process as well as flood control and drainage process. The results show that, with the pump station, the water level of inner-river decreases compared with the case of no pump station. Moreover, the greater the pumping capacity is, the larger the drawdown value of the water level. Without the pump station, parts of the river reaches have high water levels in case one compared with the case two, for the reason that the case one has a higher outer tide level. The influence of outer tide level is decreased obviously, and the water level is mainly influenced by rainfall and pumping capacity. The results are reasonable, showing that the coupling model will benefit the flood control and drainage planning in the plain tidal river network.

Keywords: Tidal river network; SWMM model; hydrodynamic model; flood control; drainage.

1 INTRODUCTION

The plain river network region has a high urbanization level and a large population. Meanwhile, the plain river network region is generally a low-lying area with lakes and rivers all around, and thus is vulnerable to floods. Recently, as the economy develops rapidly and the urbanization process increases, the loss caused by urban waterlog disaster has been more and more prominent. It not only adds the task of flood control and drainage to the city, but also causes great influence to economic construction and people's livelihood.

This paper simulated the rainfall runoff and flood control and drainage processes of the study area by adopting the SWMM hydrological model and MIKE11 hydrodynamic model, aiming at the flow characteristics in the plain river network and tidal region. Firstly, the study area was divided to several sub-regions based on the river system and underlying surface characteristics, and the rainfall-runoff of each sub-region was then calculated by the SWMM model. Secondly, the one-dimensional river network hydrodynamic model was established with the use of the MIKE11 software, which was developed by the Danish Institute of Water Conservancy. The runoff process of each sub-region, which can be regarded as the river inflow, was provided as the flow boundary condition for the hydrodynamic model. Therefore, the rainfall runoff model and hydrodynamic model was coupled, and the rainfall-runoff processes and the flood control and drainage processes of the study area were simulated. Eventually, the results were analyzed in detail.

2 SWMM AND MIKE11 HYDRODYNAMIC MODEL

2.1 SWMM model

Storm Water Management Model (SWMM) is a comprehensive mathematic model for urban storm design and management, which was developed by the U.S. Environmental Protection Agency (USEPA). SWMM can simulate the complete urban rainfall runoff process, including surface runoff as well as flow process and regulation and storage of rainfall flood in the drainage system. Also, SWMM can display the flow and water quality state of each point both in the system and in the receiving water. This model has been applied in many areas in China such as Tianjin, Shanghai and Beijing (Liu and Xu, 2001; Cong et al., 2006; Liu et al., 2006).

SWMM simulation software is composed of five modules. Runoff, transport, extran and storage/treatment make up the four calculation modules, which can process dynamic simulation for water quantity and quality of surface runoff, network of drains and sewage treatment units. While the main function of the service module is post process of calculation, such as statistics and drafting. The relationship between the modules is shown in Figure 1.

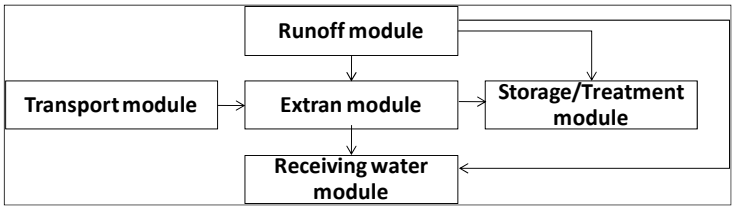

Figure 1. Relationship between the modules of SWMM (Ren et al., 2006).

2.2 MIKE11 hydrodynamic model

MIKE11 Hydrodynamic Model is based on Saint-Venant equations:

$$\begin{cases} \dfrac{\partial A}{\partial t}+\dfrac{\partial Q}{\partial x}=q \\ \dfrac{\partial Q}{\partial t}+\dfrac{\partial}{\partial x}\left(\alpha\dfrac{Q^2}{A}\right)+gA\dfrac{\partial h}{\partial x}+g\dfrac{Q|Q|}{C^2AR}=0 \end{cases} \quad [1]$$

where, x and t are spatial and temporal axes, A is the cross-sectional area, Q is the flow discharge, h is the water level, q is the uniform lateral inflow of unit length (including the rainfall runoff), C is Chezy coefficient, R is hydraulic radius, α is momentum correction coefficient, g is gravitational acceleration.

6-point implicit difference scheme is adopted. The water level and discharge at each grid point are not solved at the same time, they are alternately calculated in sequence instead, respectively marked as h and O. The format is unconditional stable, which can remain calculation stability under considerable Courant number, and a long-time step can be taken to save computational time (Wang, 2007).

3 DEVELOPMENT AND APPLICATION OF COUPLING MODEL

3.1 Basic information

The study area is located in the Pearl River Delta (PRD) area, where the eastern and southern parts are alluvial plains while the western and northern parts are hilly terraces. The central-north area is of higher grounds and the terrain leans to the southeast direction. The whole area is densely covered by river networks, sluice 1# and 2# are located at the border where the inland and the outer rivers meet. The river system of the area is shown in Figure 2.

The peripheral levee of the regional water system has already met the flood control standard, so the major problem of the water system is the internal drainage. With the speeding up of urbanization process, utilization properties of lots of lands have been changed, which will result in the decrease of water capacity of the region. When the flood and tide come at the same time, the excess water cannot be drained by the sluices, which will lead to waterlog disaster. Therefore, it is quite necessary to study this area.

3.2 Development of the model

3.2.1 Calculation of rainfall runoff

The total area of the study region is 159.4 km^2. The division of catchment areas should consider the topography, geographical features, confluence of the river network, drainage areas, arrangements of hydraulic projects, etc. There are 56 subcatches after model generalization, which are shown in Figure 3 (the serial number begins with 2). The runoff processes under different precipitation conditions at each outlet of the subcatches can be obtained by SWMM.

3.2.2 Generalization of river network

The basic principle of the river network generalization is that the results should reflect the hydraulic characteristics of the natural river network, which means that the water conveyance capacity and regulation capacity must be close to or exactly the same with the actual river networks or lakes. In the water system of plain river network areas, as river channels crisscross, there is no fixed direction of the flows. Moreover, the river system is of cyclic structure which is called as looping river network. Inside of the river network, there are lakes and hydraulic constructions such as embankments, sluices and culverts. In the calculation, the river network is usually generalized as three kinds of elements which are nodes, river channels and hydraulic constructions (Wang and Shi, 2000).

According to the basic principles of river network generalization and data of main concerned channels, the river network of the studied area is generalized, which is shown in Figure 4.

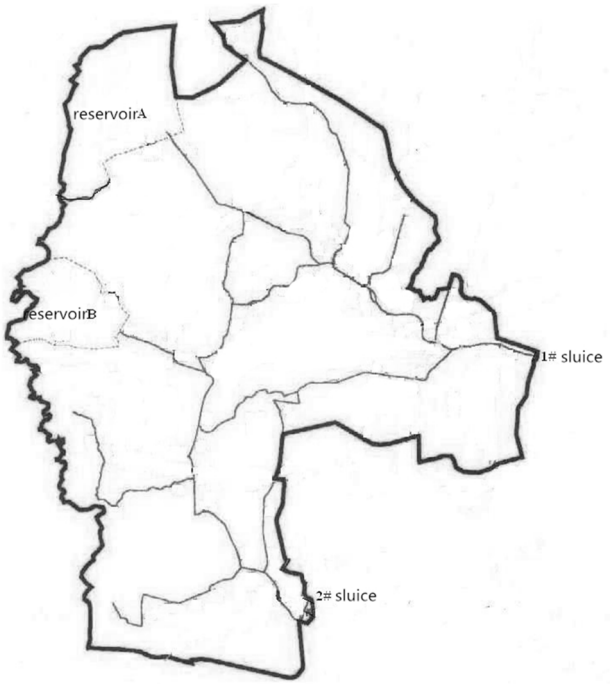

Figure 2. Water system map of the study area.

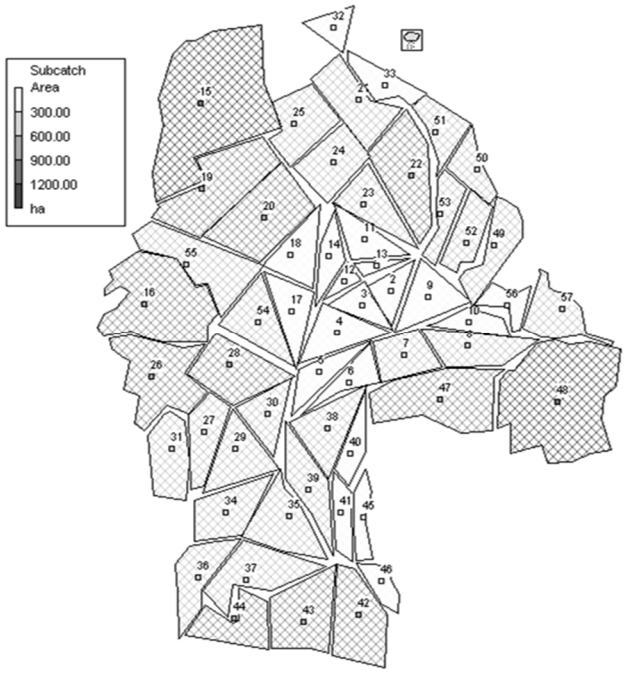

Figure 3. Schematic diagram of division of the study area.

3.2.3 Calculating cases

The study area is typical plain river network area, where the water channels crisscross. With a low-lying land, the elevations of the ground are almost the same. The rivers flow slowly and the flow directions are not fixed. The channel flow is largely influenced by boundary control structures and the outer tide. In flood season, when heavy rain occurs, self-drainage is quite difficult due to the high tide level, so water is stored in the river channels and drainage is effective only when the tide declines, thus waterlog often forms. Besides, when the astronomical tide, the waterlogging and typhoon meet together, more long-lasting high water level of the outer river and higher tidal level will come up, so is worse waterlogging disaster. There is no necessary relationship between the origins of waterlogging and the tide, as well as the probability that they occur. According to the drainage plan of the studied area, two working conditions are drafted. The first working condition is of 10-year waterlogging and 5-year high tide level. The second working condition is of 20-year waterlogging and 2-year high tide level.

In addition, pumping stations are added at the locations of 1# and 2# sluices. Three computational schemes are designed to analyze the water level changes of the inland rivers under conditions of no pumping station and different pump discharge capacites.

1. Without pumping station.
2. Except the two existing sluices, 2 pumping stations are added to improve the drainage capacity. The 1# pumping station has a discharge capacity of 50m^3/s, while the 2# pumping station has a discharge capacity of 20 m^3/s.
3. Except the two existing sluices, 2 pumping stations are added to improve drainage. The 1# pumping station has a discharge capacity of 95 m^3/s, while the 2# pumping station has a discharge capacity of 30 m^3/s.

On the whole, calculation cases of this paper are listed in Table 1.

Table 1. Calculation conditions of the model.

Working conditions	Rainfall	Tide level	Schemes
I	10-year	5-year	No pumping station A B
2	20-year	2-year	No pumping station A B

3.3 Results and analysis

3.3.1 Impacts of the pumping stations

The locations of representative sections are shown in Figure 5. And the computational results of the highest instantaneous water levels of representative sections are displayed in Table 2 and Table 3. It can be shown that highest instantaneous water levels of the inland rivers are significantly decreased. It is also shown that the larger the pump discharge is, the more the water level decreases.

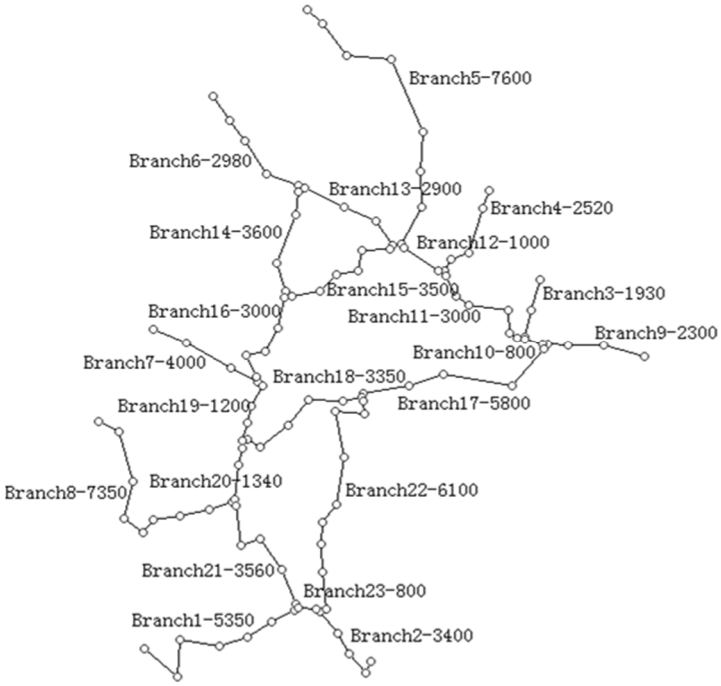

Figure 4. Generalized river network in the study area.

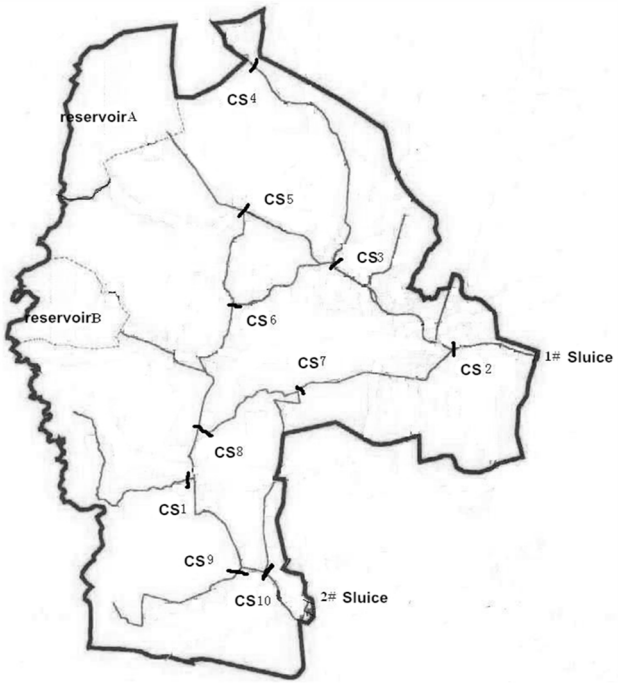

Figure 5. Location of representative sections.

Table 2. The highest water level of representative sections in the first calculation condition (m).

Cross section number	Cross sections location	No pumping station	A	B
1	branch8 7350m	3.02	2.91	2.67
2	branch9 2300m	2.84	2.65	2.41
3	branch12 1000m	2.86	2.71	2.46
4	branch5 0m	2.98	2.86	2.54
5	branch13 2900m	2.90	2.74	2.5
6	branch14 3200m	2.90	2.74	2.49
7	branch17 5800m	2.98	2.82	2.57
8	branch19 1200m	3.02	2.88	2.64
9	branch1 5350m	2.97	2.91	2.68
10	branch2 3400m	2.97	2.91	2.67

Table 3. The highest water level of representative sections in the second calculation condition (m).

Cross section number	Cross sections location	No pumping station	A	B
1	branch8 7350m	3.01	2.88	2.79
2	branch9 2300m	2.77	2.68	2.58
3	branch12 1000m	2.88	2.71	2.65
4	branch5 0m	3.07	2.78	2.72
5	branch13 2900m	2.91	2.76	2.70
6	branch14 3200m	2.9	2.74	2.70
7	branch17 5800m	2.88	2.84	2.74
8	branch19 1200m	2.96	2.87	2.79
9	branch1 5350m	3.01	2.86	2.74
10	branch2 3400m	2.99	2.87	2.72

3.3.2 Sensitivity analysis of rainfall and tide level

(1) Without pumping station

Water surface profiles of representative cross sections are given in Figure 6 and Figure 7.

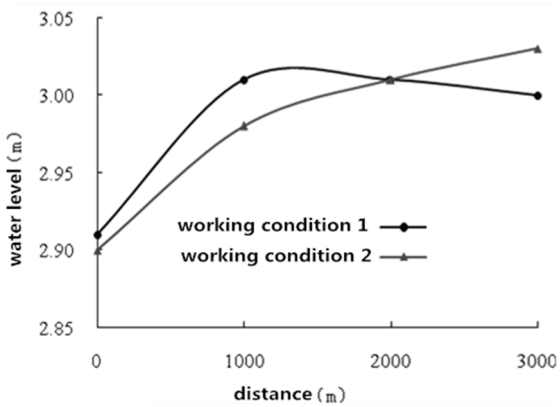

Figure 6. Water surface profile of branch16.

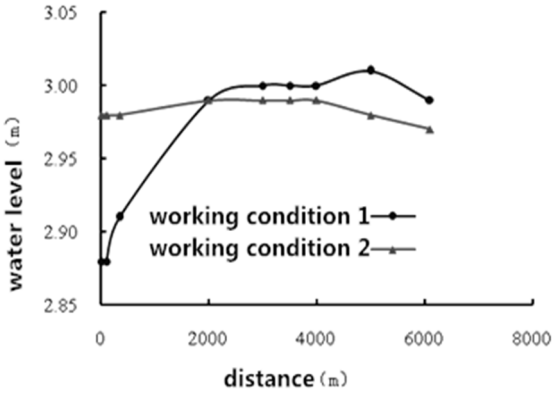

Figure 7. Water surface profile of branch 22.

(2) Scheme A
Water surface profiles of representative cross sections are given in Figure 8 and Figure 9.

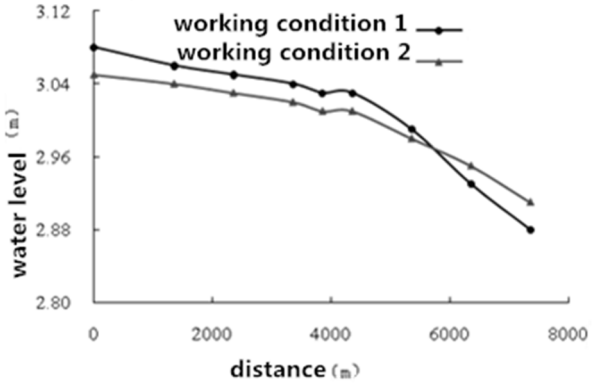

Figure 8. Water surface profile of branch 8.

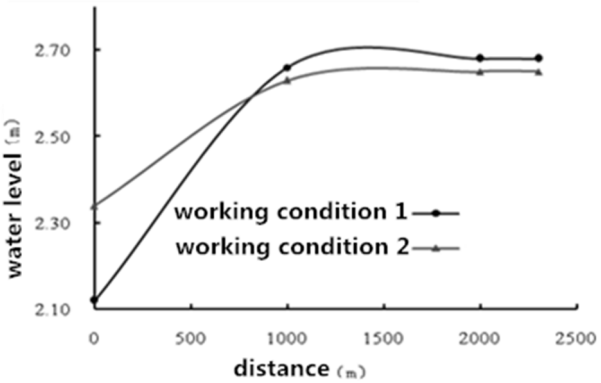

Figure 9. Water surface profile of branch 9.

(3) Scheme B
Water surface profiles of representative cross sections are given in Figure 10 and Figure 11.

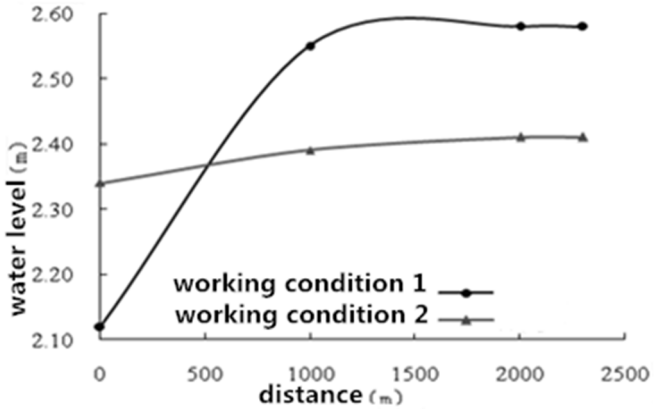

Figure 10. Water surface profile of branch 9

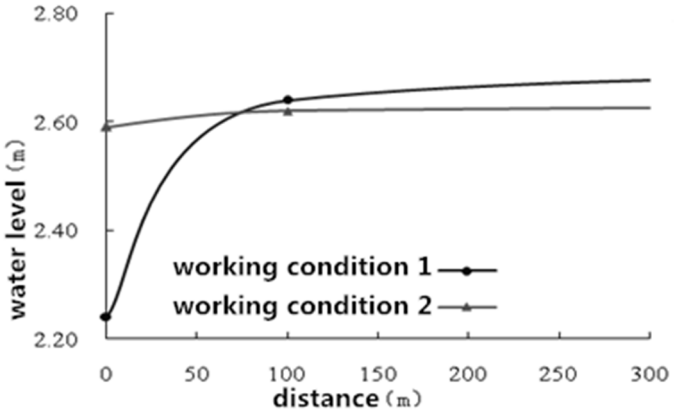

Figure 11. Water surface profile of branch 2.

It can be found in the calculation that when there's no pumping stations, some of the rivers have higher water levels in the 10-year waterlogging condition than that of the 20-year due to the higher tide level of the outer river. The range of these river reaches influenced by the tide level is shown in Figure 12(a). Besides, the ranges of river reach influenced by the tide level after the construction of pumping stations are given in Figure 12(b) and Figure 12(c). It can be seen from the figures that with the help of pumping stations, effects from the tide level are largely decreased, and the water level of the inland river is mostly influenced by the precipitation and the pump discharge capacity.

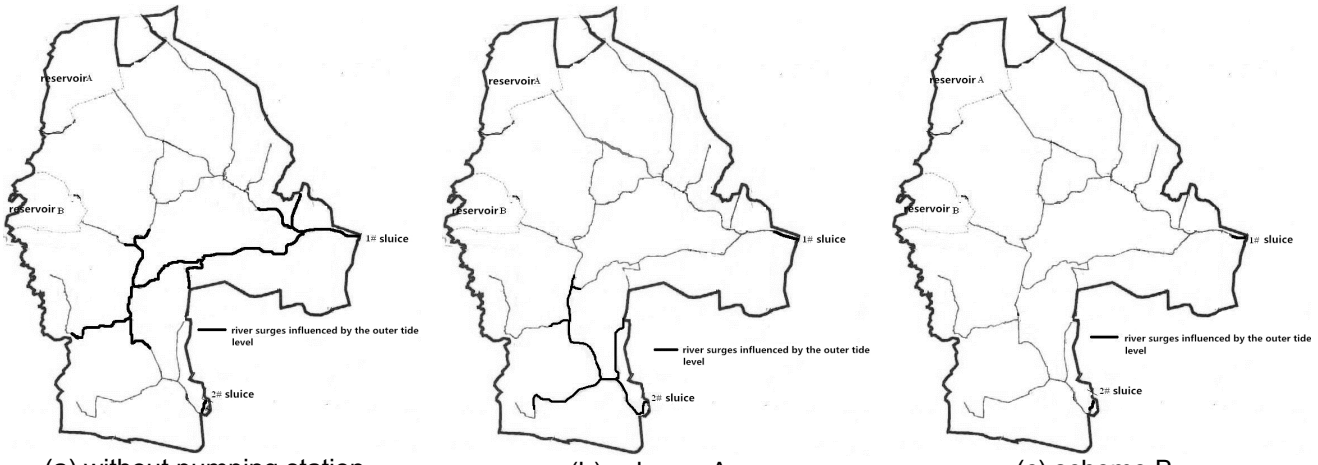

(a) without pumping station (b) scheme A (c) scheme B

Figure 12. Influence scope of river surges.

4 CONCLUSIONS

The rain-runoff process of river network and the drainage process of the study region were simulated by the SWMM rainfall-runoff model and MIKE11 hydrodynamic model in this paper. The main conclusions are as follows:

(1) With the pump station, the water level of inner-river was decreased apparently compared with the case of no pump station. Moreover, the greater the pumping capacity is, the larger the drawdown value of the water level.

(2) Without the pump station, parts of the river reaches have high water levels in case one compared with the case two, for the reason that the case one has a higher outer tide level. The influence of outer tide level is decreased obviously, and the water level is mainly influenced by rainfall and pumping capacity.

(3) The results of this paper are reasonable, indicating the coupling model have an application value for flood control and drainage planning of other plain river network districts.

ACKNOWLEDGEMENTS

The research reported herein is funded by Ministry of water resources public welfare industry special funds scientific research projects(CKSC2014638/HL), Central public welfare scientific research basic scientific research business expenses of Changjiang River Scientific Research Institute (CKSF2015004/HL, CKSF2015049/HL, CKSF2017010/HL).

REFERENCES

Cong, X.Y., Ni, G.H., Hui, S.B., Tian, F.Q. & Zhang, T. (2006). Smiulative Analysis on Storm Flood in Typical Urban Region of Beijing based on SWMM. *Water Resources and Hydropower Engineering*, 37(4), 64-67.

Liu, J. & Xu, X.Y. (2001). Application of the Urban Rain Flood Model in Drainage Analytical Calculation of the Urban Areas of Tianjin. *Haihe Water Resources*, (1), 92-111.

Liu, J., Guo, L.H., Zhang, J.T. & Lv, T. (2006). Study on Simulation of Drainage and Flooding in Urban Areas of Shanghai based on Improved SWMM. *China water & wastewater*, 22(21), 64-66.

Ren, B.Z., Deng, R.J. & Li, W.J. (2006). Principles of SWMM Model and Its Application in Xianing Port Area. *Port and Waterway Engineering*, (4), 41-44.

Wang, L.Y. (2007). Applied Research of Danish MIKE11 Hydrodynamic Module in River Network Simulation. *China Water Transport*, 7(2),106-107.

Wang, X.D. & Shi, J.H. (2000). Research and Application of River Network Model in Lixiahe Area. *Hydrology,* 20(supplement), 5-9.

GREEN ROOF: RESPONSE TOWARDS EL-NINO AND IMPACT ON RUNOFF WATER QUALITY

KHAIRUL RAHMAH AYUB[1], AMINUDDIN AB. GHANI[2] & NOR AZAZI ZAKARIA[3]

[1, 2, 3] River Engineering and Urban Drainage Research Centre (REDAC), Universiti Sains Malaysia, Engineering Campus, Penang, Malaysia
redac03@usm.my; redac02@usm.my; redac01@usm.my

ABSTRACT

Sustainable Urban Drainage Systems (SUDS) promoting numerous type of facilities in stormwater management. The facilities fall in three major group functions namely source control, site control and regional control. Control at source facilities like green roofs, permeable surface and so forth are purposely built to manage rainfall close to where it falls. Benefits of green roof around the globe are very noticeable. This paper will discuss the performance of green roof during El-Nino period and runoff water quality from high intensity rainfall. Intensive green roof is constructed on the top of car parking roof. It was observe daily for one year. Results found that green roof's contribution in cooling the indoor area of car park in tropical climate region varies during El-Nino period. Its performance relies to the surrounding temperature which during El-Nino, it can increase the surrounding temperature in the range 0.5^{o}C to 2.0^{o}C compared to normal period. However, during normal climate, green roof manage to reduce indoor area temperature in the range of 0.2^{o}C to 2.0^{o}C. This study shows the green roof manage to perform very well in delaying the outflow during high intensity rainfall. It can retain 100% of rain water or up to 6 months ARI event. However, it depends on the frequency of the events. In term of improving the rain water quality, vegetation used did not gave significance difference in improving runoff water quality. Nonetheless the parameters studied still did not permit according to the National River Water Quality Standard for Malaysia and Malaysia Drinking Water Quality Standard (Raw Water). This study concluded that application of green roof in urban infrastructure like parking areas and bus stops is very promising method for tropical climate countries.

Keywords: Intensive green roof; runoff quality; stormwater management; sustainable rrban drainage systems (SUDS); thermal.

1.0 INTRODUCTION

Climate changes are providing many challenges around the globe and one of it is El- Nino. During the El-Nino, the weather is possible to be extremely hot and people have to face and deal with the rising temperatures and changes in rainfall patterns are among other effects. People have started to prepare for climate change and are looking for suitable adaptation measures to put in place to manage its impacts. Due to this scenario, the green roof becomes a consideration. Green roofs are vegetated roofs, or roofs with vegetated spaces. The benefits of green roof have been studied widely. It brings a lot of benefits in social, economic and environment aspect. Berndtsson (2010), Getter et al. (2007), VanWoert et al. (2005) and Villareal and Bengtsson (2004; 2005) discovered that it also can create new habitat, filter pollution, decrease noise or noise buffer, improve air quality, reduce microclimate temperature and others as its benefits.

Many studies show that green roof can be effective and sustainable facilities in order to reduce the indoor temperature (He et al., 2016; La Roche & Berardi, 2014) and retain rainfall runoff impacts in urban areas (Stovin et al., 2012; 2015; 2017; Grabowiecki et al., 2012; Liaw et al., 2011). The water quality of runoff that comes from the green roof also gain attention of researchers and they found that the performance of green roof varies and relies on many factors like substrates materials, depth, slope, rainfall depth and ect. (Jung et al., 2016; Vijayaraghavan and Raja., 2014; Razzaghmanesh et al., 2014;).

In tropical climate weather like Malaysia, receiving high rainfall throughout the year is normal. Availability of big area of tropical rainforest as a water catchment area do not mean that the country is free from the water resources issues. Even though average rainfall per year is 3500mm, the country has problems related to water scarcity and back in 2016, Malaysia faced El-Nino and it worsens the problem. Thus this paper discusses the response of green roof during the El-Nino in reducing the indoor temperature and the runoff quality of rainfall after the El-Nino period.

2.0 MATERIAL AND METHODS

2.1 Study area - Car parking green roof

The study has been done in Engineering Campus, University Sains Malaysia. It is located in the Peninsular Malaysia, the state of Penang. The implementation of intensive green roof in the real condition was applied on the top of car park. Five similar structures of green roof test platforms were built on top of the car park roof for this study. These green roofs were constructed with dimension of 2.0m x 2.0m each. Each platform represent intensive green roof with slope selected value at 2^o and were constructed using bricks. Each platform consisted double layer of drainage cells (40mm each), covered with geotextile filter fabric. On top of this drainage layer. It was covered by 50mm depth of clean river sands approximately with 2.0mm grain size, followed with 200mm top soils which play a role as substrate layer. All open surfaces were covered with waterproofing membrane except for vegetation area to avoid leakage. At the lower end of the platforms, polyvinyl chloride (PVC) pipe of 10cm in diameter was attached as outlet to direct runoff through the measuring device and for water sampling purpose. The difference among these platforms was based on the vegetation species that was planted. The first platform (GR1) was planted with the *Arachis pintoi* (Family: Fabaceae) and second platform (GR2) was leaved in bare as a control green roof platform. *Zoysia matrella* (Family: Poaceae) was planted in the third platform (GR3), whereas in the fourth platform (GR4) consisted of *Kalanchoe pinnata* (Family: Crassulaceae). The mixture of these three species were planted in the fifth (GR5) and final platform.

2.2 Data collection

For thermal preliminary study, temperature under green roof car parking (indoor temperature) and under conventional car parking also was recorded and compared. Temperature was recorded daily in the morning (8.30am) and in the evening (5.00pm). Evaporation data was gained from evaporation pan logger which was located beside the green roof. The data was used in calculating potential evapotranspiration (ET_o) in study area. For calculating ET_o equation 1 has been used.

$$ETo = Kp * Epan \quad (1)$$

Where ET_o = potential evapotranspiration (mm/day), K_p = pan coefficient (Malaysian value is 0.75 as in Ng et. al. (2004)) and E_{pan} = pan evaporation (mm/day).

To gain rainfall and runoff data, measuring devices was installed only in GR5 due to the limited equipment and budget. Outlet of GR5 was installed with probe sensor which allowed continuous measurement of the water level, velocity and flow. This probe was connected to a Sigma 950 Flowmeter data logger which recorded flow every minute and was downloaded to a computer hard drive twice a week. Surface of GR5 also was installed with the water level sensor to determine the level of ponding water if it occurred. Tipping bucket rain gauge also was installed on the car park green roof. The data were recorded every minute and downloaded to the computer hard drive after rainfall events or twice a week. Rainfall intensities were categorized based on Roslan (1995) as summarized in Table 1. For runoff water quality purpose, each outlet of green roof platforms were connected to the 5 liters barrel to allow grab sampling of runoff when needed. Substrate properties were gained from laboratory experiments. Parameters tested were bulk density (1.766 g/cm^3), porosity (33.33%), permeability, k (5.084×10^{-4} cm/s) and maximum water capacity, WC_{max} (19.96%).

Table 1. Rainfall intensity categorization (Roslan, 1995)

Rainfall Intensity (mm/hr)	Remarks
< 6.5	Low
6.5 - 13	Medium
13 - 50	High
> 50	Severe

3.0 RESULTS AND DISCUSSIONS

3.1 Thermal performance

Figure 1, show the difference between car parking with green roof (GR) and car parking with conventional roof (SC). In average, temperature under green roof was 1^oC higher than conventional roof during morning and evening. It is believe due to the insulation effect of the green roof. Temperature pattern recorded shows similar results to the study done by He et al. (2016). They found that there were two phases in temperature development in green roof. The first phase was from 7.00am to 3.00pm in which the temperature sequence was; indoor air > inner surface of structural layer > roof local air > middle soil layer > outer surface of structural layer. During this period, green roof acted as a heat sink. Second phase of temperature development, He et al (2016) found that from 3.00pm to 7.00pm, the sequence was from indoor > inner surface of structural layer > outer surface of structural layer > middle soil layer > roof local air. It showed that green roof performed as a layer of thermal resistant.

Result gained in this green roof car parking study during morning (represent first phase) and evening (second phase) temperature confirmed the scenario. Base on this comparison of temperature it shows that green roof's contribution in cooling the indoor area of tropical climate region varies. Its performance relied on the surrounding temperature which in Figure 1, shows clearly the difference between February until April compared to May. It was notable on March 2016; Malaysia faced El-Nino and ended in April 2016. El-Nino effect can increase the surrounding temperature in the range 0.5°C to 2.0°C compared to normal period (Tangau, 2016). It confirms that performance of green roof as a thermal mitigation during El-Nino, slightly decreases due to the temperature was higher than normal and consequently it shows the limitation of green roof.

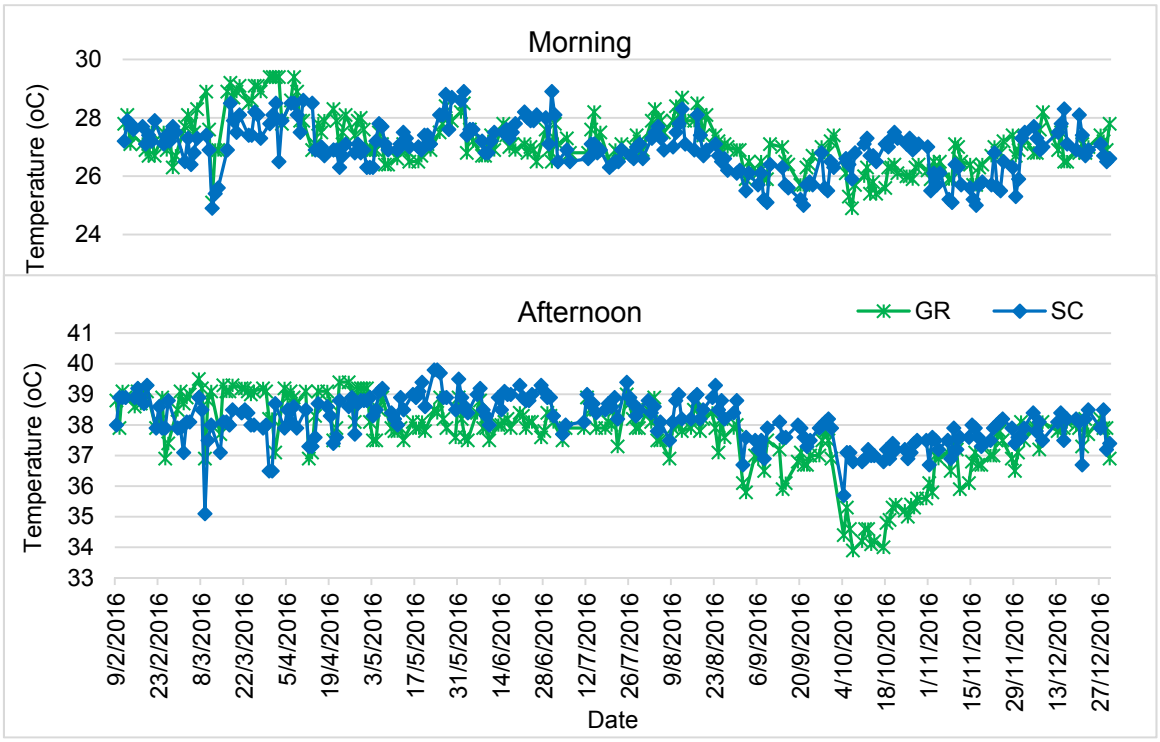

Figure 1. Temperature comparison between green and conventional roof

3.2 Flow attenuation

The total of 60 events during monitoring period occurred and measured by the rain gauge located in study area. Intensity Duration Frequency (IDF) Curve was developed based on Rainfall Station at Sungai Simpang Ampat Tangki in Penang. The selection of the station was due to being the nearest in the study area. Even though 57 events recorded shows one to six month ARI but most of the events had high rainfall depth (Figure 2) and many events were categorized as high intensity (Figure 3).

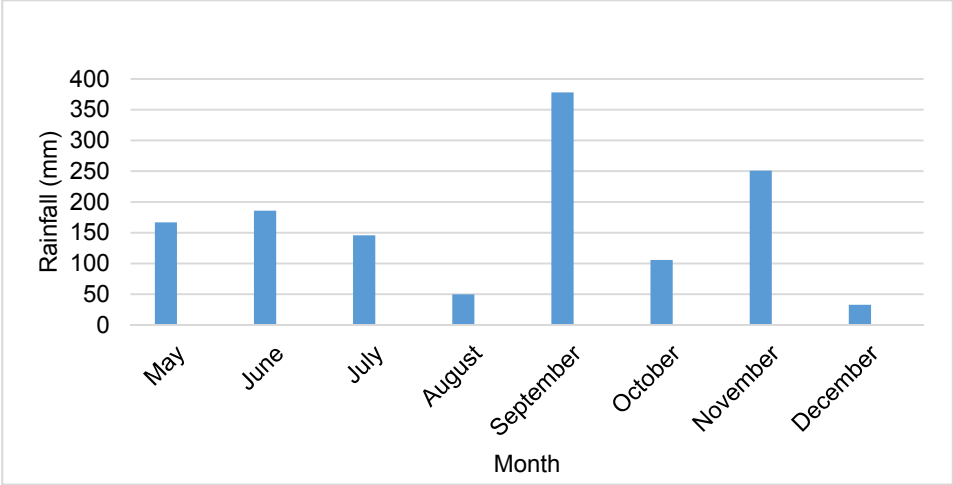

Figure 2. Rainfall depth during study period

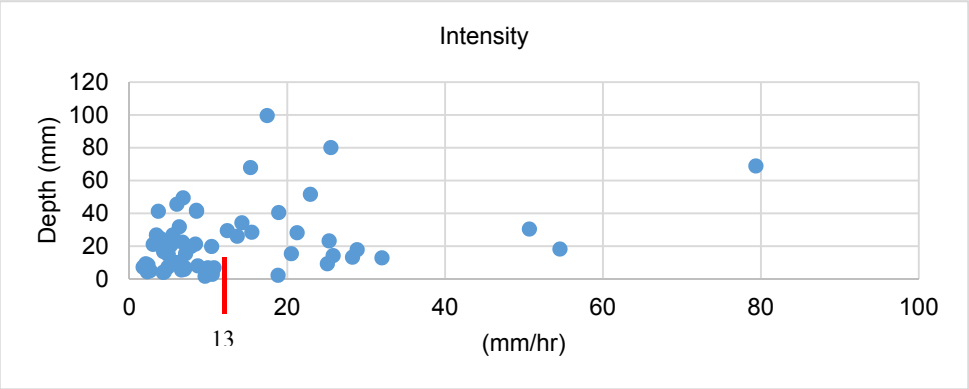

Figure 3. Rainfall intensity

However, outflow runoff did not occur from the green roof in every events. It might be due to the substrate capability in holding water. The high potential of soil substrate in holding water is believed due to high value of potential evapotranspiration rate (ET_o). In average evapotranspiration rate (ET_o was at 29.64mm/day in study area. Event on 3rd June 2016 reached 1 year ARI with the intensity of 17.47 mm/hr and green roof managed to delay (1 hour) the existence of rain water outflow and it gave a good sign in stormwater management. Figure 4 show there was attenuation of the runoff during the event. It was proven that the green roof manage to slow down the volume of the rain water before it reach to the ground. Consequently, it gave time to the surface runoff on the ground that occurred directly from the rainwater flow to the nearest water bodies or downstream area.

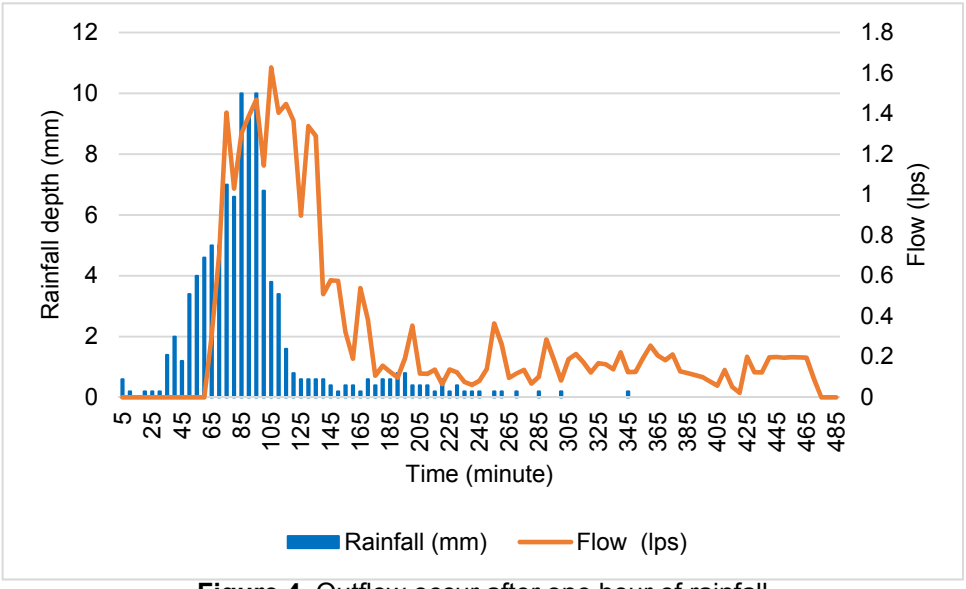

Figure 4. Outflow occur after one hour of rainfall

3.3 Runoff water quality

Vegetation used in this study showed various responses in treating rain water that fall onto the green roof surface (Figure 5). Four parameters studied were analyzed namely as Total Phosphate (TP), Total Nitrogen (TN), Ammoniacal Nitrogen (AN) and Potassium (K). Median concentration of TP in the outflow water of each green roof platform was varied. It was found to be higher compared to the rain water. The similar trend was gained for AN, TN and K too. It is believe that the substrate of the green roof itself which is the oil, contains some amount of this pollutants and it was flushed by rain water that flow through the substrate and become outflow of green roof. Although vegetation managed to uptake the nutrient, but it still does not give significant difference due to only small amount were consumed by the plants itself. Phosphate is an essential nutrient in providing energy for plants. It occurs naturally in low level and can quickly bonds to soil particles. The values of TP were found to be lower compared than study done by Ayub et al. (2016; 2015), Speak et al. (2014) and Vijayaraghavan et al. (2012). Higher concentration of TN, AN and K in outflow water was consistent with a study done by Razzaghmanesh et al. (2014) in South Australia. They also found potassium content in outflow runoff of green roof system were higher than influent. Whereas the concentration of nitrogen found to increase with time during the study period and it prove that green roof system can act as sink of nitrate (Gabriel et al., 2016; Razzaghmanesh et al., 2014; Berndtsson et al., 2009). Result in Figure 5 also shows that vegetation plays a minor role in improving rain water quality. Other than that, it can contemplate that the substrate still

haven't stabilize to act and perform for better treatment of the rain water. Nonetheless the nutrients' concentration in outflow were high in this study. The values that were permitted in the Malaysia Drinking Water Quality Standard (Raw Water) (Ammonia, 1.5mg/L & Nitrate, 10.0mg/L) and the runoff water quality fall in group 2 of the standard.

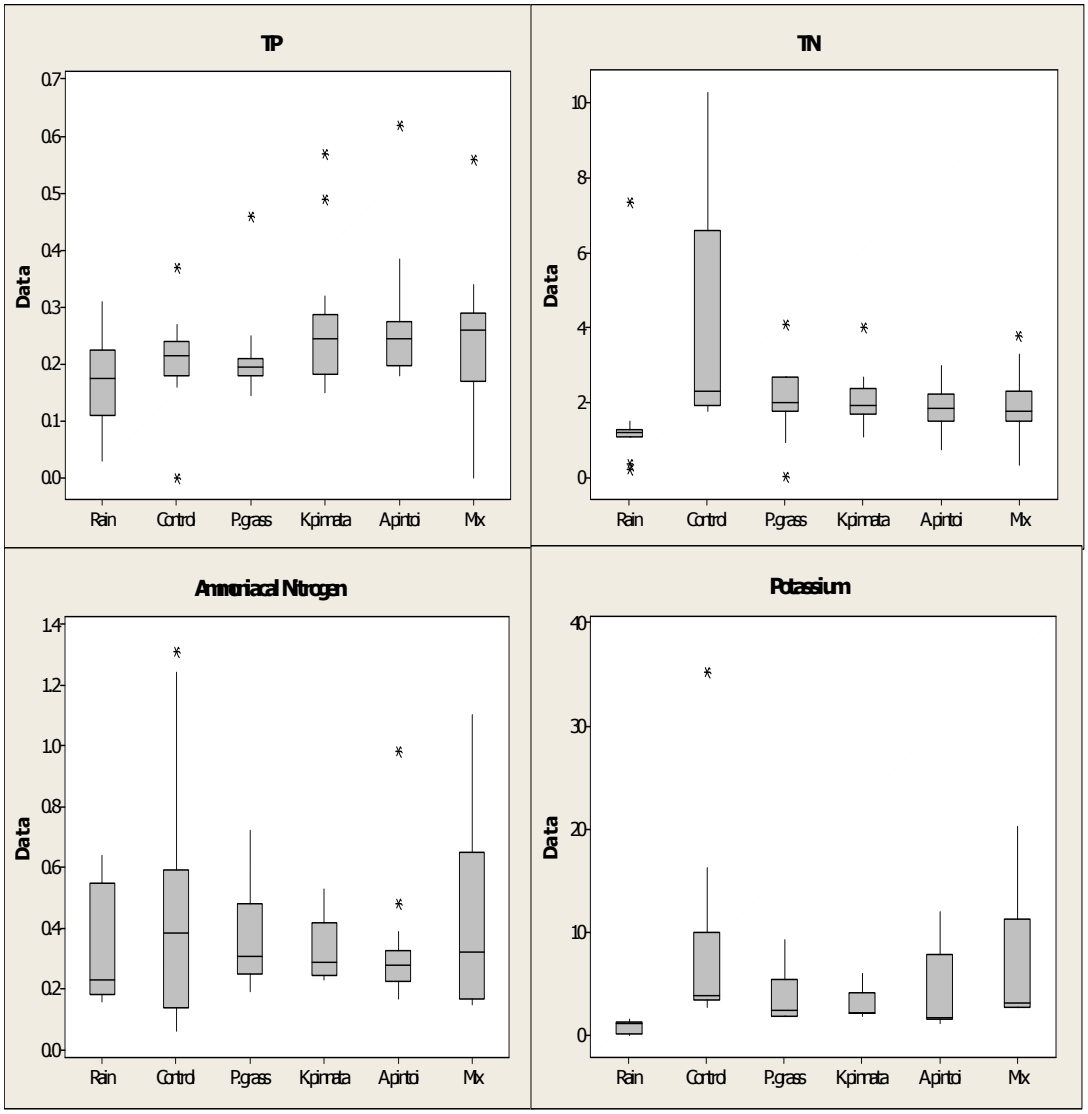

Figure 5. Boxplot of the pollutants concentration in every green roof platform compare to rain water

4.0 CONCLUSIONS

Green roof as a thermal mitigation is proven due to the ability in reducing indoor temperature especially during the sunny days (May – December 2016). However, the performance relies on the surrounding temperature and there is the limitation of the green roof in thermal mitigation (El-Nino period). Green roof's contribution in cooling the indoor area of tropical climate region varies. Other than that green roof manages to delay the rain water from reaching the ground so it gives time to the ground surface runoff flow to the downstream first. For the outflow water quality it is believed that the water quality rely more to the substrate significantly. The stabilization period of the substrate and green roof needs to be carried out in the next phase of this research.

5.0 ACKNOWLEDGEMENTS

This research is funded by Ministry of Science, Technology and Innovation, Malaysia. The authors also like to thank the Deputy Vice Chancellor (Research and Innovation), Universiti Sains Malaysia (USM). The gratitude also goes to REDAC's staff for their cooperation and involvement in this research.

REFERENCES

Ayub, K.R., Ab, Ghani, A., Zakaria, N.A. & Shaharudin, S. (2015). Efficiency of Intensive Green Roof in High Intensity Rainfall for Stormwater Treatment: Selection of Vegetations. *E-proceeding of the 26th IAHR World Congress.* 28 June – 3 July 2015. The Hague, The Netherlands.

Ayub, K.R., Ab, Ghani, A., Siang, L.C., Shaharudin, S. & Yusof, M.F. (2016). *Feasibility and Practicality of Green Roof for Stormwater Management in Malaysia*. Short term research project Report. Universiti Sains Malaysia. unpublished.

Berndtsson, J. C., Bengtsson, L. & Jinno, K. (2009). Runoff water Quality from Intensive and Extensive Vegetated Roofs. *Journal of ecological Engineering. Elsevier*. 369-380. doi: 10.1016/j.ecoleng.2008.09.020.

Berndtsson, J. C. (2010). Green Roof Performance Towards Management of Runoff Water Quantity and Quality: A Review. *Journal of Ecological Engineering*. Elsevier. doi: 10.1016/j.ecoleng.2009.12.014.

Gabriel, P.M., Pascual, F. R., Carlos, V. R., Oscar, V., Mario, D.O., Juan, P.R.S. & Correal, M.E. (2016). Assessment of Runoff Quantity and Quality for Extensive Green Roof Modular Systems. *NOVATECH Proceeding 2016.*

Getter, K. L., Rowe, D. B. & Andresen, J. A. (2007). Quantifying the Effect of Slope on Extensive Green Roof Stormwater Retention. *Journal of Ecological Engineering*. Elsevier. 225-231. doi: 10.1016/j.ecoleng.2007.06.004.

Grabowiecki, P. Tota-Maharaj, K., Tumula, P.D. & Babatunde, A. (2012). The Hydrological Assessment of Green Roofs within the Greater Manchester Area, UK. *Sixteenth International Water Technology Conference*, Istanbul Turkey.

He Y., Yu H., Dong N. & Ye H. (2016). Thermal and Energy Performance Assessment of Extensive Green Roof in Summer: A Case Study of a Lightweight Building in Shanghai. *Energy and Buildings*, 127, 762-773.

Jung, Y., Yeo, K., Oh, J., Lee, S., Park, J. & Song, C.G. (2016). The Economic Effect of Green Roofs on Non-Point Pollutants Dources Management using the Replacement Cost Approach. Water Engineering. *KSCE Journal of Civil Engineering*. doi:10.1007/s12205-016-0370-3

La Roche, P. & Berardi, U. (2014). Comfort Energy Savings with Active Green Roofs. *Energy and Buildings*, 82, 492-504.

Liaw, C.H., Huang, E.H., Lai, C.T. & Lin, S.C. (2011). The Effect of a Green Roof on Rainwater Runoff. *Institute of Electrical and Electronics Engineers*. 1798-1801.

Ng M. W., Alejandro C., Ahmad Khairi A.W. & Sobri H. (2004). Estimation Evaporation and Evapotranspiration in Malaysia Using Penman and Christiansen Methods. *Borneo Science*, 15, 23-36.

Razzaghmanesh, M., Beecham, S. & Kazemi, F. (2014). Impact of Green Roofs on Stormwater Quality in a South Australian Urban Environment. *Science of the Total Environment,* 470-471. Elsevier. 651-659. doi:10.1016totenv.2013.10.047.

Roslan, Z.A. (1995). Tanah Runtuh – Ciri-ciri, Ramalan dan Teknologi Kawalan. *Isu-isu semasa Sains dan Teknologi 1995*. Petaling Jaya, Selangor. 94-100.

Speak, A.F., Rothwell, J.J., Lindley, S.J. & Smith C.L. (2014). Metal and Nutrient Dynamics on an Aged Intensive Green Roof. *Environmental Pollution 184*. Elsevier. 33-43. doi: 10.1016/j.envpol.2013.08.017.

Stovin V., Vesuviano G. & Kasmin H (2012). The Hydological Performance of a Green Roof Test Bed Under UK Climate. *Journal of Hydrology*. Elsevier. 148-161.

Stovin V., Poe S., De-Ville S. & Beretta C (2015). The Influence of Substrate and Vegetation Configuration on Green Roof Hydrological Performance. *Ecological Engineering*. Elsevier. 159-172.

Stovin V., Vesuviano G. & De-Ville S. (2017). Defining Green Roof Detention Performance. *Urban Water Journal*. 14(6), 574-588.

Tangau M. (2016) Minister of Science, Technology and Innovation of Malaysia. *Media Statement*. 8 January 2016.

VanWoert, N. D., Rowe, D. b., Andresen, J. A., Rugh, C. L., Fernandez, R. T. & Xiao, L. (2005). Green Roof Stormwater Retention: Effects of Roof Surface, Slope, and Media Depth. *Journal of Environmental Quality*. 1036-1044. doi: 10.2134/jeq2004.0364.

Vijayaraghavan, K., Joshi, U.M. & Balasubramanian, R. (2012). A Field Study to Evaluate Runoff Quality from Green Roofs. *Water Research 46*. Elsevier. 1337-1345. doi:10.1016/j.watres.2011.12.050

Vijayaraghavan, K. & Raja, F.D. (2014). Design and Development of Green Roof Substrate to Improve Runoff Water Quality: Plant Growth Experiments and Adsorption. *Water Research 63*. 94-101.

Villareal, E. L. & Bengtsson, A. S. D. L. (2004). Inner City Stormwater Control Using a Combination of Best Management Practices. *Journal of Ecological Engineering*. Elsevier. 279-298. doi: 10.1016/j.ecoleng.2004.06.007.

Villareal, E. L. & Bengtsson, L. (2005). Response of a Sedum Green-Roof to Individual Rain Events. *Journal of Ecological Engineering*. Elsevier. 1-7. doi: 10.1016/j.ecoleng.2004.11.008.

CORRELATING HYDROLOGICAL AND METEOROLOGICAL PARAMETERS IN HYDROLOGICAL PROCESSES USING SOFT TOOL

SHRIKANT CHARHATE[1], VIDYANAND SAYAGAVI[2] & RAJENDRA MAGAR[3]

[1] Pillai HOC College of Engineering & Technology, Rasayani, New Mumbai – 410 207, India
sbcharate@yahoo.co.in

[2] M.G.M.'s College of Engineering & Technology, Kamothe, New Mumbai- 410 206 India
vgsayagavi62@gmail.com

[3] AIKTC School of Engineering & Technology, New Mumbai – 410 206, India
rajendramagar69@gmail.com

ABSTRACT

Rainfall-runoff is an important hydrological process that is complex in its nature involving in-depth study of hydrological and meteorological parameters. Hydrological processes are dynamic, chaotic and non–linear. Accurate estimation of hydrological parameters could be carried out with the study of influence of meteorological parameter by performing sensitivity analysis and so on. Generally, the process governs with rainfall as the major factor, however in monsoon season some meteorological parameters may have the greater influence which may lead to enhance the model accuracy in the estimation of runoff. Some meteorological parameters; temperatures, relative humidity and pan evaporation could influence the process. The rainfall and runoff may affect evaporation, humidity and temperature. Meteorological parameters like maximum temperature and minimum temperature affect humidity, evaporation and runoff of a catchment. This paper is mainly focuses on the study of influence of meteorological parameters in the rainfall-runoff processes and importance of meteorological parameters in such process. The tools used here are Multiple Linear Regression and soft computing tool, Artificial Neural Network. The study area selected for the purpose is Shivade catchment of upper Krishna basin, Maharashtra State in India. The meteorological parameters collected includes pan evaporation, average temperatures, average wind speed, relative humidity and hydrological parameters; rainfall and runoff. The correlation analysis amongst all the parameters is carried out to perform overall sensitivity analysis. The effect of all the parameters on each other is studied. The meteorological parameters namely maximum temperature and minimum temperature along with some other parameters have been studied using MLR and ANN model building. Amongst the two methods, ANN models exhibited better estimation of both hydrological and meteorological parameters. The statistical analysis and the qualitative analysis showed influence of parameters on each other, however few parameters do not show correlation but are significant in the processes as observed in model development.

Keywords: Hydrological parameters; meteorological parameters; average rainfall; runoff; temperature.

1 INTRODUCTION

The estimation of hydrological and meteorological parameters is a challenging task. Meteorological processes and hydrological processes are dynamic, chaotic and non–linear. Estimation of these parameters plays vital role and majorly contributes in the influence of these process and depends on the accurate measurement of parameter. The accuracy in the estimation can be increased by using greater data length which was tried to achieve in the present study. The dependability of the hydrological process and meteorological process is important to decide upon role which parameters are having more influence on each other and vice versa. The same was analyzed by statistical tool, MLR and compared with ANN. Over few decades, ANN has been a popular software tool explored by many researchers for hydrological problems. Thirumalaiah and Deo (2000), Chang et al. (2002), Rajurkar et al. (2004), Srinivasulu and Jain (2006), Zhang and Chiew (2009), Charhate and Kote (2009), Googhari et al. (2010), Londhe and Charhate (2010), Jothiprakash and Magar (2012), Wu (2011), Arunkumar and Jothiprakash (2014), Fathima and Jothiprakash (2014), Mehr et al. (2015), Chang et al.(2014), Wu et al.(2014), Aichouri et al. (2015), Pandhiani (2015), Patel and Ramachandra (2015), Youngmin et al. (2015) and others showed the capability of ANN in solving hydrological problems.

The meteorological factors that affect runoff are temperature, relative humidity, wind velocity, pressure difference. Maximum temperature is considered as the highest temperature recorded during a specified period of time. The most common reference is to the daily maximum temperature. Average wind speed and time-averaged wind speed are averaged over a specified time interval. The mean wind speed varies with elevation above mean sea level and the averaging time interval while a standard reference elevation is 10 m and a standard time interval is 1 hour. The best model for meteorological parameters can be developed with Jordan

Elman Network as recommended by Afzali et al. (2011) and Multilayer Perceptron as recommended by Abhishek et al. (2012) and Baboo and Shereef (2010). A comparison between the MLR and ANN model for the same input shows that ANN models produced better correlation between the estimated parameter and the observed parameter as seen in De and Debanth (2009). Hence capacity of ANN was judged as a better estimation method than the traditional MLR method as recommended by Mohammed (2011) and by El Shafie et al. (2011).

The following section gives an idea about the best correlation of the meteorological parameters and their importance in the process. This paper discusses the correlation amongst all the parameters and also the effect on the process of runoff to estimate the accurate values in the process. The correlations of the parameters were found out by building models on the database of Shivade catchment. The common statistical methods were used for initial analysis. The MLR and ANN models were developed by studying the influence of each parameter.

2 METHODOLOGY AND DATA COLLECTION

In this paper two approaches were used to solve the problem, the Multiple Linear Regression (MLR) and Artificial Neural Networks (ANN). Over few decades, ANN has become one of the promising software computing tool in hydrological and meteorological parameter estimations. MLR is a method use to model the linear relationship between a dependent variable and one or more independent variables. The dependent variable is sometimes also called the predict, and the independent variables the predictors. Artificial neural networks are 'biologically' inspired networks and works on the cognition of human brains. The ANN has the ability to learn from empirical data information. The most common types are feed forward neural networks (FFNNs), typically shown in Figure 1 and recurrent neural networks (RNNs). Various types of neural network architectures can be used in the estimation process e.g. single-layer feed forward networks, multi-layer feed forward networks, recurrent neural networks, radial basic function, Jordan Elman network, etc.

The area selected for the present study was Upper Krishna basin located in the western regions of Maharashtra, India, lying between latitudes 13° 07' N and 19° 20' N and longitudes 73° 22' E and 81° 10' E. The study area has eighteen rain gauge stations in its catchment (Figure 2). The total area of Shivade catchment is 3261.03 sq. km with 67 km length of river in watershed up to gauge discharge site as 20.82 km. The average annual rainfall in the Krishna basin is 784 mm. The south west monsoon sets in the middle of June and withdraws during mid of October. About 90% of the rainfall occurs during the monsoon period of which more than 70% of the annual rainfall occurs during July, August and September. The duration of data for the present study is 2002 to 2010 (9 years).

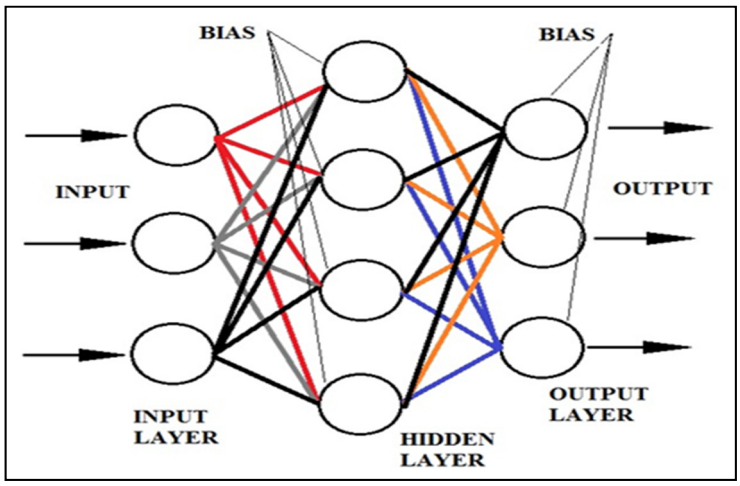

Figure 1. Feed forward neural network.

The models were developed with Artificial Neural Network (ANN) and MLR with similar data divisions with various combinations of inputs after studying the correlation amongst each other. The performance of the models was judged by quantitative analysis by evaluating them with correlation coefficient and error measures such as Mean Absolute Error (MAE), Mean Square Error (MSE), and Root Mean Square Error (RMSE). The model performance was also judged by qualitative analysis by drawing scatter plots and time series plots.

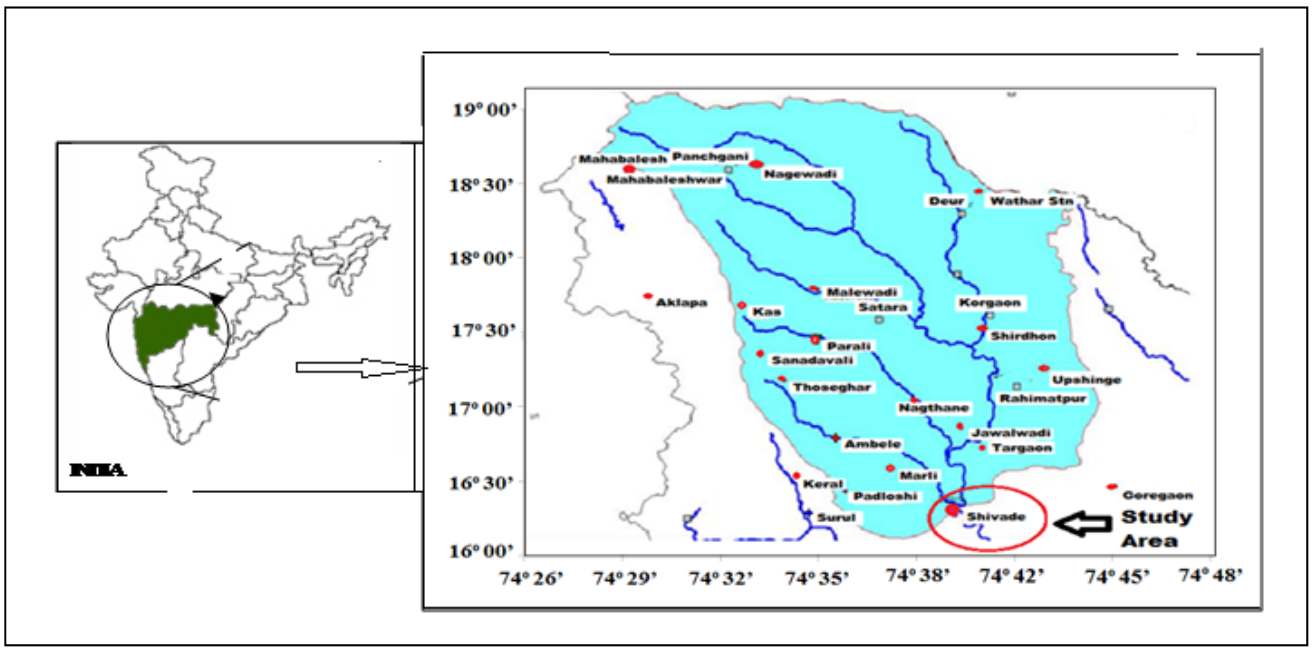

Figure 2. Map showing catchment details of Shivade Catchment, Krishna Basin Maharashtra, India.

3 RESULTS AND DISCUSSIONS

Initially data was analyzed by performing data trend analysis and gap filling by interpolation. The data was analyzed statistically by normalizing the values, performing analysis for standard deviation, kurtosis, median, mean and correlation. The estimation process involves developing models to find the correlation of each parameter to decide upon the maximum impact of input parameter. This was done to check the influence of each parameter in the hydrological process. This study has given an insight of all parameters and influence on each other, this helps to build the required models and the unnecessary data input will be restricted. The MLR and ANN models has been developed using the data of monsoon months for a period 2002 to 2010. From the available data ,70% of the observed values were considered to build the model while 30% of unseen data was used to test the models. The data division was finalized based on the number of trail conducted to arrive at the most accurate results. The meteorological parameters considered for analysis are pan evaporation, relative humidity, dry bulb temperature, minimum temperature, wet bulb temperature, maximum temperature and average wind speed. Data of nine years was processed to obtain the results and to arrive at a conclusion. For arriving at the most accurate estimation the correlation analysis was performed on all the parameters using statistical tools. The results of inter correlation of each hydrological and meteorological parameters are given in Table 1.

Table 1. Correlation of hydrological and meteorological parameters.

PARAMETERS	AVG MPS	HQC	MHS	MWS	MEP	MTD	MTN	MTW	MTX
AVG MPS	1	0.712	0.412	0.280	-0.426	-0.501	-0.196	-0.358	-0.565
HQC	0.712	1	0.318	0.222	-0.419	-0.398	-0.213	-0.293	-0.465
MHS	0.412	0.318	1	0.025	-0.539	-0.716	0.092	0.045	-0.636
MWS	0.280	0.222	0.109	1	0.043	-0.125	0.383	-0.071	-0.123
MEP	-0.426	-0.419	-0.539	0.043	1	0.778	0.335	0.523	0.820
MTD	-0.501	-0.398	-0.716	-0.125	0.778	1	0.174	0.653	0.907
MTN	-0.196	-0.213	0.092	0.011	0.335	0.174	1	0.297	0.235
MTW	-0.358	-0.293	0.045	-0.071	0.523	0.653	0.297	1	0.604
MTX	-0.565	-0.465	-0.636	-0.123	0.820	0.907	0.235	0.604	1

where AVG MPS=Average Rainfall in mm, HQC=Runoff in m^3/sec, MHS= Relative Humidity %, MWS= Maximum average Wind Speed, MEP= Pan Evaporation in mm, MTD= Dry Bulb Temp, MTN =Minimum Daily Temperature, MTW = Wet Bulb Temperature, MTX= Maximum Daily Temperature ºC.

From Table 1, it is seen that the hydrological parameters i.e. AVG MPS (rainfall) and HQC (runoff) have positive correlation with MHS (relative humidity) and MWS (wind speed). In the case meteorological parameters MEP has positive correlation with MTD (dry bulb temperature), MTN (minimum temperature), MTW (wet bulb temperature) and MWS while MHS has positive correlation with MTN,MTW and MWS; MTD has positive correlation on MEP,MTN,MTW,MTX (maximum temperature); MTN has positive correlation on MEP, MHS, MTD, MTW and MTX; MTW has positive correlation on MEP,MHS,MTD,MTN and MTX; MTX has

positive correlation on MEP, MTD, MTN, and MTW and MWS has positive correlation on AVG MPS, HQC, MEP and MHS. From above it is observed that HQC is closely affected by meteorological parameters such as relative humidity and average wind speed. The analysis was carried out taking into account these factors also. The following analysis gives estimation of some of the hydrological and metrological parameters considering their influence on each other. The negative correlation between some parameters indicates that they hardly contribute in the processes, especially in estimating runoff however estimation of such parameters may be useful in determining the other aspect of the process.

3.1 Runoff (HQC)

As seen in Table 1, HQC (runoff) has positive correlation with three parameters namely average rainfall (AVG MPS), relative humidity (MHS) and average wind speed (MWS). MLR models were developed using all three parameters and also by eliminating the parameters having lower correlation one by one. It was observed that the correlation between actual values of HQC and estimated values of HQC found to be highest when AVG MPS alone was used to develop the MLR having correlation coefficient=0.702 and less error measures with this combination. The resulting equation is shown in Eq. [1]:

$$HQC=37.27833741 +9.880741453 \text{ AVG MPS} \quad [1]$$

ANN model was developed using similar data division and similar process discussed above. Various networks were tried to achieve maximum accuracy however model developed with Jordan Elman network exhibited good results with correlation coefficient for testing as 0.865 and the MAE value 62.46. The correlation of the observed HQC and estimated HQC by ANN found to be good. The time series plot between observed values of HQC and estimated values of HQC by MLR and ANN are plotted in Figure 3. The estimated values of HQC using ANN are in agreement with observed values. The results of the models testing are given in Table 2 showing the performance of all the input methods used in the model building. From Table 2 it is seen that addition of some meteorological parameters having positive correlations contributed in the accuracy of model.

Table 2. Results for runoff estimation analysis.

INPUT	OUTPUT	TESTING							
		r		MAE		MSE		RMSE	
		MLR	ANN	MLR	ANN	MLR	ANN	MLR	ANN
AVG MPS	HQC	0.702	0.843	73.61	57.828	16053.5	10569.7	126.70	102.80
AVG MPS, MHS	HQC	0.698	0.848	79.01	67.200	16698.4	12793.1	129.22	113.10
AVG MPS, MHS,MWS	HQC	0.693	0.865	80.71	62.462	16967.8	11358.6	130.26	104.57

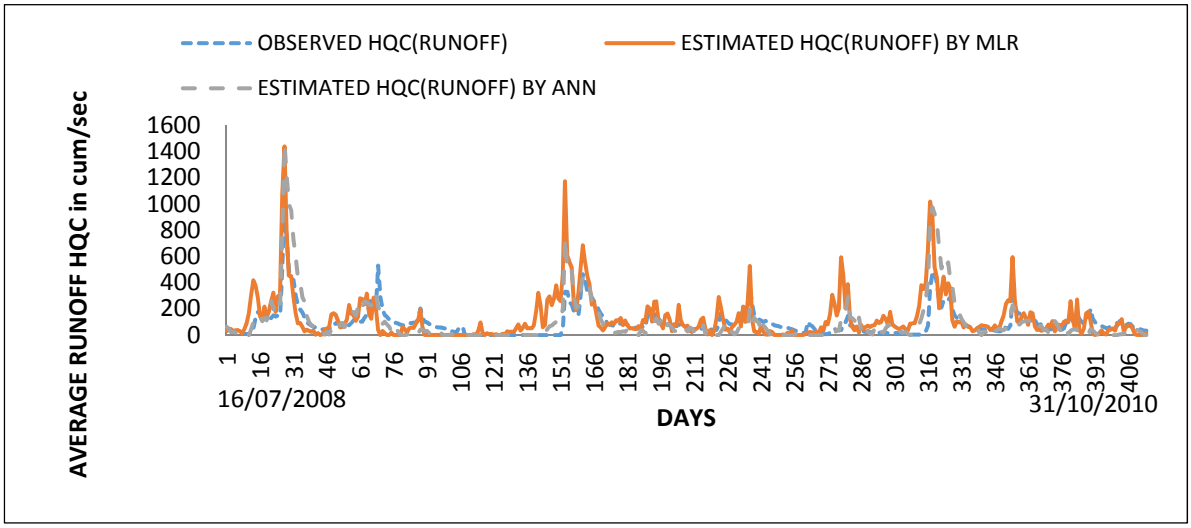

Figure 3. Time series plot of estimated runoff by MLR and ANN using input AVG MPS, MHS and MWS.

3.2 Estimation of meteorological parameters

The MLR and ANN models were developed for seven meteorological parameters namely pan evaporation (MEP), relative humidity (MHS), dry bulb temperature (MTD), minimum temperature (MTN), wet bulb temperature (MTW) and maximum temperature (MTX). However, in this paper model performances of

two meteorological parameters namely maximum temperature (MTX) and Minimum temperature (MTN) are presented.

3.3 Maximum Temperature (MTX)

As seen in Table 1 Maximum temperature (MTX) has positive correlation with four parameters namely dry bulb temperature (MTD), pan evaporation (MEP), wet bulb temperature (MTW) and minimum temperature (MTN). MLR models were built using all four parameters and also by eliminating the parameters having lower correlation values one by one. This was done to check the influence of inclusion of parameters. It was observed that the correlation between estimated and actual values of MTX was found to be highest when MTD and MEP was used in MLR model development. Hence the MLR model developed with MTD and MEP is considered as acceptable model with correlation (r) for testing 0.77 and mean absolute error 1.145. The equation of the MLR model developed is given in Eq. [2]:

$$MTX=8.311223+0.676894MTD+1.244856MEP \quad [2]$$

The ANN models were developed using all the parameters having positive correlation and then by eliminating the parameters with lower correlation one by one as discussed in case of MLR model building. Hence the ANN model has been developed with 4, 3, 2 and 1 parameter as input. Similar data division was used as MLR, to this data Jordan/Elman network showed good results. The transfer function employed was Tanh Axon with 1 hidden layer. The correlation between the actual MTX and the estimated MTX is highest when the ANN model was built using MTD and MEP. The correlation of testing for this model is 0.89 and its MAE is 1.065885 which outperforms the MLR model results. The results obtained by MLR and ANN models are tabulated in Table 3. The qualitative analysis of this model is as shown in Figure 4. The time series plot between estimated observed values of MTX by ANN are plotted in Figure 5. The estimated values of MTX are matching well with the observed values of MTX.

Table 3. Results of MLR for maximum temperature.

INPUT	OUTPUT	TESTING							
		r		MAE		MSE		RMSE	
		MLR	ANN	MLR	ANN	MLR	ANN	MLR	ANN
MTD	MTX	0.755	0.881	1.213	1.1455	2.3594	2.04165	1.536	1.4288
MTD,MEP	MTX	0.77	0.897	1.145	1.0658	2.0632	1.80873	1.436	1.3448
MTD,MEP,MTW	MTX	0.764	0.887	1.201	1.1145	2.3077	1.97640	1.519	1.4058
MTD,MEP,MTW,MTN	MTX	0.764	0.891	1.200	1.0838	2.3072	1.87985	1.518	1.3710

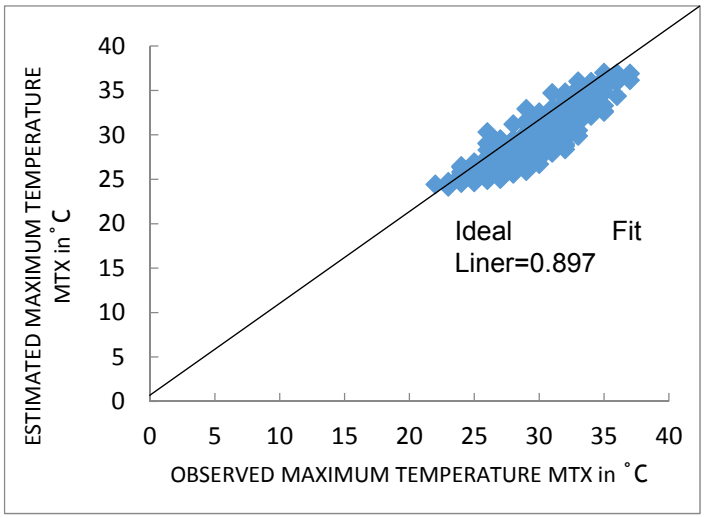

Figure 4. Scatter plot of observed maximum temperature versus maximum temperature estimated by ANN.

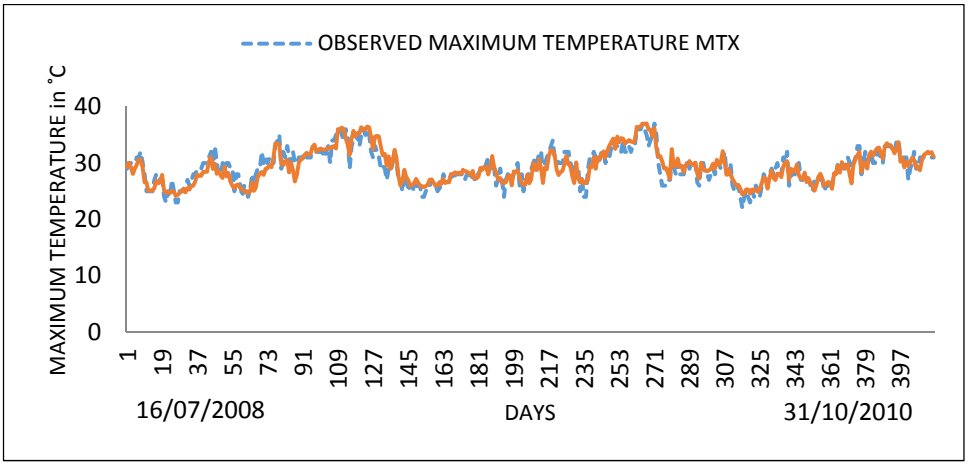

Figure 5. Time series plot of observed maximum temperature and estimated maximum temperature by ANN with input MTD, MEP.

3.4 Minimum Temperature (MTN)

As seen in Table 1, Minimum temperature (MTN) has positive correlation with six parameters namely average wind speed (MWS), pan evaporation (MEP), wet bulb temperature (MTW), maximum temperature (MTX), dry bulb temperature (MTD) and relative humidity (MHS). MLR models were developed using all six parameters and also by eliminating parameters one by one having lower correlation. It is observed that the correlation between estimated and observed values of MTN are maximum when MWS, MEP and MTW and MTX are used. The resulting correlation of MLR model developed with MWS, MEP and MTW was found to be 0.631 and mean absolute error 1.215. The accuracy obtained by model was very less. The equation of the MLR model developed is given in Eq. [3]:

$$MTN = 14.07557 + 0.340334MWS + 0.446377MEP + 0.118186MTW + 0.123067MTX \quad [3]$$

Based on the correlation analysis and MLR model building, similar parameters were used to developed ANN models keeping similar data division. ANN model was built using 70% data for training and 30% data was used to test the accuracy of the model. The network used to develop this model was Jordan/Elman. The transfer function employed was Tanh Axon with 1 hidden layer. The maximum accuracy was found with 2000 iterations. The correlation in testing for this model exhibited 0.7126 and its MAE found to be 1.075449. It is seen that model developed with ANN performed better in this case. The qualitative analysis of this model is shown by drawing scatter plot (Figure 6) where it is seen that estimated values are very close to the observed one. The correlation of estimated and observed MTN by ANN found to be good. The time series plot between observed and the estimated values by ANN as seen in Figure 7 confirms the trend followed by the estimated values.

Table 4. Results of minimum temperature.

INPUT	OUTPUT	TESTING							
		r		MAE		MSE		RMSE	
		MLR	ANN	MLR	ANN	MLR	ANN	MLR	ANN
MWS	MTN	0.244	0.285	1.380	1.362	3.617	3.548	1.901	1.883
MWS,MEP	MTN	0.567	0.633	1.203	1.135	2.627	2.374	1.62	1.540
MWS,MEP,MTW	MTN	0.575	0.649	1.215	1.152	2.564	2.472	1.601	1.572
MWS,MEP,MTW,MTX	MTN	0.631	0.655	1.229	1.113	2.691	2.297	1.64	1.515
MWS,MEP,MTW,MTX,MTD	MTN	0.573	0.639	1.229	1.117	2.693	2.372	1.641	1.540
MWS,MEP,MTW,MTX,MTD,MHS	MTN	0.579	0.596	1.227	1.182	2.680	2.583	1.637	1.607

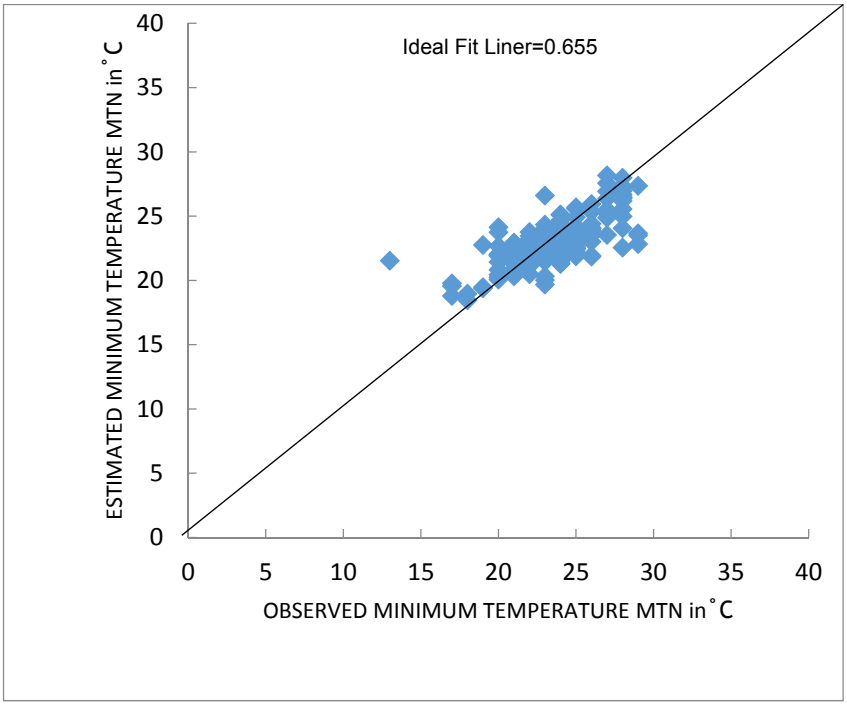

Figure 6. Scatter plot of observed minimum temperature versus minimum temperature estimated by ANN.

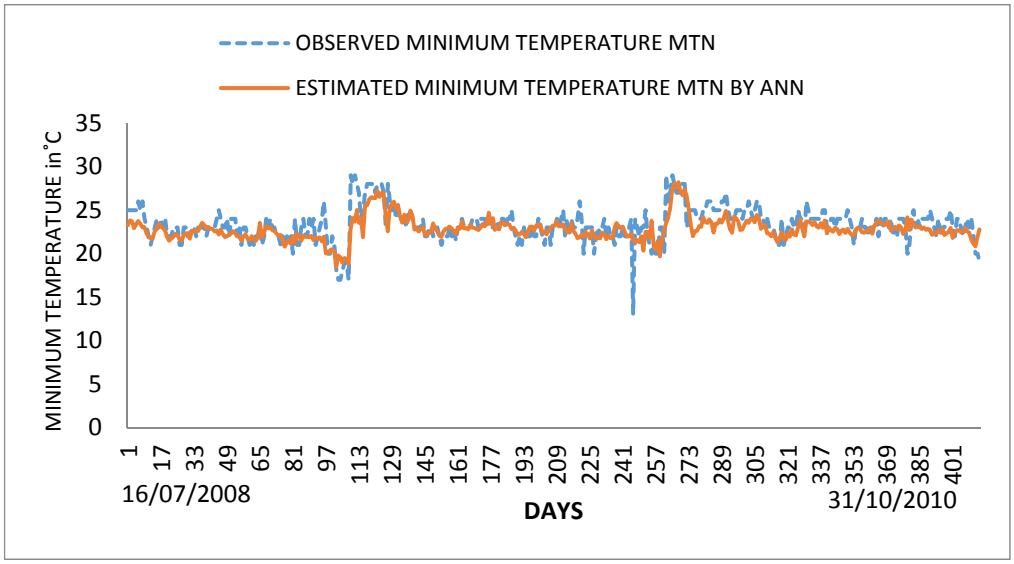

Figure 7. Time series plot of observed dry bulb temperature and estimated dry bulb temperature by ANN with input MWS, MEP, MTW, and MTX.

4 CONCLUSIONS

The correlation amongst all the hydrological and meteorological parameters and their effect on each other was studied using statistical analysis. The influence of these parameters plays vital role in hydrological process and their influence on each other was largely felt during model building. Based on correlation amongst some meteorological parameters, the model building was executed for maximum temperature, minimum temperature, wet bulb, dry bulb temperature and relative humidity. Hydrological parameters namely average rainfall and runoff were modeled using MLR and soft tool, ANN. The number of input parameters in building models were increased one by one according to their correlation effect. The parameter having highest positive correlation was used to develop the models. The hydrological models developed i.e. runoff using ANN showed good correlation when tested on an unseen data. Similarly, the maximum and minimum temperature estimation also proved that ANN is capable in estimating values close to the observed with high accuracy in such meteorological process too. Also, addition of meteorological parameters such as relative humidity, average wind speed has shown considerable effect as reflected in model output giving improved results. The main aim of this study was to see the effect of influence on each other. It was observed that even some parameters showed minimum correlation, however their contribution was largely felt and reflected in giving the accurate results.

REFERENCES

Abhishek, K., Kumar, A., Ranjan, R. & Kumar, S. (2012). A Rainfall Prediction Model using Artificial Neural Network*. In Control and System Graduate Research Colloquium (ICSGRC)* 2012, 82-87.

Afzali, M, Afzali A. & Zahedi, G. (2011). Ambient Air Temperature Forecasting Using Artificial Neural Network Approach, International Conference on Environmental and Computer Science IPCBEEvol.19(2011), IACSIT Press, Singapore, pp.176-180, 2011.

Aichouri, I., Hani, A., Bougherira, N., Djabri, L., Chaffai, H. & Lallahem, S. (2015). River Flow Model using Artificial Neural Networks. *Energy Procedia*, *74*, 1007-1014.

Arunkumar, R. & Jothiprakash, V. (2014). Multi-Reservoir Optimization for Hydropower Production Using NLP Technique. *KSCE Journal of Civil Engineering,* 18(1), 344-354.

Baboo, S.S. & Shereef, I.K. (2010). An Efficient Weather Forecasting System using Artificial Neural Network. *International journal of environmental science and development*, 1(4), 321.

Chang, F., Chang, L.C., & Huang, H.L. (2002). Real-Time Recurrent Learning Neural Network for Stream-Flow Forecasting. *Hydrological processes*, 16(13), 2577-2588.

Chang, F.J., Chen, P.A., Lu, Y.R., Huang, E. & Chang, K.Y. (2014). Real-Time Multi-Step-Ahead Water Level Forecasting by Recurrent Neural Networks for Urban Flood Control. *Journal of Hydrology*, *517*, 836-846.

Charhate, S.B. & Kote, A.S. (2009) Seasonal Reservoir Inflow Prediction Using Advance Data Driven Method, Journal of Applied Hydrology, Vol.-XXII, No-2, 76-83 2009.

De, S.S. & Debnath, A. (2009). Artificial Neural Network based Prediction of Maximum and Minimum Temperature in the Summer Monsoon Months over India. *Applied Physics Research*, 1(2), 37-44.

El-Shafie, A., Mukhlisin, M., Najah, A.A. & Taha, M.R. (2011). Performance of Artificial Neural Network and Regression Techniques for Rainfall-Runoff Prediction. *International Journal of Physical Sciences*, 6(8), 1997-2003.

Fathima, T.A. & Jothiprakash, V. (2014). Behavioural Analysis of a Time Series–A Chaotic Approach. *Sadhana*, 39(3), 659-676.

Googhari, S.K, Huang, Y.F., Abdul Halim, Ghazali, B. & Lee, T.S. (2010). Neural Networks for Forecasting Daily Reservoir Inflows. *Pertanika Journal Science & Technology.* 18(1), 33–4.

Jothiprakash, V. & Magar, R.B. (2012). Multi-Time-Step Ahead Daily and Hourly Intermittent Reservoir Inflow Prediction by Artificial Intelligent Techniques using Lumped and Distributed Data. *Journal of Hydrology*, 450, 293-307.

Londhe, S. & Charhate, S. (2010). Comparison of Data-Driven Modelling Techniques for River Flow Forecasting. *Hydrological Sciences Journal–Journal des Sciences Hydrologiques*, 55(7), 1163-1174.

Mehr, A.D., Kahya, E., Şahin, A. & Nazemosadat, M.J. (2015). Successive-Station Monthly Streamflow Prediction using Different Artificial Neural Network Algorithms. *International Journal of Environmental Science and Technology*, 12(7), 2191-2200.

Mohammad, A.S. (2011). Weather Temperature Forecasting Using Artificial Neural Network. *Journal of Engineering and Development*, 15(2).

Pandhiani, S.M. (2015). Time Series Forecasting by Using Hybrid Models for Monthly Stream Flow Data. Applied Mathematical Sciences, Vol. 9, 2015, no. 57, 2809 – 2829.2015.

Patel, S. S. & Ramachandran, P. (2015). A Comparison of Machine Learning Techniques for Modeling River Flow Time Series: The Case of Upper Cauvery River Basin. *Water Resources Management*, 29(2), 589-602.

Rajurkar, M.P., Kothyari, U.C. & Chaube, U.C. (2004). Modeling of The Daily Rainfall-Runoff Relationship with Artificial Neural Network. *Journal of Hydrology*, 285(1), 96-113.

Srinivasulu, S. & Jain, A. (2006). A Comparative Analysis of Training Methods for Artificial Neural Network Rainfall–Runoff Models. *Applied Soft Computing,* 6(3), 295-306.

Thirumalaiah, K. & Deo, M.C. (2000). Hydrological Forecasting using Neural Networks. *Journal of Hydrologic Engineering*, 5(2), 180-189.

Wu, C.L. & Chau, K.W. (2011). Rainfall–Runoff Modeling using Artificial Neural Network Coupled with Singular Spectrum Analysis. *Journal of Hydrology*, 399(3), 394-409.

Wu, J., Long, J. & Liu, M. (2014). Evolving RBF Neural Networks for Rainfall Prediction Using Hybrid Particle Swarm Optimization and Genetic Algorithm Neuro Computing, 148, 136–142.

Youngmin, S.K., Kisi, O. & Singh, V.P. (2015). Daily Water Level Forecasting using Wavelet Decomposition and Artificial Intelligence Techniques. *Journal of Hydrology,* 520, 224–243.

Zhang, Y. & Chiew, F.H. (2009). Relative Merits of Different Methods for Runoff Predictions in Ungauged Catchments. *Water Resources Research*, 45(7).

INFILTRATION AND SURFACE RUNOFF PROCESSES ON SLOPE AND SOIL COMPACTION WITH RAINFALL SIMULATOR EXPERIMENT

D NOORVY KHAERUDIN[1], AGUS SUHARYANTO[2], DONNY HARISUSENO[3] & LILY MONTARCIH[4]

[1] Tribhuwana Tunggadewi University, Malang, Indonesia
dianoorvykhaerudin@gmail.com
[2,3,4] Brawijaya University, Malang, Indonesia
Agus.s@ub.ac.id; donnyhari@ub.ac.id; lilymont2001@gmail.com

ABSTRACT

The hydrological processes in the urban drainage are known as rainfall, runoff, and infiltration. This research aims to find out how the relationship of soil density, initial moisture content, and slope of lands influences the rain, runoff, and infiltration process. This research is conducted in a laboratory using a rainfall simulator plot tank. The size of the plot tank is 1.17 m x 0.97 m x 0.30 m. The plot tank is filled with soil of the same specific gravity for different initial water content in soil compaction land slope variation. The experiment carried out on steady rain intensity where every point in the plot is assumed to have uniform velocity. The method describes the compaction of urban land using prototype that influences the infiltration rate. Runoff processes. Infiltration rate was calculated by reducing intensity of rain and runoff as output data from a running rainfall simulator. The processes are explained in water balance concept in urban drainage. Based on the results of the study, the compaction and the slope will positively affect against the runoff where the higher the compaction, the greater the runoff will be. However, it will negatively affect the infiltration.

Keywords: Soil compaction; infiltration rate; runoff; rainfall simulator; urban drainage.

1 INTRODUCTION

Rainfall in urban areas uses drainage principle of which rainfall is contained and controlled to prevent floods and runoffs. Rainfall will be contained and let pass as described by the continuity law of the water balance concept. Water balance concept explains the hydrological process, runoff, surface puddle, evaporation and infiltration (Bedient, 2008). Surface puddle is counted as runoff while evaporation is disregarded which leaves us with infiltration as the only loss factor.

The limitation of lands in urban areas decreases the environmental support. Conventional urban drainage concept expects rainwater to be conveyed away as quickly as possible to underground pipes or main drainage waterways or even to the sea. However rainfall can also be absorbed temporarily by soil and the infiltration for water storage can be planned in urban areas.

Buildings in urban areas affect soil density (Fox et al., 1997) Increased soil density will make the infiltration lower. Runoffs will be much larger because water flow depends on land slope, land condition, and rain itself. Rainwater will flow for sometimes, at times, water will reach the maximum level depending on drainage conditions in lands, waterways, or pipes.

Rain process and runoffs in overland flow are influenced by rain intensities, land slope, and condition. The land condition, which includes soil texture variations, structure, and layer interface (Ames et al., 2001), among other effects, affect rain process, runoffs, and infiltration. Land slope also affects runoffs and infiltrations (Chen et al., 2011) so does land prior conditions, such as initial water content.

The problem is how those 3 parameters simultaneously affect rain process, runoff, and infiltrations which is connected by time using a rain simulator tool. The purpose of this research is to understand runoff and infiltration conditions in initial water content using density and slope as variables. Another purpose includes getting the statistics between runoff and infiltration as the mentioned parameters, while also gaining the time analysis, which happens in rain process, runoff, and infiltration.

2 MATERIAL AND METHOD

2.1 Overland flow concept

Rain process, runoff, and infiltration happen in overland flow drainage. This is a concept where continuity law meets momentum law. Infiltration acts as a reduction factor in rain process and runoff.

Continuity equation for overland flow (Bedient, 2008)

$$\frac{\partial q_o}{\partial x} + \frac{\partial y_o}{\partial t} = i - f \qquad [1]$$

With i-f is the rainfall rate minus infiltration (mm/s), qo is the unit width flow rate (m^2/s/m'), yo flow depth (m).

2.1.2 Momentum equation

Considering the steady uniform flow and free air pressure are disregarded, then the basic slope equals the energy line slope. Momentum equation was taken from second Newton law in Eq. [2] :

$$F = \frac{d(mv)}{dt}$$

$$\frac{d(mv)}{dt} = m\frac{dv}{dt} + v\frac{dm}{dt} = \rho A \Delta x \frac{dv}{dt} + \rho v q \Delta x \quad [2]$$

Equation becomes:

$$S_o - S_f = 0 \quad [3]$$

Then :

$$Q = \frac{So^{1/2}}{n} . A^m \quad [4]$$

The surface runoff phenomenon is shown through the water balance theory in the continuity equation below: (Bedient, 2008)

Real rainfall rate = Puddle + evaporation + infiltration + surface runoff

The puddle is included in surface runoff and disregarding evaporation, then effective rainfall rate obtained equals to surface runoff as shown below:

Effective rainfall rate = Real rainfall rate – (infiltration and surface runoff).

Based on that, time distribution is essential to be known in effective rainfall rate. Time distribution of effective rainfall rate, which was interpreted as runoff and infiltration, was obtained and observed through uniform flow rate in constant rainfall.

Water balance in the relationship between rainfall rate and infiltration as shown in Figure 1.

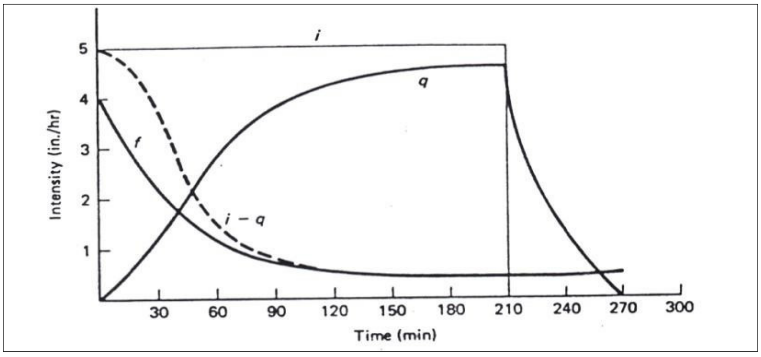

Figure 1. Water balance in overland flow. Source **:** Gupta (1989, p.87).

2.2 Runoff

Runoff can be described as water flow from land to surface waterways. Runoff which flows to channel is dependent on time. Effective rainfall, which flows from land to waterways is called overland flow (Subramanya, 2002). Whereas overland flow which goes to smaller waterways and then joins a bigger waterway with the hydraulics flow of an open waterway is called surface runoff. Time, which differentiates between the two, depends on certain parameters on land and waterways during the water flow process.

Different processes of overland flow and surface runoff occurred from q and flow media. In overland flow, q is unit of width flow rate, whereas surface runoff is Q with wetted media. Flow depth in overland flow occurred because of infiltration, whereas flow depth in surface runoff is water depth from the ground channel. Based on that, the parameters that affect each flow are different. From this runoff process, the time-concentration in each case will be solved differently, although still in water balance concept.

2.3 Infiltration

A loss water factor which affected the amount of surface runoff will be different with the overland flow. In a surface runoff, water loss occurred because of waterways curves, basic material, ground roughness, and dimension. Whereas in overland flow the affecting factor of water loss was infiltration, then for overland flow was rain process and runoff.

Infiltration process was observed through the reduction of stored runoff from rainfall rate (Wilson, 1990). Factors affecting infiltration rate are soil characteristics, land lid condition, and slope. Land lid condition can be observed through the density, which can be measured by its dry weight. The land characteristic can be observed through certain parameters, pores value, saturation degree, porosity, specific gravity, water rate, and land slope.

Infiltration rate was affected by land slope. The steeper the land, the lower the infiltration rate was (D.M, 1997). If infiltration rate was lower, then concentration time, which is the time when the soil condition reaches maximum and constant, was longer.

Infiltration rate models:

a. Kostiyakov Model

Kostiakov Model relates infiltration to time as a power function while excluding initial and final water content (constant infiltration rate). Infiltration rate and equation are shown below:

$$F = at^b \qquad 0 < b < 1 \qquad [5]$$

$$f = \frac{dF}{dt} = abt^{b-1} \qquad [6]$$

Where *a* and *b* are constants that depend on the soil characteristics and initial water content. These constants cannot be measured before and usually obtained by pulling a straight line on a figure paper for empirical data or by using the smallest quarter method.

b. Horton Model (1930), (Subramaya, 2002):

$$f_{ct} = f_{cf} + \left(f_{co} - f_{cf}\right)e^{-Kht} \qquad \text{for } 0 \geq t \leq t_d \qquad [7]$$

Where :

f_{ct} = the infiltration capacity or potential infiltration rate (cm/h)
f_{cf} = the final constant infiltration rate (cm/h)
f_{co} = the infiltration capacity at (cm/h) t = 0
Kh = geophysics constant which depends on soil characteristics and land lid
t_d = rainfall time

2.4 Time of concentration

Time of concentration had two definitions based on the development of kinematic wave theory (Bedient, 2008), which are 1) time of concentration is the time required for water to travel from the most hydraulically-remote portion of a watershed to the channel, and the second definition is 2) time of concentration balance time in a watershed with constant rain intensities. Time of concentration according to (Richard, 1984) is the time required for water to travel from the most hydraulically-remote portion of a watershed to a location of interest.

In land, time of concentration equation is: (Richard, 1984)

$$Tc = 0{,}04690.L_f^{0{,}4450}.i_2^{-0{,}7231}.\theta^{0{,}5517}.S_{fm}^{-0{,}2260} \qquad [8]$$

Where

L_f = overland flow path of distance
i_2 = 2 years rain intensities
S_{fm} = slope
Φ = stored flow variable

2.5 Parameter optimization

Januardin (2008) states that the higher the soil density, the lower the rate of infiltration. Soil density occurred because of collisions between rain and the soil surface. Vegetated soil usually had a higher infiltration rate than the open soil surface. This was caused by vegetation roots which make porosity higher which had higher rain collision energy so infiltration rate was higher.

Soil density also affected surface runoffs. Soil density occurred in urban areas because urban land was used a lot more than rural areas, such as crowded human habitation and skyscrapers (Noorvy, 2014)

Pore size and amount affect infiltration rate as well. The more and bigger pores make higher infiltration rate. In accordance with that, clay is dominated with small pores whereas sand is with big pores. So it can be concluded that infiltration in sandy soil is a lot higher than those in clay (Lipiec, 2006)

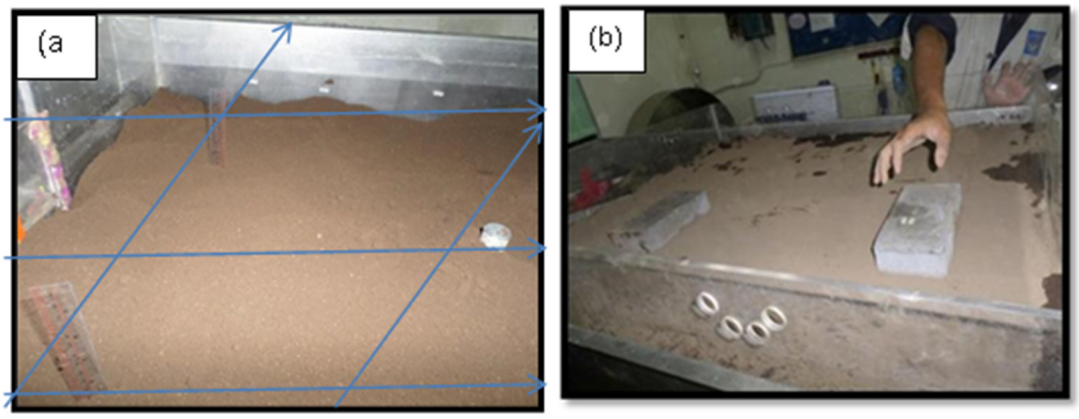

Figure 2. (a) Soil height measurement; (b) Soil density measurement.

As much as 120 kg of soil was mixed with water where the amount was 20% of the soil used, which then was divided into 3 density layers following the Proctor Test rule. Soil used in this experiment had to be dried and passed through filter no. 10. Put the soil into the testing box, and compact it using a 2.9 kg pounder.

The initial water content variable was obtained by determining water mix in the experimental soil, which was 20% water from soil weight. After mixing was done, groundwater was flowed through the still soil for 2 hours, 2 days, and 4 days with the initial water content measured at each time.

A concrete weight was dropped to soil layers from 10 cm above ground. The weight falls horizontally and vertically to make the density to be spreaded evenly. Soil heights before and after pounding were measured by dividing the soil to 3 parts horizontally and 2 parts vertically. After the first layer was pounded, the second layer was added. The same thing goes for the third layer.

Soil density was measured in 2 spins (d1), 4 spins (d2), and 6 spins (d3) in order to get various densities in an evenly pondered soil. Each of the three soil layers was pounded evenly. Each density gets 4 initial water content treatment, w1, w2, w3, and w4. Every density and initial water content get 3 slope treatment: S1, S2, and S3. Experiment design is shown in Table 1.

2.6 Experiment set up

The relationship between runoff amount and time (t) will be obtained as the result. The relationship between rain and runoff was that the higher the rainfall rate, the higher the runoff is and vice versa. When runoff is constant, the soil will be water saturated and has constant infiltration as well.

The relationship between rain and runoff is often used in hydrological design and analysis using factors that affect runoff as a parameter. Hydrography is a Figure that shows height, amount, velocity, and other characteristics of time-dependent water.

The experiment was done in a hydrological laboratory in Water Engineering of Brawijaya University using a rainfall simulator S12-MKII Hydrology System from Armfield UK. Machine specifications are shown in Figure 3. The output of the experiment is the surface runoff amount.

The data achieved were primary data from the laboratory, which means, it was directly observed in a laboratory using Rainfall Simulator with soil density and slope as variables.

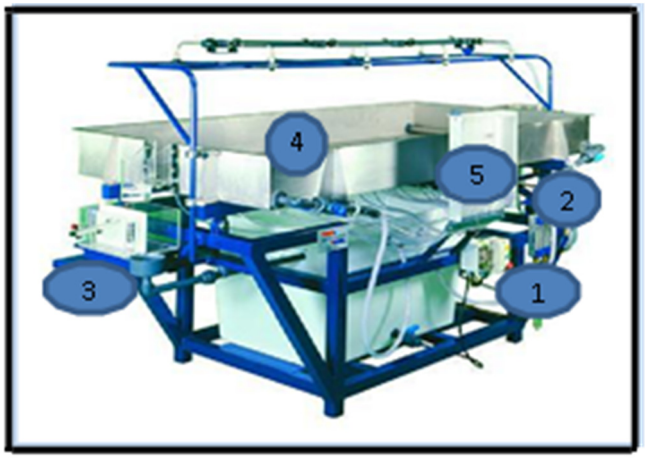

Figure 3. Rainfall Simulator S12-MKII Hydrology System, Armfield UK parts used in the machine are: (1) rain intensities control, (2) rain intensities control, (3) slope control, (4) runoff control, (5) material tank and (6) infiltration height gauge (multi-tube manometer).

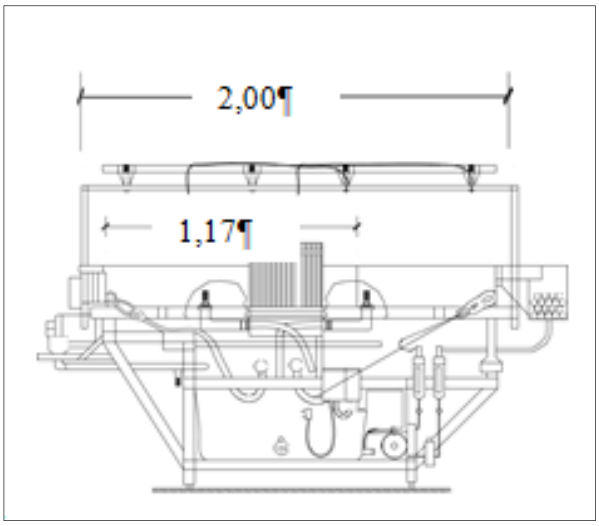

Figure 4. The nozzle on the top controls rainwater size.

Rainfall Simulator shows the hydrological event in the surface land. This machine has a 2x1.2x0.3 meter plot tank. While in this experiment it has been modified to 1.17x0.97x0.30 meter as shown on Fig. 4. The nozzle on the top controls rainwater size. This tank also has two porous pipes and two gauge flow tank.

Table 1. Experimental design of Relationship between rain, runoff, and infiltration.

Compaction	Intial water content	Slope	Compaction	Intial water content	Slope	Compaction	Intial water content	Slope
d1	w1	S1	d2	w1	S1	d3	w1	S1
		S2			S2			S2
		S3			S3			S3
	w2	S1		w2	S1		w2	S1
		S2			S2			S2
		S3			S3			S3
	w3	S1		w3	S1		w3	S1
		S2			S2			S2
		S3			S3			S3
	w4	S1		w4	S1		w4	S1
		S2			S2			S2
								S3

Where :
d1, d2, d3 : soil compaction
w1,w2,w3,w4 : Initial water content
S1, S2, S3 : land slope

3 RESULTS

3.1 Runoff analysis

Runoff happens when rainfall rate was higher than the infiltration capacity of soil. In this research, surface runoff occurred on water saturated and unsaturated soils.

1 The first kind of flow occurred on the unsaturated soil. In this case, soil can be dry by adding 20% water (of soil weight) into *Rainfall Simulator*.

2 The second kind of flow occurred when soil had become saturated and there were no empty pores left to be infiltrated. This soil layer condition happens because the soil had become saturated prior to rainfall, so infiltration stops. Below were the results of runoff observation before and after saturation when rain was stopped at every minute:

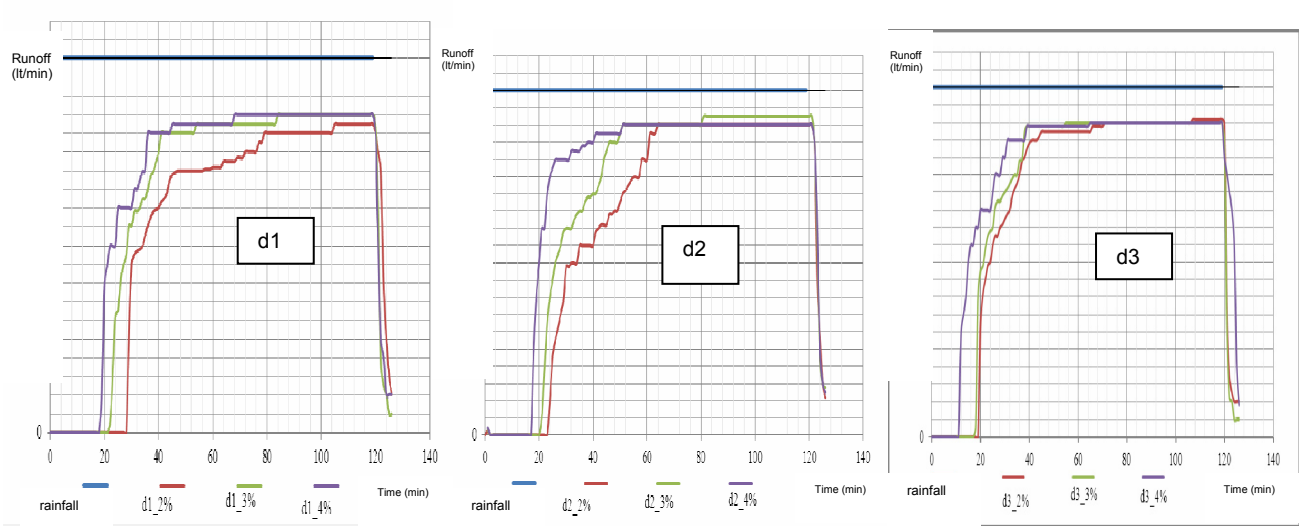

Figure 5. Runoff curve in density 2, 4, 6 spin (d1, d2, d3) and slope 2,3,4%.

Curves on the Fig. 5, show rainfall and runoff in 120 minutes of soil sample with density 2, 4, 6, and slope spins of 2%, 3%, 4%. At d (1), the curve shows times when runoff starts, increase, summit, constant start, and constant. It also shows that at steeper land, runoff starting time was faster and time to reach constant was also faster.

For runoff starting time, the steeper the land, runoff starting time was faster. In density 4 spin, the steeper the land, the faster it was to reach constant. It can be seen in the 4% curve that runoff process was steeper than 4% in 2 spins (d1). This showed that alongside slope, density also the affect runoff process rate. Fig. 5 curves (d3) showed that runoff starting time and constant starting time in density 6 spin slopes was 2%, 3%, and 4 %. Curve below shows that the denser the soil, the faster the runoff starting time will be. The curve goes up in 6 spin (d3) and was tighter than d2. This showed that rain process and runoff were affected by slope and density.

Curve tightness in the highest density showed that runoff and infiltration will reach rain value depending on the soil treatment. The denser the closer. This water content variable was observed for runoff process and infiltration. Below are the Figures for this condition, Figure 6:

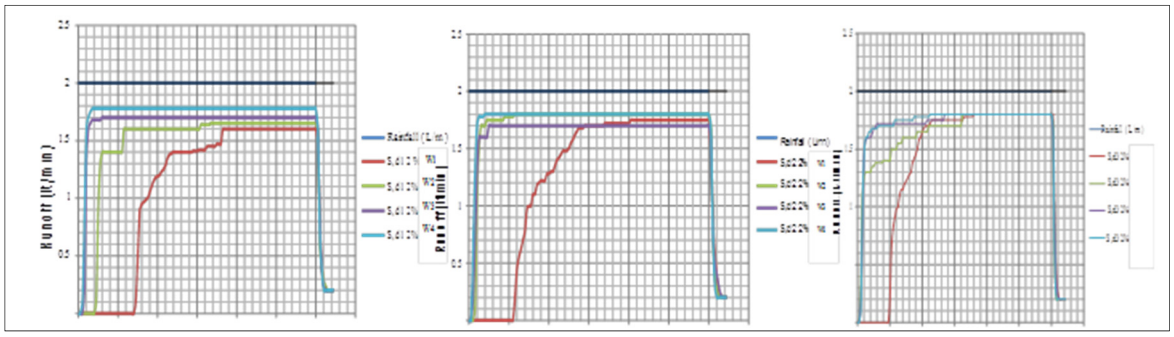

Figure 6. Runoff and time at d1, d2, d3_S 2% different water content.

Initial water content at the same slope and density means a faster constant time. This showed that soil in same density and slope had pores that were fully filled with water. Runoff was higher at same density and

slope, but high water content was present as well. This was because the soil was filled with water. So for the runoff starting time, the higher water content means faster runoff starting time, as shown in Fig. 6.

3.3 Infiltration analysis

During rainfall water infiltrates the soil from the surface and redistributes in the unsaturated zone. The distribution process depends upon the soil moisture conditions, water pressure, and unsaturated permeability (Gavin and Xue, 2008). According to (Arfan and Pratama, 2012), the relationship between infiltration and rain intensities variables, density and slope, were directly proportional. Infiltration will increase when rain intensity was increased. The relationship between infiltration and the density was inverted. Infiltration will increase if the density was decreased. Relationship between infiltration and slope variable was inverted; infiltration will decrease if the slope was increased.

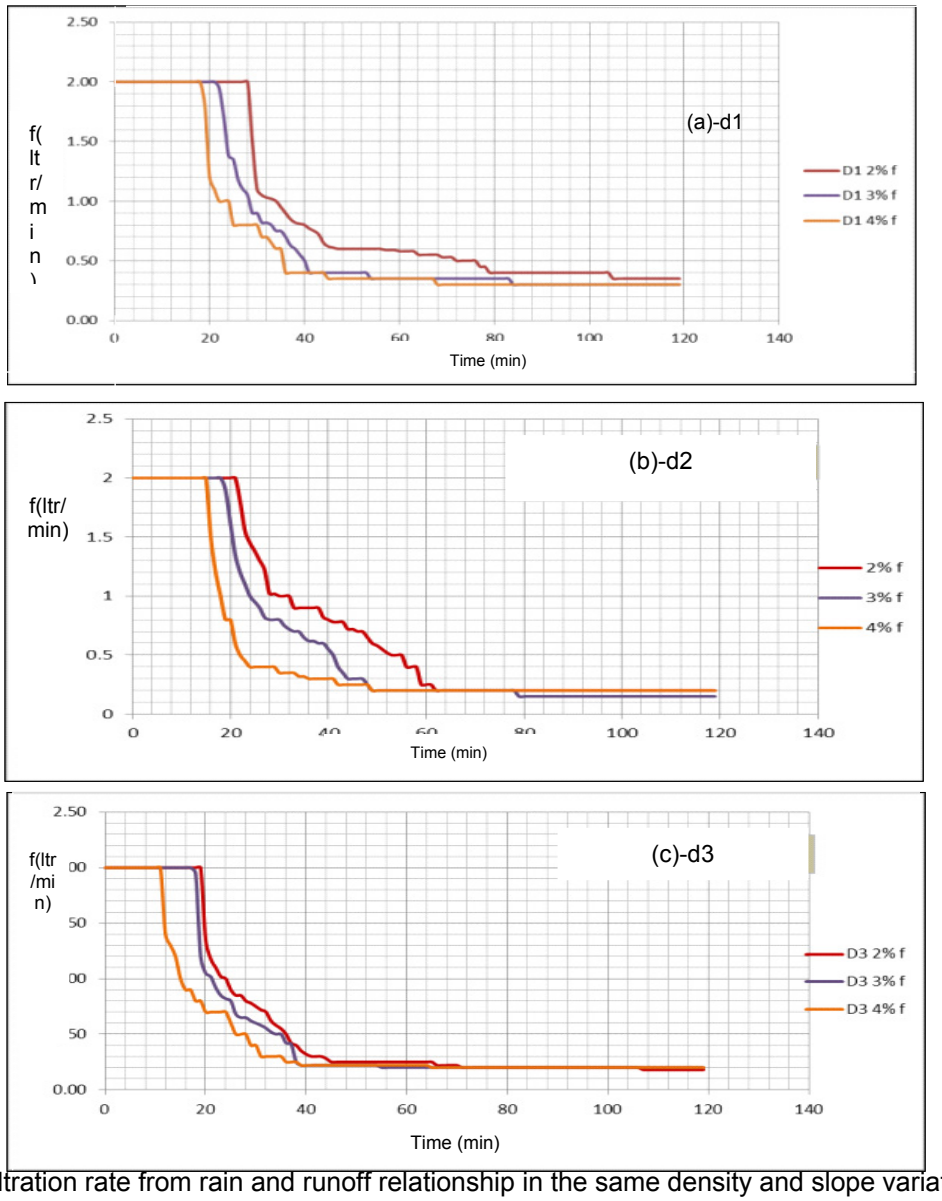

Figure 7. Infiltration rate from rain and runoff relationship in the same density and slope variation at (a)-d1, (b)-d2, and (c)-d3.

Based on Figure 7 a), b), and c), it can be seen that infiltration rate was the same in density d2, and d3 at slope of 2%, 3%, 4%, but density d1 had a higher result. Density d1 at slope 2%, 3%, 4% had an approximately same result for those of d2 and d3. So it can be concluded that maximum infiltration capacity will be the same at a uniformed density but slopes will affect the runoff rate to reach constant infiltration capacity.

From Figure 8 (a, b, c), it can be seen that at same slope, the higher density will cause lesser infiltration. Density of soil will decrease the infiltration rate up to 70% to 90% (Gregory, 2006). At a denser soil, the infiltration capacity rate had similar value and tighter which shows that infiltration rate was similar in different density at uniformed slopes.

But in density d1, there were spaces between each density. This means that there were other effects in rain process, runoff, and infiltration. The factor is initial water content. Initial water content affects the process of filling pores in soil density process. The soil density process was stated as SG (Specific Gravity) and pore value was inversed. A higher SG means higher soil density (dry soil volume), whereas a higher pore value (e) means lesser soil density. Which means high density will give rise to a decline in rate of infiltration.

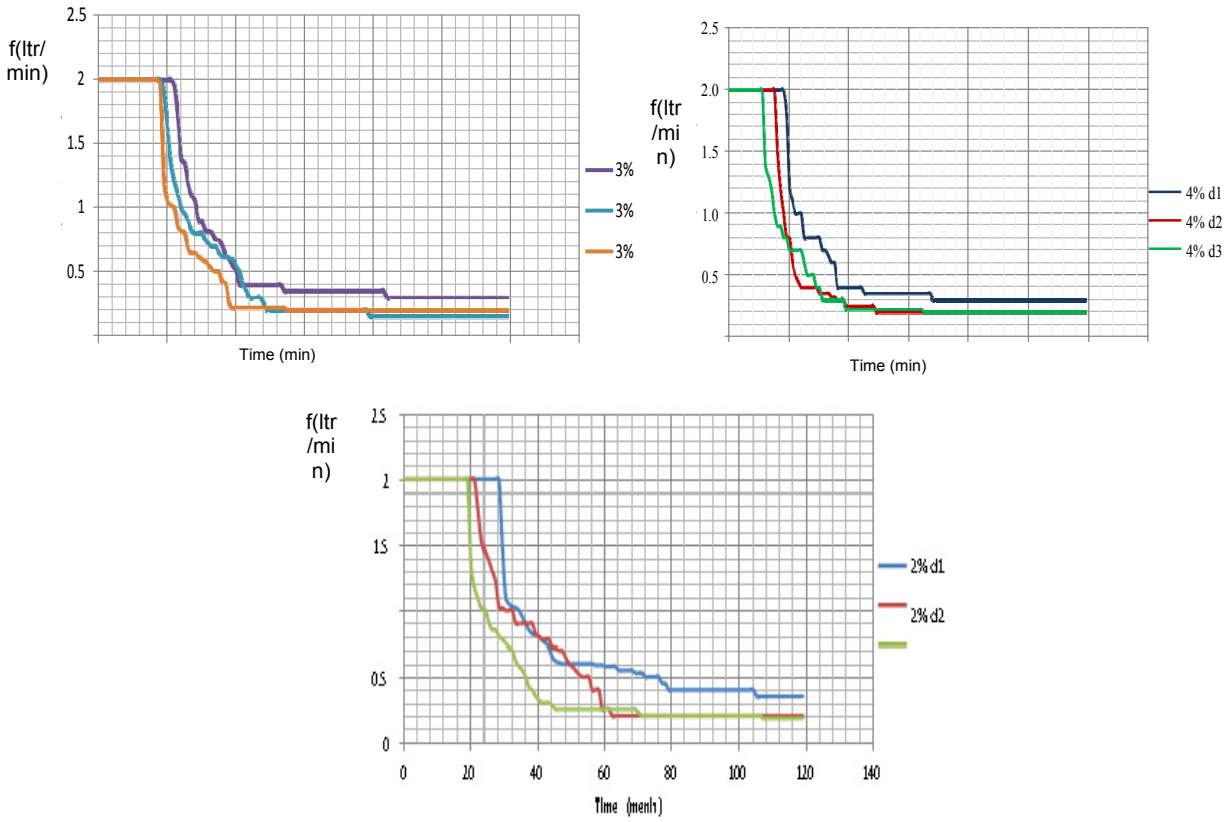

Figure 8. Infiltration rate on rain and runoff relationship in the same slope density variation S2%, S3%, S4%_d1, d2, d3.

3.4 Rainfall, runoff and infiltration processes analysis

Rain and runoff process use the concept of water balance with infiltration as the only loss factor in overland flow. Rain, runoff, and infiltration curve show three moments of rain, runoff, and infiltration processes. Those were rainfall and infiltration moment, runoff moment when infiltration was lower than rainfall until the meeting point of runoff and infiltration curves, the last was when infiltration and runoff have reached constant.

In this curve, runoff starting time and constant infiltration will be shown at the same time. This explanation was part of water balance concept. Figure 9 shows result from relationship data of runoff and rain. Runoff and infiltration relationship also showed a meeting point at certain times when runoff and infiltration were the same amount. Because the rainfall rate was 2 Litre /minute, it showed that runoff and infiltration were in balance which was 1 Liter/minute. The steeper the slope, the faster meeting point happens. Figure 9 shows water balance time of which meeting point between runoff and infiltration on a denser soil means the faster balance between rain, runoff, and infiltration occurred. This time showed the runoff starting point after infiltration process. This time balance occurs in density with the same initial water content and slope .

Infiltration happens on a denser soil, steeper slope where higher initial water content was faster. Infiltration capacity with units of liters / minute was the flow capacity in the soil over time. The maximum capacity of the ground to collect rain water that was at constant on the amount of time concentration. So the maximum capacity of the ground to collect rain water that comes from a reduction in the discharge of rain had reduced runoff (Hjelmfelt, 1978).

Rain and runoff process used the concept of the balance of water by infiltration as the sole factor in the loss of the flow of surface land. Curve of rain, runoff and infiltration showed three times the incidence of the rain, runoff and infiltration. The third time was when it began to rain and there was water infiltration, time begins to flow, namely when infiltration was smaller than the rain and up at the meeting point of the line between the curves of runoff and curves of infiltration. This is the time where infiltration and runoff have reached constant conditions.

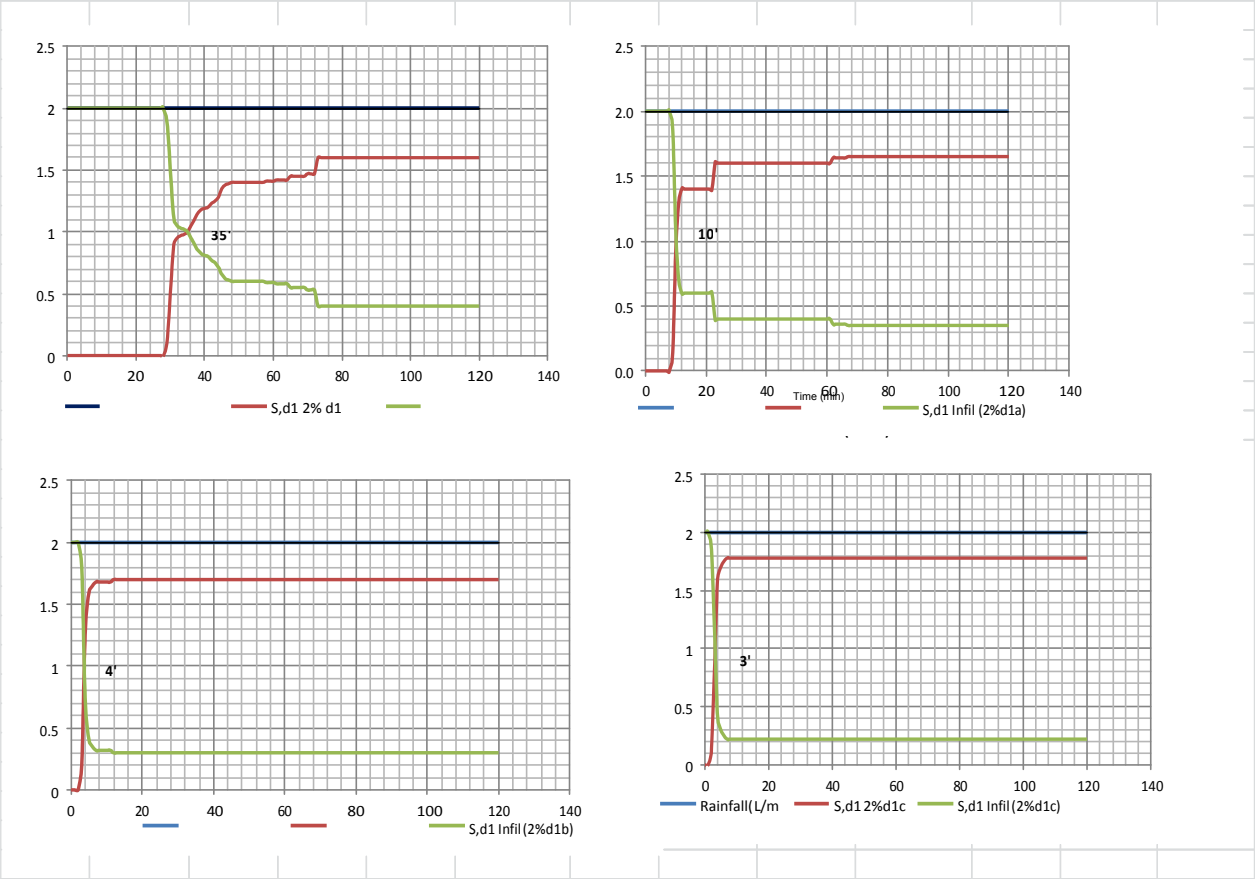

Figure 9. Relationship between rain, runoff, and infiltration for d1_2%_w1,w2,w3,w4.

4 CONCLUSION

Density variation of d1, d2, d3 will affect infiltration rate. The denser the soil, water in the tank will runoff faster and infiltrated lesser. While at a variation of slopes but same density, runoff water will be faster with steeper soil. Runoff amount will be uniform at last. Initial water content also affects infiltration and initial water content affect pores fill so water infiltrate lesser when initial water content is increased. The same thing applies to soil of different kind and different pore value.

When density is the same and the slope is steeper, infiltration rate at constant will be less. When the slope is the same and density is higher, infiltration rate at constant will be less. Based on the relationship of rain and runoff in water balance and in wave kinematic law, time of concentration will be read in runoff process. Runoff happens when runoff curve goes up until it becomes constant. Infiltration as rain absorption also has the same condition.

ACKNOWLEDGEMENTS

This research is funded by Kemenristek DIKTI as a doctoral scholarship program at Brawijaya University. The author appreciates the help from Hydrological Laboratory in Brawijaya University.

REFFERENCE

Arfan, H., & Pratama, A. (2012). *Model Eksperimen Pengaruh Kepadatan, Intensitas Curah Hujan dan Kemiringan Terhadap Resapan Pada Tanah Organik*. Jurusan Teknik Sipil Fakultas Teknik Universitas Hasanuddin. Makassar, 1-8.

Ames, K.C., Inkpen, E.L., Frans, L.M. & Bidlake, W.R. (2001). *Preliminary Assessment of Infiltration Rates and Effects on Water Quality of Selected Infiltration Media for use in Highway Runoff Retention Basins in Washington State*, US Geological Survey in cooperation with Washington State Department of Transportation (WSDOT).

Bedient. (2008). *Hydrology and Floodplain Analysis*. Canada: Prentice Hall, Pearson Education International, 816.

Chen, R.H., Kuo, K.J. & Chang, C.M. (2011). Experiment on the Stability of Granular Soil Slopes by Rainfall Infiltration. In *5th International Conference on Debris-Flow Hazards Mitigation, Mechanics, Prediction and Assessment*, 303-31.

Fox, D.M., Bryan, R.B. & Price, A.G. (1997). The Influence of Slope Angle on Final Infiltration Rate for Interrill Conditions. *Geoderma*, 80(1-2), 181-194.

Gavin, K., & Xue, J. (2008). A Simple Method to Analyze Infiltration into Unsaturated Soil Slopes. *Computers and Geotechnics*, 35(2), 223-230.

Hjelmfelt, A. (1978). Influence Of Infiltration On Overland Flow . Journal Of Hydrology, 36(1-2), 179-185.

Januardin. (2008). *Pengukuran Laju Infiltrasi pada Tata Guna Lahan yang Berbeda di Desa Tanjung Selamat Kecamatan Medan Tuntungan Medan. Medan*: Departemen Ilmu Tanah FP USU.

Lipiec, J., Kuś, J., Słowińska-Jurkiewicz, A. & Nosalewicz, A. (2006). Soil Porosity and Water Infiltration as Influenced by Tillage Methods. *Soil and Tillage research*, 89(2), 210-220.

Noorvy, D. (2014). Effect of Density Soil to Water Recharge (Infiltration) in Urban Overland Flow. *International Conference on Suistanable Built Environment*. Yogyakarta: Universitas Islam Indonesia, 87-94.

Subramaya. (2002). *Engineering Hydrology*. New Delhi: Mc Graw – Hill, 392.

Wilson, E.M. (1990). *Engineering Hydrology*. Macmillan Education UK, 1-49.

IMPACT OF LANDUSE CHANGE ON URBAN RUNOFF: A CASE STUDY OF JAIPUR CITY, INDIA

DEEPAK KHARE [(1)], LAKHWINDER SINGH [(2)] & MAHESH KUMAR JAT [(3)]

[(1, 2)] Water Resources Development and Management Department, Indian Institute of Technology Roorkee, Roorkee, India
kharefwt@gmail.com; lakhwinder108@gmail.com
[(3)] Civil Engineering Department, Malaviya National Institute of Technology, Jaipur, India.
mahesh.mnit@gmail.com

ABSTRACT

The present study shows that land use change has major impact on runoff of urban catchment. The land use from the year 1980 and 2011 have been prepared and used in the SWAT model. It has been found that the runoff increases by 14.95% at the major outlet of urban watershed of the Jaipur city. The urbanization has shown considerable increase in the urban area from 39.23 km^2 to 97.89 km^2 i.e. 149.53% over a span of 21 years. Similarly, other condition were also calculated for land use change as in this present study. Increasing urban runoff results in urban flooding, therefore assessment of quantum of increase can help the water resources planner of the city to plan adaptation techniques. The present study is an attempt to provide the impact of urbanization over the total horizon of around 44 years with digital data presented from 1972, though only one such result is indicated. For high accurate elevation value Cartosat-1 Digital Elevation Model (DEM) with 30m spatial resolution is used, provided by ISRO Bhuvan Data Portal. Cartosat-1 V3 DEM are highly accurate due to fixed elevation on water bodies, which does not impact during simulation. Model is simulated with each change in land use and runoff, groundwater is calculated. Simulation was run on number of times with the changing of land use considering same rainfall to calculate runoff at the outlet with land use change.

Keywords: Surface runoff, impact of land use; urban watershed; urban hydrology; discharge and land use.

1 INTRODUCTION

Change in the availability of water in general, and change in surface runoff in particular, of an area can affect the land cover land use (LCLU). Change in LCLU is normally induced by human activities rather than natural events. Such changes can have great impact on the environment of watersheds as they alter the hydrological processes such as infiltration, groundwater recharge, base flow and runoff (Niehoff et al., 2002). Study of change in runoff characteristics due to human activities has an important role in understanding the effects of LCLU change on hydrological processes over the earth surface (Shi et al., 2007). To understand the future effects of land use change on runoff characteristics, it is important to have an understanding of the effects that historic changes in land use have had on runoff (Crooks et al., 2000). Hence it is imperative that the effect of change in land use on the runoff characteristics of a region to be assessed (Shi et al., 2007). Numerous watershed models with varying capabilities, strengths, and weaknesses are available in each of these categories (Randall et al., 1998). Among watershed models, the Soil and Water Assessment Tool (SWAT) is a versatile watershed model as it has the capability of simulating many processes right from rainfall-runoff process up to plant growth (Neitsch et al., 2002; Gassman et al., 2007). The SWAT is a computationally efficient agro-hydrological watershed scale model and is well-suited for studying the large-scale impacts of land use changes (Breuer et al., 2009). Components of the model include weather, hydrology, soil characteristics, plant growth, nutrients, pesticides and land management (Gassman et al., 2007). Many attempts have been made for modelling runoff in an ungauged watershed with little or no calibration efforts (Arnold et al., 1998). Here, ungauged watersheds refer to the watersheds for which topographic and climatic properties are available, but discharge data are not available. The SWAT model could simulate runoff from a watershed in Jaipur with reasonable accuracy even without any calibration data (Jayasree and Sajikumar, 2012). Wang et al. (2012) compared the effect of change in land use by utilizing the SWAT and partial least square method. Githui et al. (2009) used SWAT model for assessing the impact of land use change on runoff characteristics and found that varying degree of dependence of land use change on the runoff characteristics. Several such studies have been conducted by many investigators for assessing the effect of land use change on runoff characteristics (Li et al., 2009; Wang et al., 2012; Alibuyog et al., 2009). These studies indicate that impact of land use changes on runoff characteristics varies from place to place. Therefore it becomes imperative to assess the effect of LCLU change on runoff characteristics in the area of interest, especially where unique features exist in such area. Hence the objectives of the current study are set as:

- To assess the effect of local land use change on the runoff characteristics of some of the typical watersheds in Jaipur, India where slope of the terrain changes drastically within a relatively smaller length of the river.
- To appraise how the change in land use in the last few decades affected the runoff characteristics of these watersheds.
- To assess groundwater recharge in urban watershed.

2 MATERIALS AND METHODS

2.1 Study area

The current study focuses on the effect of land use landcover change on runoff characteristics of watersheds Jaipur urban. All three watershed has area within city and some area outer of city. Jaipur is city of Rajasthan, a state in India, located in limits of 26°45'8.7"N to 27°1'55.42" and 75°41"40.86" E to 75°51"14.80" E as shown in Figure 1. This area receives 548mm total average rainfall in a year. Beyond this region rainfall toward west has decreasing trend in all years. Figure 2 shows annual rainfall pattern of rainfall area around each grid surrounded by this region. This Grid is generated with India Meteorological Department (IMD) rainfall data. Rainfall in an area is always in limits of rainfall of its surrounding area. This growth also increased the amount of runoff from urban catchment. Total area of Jaipur city is after considering 2016 urban expansion is 316.29 km^2. This area has significant changes in land use over 44 years which also impact urban runoff. Change in land use also change groundwater recharge which might change the lower groundwater level in long span of time and also reduce quality of groundwater. In long time, most of land use changed and most of agriculture area is reduced. This type of study for this area has never been carried out. So, an attempt has been made to quantify runoff with the changing of land use.

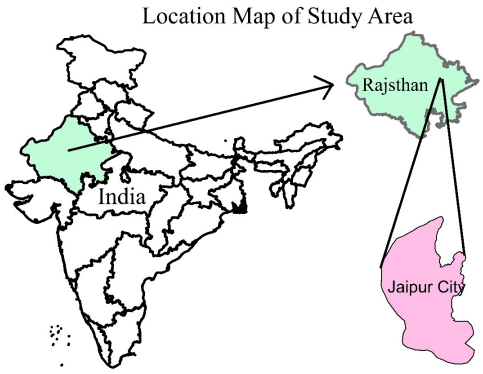

Figure 1. Study area.

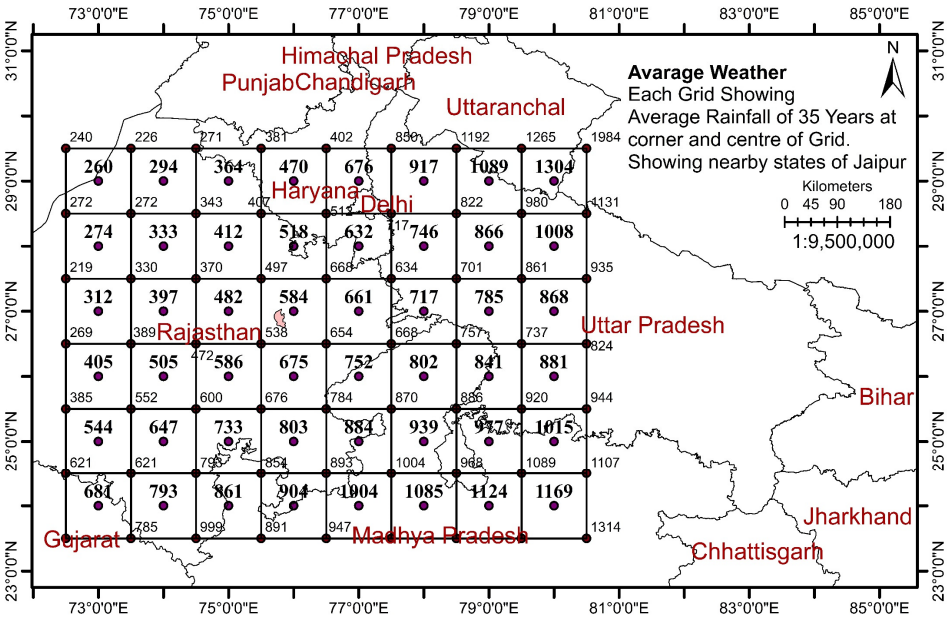

Figure 2. Weather grid surrounding by Jaipur.

2.2 Data sources

Weather data was used from Indian Metrological Department Processed by SWAT (Soil and Water Assessment Tool) and CFSR (Climate Forecast System Reanalysis). It provide 36 year of compiled weather data of Temperature, Daily rainfall, Humidity, wind speed and solar radiation. We also used data from IMD for simulation of watershed on different conditions with all climate parameter average and this was data updated in SWAT database with a certain format required for SWAT before processing. It was later, converted to Grid format for processing requirements where more details about processing of this data will be found in research paper on climate data (Dile and Srinivasan 2014; Fuka et al., 2014). Table 1 Shows details of Satellite image used.

Table 1. Detail of satellite data used.

Satellite	Sensor	Date taken	Resolution
L 1	MSS multi-spectral	04-09-1972	60 meter
L 3	TM multi-spectral	08-01-1980	60 meter
L 5	TM	13-09-2000	30 meter
L 5	ETM+ multi-spectral	22-10-2011	30 meter
L 8	OLI and TIRS	17-09-2016	30 meter

Digital Elevation Model of Cartosat-1 of Version 3 was used for watershed generation and simulation. Soil Map by FAO was used and soil properties provided by FAO were set into database of SWAT Details of Jaipur Soil properties as shown in Table 2. The area of each soil has been calculated and values were steeled in model.

Table 2. Soil properties of Jaipur urban watersheds.

Term	Loam Soil	Sandy Loam
FAO Soil code	Be76-2b-3677	Qc49-la-3840
Hydrological Soil Group	D	C
Area	212.25km^2	16.78km^2
Soil K (Layer 1 and 2)	4.63 mm/hr, 4.23 mm/hr	9.1 mm/hr, 9.99 mm/hr
Clay (Layer 1 and 2)	25%, 28%	14%, 17%
Silt (Layer 1 and 2)	36%, 36%	32%, 32%
Sand (Layer 1 and 2)	39%, 35%	54%, 51%

Calculated and Identified in Model, Data Source FAO

2.3 Methodology

Hydrologic modelling and analysis of urban watersheds of Jaipur was carried out using the ArcSWAT interface for SWAT in ArcGIS. The surface runoff simulation in SWAT was brought out using various input data such as topography, land use, soil properties and weather data in the watersheds. The watersheds were initially divided into Hydrologic Response Units (HRUs) on the basis of unique combinations of land use, soil distribution, and slope. Total 15 Hydrological Unit was generated for the whole watershed area. Total of 3 outlets are identified after generation of drainage network over surface area. Each outlet and watershed has been numbered from 1 to 3. Hydrological units provide best estimation for simulation model to simulate soil properties and rainfall (Neitsch et al., 2002). Based on daily components of hydrologic cycle (precipitation, runoff, evapotranspiration, percolation, sub- surface return flow, groundwater flow, and changes in water storage), a daily water budget in each HRU was calculated (Neitsch et al., 2002).

The hydrologic cycle is simulated by the SWAT model on the basis of the following water balance Eq. [1].

$$SW_t = SW_O + \sum_{t=1}^{t}(R_t - Q_t - ET_t - P_t - QR_t) \qquad [1]$$

where, SW_O and SW_t are the soil water content at the beginning and end of a time period for which water balance equation is written. The unit used in the equation is mm.R_t,Q_t,ET_t, P_t and QR_t are the rainfall, the surface runoff, the evapotranspiration, the percolation and the lateral flow respectively.

Two methods for estimating surface runoff are available in the SWAT: The SCS curve number procedure and the Green and Ampt infiltration method. In this study, the SCS method was used. The SCS curve number method estimates surface runoff from daily rainfall using initial abstractions (surface storage, interception, and infiltration prior to runoff) and a retention parameter which varies with respect to changes in soil, land use management, slope and soil water content. It may be noted that this computation had been carried out at the watershed level but not at the HRU level. The sizes of HRUs are much smaller than that of watershed. Though the CN method has certain inherent drawbacks, it was proved to be useful in simulating the historical runoffs, especially when the watershed was considered to have a large number of sub-basins and the flow are routed through channels by hydrologic routing as in case of the SWAT model (Raneesh and Thampi, 2011; Jayasree

and Sajikumar, 2012).The SWAT model is proved to be useful in simulating the daily surface runoff, sediment yield and nutrient load, even though it utilizes the CN method for computing surface runoff (Raneesh et al., 2010).

Once the surface runoff is calculated with the curve number method, the amount of surface runoff released to the main channel is calculated from each sub-watershed and is then routed through the channel network. Three methods of estimating Potential Evapotranspiration (PET) are available in the SWAT. The readers are referred to Neitsch et al. (2002) for complete description of the methodology of the SWAT model.

Groundwater Recharge is calculated with following Eq. [2].

$$w_{rchrg,j} = \left(1 - \exp\left[-\frac{1}{\delta_{gw}}\right]\right).w_{seep} + \exp\left[-\frac{1}{\delta_{gw}}\right].w_{rchrg,i-1} \qquad [2]$$

where, $w_{rchrg,j}$ is amount of recharge entering the aquifer on day i, δ_{gw} is the delay time or drainage time of the overlaying geologic formation (days), w_{seep} is the total amount of water exiting the bottom of the soil profile on day i, and $w_{rchrg,i-1}$ is the amount of recharge entering the aquifer on day i-1. The total amount of water exiting the bottom of the soil profile on day I is calculated as per Eq. [3]:

$$w_{seep} = w_{prec,ly=n} + w_{crk,btm} \qquad [3]$$

where, w_{seep} is the total amount of water exiting the bottom of the soil profile on day i , where $w_{prec,ly=n}$ is the amount of water percolating out of the lowest layer, n, in the soil profile on day i, and $w_{crk,btm}$ is the amount of water flow past the lower boundary of the soil profile to bypass on day *i* (mmH_2O)

The delay time δ_{gw} cannot be directly measured. It can be estimated by simulating aquifer recharge using different values for δ_{gw} and comparing the simulated variations in water table level with observed values. Johnson (1977) developed a simple program to iteratively test statistically evaluate different delay times for the watershed. Sangrey et al. (1984) noted that monitoring wells in the same area had similar values forδ_{gw}, so once a delay time value for a geomorphic area was defined; similar delay time can be used in adjoining watershed within the same geomorphic province.

2.4 Model setup

We have divided total watershed using 3 outlets by manual identification. Landuse pattern in each watershed was calculated. But it's found that only watershed No. 3 had major impact of land use change due to its covering of maximum area of city. So we focused on this watershed, weather details of all watershed are also calculated. Watershed map and detail of land use changing over time in each watershed is shown in Figure 3 and Table 3, 4 and 5 in result section of this paper. We have given 15% (Landuse), 10 %(soil). 20 %(slope) weight to HRU classes as recommended by SWAT.

The simulation period can be set according to the requirement, but here it was fixed based on the availability of data for validating the model. Hence, the period of simulation was fixed to 2016 with different land use i.e. 1972, 1980, 2000, 2011 and 2016. It may be noted that ungauged watershed scenario was simulated and was assumed that no runoff data is available for calibration of the model. The parameters used in the model were not derived from an actual runoff data rather derived by simulation as actual condition.

3 RESULTS AND DISCUSSIONS

3.1 Simulation of runoff and its dependence on land use

As the aim of the current study is to assess the effect of land use and land cover on the runoff characteristics, the SWAT model was run to simulate the surface runoff in selected watersheds. The study was expected to be conducted in a data scarce situation as the lack of sufficient number of gauging stations was a common hurdle in many water resources applications, at least in the region under consideration. Hence, the selected SWAT model was run with the minimum data possible. The land use data was prepared using Landsat.

These processed data along with other local data such as soil and weather data were used for running the model. It is seen that the simulated flow varies appreciably from the measured one. This can also be seen from the Table 3 which shows the annual average values of various components in the runoff processes. This values are based on actual data, and repressing that changing in land use also impact on groundwater recharge and other hydrological parameters. To identify impact of land use we have used same weather data as of 2011 for year 1980 with changing land use. So, that only impact of land use change can be identified. It is found that groundwater recharge is reduced in 2011 due to change in land use.

Table 3. Groundwater recharge and annual basin values by considering same rainfall.

Term	1980 Landuse	2011 Landuse
Precipitation	1360.8 mm	1360.8 mm
Surface runoff Q	540.30 mm	672.09 mm
Lateral soil Q	11.70 mm	11.34 mm
Groundwater (SHAL AQ) Q	227.09 mm	115.97 mm
Groundwater (DEEP AQ) Q	8.92 mm	5.16 mm
Revap* (SHAL AQ => SOIL/PLANTS)	44.03 mm	44.03 mm
Deep aquifer recharge	14.27 mm	8.34 mm
Total aquifer recharge	**285.35 mm**	**166.85 mm**
Total water yield	788.00 mm	804.56 mm
Percolation out of soil	290.12 mm	169.82 mm
Evapotranspiration	472.1 mm	449.8 mm
Total sediment loading	143.09 T/HA	131.69 T/HA

It is found that groundwater recharge was 285 mm in year 1980 which later was reduced to 166.85 mm. The lower the groundwater recharge, the lower the groundwater level. Similarly, as in Table 3, recharge of shallow aquifer is also reduced. But water yield is increased. Surface runoff also increased from 540m to 672mm. Due to loss in vegetation evapotranspiration was also reduced. Urban area has increased in speedy way and Table 4 is showing the area changes from 1972-2016 in km2. Table 4 is also showing the changing pattern of land use in percentage. It is clear that urban area has increased by 179 km2 from 1972 to 2015. Figure 3 shows changing pattern on land use of urban area of Jaipur city. Built up area of Jaipur have undergone a very fast rate of growth and it is growing at the rate of 4.06 km2/year (Average calculate by comparing 1972 and 2016 data). Whereas agriculture land loss is about 126.23km2 and this loss has an average rate of 2.86 km2/year. Vegetation loss was about 53.64 km2. Most of agriculture land were converted into built up area. Natural vegetation appears to be more in year 1980 and 2001 but in 2011 it also recorded a decrease in the area. Most of population is found in north side of Jaipur where build up is too dense. West side has the most agriculture and natural vegetation. Growth of Jaipur city starts form Jaipur Lake and move towards west side of city. This city is more extended towards the North and south side and less extended in the east and west side. Due to being a tourist place it is increasing at rapid speed. Table 4 shows the changes in land use and Table 5 shows the change in detection matrix for each class from 1972 to 2016

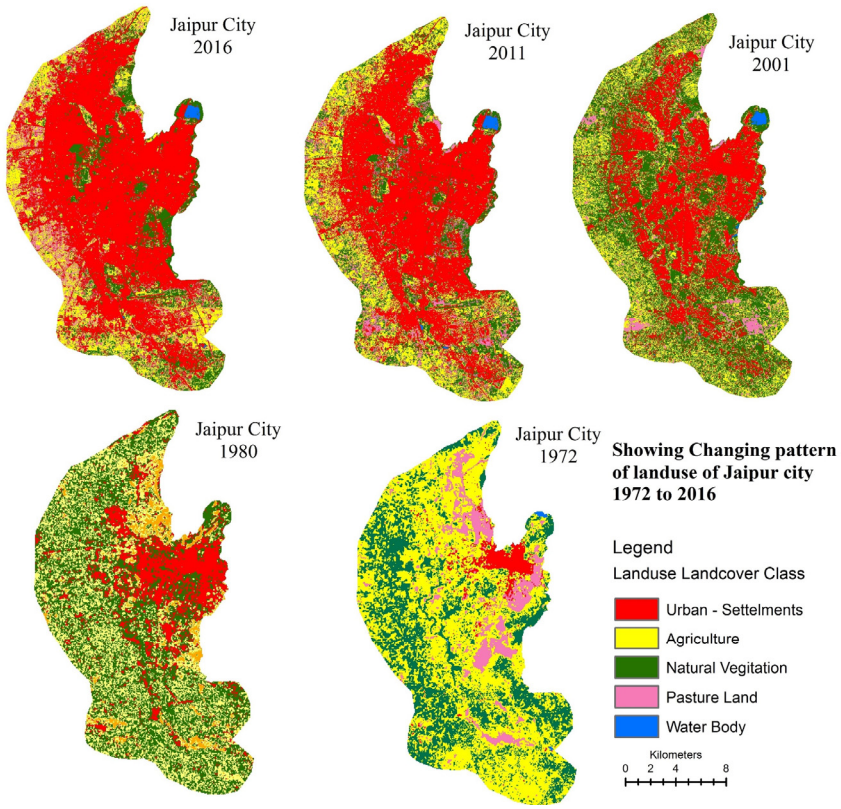

Figure 3. Landuse of Jaipur from 1972 to 2016.

Table 4 Area in km^2 and percentage in Brackets.

Name	2016	2011	2001	1980	1972
Built Up	191.67 (60.50)	167.41 (52.84)	108.86 (34.36)	56.86 (17.95)	12.26 (3.87)
Agriculture	50.45 (15.92)	67.79 (21.40)	68.86 (21.74)	106.39 (33.58)	176.68 (55.77)
Vegetation	44.31 (13.98)	55.49 (17.51)	126.23 (39.84)	137.47 (43.39)	97.95 (30.92)
Pasture Land	29.18 (9.21)	24.89 (7.86)	11.42 (3.61)	16.10 (5.08)	29.44 (9.29)
Water Body	1.22 (0.39)	1.25 (0.39)	1.45 (0.46)	0.00 (0.00)	0.50 (0.16)

Table 5. Change detection matrix of Jaipur 1972 vs 2016 (area in km^2).

	Built up	Agriculture	Vegetation	Fallow Land	Water Body	Total 2016
Built up	10.34	107.09	52.93	21.18	0.13	191.68
Agriculture	0.56	29.03	18.24	2.32	0.09	50.23
Vegetation	1.10	24.45	13.63	4.60	0.26	44.05
Pasture	0.23	15.27	12.39	1.20	0.02	29.11
Water Body	0.01	0.56	0.54	0.11	0.00	1.22
Total 1972	12.24	176.40	97.74	29.42	0.50	

Table 6. Detail of urban watershed based on outlets.

Outlet Number	Area km^2
Outlet 1	26.02
Outlet 2	51.18
Outlet 3	151.82
Total Area of Watersheds	229.02

The change detection matrix is showing how each class obtained values from other class during changing land use of 44 years. As built-up in 2016 takes up to 107.09 km^2 from 1972. Elevation map of Jaipur shows higher elevation at north side of Jaipur and lower are at south side of Jaipur as shown in Figure 4. Much variation was found in elevation means and more in water flow. This type of area required a great deal of water management practices. On other side rainfall of Jaipur which is derived from IMD data and interpolated variation according to city level is showing a micro pattern of rainfall found in the city and it was derived from 35 years of climate average data. It receives more rainfall at east side and less rainfall at west side. This was the reason that deserts were found in west side of continent. Since it is a very small variation it does not impact much. But this variation is important to contribute to runoff. Area of soil under each watershed is shown in Table 8. The major types of soils were loam and sandy loam. Major area of watershed was found under loam soil and very less area is under sandy loam soil. Properties of all soil had already been discussed in Table 2 and soil map is shown in Figure 7. Loam soil has a coverage of 212 km^2 and sandy loam soil is 17 km^2.

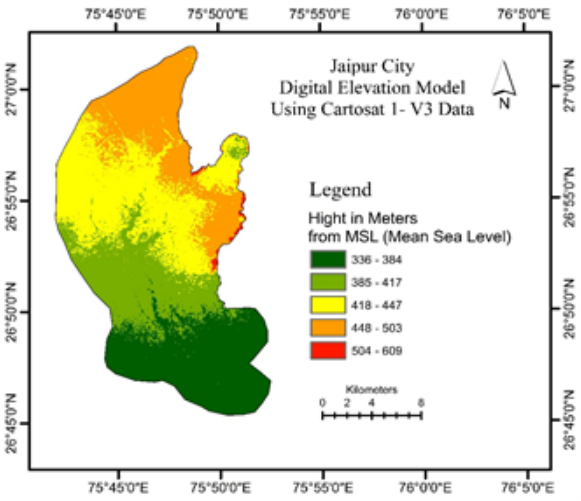

Figure 4. Elevation map of Jaipur.

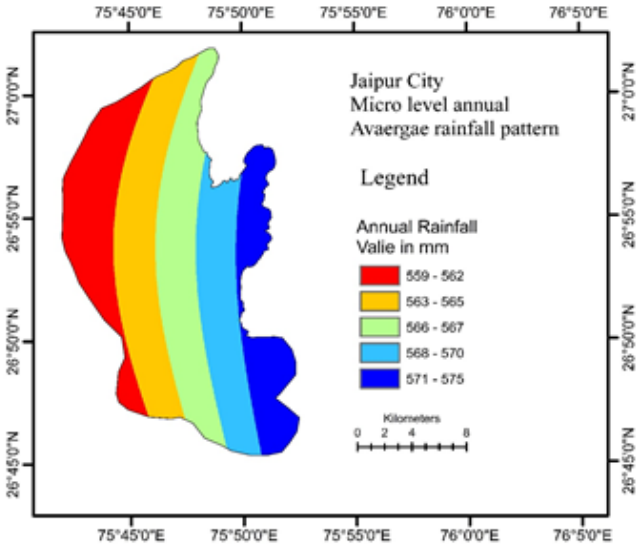

Figure 5. Micro level rainfall variation.

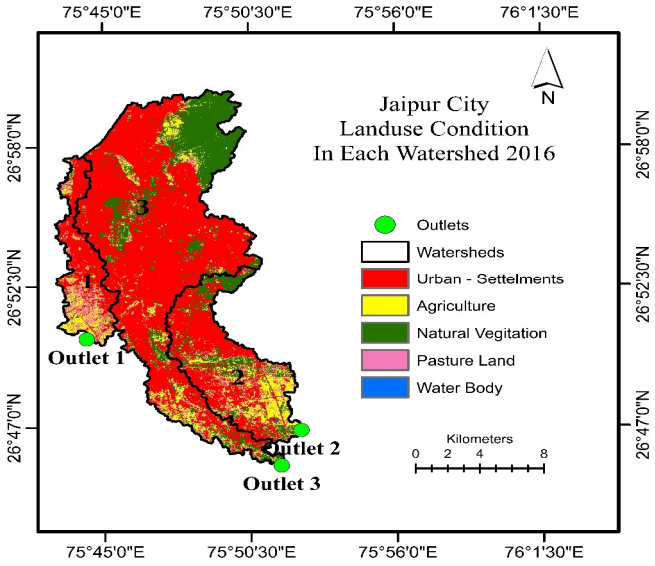

Figure 6. Land use in each watershed.

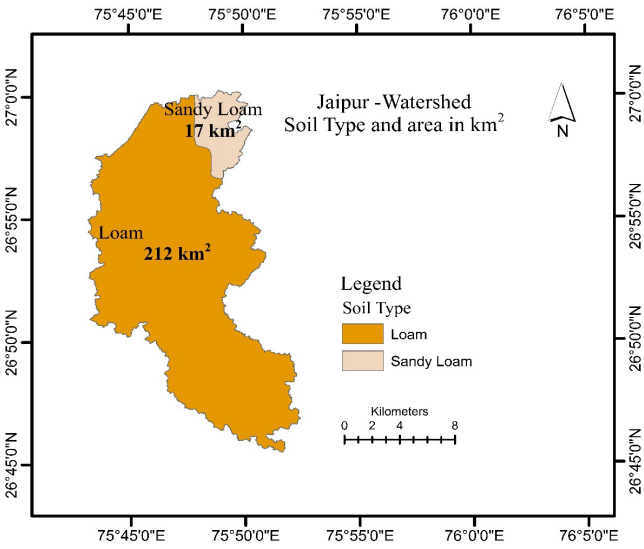

Figure 7. Soil map of Jaipur.

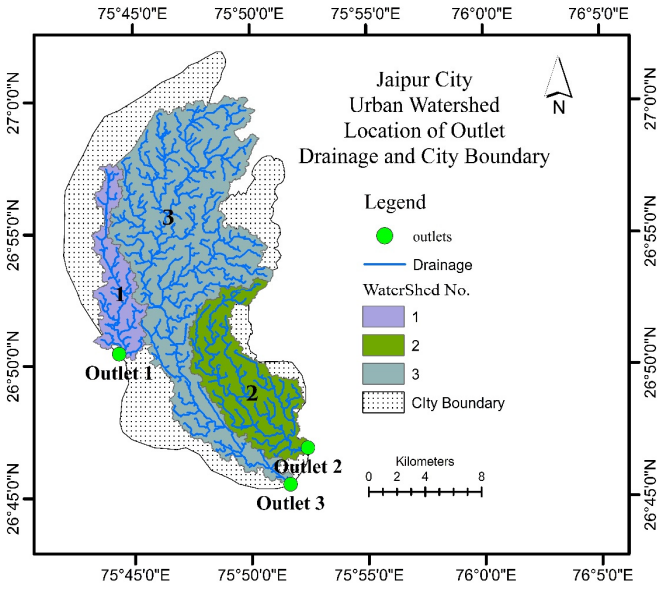

Figure 8. Urban watershed and outlet of Jaipur.

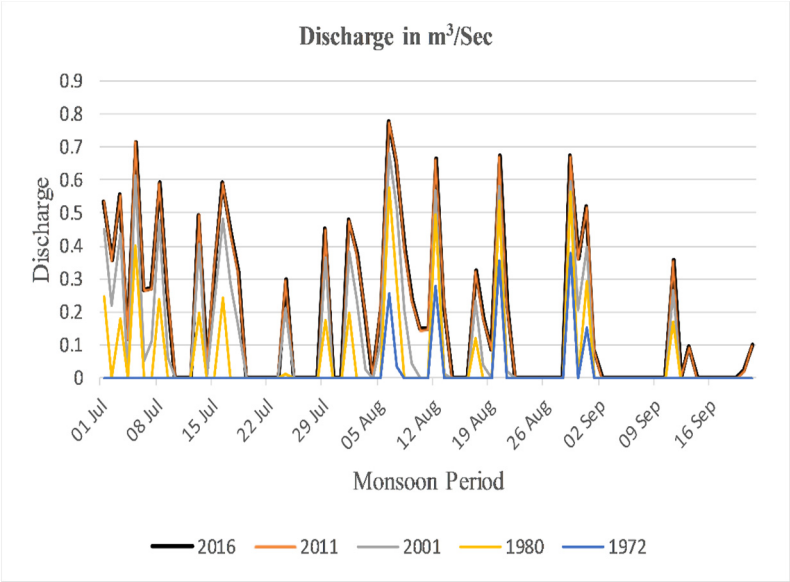

Figure 9. Discharge vs landuse.

It is found that urban area has reached its maximum possible extent of watershed boundary. It is not possible to increase more urban area in that watershed as shown in Figure 6 In the center of map, a whole watershed is covered by urban development.

3.2 Runoff land use

Simulation was run for all three watersheds for a whole year. But only the major watershed is important and so only it is considered and monsoon period data is calculated. Change in land use impact on discharge and total amount of water also were calculated. We have found that urban area is expanding and amount of runoff from city is increasing. Both are increasing at linear rate combination as in reported results. But it has limits, because if urban area reached maximum extent of watershed then more increase in runoff is not possible. This is because no further expansion of urban is possible in a watershed. But this results and derived relation is applicable on area of similar properties. After simulation, we get results of runoff versus land use as shown in Figure 9. It is clear from figure that runoff is increasing with expending urban area. As of in August discharge was 0.25m3/sec in 1972 and it had increased up to 0.80m3/sec in 2016. Same trend was visible in all years during monsoon. Jaipur is centered at the location on earth where desert is near and it receives very less monsoon rainfall. Table 8 shows how runoff is changing with respect to land use. We have calculated it in both way by considering 1972 as base year and compare changes with previous years. From Table 9 it is clear that urban area has increased up to 1306% compared to 1972 with 2016. Similarly, runoff had increased by 918% compared to 1972 with 2016. But when compared to 2011 urban area in major watershed had increased by

6.02% and runoff compared to 2011 vs 2016 is just 0.63%. This is because no further expansion is possible in urban area of major watershed. But overall till it reach boundary of watershed it is following a positive and linear relationship between runoff and land use as shown in Figure 10 and Table 7. It is clear from the figure where it has an r2 value of 0.99 which is nearly about exact positive approach. Trend line and actual data were following the same slope. So by using this linear Equation of runoff and land use we can predict land use change and runoff relation of similar area with same properties. Table 9 also shows changing volume of runoff with changing of urban area.

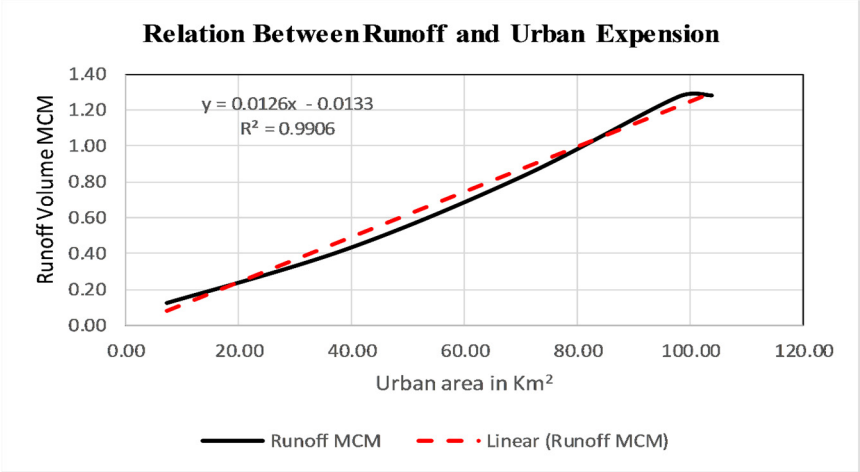

Figure 10. Runoff volume vs urban area.

Table 7. Landuse pattern on whole watershed (area in km^2).

Whole Watershed	2016	2011	2001	1980	1972
Built up	145.27	132.41	88.53	46.49	7.59
Agriculture	23.81	30.88	37.07	70.31	125.43
Vegetation	44.95	49.95	95.19	98.30	71.71
Pasture	14.81	15.55	6.49	13.92	24.12
Water Body	0.19	0.23	1.75	0.00	0.18

Table 8. Runoff changes due to changes in land use of urban watershed (in Percentage).

	Urban Expansion in Major Watershed		Change in Runoff Volume (MCM)	
Year	Change vs Previous Period	Change vs 1972	Change vs Previous Period	Change vs 1972
2016	6.02	1306.23	0.63	918.25
2011	38.87	1226.42	52.88	911.9
2001	79.68	855.15	95.77	561.9
1980	431.57	431.57	238.1	238.1
1972	Base Year			

Table 9. Urban area vs runoff volume with land use change (Major Watershed).

Year	Urban	Runoff MCM
2016	103.78	1.283
2011	97.89	1.275
2001	70.49	0.834
1980	39.23	0.426
1972	7.38	0.126

4 CONCLUSIONS

It is apparent from the results that land use change has an impact on the runoff and groundwater. Runoff was only 0.126 MCM in 1972 and increased to 1.283 MCM in 2016. During the same period urban area also increased from 7.59 km^2 to 145.27 km^2 in the watershed. Urban expansion has also an additional impact because it reduced aquifer recharge from 285.35 mm to 166.85 mm. Changes in the extent of urban area also impacts on natural process of hydrological cycle. Later this changes impact the human in form of flash flood and overloaded water in urban catchment. Urban areas build on natural flow path of water and this causes flood due to flood water following its old flowing pattern. Our study shows the drainages also have increased speed of water flow with changing pattern on urban area. This water must be managed to avoid damage to properties.

So, before expansion of urban area it is better to quantify the impact of land use with hydrology method to build a better urban city.

REFERENCES

Alibuyog, N.R., Ella, V.B., Reyes, M.R., Srinivasan, R., Heatwole, C. & Dillaha, T. (2009). Predicting The Efffects of Land Use Change on Runoff And Sediment Yield in Manupali River Subwatersheds Using the SWAT model. *Int. Agric. Eng. J.*, 18(1e2), 15-25.

Arnold, J.G., Srinivasan, R., Muttiah, S. & Williams, J.R. (1998). Large Area Hydrologic Modeling and Asessment Part 1. J. Am. *Water Resour. Assoc*., 34(1), 73-89.

Breuer, L., Huisman, J.A., Willems, P., Bormann, H., Bronstert, A., Croke, B.F.W., Frede, H.G., Graff, T., Hubrechts, L., Jakeman, A.J., Kite, G., Lanini, J., Leavesley, G., Lettenmaier, D.P., Lindstrom, G., Seibert, J., Sivapalan, M., Viney & N.R. (2009). Assessing The Impact of Land Use Change on Hydrology by Ensemble Modeling (LUCHEM). *Adv. Water Resour*. 32(2), 129-146.

Crooks, S., Davies, H. & Goodsell, G. (2000). Rainfall Modelling and the Impact of Land use Change in the Thames Catchment. PIK Report No. 65 edited by: Bronstert, A Bismuth, B Menzel, L. Proceedings of *European Conference on Advances in Flood Research*, November 2000.

Deepa (2000). Landscape Evaluation of Peechi-vazhani Wildlife Sanctuary with Special Reference to Peechi Region Using Remote Sensing Techniques. *MSc Thesis*. School of Environmental Sciences, MG University, Kottayam.

Dile, Yihun Taddele & Raghavan Srinivasan (2014). Evaluation of CFSR Climate Data for Hydrologic Prediction in Data-Scarce Watersheds: An Application in the Blue Nile River Basin. *Journal of the American Water Resources Association,* 50(5), 1226–41.

Fuka, D. R., Walter, M. T., MacAlister, C., Degaetano, A. T., Steenhuis, T. S. & Easton, Z. M. (2014). Using The Climate Forecast System Reanalysis as Weather Input Data for Watershed Models. *Hydrological Processes*, 28(22), 5613-5623.

Garzuzi, J, N Goldshleger, E Ben-dor & L Asaf. (2002). Impacts of Land Use on Quantity and Quality of Urban Runoff (Herzliya and Ra'anana Case Study). *Environment,* (2001), 153–57.

Gassman, P.W., Reyes, M.R., Green, C.H. & Arnold, J.G. (2007). The Soil and Water Assessment Tool: Historical Development, Applications, and Future Research Directions. *Trans. ASABE*, 50(4), 1211-1250.

Githui, F., Mutua, F. & Bauwens, W. (2009). Estimating The Impacts of Land-Cover Change on Runoff Using The Soil and Water Assessment Tool (SWAT): Case Study of Nzoia Catchment, Kenya. *Hydrol. Sci. J.*, 54 (5), 899-908.

Jayasree, M.S. & Sajikumar N. (2012). Runoff Prediction in Manali River Using SWAT. In: *Proceedings of the 24th Kerala Science Congress*, 376-378.

Li, Z., Liu, W., Zhang, X. & Zheng, F. (2009). Impacts of Land Use Change and Climate Variability on Hydrology in an Agricultural Catchment on The Loess Plateau of China. *J. Hydrol*. 377, 35-42.

Meshesha, Tesfa Worku, S. K. Tripathi & Deepak Khare. (2016). Analyses of Land Use and Land Cover Change Dynamics Using GIS and Remote Sensing during 1984 and 2015 in the Beressa Watershed Northern Central Highland of Ethiopia. *Modeling Earth Systems and Environment.* 2(4), 168. Retrieved (http://link.springer.com/10.1007/s40808-016-0233-4).

Neitsch, S.L., Neitsch, J.G., Arnold, J.R., Kiniry, J.R., Williams, J.R., King, K.W., Srinivasan, Willia & M.S. (2002). *Soil and Water Assessment Tool Theoretical Documentation*.

Niehoff, D., Bronstert, A.& Burger, G. (2002). Effects of Climate and Land-Use Change on Storm Runoff Generation: Present Knowledge and Modelling Capabilities. *Hydrol. Processes*, 16, 509-529.

Randall, D., Curry, J., Battisti, D., Flato, G., Grumbine, R., Hakkinen, S., Martinson, D., Preller, R., Walsh, J. & Weatherly, J. (1998). Status of and Outlook for Large-Scale Modeling of Atmosphere-Ice-Ocean Interactions in The Arctic. Bull. Am. *Meteorol. Soc*. 79 (2), 197-219.

Raneesh, K.Y., Thampi & S.G. (2011). A Study on The Impact of Climate Change on Streamflow at The Watershed Scale in The Humid Tropics. *Hydrol. Sci. J.*, 56 (6), 946-965.

Raneesh, K.Y., Surya, T.V., Thampi & S.G. (2010). Prediction of Stream Flow, Sediment Yield, and Nutrient Load in The Chaliyar River Basin, Kerala, India. *Int. J. Earth Sci. Eng*., 3(5), 654-661.

Wang, G., Yang, H., Wang, L., Xu, Z. & Xue, B. (2012). Using the SWAT model to Assess Impacts of Land Use Changes on Runoff Generation in Headwaters. *Hydrol. Processes*. http://dx.doi.org/10.1002/hyp.96.

Xie, Xianhong & Yuanlai Cui. (2011). Development and Test of SWAT for Modeling Hydrological Processes in Irrigation Districts with Paddy Rice. *Journal of Hydrology,* 396(1–2), 61–71. http://dx.doi.org/10.1016/j.jhydrol.2010.10.032.

SIMULATION OF HYDROLOGIC BEHAVIOR OF LOWER TAPI BASIN USING HEC-HMS AND GEOSPATIAL TECHNOLOGY

PAWAN N. BHAVSAR[1] & JAYANTILAL N. PATEL[2]

[1] S.V. National Institute of Technology, Surat, India,
pawanbhavsar@gmail.com

[2] Civil Engineering Department, S.V. National Institute of Technology, Surat, India,
jnp@ced.svnit.ac.in

ABSTRACT

Today, it is essential to use a hydrological model to assess and predict the water availability of river basins due to climate change. Event based rainfall-runoff modeling is carried out using HEC-HMS. In the present study, Linear imaging self-scanning sensor (LISS-III) satellite images are used to delineate the river basin by using ARCGIS. Penman-Montieth model is used for the estimation of evapotranspiration loss. Green- Ampt model and Snyder's method are compared and best suitable method is adopted to transform rainfall into runoff. Uncertainty analysis is carried out to increase the model efficiency. The condition number is being used for the sensitivity analysis to ascertain the most sensitive parameters. Only sensitive parameters are used for the uncertainty analysis. The Model is separately run, calibrated, and validated for the years 2011-2015 events. Green – Ampt and Snyder models are compared for the predictive capability and it has been concluded that Green –Ampt model is better suitable for the study area. The objective of the present study is to develop rainfall runoff model for the Lower Tapi Basin and carried out the uncertainty analysis to estimate the better model parameters for the simulation of rainfall events. For the uncertainty analysis, Monte-Carlo method is used by taking Nash –Sutcliffe coefficient as an objective function, which is to be maximized for the better simulation of rainfall runoff process.

Keywords: HEC-HMS; monte-carlo method; sensitivity analysis; rainfall runoff modeling.

1 INTRODUCTION

Rainfall-runoff is a complex phenomenon to represent in mathematical form. In the real world system, rainfall runoff process is influenced by each and every physical characteristics of the catchment. To generalize all physical characteristics of the catchment is really a difficult task. Consider the infiltration phenomenon which has a direct influence on the runoff process, when infiltration is observed at different sites in the catchment it comes out to be a wide range of infiltration rates. In a case of lumped hydrological model, representation of such wide range of the values are difficult because parameter values are to be averaged for the particular catchment. Climatological parameters are also having great influence on the runoff process. Consider the evapotranspiration process it is influenced by the temperature, wind speed, vapor pressure and other parameters. Getting proper data for all these parameters is itself is the difficult task. Even if omitted the single parameters can lead to the imprecise estimation of any process.

Today's advanced computing techniques have overcome the most of the real world complexity. It is possible to represent even a complex phenomenon in a fairly good way. Using the gridded distributed models it is possible to represent the catchment in a more realistic way. Watershed management is really an important subject which will helpful in the future planning of Hydro projects and natural resources management. The HEC - HMS tool is used to predict the runoff process in a Lower Tapi basin at all below mention gauging stations.

Hydrological model of HEC-HMS is designed based on simulation of rainfall-runoff in watersheds that can solve rainfall-runoff process in the graphical interface (Elham et al., 2012). Hydrographs produced by program use directly or in conjunction with other software for studies of urban drainage, water availability, future urbanization impact, flow forecasting, flood damage reduction, floodplain regulation and systems operation. Most of the calculations in HEC-HMS include loss calculations, conversion of extreme precipitation to run off, baseflow estimation, routing in reaches and reservoirs. Radmanesh et al. (2006) calibrated and validated the HEC-HMS model in Yellow River watershed in southwestern Iran. Rostami et al. (2012) used the HEC-HMS and GIS to simulate the rainfall-runoff process in Amirkabir watershed. Sabzevari et al. (2009) estimated the flood hydrograph in no statistical watersheds using HEC-HMS model and GIS in Kasi-lian watershed. Shaghaeghi fallah (2001) applied HEC-HMS model to simulate river flow in Mohammadabad watershed (located in the north of Iran). There are different methods for surface runoff simulation in HEC-HMS and these methods have different results (Elham et al., 2012). Yusop (2007) used the HEC-HMS for predicting the runoff in oil Palm catchment.

Yener et al. (2007) simulated the rainfall runoff process by dividing the basin into three sub-basins: Kirazdere, Kazandere, and Serindere and each sub-basin is modeled with its own parameters. For the hydrologic modelling studies, the new version of HEC-HMS hydrologic modelling software released in April 2006 by the US Army Corps of Engineers is used. Modeling consists of two things, event-based hourly simulations and runoff scenarios using intensity-duration-frequency curves. Infiltration loss and baseflow parameters of each sub-basin are calibrated with hourly simulations. This study concludes that the simulated runoff values can be used for flood control and flood damage estimations.

Arekhi et al. (2011) compared the different methods of precipitation loss which are Constant loss, Initial and constant loss rate, Deficit and Green & Ampt. The objective of this study was to fit the peak flow discharges and the total volume of flow in HEC-HMS. Results showed that for two objective functions, Initial and constant loss rate method shown the best results had fewer changes percent of simulated to observed discharges in 70% events and Green & Ampt and Initial Deficit and Constant loss rate methods placed in next preferences.

Majidi and Shahedi (2012) used the HEC-HMS hydrological model version 3.4 to simulate the rainfall-runoff process in Abnama watershed located in the south of Iran. To compute infiltration, rainfall excess and flow routing, Green-Ampt, SCS Unit hydrograph and Muskingum routing were chosen, respectively. Rainfall-runoff simulation were conducted using five rainstorm events. Initial results showed that there is a clear difference between observed and simulated peak flows. Therefore model calibration with optimization method and sensitivity analysis has been done. The results showed that lag time is a sensitive parameter. Model validation using optimized lag time parameter showed the reasonable difference in peak flow. Finally, it's been concluded that model can be used with the reasonable approximation in hydrologic simulation in Abnama watershed.

There are many methods available to carry out uncertainty analysis viz, Monte-Carlo method, (Shamsudin et al., 2011; Kuczera and Parent, 1998) Generalizes Likelihood Uncertainty Estimation, (GLUE) (Beven and Binly, 1992) Model error analysis methods (Montanari and Brath, 2004) and methods based on fuzzy set theory (Maskey et al., 2004). Amongst these methods, some of are the sampling based method (Monte-Carlo method) to be used when the quantity and quality of data are not satisfactorily available and some of are categorized under Bayesian methods (Shrestha et al., 2009) to be used when the quantity and quality of the data are satisfactorily available. Pappenberger et al. (2006) has given decision tree to choose the method applied to the given problem.

In the present study, HEC-HMS (Hydrologic Engineering Center's Hydrologic Modeling System) model is used to simulate the rainfall-runoff process. Linear imaging self-scanning sensor (LISS-III) satellite images are used to delineate the Tapi river basin in ARCGIS. Penman-Montieth model is used for the estimation of evapotranspiration loss. Green & Ampt model and Snyder's method are compared and best suitable method is adopted to transform rainfall into runoff. Uncertainty analysis is carried out by using Monte-Carlo method in order to increase the model efficiency. The condition number is being used for the sensitivity analysis to ascertain the most sensitive parameters. Only sensitive parameters are used for the uncertainty analysis. Uncertainty analysis involves in optimizing the parameters involved in the model. Optimized parameters are may not be a global optimum parameter of the basin, optimized parameters only suitable to the catchment for which uncertainty analysis is being carried out. Many researchers have tried to optimize the model parameters by using Monte-Carlo methods using readily available tools (Shamsudin, 2014), but still, proper explanation and proper algorithm to carry out uncertainty analysis are still missing. Thus, this study also demonstrates the proper algorithm to carry out uncertainty analysis of the rainfall-runoff model.

2 STUDY AREA AND DATA COLLETCTION

Tapi River is a river in Central India. Tapti, Tapee, Taapi are the various names used to denote Tapi River. Also known as the daughter of Sun God, its basin extends over an area of 65, 145 km^2 - a whooping area which totals to 2% of the total area of India. In India, Tapt River originates at Multani of Betul District (Madhya Pradesh). The Basin of Tapi River lays in three Indian States, namely, Gujarat, Madhya Pradesh and Maharashtra. Covering an area about 3,837 km^2, 9,804 km^2 and 51,504 km^2 respectively. For the present study, only part of the Tapi basin is being considered, along with the river called Girna, which joins Tapi river at Nanded in Maharashta state. Girna is the second biggest tributary of Tapi in terms of the catchment area. Basin map is shown in figure 1.

Daily rainfall data and discharge data of the catchment area under consideration is procured from the Gujarat State Data Centre (GSDC) for the period of 2011 to 2015. For the present study, 12 rain gauges are used after applying missing data analysis wherever it was required. Discharge is measured at the causeway downstream of Tapi River.

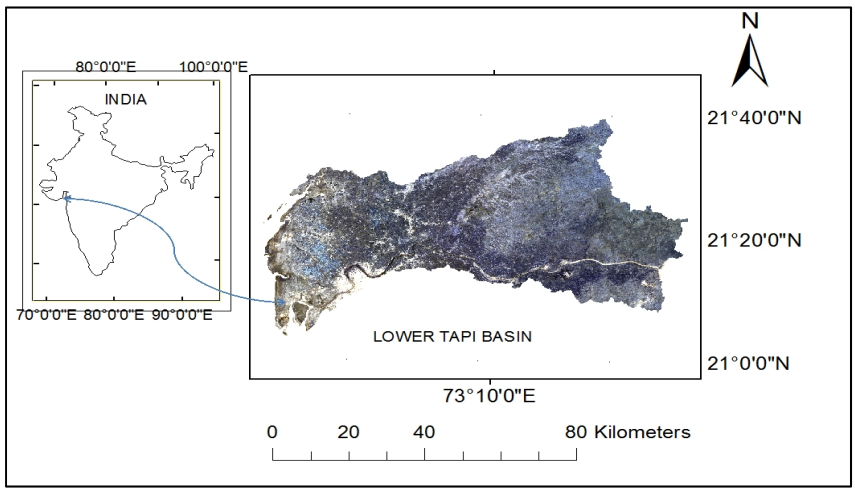

Figure 1. Study area of Lower Tapi Basin

3 METHODOLOGY

3.1 Green-Ampt Model

The Green-Ampt model is a conceptual model to calculate rainfall loss in permeable surfaces in a specific period, Majidi (2012), Saleh (2012). Initial content (it is a volumetric moisture content at the time of simulation), saturated content (it is the maximum moisture content that soil can hold), suction head (mm), hydraulic conductivity (mm/hr) and imperviousness (%) are the parameters of the Green-Ampt model. All these parameters depend on the type of soil present in the catchment. For known soil type suction head, conductivity can be taken from the Green-Ampt parameter table given by Chow (1988). Saturated content can be known based on the type of the soil. Initial content can be set based on the type of soil and time gap from the previous rainfall event. Percentage of impervious surface for each sub-basin determined using topography maps in ArcGIS by supervised classification.

3.2 Snyder method

The Snyder's method is a synthetic unit hydrograph. Snyder considered the shape and area of the basin. After analyzing a large number of hydrographs from drainage basins of areas from 25 to 25000 km^2 it gave the following empirical equations. The hydrograph characteristics are the peak direct runoff rate (qp), the basin lag time (t_l) and the effective rainfall duration (tr), From these characteristics, five characteristics of a required unit

Hydrograph for a given effective rainfall duration may be calculated the peak discharge per unit of watershed area (*qp'*), the base time(t_b), the basin lagn (t_l), and the widths, *W* (in time units) of the unit hydrograph at 50 and 75% of the peak discharge.

Lag time or basin lag: The lag time was defined as the time from the center of mass of effective rainfall to the peak rate of flow. The basin lag is given by:

$$t_l = C_t(LL_c)^{0.3} \quad [1]$$

where t_l = the basin lag (hours), C_t = a coefficient which depends upon the characteristics of the basin, L = length of the main stream of the catchment (km), L_c = distance from the basin outlet to a point on the stream which is nearest to the centroid of the area of the basin (km).

Rainfall Duration: The duration of rainfall excess for Snyder's synthetic unit- hydrograph development is a function of lag time. The unit duration of the storm was given as follows (Arora, 2004):

$$t_r = \frac{t_l}{5.5} \quad [2]$$

where, tr = the unit duration of the storm (hours), tl= the basin lag (hours).

Peak discharge: Peak discharge is the highest volume of runoff over the basin. It is a function of the hydrographic time relation parameters. The determination and knowledge of peak discharge are very essential in hydraulic designs and flood characteristics in basins (Ifabiyi, 2004):

$$Qp = \frac{2.78CpA}{t_l} \quad [3]$$

The peak discharge per unit area is given by the equation below (Arora, 2004):

$$qp' = \frac{Qp}{A} = \frac{2.78Cp}{t_l} \quad [4]$$

where: Qp =the peak discharge (m3/s), Cp = the coefficient which depends upon the retention And storage characteristics of the basin (Values of Cp vary from 0.3 to 0.93). A = area of the Basin (km^2); t_l = the basin lag (hours).
Time base or base period: The time base of a hydrograph is the time from which the Concentration curve (rising portion of a hydrograph) begins until the direct runoff component reaches zero. The base period (T) of the unit hydrograph is given by:

$$T = 3 + \frac{3t_l}{24} \quad [5]$$

where: T = the base period (days), t_l= the basin lag (hours).
Hydrograph time widths of 50 and 75% of peak flow: As a general rule of thumb, the time Width at W50 and W75 ordinates should be proportioned to each side of the peak in a ratio of 1:2with the short time side on the left of the synthetic unit- hydrograph. U.S. Army Corps of Engineers gave the following expressions for W50 and W75 (Arora, 2004):

$$W50 = \frac{5.9}{qp'^{1.08}} \quad [6]$$

$$W75 = \frac{3.4}{qp'^{1.08}} \quad [7]$$

4 MONTE CARLO UNCERTAINTY METHOD

Monte Carlo method in context to the uncertainty analysis of rainfall-runoff model involves generating uniform random parameter(s) values from the known upper and lower limit of the parameter. After generating the uniform random numbers of the parameters, a possible combination of all parameters is formed. Each parameter set is fed into the rainfall-runoff model and model efficiency is calculated. Model efficiency can be calculated by using the index of agreement, Nash & Sutcliffe formula, The explanation for model efficiencies and comparison were reported (Krause 2005). Model efficiency, in this case, is known as the objective function which maximize in case of Nash-Sutcliffe.

5 RAINFALL-RUNOFF MODELLING

Main objective of this study is to simulate event based rainfall runoff process. For the present study five events are considered between 2011-2014. Model is calibrated for the first three events independently and validated for rest of the two events. Parameters thus obtained are subjected to uncertainty analysis using monte-carlo method. Parameter values for different soil can be found in (Chow et. al, 1964; 1988), Model parameters are given in table 1.

In the rainfall runoff modeling Thiessen polygon method is applied for the different rain gauges to get proper rainfall influence area using ARCGIS. Lag-time for the respective polygons is computed from the discharge gauging stations.

Runoff from the all the Thiessen polygons will be accumulated or measured at the Causeway which is the last discharge gauging station to the lower Tapi River. There is a release form the Ukai dam, which is at the upstream of the catchment, release data are added to the total runoff data accumulated from the catchment.

Table 1. Model parameters (Chow et al., 1964; 1988).

Soil Type	Parameter (units)	Ranges
Black Cotton	Initial content (Wi) (volume ratio)	0.10-0.25
	Saturated content (Sr) (volume ratio)	0.3-0.5
	Suction head (ψ) (mm)	110-270
	Conductivity (k) (mm/hr)	0.1-11
	Impervious (i) (%)	5-20
	Lag Time (Lg) Hours	4-10

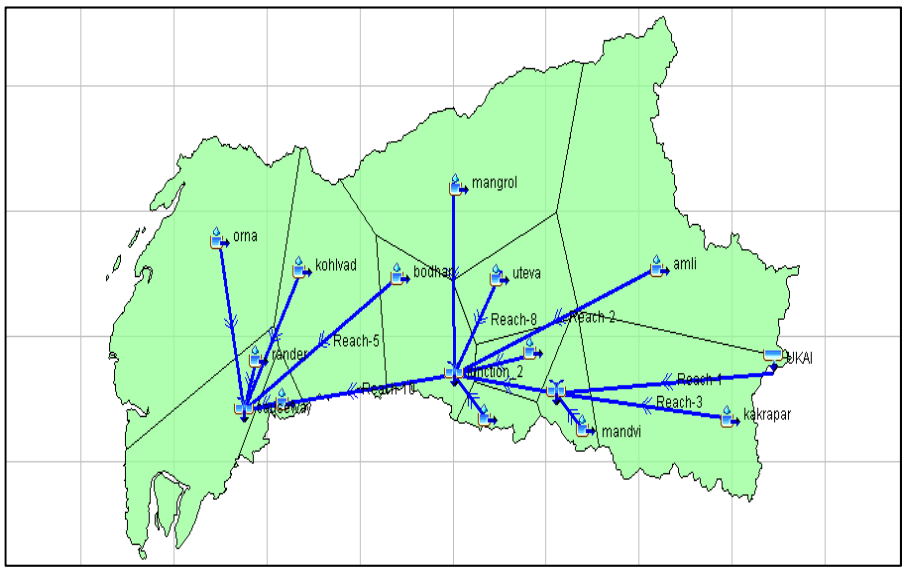

Figure 2. Lower Tapi river showing Thiessen Polygons and the location of different rain gauges and discharge stations.

6 RESULTS AND DISCUSSIONS

6.1 Rainfall Runoff Modeling

In the present study, the Model is separately run by Green Ampt method and Snyder's method. The results are shown in the following table 2. Form the below figure it can be seen that Green-Ampt model performed better than the Snyder method. Hence for the present study Green Ampt model is adopted for the estimation of runoff. Table 2 shows the global summary of both the models. Figure 3 and 4 shows the runoff event (1 Aug 2013 to 5 Aug2013) during model development for the parameter given in Table 3.

Table 2. Model efficiency parameters.

Sr No	Parameters	Green Ampt Model	Snyder's Model
1	Peak Discharge	4699.1 M^3/S	4699.1 M^3/S
2	Nash –Sutcliffe	0.811	0.351
3	Mean Abs Error	413.7 M^3/S	632.4 M^3/S
4	RMS Error	478.3 M^3/S	885.5 M^3/S

Table 3. Initial model parameters.

Sr No	Parameters name and unit	Green Ampt Model
1	Initial content (Wi) (volume ratio)	0.2
2	Saturated content (Sr) (volume ratio)	0.35
3	Suction head (ψ) (mm)	250
4	Conductivity (k) (mm/hr)	0.4

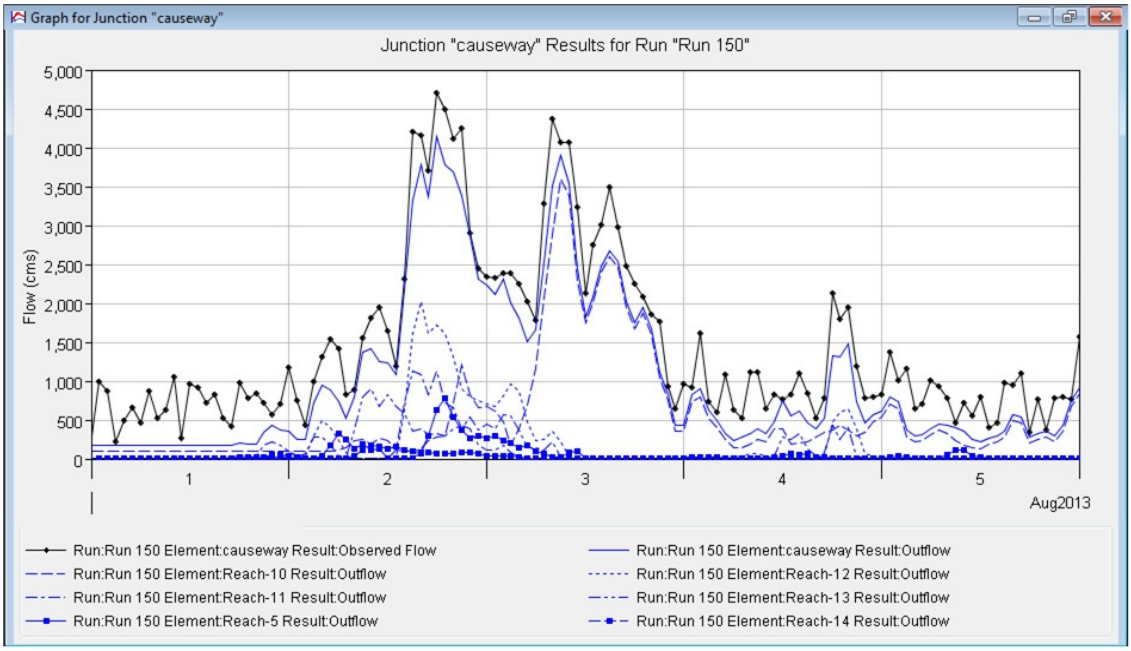

Figure 3. Observed and predicted discharge by Green Ampt Model.

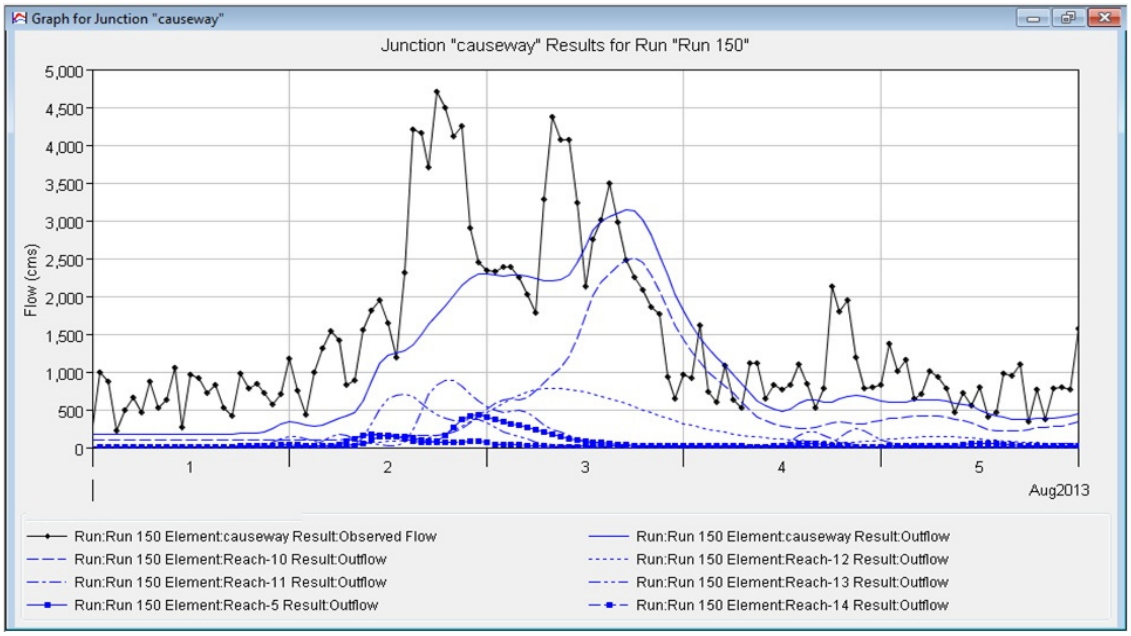

Figure 4. Observed and predicted discharge by Snyder's Model

6.1 Uncertainty analysis

6.1.1 Sampling

Parameters after are distributed uniformly within the given range as shown in Table 1. The reason behind for considering the uniform distribution is that presently what value of parameters is best suitable for the area under consideration is not known. Once the samples are uniformly distributed, the combination of parameters is to be formed with each other. A number of combinations of parameters may go to 15000 or so. Out of all set of combination of parameters, only those set of parameters are retained which gives the better model efficiency. Those retained parameters are known as behavioural parameters and those which are discarded are known as the non-behavioural parameters.

6.1.2 Uncertainty analysis results

As per Monte Carlo Algorithm once the parameter combinations are formed next step is to simulate the rainfall-runoff model for every parameter combination. Total 1500 model simulations and uncertainty analysis

was carried out by developing MatLab code. Out of all simulation representative, 6 model combinations are as shown below in Figure 5.

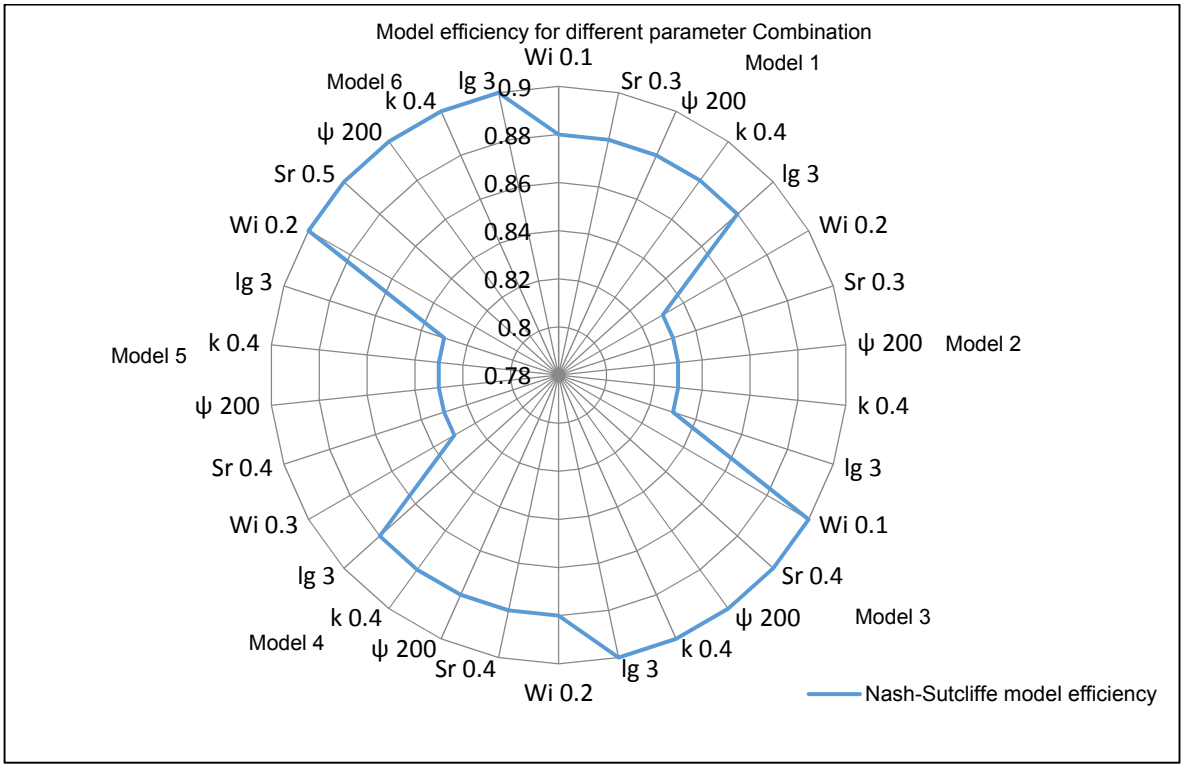

Figure 5. Model simulation results.

Figure 5 shows the Nash–Sutcliffe coefficient for the different parameter combinations. From the above figure it can be seen that there are two sets of the parameter (Model 3 and 6) which gives the very good model efficiency. These model parameters are retained for the model validation. Table 4 shows the optimal parameter range.

Table 4. Optimum Green Ampt parameter range for Lower Tapi River.

Wi	0.1-0.3
Sr	0.3-0.5
ψ	200-250
k	0.4-0.6

6.2 Model validation

Parameters were optimised for the year 2013 on Lower Tapi Basin catchment but it has to be validated for independent data set. It can be seen that model predicts good when the discharge is low, but at the peak discharge model is under-predicting. It may be due to an error in observed data or large change in a geographical feature of the catchment. Its interesting note that only at the two events of rainfall model is under-predicting and at the rest of the event model is predicting satisfactorily hence above justification seems to be true. Validation results are shown in Table 5. Scatter plot between observed and predicted discharge is also shown in Figure 7. Runoff Hydrograph for the year 2013 is as shown in Figure 5

Table 5. Validation Results for the event 1st Aug 2013 to 2nd Aug 2013.

Parameter	Parameter Value	Nash efficiency
Wi	0.2	0.94
Sr	0.3	
ψ	200	
`k	0.4	

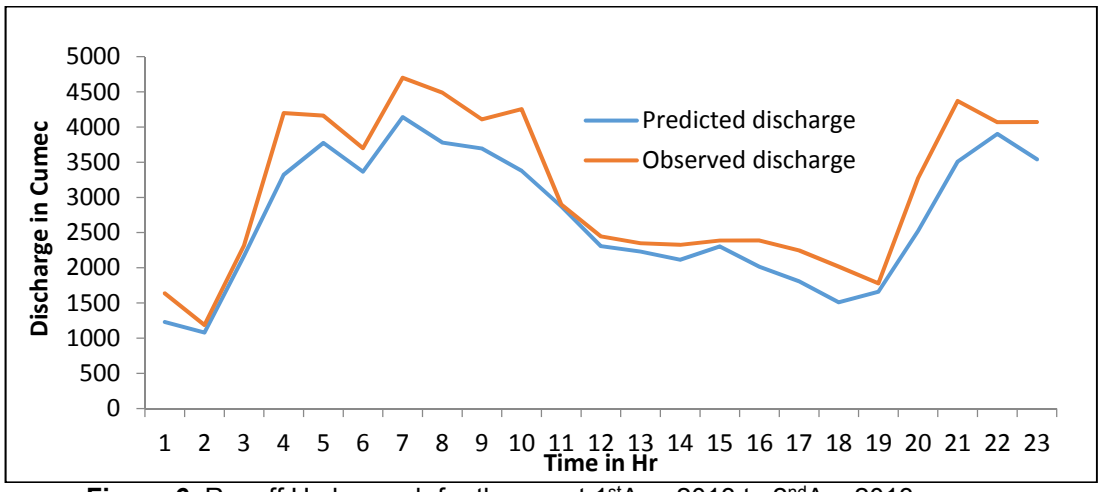

Figure 6. Runoff Hydrograph for the event 1st Aug 2013 to 2nd Aug2013.

7 CONCLUSIONS

Event Based Rainfall Runoff model is being carried out to estimate surface runoff. In the present study widely used Snyder model and Green-Ampt models are compared for the suitability of the model for the present study area. Amongst both the model Green-Ampt model is found to be more suitable. Green Ampt parameters such as initial water content, saturated water content, suction head, conductivity, and lagtime are considered for the uncertainty analysis. It has been observed that HEC-HMS is very less sensitive towards the percentage imperviousness and most sensitive toward the suction head (ψ) and lag time (lg). Total 1500 simulations are performed and best suitable parameters are obtained for the Lower Tapi Basin. Model no. 3 and 6 with the initial water content 0.2, saturated water content 0.3, suction head 200 mm, conductivity 0.4mm/here are most suitable parameters for the Lower Tapi Basin. Model calibrated and validated by taking the independent data set and found Nash efficiency greater than 0.85. Hence HEC-HMS model can be used for the rainfall-runoff model after performing uncertainty analysis.

REFERENCES

Arekhi, S. Rostamizad, G. & Rostami, N. (2011). Evaluation of HEC-HMS Methods in Surface Runoff Simulation (Case Study: Kan Watershed, Iran). *Advances in Environ-mental Biology,* 1316-1321.

Arora, K.R. (2004). Irrigation, Water Power and Water Resources Engineering, Standard Publishers Distributors, Delhi, 96-99.

Beven, K. & Binley, A. (1992). The Future of Distributed Models: Model Calibration and Uncertainty Prediction. *Hydrological processes*, 6(3), 279-298.

Chow, V. (1964). *Handbook of applied hydrology*. McGraw-Hill, New York, NY, USA

Chow, V.T., Maidment, D.R. & Mays, L.W. (1988). *Applied hydrology*.

Elham, R., Noredin, R., Shahram, K.S. & Somaieh, T. (2012). "Calibration of Loss Estimation Methods in HEC-HMS for Simulation of Surface Runoff (Case Study: Amirkabir Dam Watershed, Iran)", *Advances in Environmental Biology*, 6(1), 343-348.

Ifabiyi, I.P. (2004). Agricultural Implication of Subsurface Flow in Parts of the Basement Complex of Northern; Nigeria. *Agrosearch,* 6(1-2), 29-37.

Krause, P., Boyle, D.P. & Bäse, F. (2005). Comparison of Different Efficiency Criteria for Hydrological Model Assessment. *Advances in Geosciences*, 5, 89-97.

Kuczera, G. & Parent, E. (1998). Monte Carlo Assessment of Parameter Uncertainty in Conceptual Catchment Models: The Metropolis Algorithm. *Journal of Hydrology*, 211(1), 69-85.

Majidi, A. & Shahedi, K. (2012). Simulation of Rainfall-Runoff Process using Green-Ampt Method and HEC-HMS model (Case study: Abnama Watershed, Iran). *International Journal of Hydraulic Engineering*, 1(1), 5-9.

Maskey, S., Guinot, V. & Price, R.K. (2004). Treatment of Precipitation Uncertainty in Rainfall-Runoff Modelling: a Fuzzy Set Approach. *Advances in Water Resources*, *27*(9), 889-898.

Pappenberger, F., Harvey, H., Beven, K., Hall, J. & Meadowcroft, I. (2006). Decision Tree for Choosing an Uncertainty Analysis Methodology: a Wiki Experiment http://www. floodrisknet. org. uk/methodshttp://www. floodrisk. net. Hydrological Processes, 20(17), 3793-3798.

Radmanesh, F., PorHemat, J., Behnia, A. & Akhondali, A.M. (2006), Calibration and Assessment of HEC-HMS Model in Roodzard Watershed, *17th international conference of river engineering, university of Shahid Chamran, Ahvaz*. 1-9.

Rostami, N., Sardoii, E.R., Sigaroudi, S.K. & Taheri, S. (2012). Calibration of Loss Estimation Methods in HEC-HMS for Simulation of Surface Runoff (Case Study: Amirkabir Dam Watershed, Iran). *Advances in Environmental Biology,* 343-349.

Sabzevari, T., Ardakanian, R., Shamsaee, A. & Talebi, A. (2009). Estimation of flood hydrograph in no statistical watersheds using HEC-HMS model and GIS (Case study: Kasi-lian watershed), *Journal of Water Engineering*, 4, 1-11.

Sardoii, E.R., Rostami, N., Sigaroudi, S.K. & Taheri, S. (2012). Calibration of Loss Estimation Methods in HEC-HMS for Simulation of Surface Runoff (Case Study: Amirkabir Dam Watershed, Iran). *Advances in Environmental Biology*, 343-349.

Shaghaeghi fallah, R., (2001). Simulation of maximum peak discharge in river Tributaries using HEC-HMS model (Case study: Mohammadabad watershed, Golestan province), *Thesis of M.Sc*. Natural Resources Faculty, University of Gorgan*. International Journal of Modelling and Simulation*, 31(4), 279-286.

Shamsudin, S., Dan'azumi, S. & Ab Rahman, A. (2011). Uncertainty Analysis of HEC-HMS Model Parameters Using Monte Carlo Simulation.

Shrestha, D.L., Kayastha, N. & Solomatine, D.P. (2009). A Novel Approach to Parameter Uncertainty Analysis of Hydrological Models Using Neural Networks*. Hydrology and Earth System Sciences,* 13(7), 1235-1248.

Yener, M.K., Şorman, A.A. & Gezgin, T. (2013). Modeling Studies with Hec-Hms and Runoff Scenarios. *International Congress On River Basin Management,* 621-634.

Yusop, Z., Chan, C.H. & Katimon, A. (2007). Runoff Characteristics and Application of HEC-HMS for Modelling Stormflow Hydrograph in an Oil Palm Catchment. *Water Science and Technology*, 56(8), 41-48.

Proceedings of the 37th IAHR World Congress
August 13 – 18, 2017, Kuala Lumpur, Malaysia

SIMULATION OF STREAMFLOW IN LOWER MAHI BASIN USING ARCSWAT

G. K. JIDHI [(1)], PRAVEEN RATHOD[(2)] & VIVEK L.MANEKAR[(3)]

[(1,2)] S.V. National Institute of Technology, Surat, India,
praeenrathodsh03@gmail.com
[(3)] Civil Engineering Department, S.V. National Institute of Technology, Surat, India,
e-mail- vlm@ced.svnit.ac.in

ABSTRACT

The hydrological modelling can be done in a better way through semi-distributed approach. The objective of this study is to simulate streamflow for lower Mahi basin, Gujarat, India using a semi distributed SWAT model. Geospatial techniques are essential tools in hydrological modelling. Geographic Information System (GIS) and Remote Sensing (RS) are used for the preparation of spatially varied input thematic layer (e.g.: land use map, soil map, slope map etc.). The developed streamflow model was calibrated and validated using semi - automated SUFI 2 calibration technique in SWAT-CUP program. Coefficient of determination (R^2) and Nash Sutcliffe efficiency (NSE) were used as model performance indicators for the calibration and validation of the developed streamflow model. The results of the model performance indicators show good performance of the developed model. It can be concluded that SWAT model performs well for the simulation of streamflow.

Keywords: Streamflow; semi distributed model; ArcSWAT; GIS; uncertainty.

1 INTRODUCTION

Hydrologic models are simplified representations of a hydrologic cycle used for the prediction and understanding of hydrologic processes. The basic concept of the hydrological cycle is the movement of water through it and in which a major measurable portion is streamflow. The proper management of watershed is only possible through the evaluation of streamflow and other hydrologic processes. Hydrologic models are broadly classified into three categories viz. empirical models, conceptual models, and process-based models. In recent decades, several hydrologic models have been developed for simulating streamflow and understanding the spatial and temporal complexities of the watershed catchment response. These models vary considerably in their objectives, time and spatial scales involved. Some of the models are Soil Water Assessment Tool (SWAT), Annualized Agricultural Non-Point Source model (AGNPS), Areal Non-point Source Watershed Environment Response Simulation (ANSWERS), Hydrological Simulation Program–Fortran Model (HSPF), ArcView-based Generalized Watershed Loading Function model (GWLF), Water Erosion Prediction Project (WEPP), etc. Among these models, the freely available geographic information system (GIS)-based ArcSWAT watershed model is well supported by the model developers, and is recognized by many regulating authorities such as the EPA (US Environmental Protection Agency). The application of the SWAT model has increased significantly across the world in the last 5 years but limited studies on the application of SWAT have been reported from India (Gassman et al., 2007).

Generation of input data in conventional models are proven to be too costly, time consuming and having limitations on its data generation. Hydrologic models have increasingly been attributed to the fast growth of both geographic Information Systems (GISs) and computer technology. With the advent of remote sensing technology, deriving the spatial information on input parameters has become more handy and cost-effective. Multi-temporal satellite images provide valuable information related to seasonal land use dynamics, erosional features, rainfall interception by vegetation, and vegetation cover factor. GIS technologies are valuable tools in developing environmental models through their advance features of data storage, management, analysis, and display. The Remote Sensing (RS) technology has been used to provide the land use/cover information by using digital image processing techniques. Accuracy and reliability of input data generated by using geospatial technologies have been increased to great extend with extended computational capabilities.

In the present study, a SWAT model was developed for the study area as lower Mahi basin, Gujarat, India, which spreads over an area of 2901.187 km^2, to simulate the stream flow in Mahi River. Generally, SWAT needs a GIS interface to work and they are jointly known as ArcSWAT. In this study, latest version of SWAT 2012 was interfaced with ArcMap 10.1.

2 OVERVIEW OF SWAT MODEL

Soil and Water Assessment Tool commonly known as SWAT, developed by the United States Department of Agriculture's Agricultural Research Station. SWAT is a semi-distributed, time continuous watershed simulator operating on a daily time step (Arnold et al., 1998). It is developed for assessing the

impact of management and climate on water supplies, sediment, and agricultural chemical yields in watersheds and larger river basins. The model is physically based, and allows simulation of a high level of spatial detail by dividing the watershed into a large number of sub-watersheds (Abbaspour et al., 2007). In SWAT, a watershed is divided into multiple sub watersheds, which are then further subdivided into hydrologic response units (HRUs) that consist of homogeneous land use, management, topographical, and soil characteristics (Arnold et al., 2012). The HRUs are represented as percentage of area covered by the sub watershed and may not be continuous or spatially identified within a SWAT simulation. The driving force behind all the processes in SWAT is water balance and it is represented in equation form as (Neitsch et al., 2009):

$$SW_t = SW_o + \sum_{i=1}^{t}(R_{day} - Q_{surf} - E_a - w_{seep} - Q_{gw}) \quad [1]$$

where SW_t is the final soil water content (mm H_2O), SW_o is the initial soil water content on day i, t is the time (days), R_{day} (mm H_2O) is the amount of precipitation on day i, Q_{surf} (mm H_2O) is the amount of surface runoff on day i, E_a (mm H_2O) is the amount of evapotranspiration on day i, w_{seep} (mm H_2O) is the amount of water entering the vadose zone from the soil profile on day i, and Q_{gw} (mm H_2O) is the amount of return flow on day i. The different inputs and processes involved in this phase of the hydrologic cycle are summarized in the following sections.

SWAT processes can be mainly divided into land phase of the hydrologic cycle and routing phase of hydrologic cycle. The major components of SWAT model are climate, hydrology, plant growth, erosion, flood routing and sediment routing. The main advantage of SWAT is that it has the flexibility to choose from various alternative models available for each component of the hydrological cycle (Arnold et al., 2012). For the simulation of surface runoff, SCS curve number procedure (SCS, 1972) or the Green & Ampt infiltration method (1911) can be used. Generally, SCS-CN method is used since subdaily precipitation data is required for Green & Ampt infiltration method. For the Potential Evapotranspiration (PET), three methods have been incorporated into SWAT; which are the Penman-Monteith method (Monteith, 1965), the Priestley-Taylor method (Priestley and Taylor, 1972) and the Hargreaves method (Hargreaves et al., 1985), among which Penman-Monteith method is the accurate one. For the estimation of sediment yield for each HRU, Modified Universal Soil Loss Equation (MUSLE) (Williams, 1975) is used. Flood routing can be done using a variable storage coefficient method developed by Williams (1969) or the Muskingum routing method. For sediment routing in channel, simplified stream power equation of Bagnold's (1977) equation is used.

3 STUDY AREA

Study area is a part of Mahi river basin, which is one of the major West-flowing rivers running into the Gulf of Cambay. The catchment is situated in the lower Mahi basin exactly, which starts from below the Wanakbori weir and extends up to the mouth of the river, having a catchment area of 2,901.187 km^2. The area is located between 73° 00' E to 73° 50' E longitude and 22° 16' N to 23° 00' N latitude as shown in the figure 1. It is the lowest portion of a large river basin; hence the area is a flat, fertile and well developed alluvial land. Major portion of the study area is occupied with agricultural land for about 48.91% of the total area, 28.28% of area is covered by pasture land, 10.18% is covered by forest land, water bodies spreads over 0.95% and 0.71% of the area is covered by urban land. In this particular study area, seven small tributaries merges to the Mahi River. They are Kun, Mahia, Mesari, Kuvach, Goma, Kharod and Meni. The catchment area comes under tropical wet climatic region. Types of soil which are seen in the catchment are orthic acrisols, eutric cambisols, calcaric fluvisols and chromic vertisols. The mean annual rainfall in the catchment is 1090.343mm. 57% of the total catchment area comes under the elevation zone of 2-6% of slope.

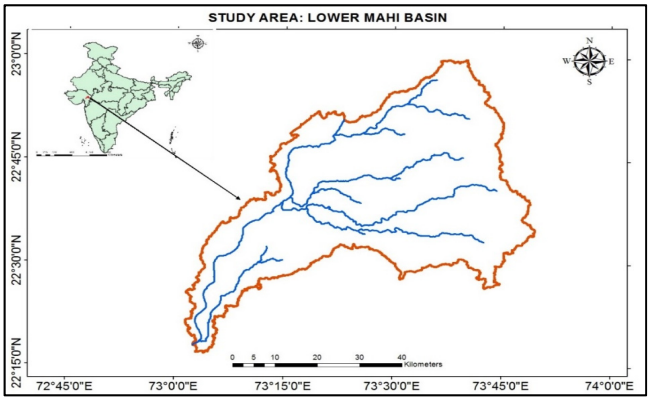

Figure 1. Study area with watershed boundary and stream network.

4 PREPARATION OF MODEL INPUT

As far as SWAT model is concerned, like any other physically based hydrological model, SWAT also requires large amount of data. Preparation of data to be fed to SWAT itself is an important and time consuming step. It essentially requires input of hydrological data, meteorological data, digital elevation model (DEM), land use/land cover (LULC) map and soil map.

Daily meteorological data (rain fall, minimum and maximum temperature, relative humidity and solar radiation) were collected from State Water Data Centre (SWDC), Gandhinagar, Gujarat for a period of 2003-2008. The catchment comprised of 12 rain gauge stations and 3 climatic stations. Few data points were missing from some gauging stations. Thus, missing data analysis was performed by using Inverse Weightage Distance Method (IWD). SWAT needs metrological data inputs in a particular format and for making input files in this format, 'SWAT Weather Database' tool was used. It is a user-friendly tool, used to store daily weather information, to create .txt files (used as input information during an ArcSWAT project setup) easily and to calculate the WGEN statistics of several weather stations efficiently.

The study area starts from below the Wanakbori weir and extends up to the mouth of the river. Hence, discharge from the Wanakbori weir was used as an inlet to the catchment in SWAT model. Stream flow was gauged at the station point Khanpur in the catchment. The daily discharge data from Khanpur station and daily gauge data from Wanakbori weir were collected from Central Water Commission (CWC), Gandhinagar for a period of 2003 to 2008.

SRTM 1 arc second (30m) Digital elevation model (DEM) were downloaded from USGS Earth Explorer website and preprocessed in ArcMap 10.1. To produce the land use/ land cover map, satellite images of Resourcesat-1, using LISS-III sensor with spatial resolution of 23.5 m were downloaded from Bhuvan-NRSC (National Remote Sensing Centre). The downloaded 19 toposheets were analyzed in ArcMap 10.1 using image classification tool and the study was divided in to 7 land use classes as shown in figure 2. Soil map used in this study was produced by Food and Agriculture Organization (FAO) and the required portion was clipped and pre-processed in ArcMap 10.1.

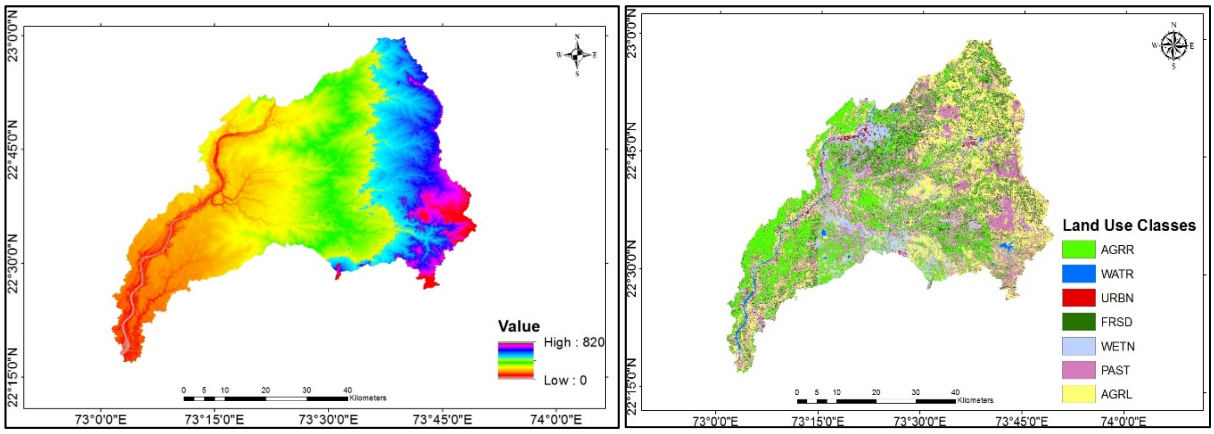

(a) (b)

Figure 2. (a) DEM and (b) Land use map for the catchment.

5 METHODOLOGY

A new ArcSWAT project was setup in the ArcSWAT interface. SWAT possess an automatic watershed delineation menu for the delineation of the catchment. Preprocessed DEM was the primary input to the SWAT model. Stream definition was done using DEM-based approach controlled by threshold area (59.94 km^2). Apart from the outlet generated by stream definition tool, two outlet points were added. One was at the Khanpur station, CWC gauging station and another was at the mouth of the river to delineate the whole catchment. Accordingly, discharge from the Wanakbori weir was entered as inlet to the catchment which contributed from the upper part of the basin. Hydrologically connected subbasins were formed using delineation tool and subbasin parameter were calculated. Land use map and soil map were inputted into the HRU analysis menu and slope map was generated by using the DEM. 259, HRUs were generated for the catchment.

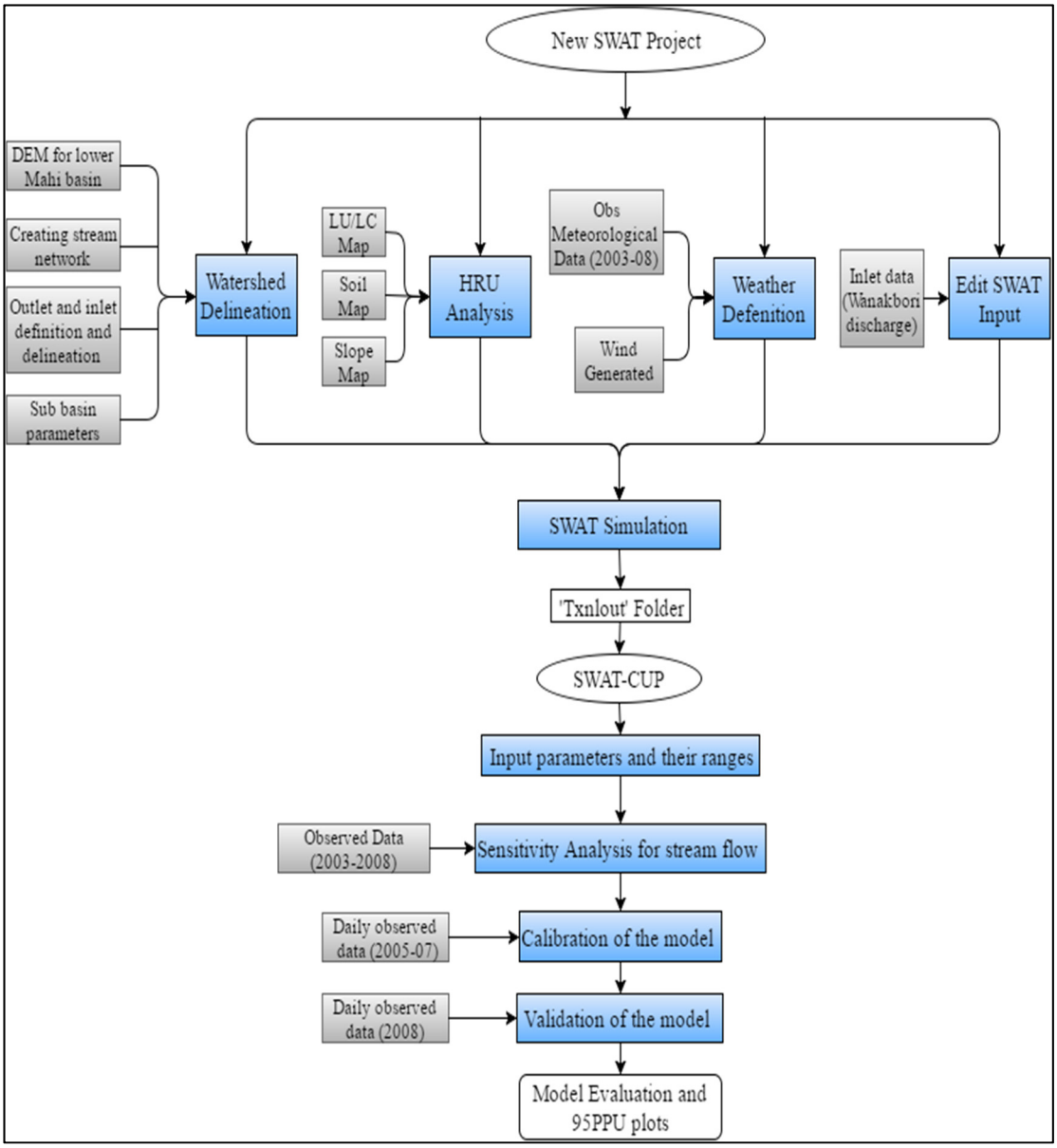

Figure 3. Algorithm of SWAT model.

Observed daily weather data, such as rainfall (mm), relative humidity (fractional), maximum temperature and minimum temperature (℃) and solar radiation (W/m^2) data for 6-year period (2003 to 2008) were processed using SWAT Weather Database tool and inputted in to weather station menu. Generated wind data by weather generator option was used and the required input tables for the simulation of SWAT was created. Inlet discharge data at Wanakbori was given in edit SWAT input menu.

SWAT simulation is the process of predicting all variables associated with a hydrological model for a given period of time. Since hydrological model needs a warmup period to produce accurate result, the starting period of 2 years were given as NYSKIP. For the evaluation of streamflow daily simulations were used. A preliminary results analysis was done using 'output.std' flies and the SWAT Checker program. Sensitivity analysis, calibration and validation of SWAT model was done in SWAT CUP interface using SUFI 2 optimization technique.

6 RESULTS AND DISCUSSIONS

A SWAT model was set up for the lower Mahi basin to predict the streamflow for the monsoon period of 2005 to 2008. As far as a semi-distributed hydrological model is concerned, sensitivity analysis, uncertainty analysis, calibration and validations are important tools to authenticate the model. For this, a SWAT-CUP interface was used with the assistance of the tool, SUFI (Sequential Uncertainty Fitting) version 2. Sensitivity analysis is the process of determining the rate of change in model output with respect to changes in model inputs, i.e. parameters (Arnold et al., 2012). Determination of the most sensitive parameters for the study area is the first step for the calibration and validation process in SWAT. Absolute sensitivity analysis was done by changing the parameter values one at a time while keeping other parameters constant using Latin Hypercube

(LH) sampling. Parameterization can be done based on the information of hydrological processes and the spatial distribution of soil, land use and slope classes. It could be defined as "the process of imparting the analyst's knowledge of the physical processes of the watershed to the model" (Arnold et al., 2012).

17 parameters which may affect the flow were loaded to the SUFI interface and 11 parameters were found to be sensitive. The five most sensitive parameters are curve number (CN2), Manning's n value for the main channel (CH_N2), bulk density (SOL_BD), deep aquifer percolation factor (RCHRG_DP) and Manning's n value for overland flow (OV_N). The 11 parameters which are sensitive to the streamflow and their parameter ranges are given in Table 1.

Table 1. List of parameters used in the SWAT model.

Sl No	Parameters	Lower Limit	Upper Limit
1	SCS Curve number for moisture condition II (CN2)	38.5	97.9
2	Manning's 'n' value for overland flow (OV_N)	0.025	0.45
3	Manning's 'n' value for main channel (CH_N2)	0.01	0.3
4	Base flow alpha Factor (1/days) (ALPHA_BF)	0.1	1
5	Effective hydraulic conductivity in main channel alluvium in mm/hr (CH_K2)	0	2.5
6	Ground water delay time in days (GW_DELAY)	0	60
7	Threshold depth of water in the shallow aquifer required for return flow to occur in mm H_2O (GWQMN)	2000	4500
8	Available water capacity of soil layer in mm H_2O (SOL_AWC)	0.21	1.05
9	Saturated hydraulic conductivity in mm/hr (SOL_K)	0.65	38
10	Deep aquifer percolation factor (RCHRG_DP)	0	0.5
11	Moist bulk density in Mg/m^3 (SOL_BD)	0.96	2.38

In SWAT-CUP, 95 PPU represents the prediction uncertainty in the model. Based on this, SUFI2 have two statistics. The percent of measured data enveloped by 95PPU band is termed as P-factor, where the thickness of 95PPU envelope is the R-factor. Sensitivity analysis in SUFI2 aims to find reasonable value to the mentioned factors. For discharge, P-factor of >70% and R-factor <1 are required (Abbaspour et al., 2004).
The model performance was evaluated using different statistical techniques. The most widely used two statistics reported in SWAT studies for calibration and validation are R^2 (Coefficient of determination) and NSE (Nash-Sutcliffe efficiency). Coefficient of determination shows a measure of how well observed outcomes are replicated by the model outputs whereas Nash-Sutcliffe efficiency is the predictive power of a hydrological model. The value of R^2 ranges from 0 to 1, where 1 represents a perfect model. While the value of NSE ranges from -∞ to 1. A model is considered to be good performing if NSE>0.5 and excellent performing model when NSE>0.75. R^2 and NSE were calculated by using following equation where Q is a variable, and m and s represent for measured and simulated, respectively, and the bar represent for average value.

$$R^2 = \frac{\left[\sum_i (Q_{m,i} - \overline{Q_m})(Q_{s,i} - \overline{Q_s})\right]^2}{\sum_i (Q_{m,i} - \overline{Q_m})^2 \sum_i (Q_{s,i} - \overline{Q_s})^2} \quad [2]$$

$$E = 1 - \frac{\sum_{i=1}^{n} (Q_m - Q_s)_i^2}{\sum_{i=1}^{n} (Q_{m,i} - \overline{Q_m})^2} \quad [3]$$

Calibration is a process of improved parameterization of model for the study area conditions to get a lower prediction uncertainty (Arnold et al., 2012). In validation process, model is run for the parameters and their ranges that are obtained from the calibration and predictions are compared with observed data which is not used in the calibration. Calibration and validation process were carried out with the monsoon period data. For the calibration and validation of the streamflow variable, 3 (2005-2007) years were chosen for the calibration and one year for validation (2008). Results from calibration and validation of the model for streamflow are given in table 2. Figure 4 shows the calibration of stream flow. From the Figure 4, it can be seen that almost all the events are simulated very accurately. Figure 5 shows the validation of stream flow from the independent data set for the year 2008.

Table 2. SWAT model performance evaluation.

Sl No	Model Performance Evaluation	Calibration 2005-2007	Validation 2008
1	P factor	0.60	0.80
2	R factor	0.07	0.47
3	NSE	0.75	0.86
4	R^2	0.83	0.86

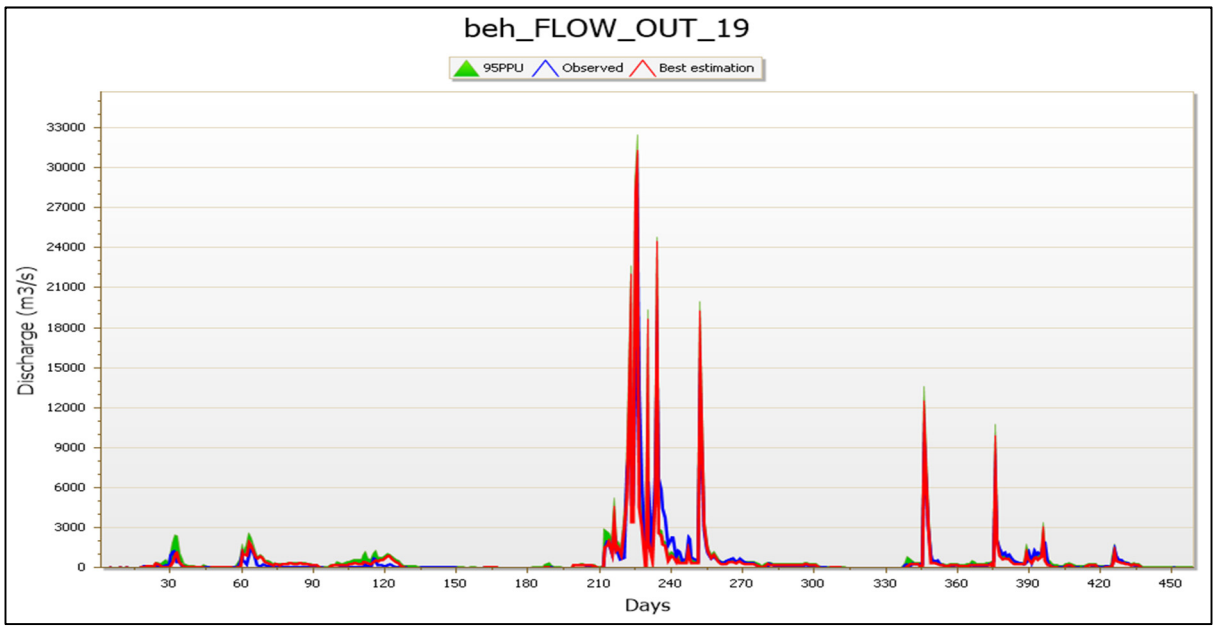

Figure 4. 95PPU plot for streamflow calibration.

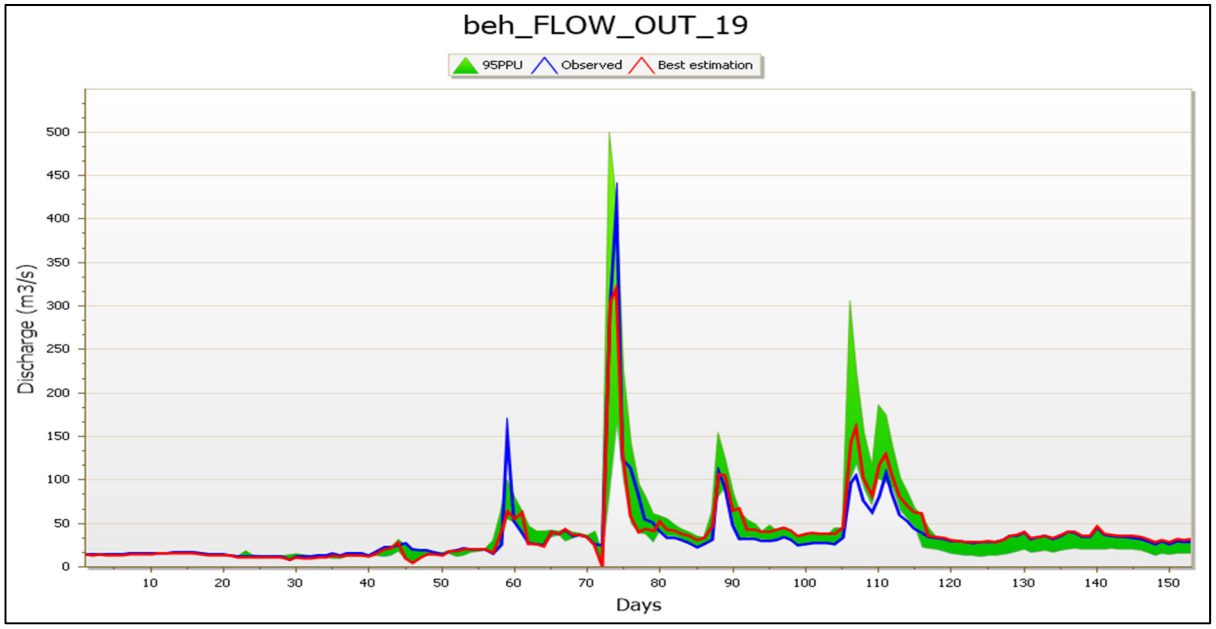

Figure 5. 95PPU plot for streamflow validation.

7 CONCLUSIONS

SWAT is a physically semi-distributed model, it requires large amount of data and it have the capability to account almost all physical process. Simulation of streamflow for lower Mahi basin was done by using SWAT model. SWAT model was executed in the ArcSWAT interface in the GIS environment and input thematic layers were prepared by using the ArcMap 10.1 version. Digital Elevation Model (DEM) was used as a primary input in SWAT and its resolution directly affects the model efficiency. From sensitivity analysis, it was found that 11 are sensitive to streamflow and the five most sensitive parameters are CN2, CH_N2, SOL_BD, RCHRG_DP and OV_N. These parameters are associated with surface runoff, Manning's resistance coefficient, soil characteristics and ground water component. Hence, streamflow is mainly affected by the mentioned processes. From the calibration and validation of the model, it can be concluded that SWAT model produces good results for the simulation of streamflow.

ACKNOWLEDGEMENTS

The authors are very thankful to Central Water Commission (CWC), Gandhinagar and State Water Data Centre (SWDC), Gandhinagar, Gujarat for providing the required data and adequate information for the study.

REFERENCES

Abbaspour, K.C., Johnson, C.A. & Van Genuchten, M.T. (2004). Estimating Uncertain Flow and Transport Parameters Using a Sequential Uncertainty Fitting Procedure. *Vadose Zone Journal*, 3(4), 1340-1352.

Abbaspour, K.C., Yang, J., Maximov, I., Siber, R., Bogner, K., Mieleitner, J. & Srinivasan, R. (2007). Modelling Hydrology and Water Quality in the Pre-Alpine/Alpine Thur watershed using SWAT. *Journal of hydrology*, 333(2), 413-430.

Arnold, J.G., Moriasi, D.N., Gassman, P.W., Abbaspour, K.C., White, M.J., Srinivasan, R. & Kannan, N. (2012). SWAT: Model use, Calibration, and Validation. *Transactions of the ASABE*, 55(4), 1491-1508.

Arnold, J.G., Srinivasan, R., Muttiah, R.S. & Williams, J.R. (1998). Large Area Hydrologic Modeling and Assessment Part I: Model development1.

Behera, S. & Panda, R.K. (2006). Evaluation of Management Alternatives for an Agricultural Watershed in a Sub-Humid Subtropical Region using a Physical Process based Model. *Agriculture, ecosystems & environment*, 113(1), 62-72.

Benaman, J., Shoemaker, C.A. & Haith, D.A. (2005). Calibration and Validation of Soil and Water Assessment Tool on an Agricultural Watershed in Upstate New York. *Journal of Hydrologic Engineering*, 10(5), 363-374.

Di Luzio, M., Arnold, J.G. & Srinivasan, R. (2005). Effect of GIS Data Quality on Small Watershed Stream Flow and Sediment Simulations. *Hydrological Processes*, 19(3), 629-650.

Kaur, R., Srinivasan, R., Mishra, K., Dutta, D., Prasad, D. & Bansal, G. (2003). Assessment of a SWAT Model for Soil and Water Management in India. *Land Use and Water Resources Research*, 3, 1-7.

Krause, P., Boyle, D.P. & Bäse, F. (2005). Comparison of Different Efficiency Criteria for Hydrological Model Assessment. *Advances in Geosciences*, *5*, 89-97.

Moriasi, D.N., Arnold, J.G., Van Liew, M.W., Bingner, R.L., Harmel, R.D. & Veith, T.L. (2007). Model Evaluation Guidelines for Systematic Quantification of Accuracy in Watershed Simulations. *Trans. Asabe*, 50(3), 885-900.

Prabhanjan, A., Rao, E.P. & Eldho, T.I. (2014). Application of SWAT Model and Geospatial Techniques for Sediment-Yield Modeling in Ungauged Watersheds. *Journal of Hydrologic Engineering*, 20(6), C6014005.

Refsgaard, J.C. (1997). Parameterisation, Calibration and Validation of Distributed Hydrological Models. *Journal of hydrology*, 198(1), 69-97.

Wheater, H.S., Jakeman, A.J. & Beven, K.J. (1993). Progress and Directions in Rainfall-Runoff Modelling.

HYBRID OF ANNS AND CLA FOR PREDICTION OF RAINFALL

REZA MOHAMMADPOUR[1], ZAHRA ASAEI[2] & AMINUDDIN AB GHANI[3]

[1] Department of civil engineering, Estahban Branch, Islamic Azad University, Estahban Iran, reza564@gmail.com
[2] Islamic Azad University, Science and Research Branch-Bushehr, Bushehr, Iran, Zahraasaie@gmail.com
[3] REDAC, Universiti Sains Malaysia, Engineering Campus, Seri Ampangan, 14300 Nibong Tebal, Penang, Malaysia, redac02@usm.my

ABSTRACT

Prediction of rainfall is extremely important for management of water resources. In urban areas, rainfall has a great impact on traffic, sewer systems, and other human activities. In this study, Learning - Cellular Automation (CLA) and artificial neural networks (ANNs) were used for classification of rainy and no-rainy days. For classification of data, a comparison between CAL and ANNs indicated that accuracy of CLA with R^2=0.796 and RMSE=0.407 is better than ANNs (R^2=0.556 and RMSE=0.431). In order to predict daily rainfall, three methods were employed including ANNs with two learning functions of LM and BFGS and hybrid of ANNs-CLA. Although the ANN with learning function of LM predicts the rainfall with high accuracy (R^2=0.839 and RMSE= 0.222), a hybrid of ANNs-CLA provides better results with higher accuracy (R^2 = 0.88 and RMSE= 0.202).

Keywords: Neural network; rainfall; CLA; modelling; urban water.

1 INTRODUCTION

Prediction of rainfall is extremely important for management of water resources. In urban areas, rainfall has a great impact on traffic, sewer systems, and other human activities. However, it is one of the most complex issues in the context of understanding and modeling and has become one of the biggest challenges in water science (Olsson et al., 2004). Notable number of methods have been developed for prediction of rainfall. Due to the temporal and spatial variation of rainfall, prediction of rainfall with high accuracy is difficult and each method has ability to forecast rainfall with different accuracy (Georgakakos, 1984; Partal and Ki, 2007).

In recent decades, the artificial neural networks (ANNs) have been successfully employed in many hydraulic and hydrology studies (Gazzaz et al., 2012; Song et al., 2013; Li et al., 2014; Mohammadpour et al., 2013a; Mohammadpour et al., 2013b; Mohammadpour et al., 2015a; Mohammadpour et al., 2015b). Abhishek et al. (2012) have used different types of neural networks and multiple linear regressions (MLR) to estimate the total rainfall in Sparta. Wu et al. (2015) used a hybrid model of wavelet neural network and particle swarm optimization with mutual information to forecast monthly precipitation. El-Shafie et al. (2011a) employed the ANNs and Multi Linear Regression model (MLR) for prediction of rainfall in Egypt. They have used several statistical parameters for evaluation of the methods. A comparison between results indicated that ANNs provides better performance than MLR model. Geetha and Selvaraj (2011) developed ANNs with back propagation technique to predict mean monthly rainfall in India. The performance of ANNs was acceptable for prediction of independent periods of rainfall.

For prediction of temporal dimension of the rainfall pattern, El-Shafie et al. (2012) used three different neural networks namely; Input Delay Neural Network (IDNN), Multi-Layer Perceptron Neural network (MLP-NN) and Radial Basis Function Neural Network (RBFNN). The IDNN provides better result in comparison with other methods.

Recently, to access a high accuracy, the ANNs have been merged with the other techniques. He et al. (2015) developed a hybrid wavelet neural network and particle swarm optimization to predict monthly rainfall. Partal and Cigizoglu (2009) employed a combination of wavelet and ANN to forecast daily rainfall in Turkey. The results showed that ANN is able to predict the daily rainfall peaks with high accuracy. For short term rainfall prediction, a hybrid of ANNs and genetic algorithm (GA) was developed by Nasseri et al. (2008). Chau and Wu (2010) utilized a combination of singular spectrum analysis (SSA) and ANN-support vector regression (SVR) for daily rainfall prediction. They showed that SSA is successfully able to improve the ANN performance. A hybrid of ANNs and wavelet was developed by Nizar et al. (2011) to forecast monthly rainfall. They have used different geographical region to test the proposed method and found that this technique was capable to predict monthly rainfall with good accuracy.

In the last decades, the learning automata (LA) has been considered as a powerful tool for classification of data and a group of learning automata is able to solve difficult problems. A number of applications for CLA

have been developed in different fields (D'ambrosio et al., 2001; Folino et al., 2006; Feng et al., 2011; Ravazzani et al., 2011). Prasetya et al. (2015) developed cellular learning automata (CLA) to determine the direction of the spread flooding. The ability of CLA was evaluated using two dimensional images. Previous studies indicated that CLA was generally used to classify data and ANN was mostly employed to predict participation. Generally, weather stations provide a dataset including both rainy and dry days. However, combination of CLA and ANNs can be employed as a robust technique to automatically classify and predict daily rainfall for a group of data that include both rainy and dry days.

The aim of this research is to predict rainy days. At first, ability of both ANNs and CLA was evaluated to classify dataset into rainy and no-rainy days. Then, three methods were used to predict daily rainfall including, ANNs with learning function of LM (Levenberg-Marqwardt), ANNs with learning function of BFGS (Broyden, Fletcher, Goldfarb, Shanno) and hybrid of CLA-ANN. Finally, accuracy of CLA-ANN was compared with other methods.

2 MATERIALS AND METHODS

In this study, the data were collected from Shiraz synoptic stations. Shiraz is capital city of Fars province with over 56 years of rainfall data. The data used in this study included daily minimum temperature (Tmin), the maximum temperature (Tmax), average temperature (Tmean), minimum humidity (Hmin), the maximum humidity (Hmax), maximum wind speed (Wmax), average wind speed (Wavg), minmum pressure (Pmin), mean pressure (Pmean) and daily rainfall. In this study, 2249 datasets were collected to predict rainfall and ranges of collected parameters are shown in Table 1.

Table 1. Range of collected data.

Parameter	minimum	maximum	Standard deviation
Tmin (centigrade)	-9	26	8.5
Tmax (centigrade)	1	41	21
Tmean (centigrade)	-3	33.5	15.25
Hmin (%)	0	97	48.5
Hmax (%)	0	100	50
Wmax (m/s)	0	29	14.5
Wavg (m/s)	0	13.2	6.6
Pmin (milli-bar)	839	861	849.55
Pmean (milli-bar)	995	1029	1011.6
Daily Rainfall (mm)	0	99	49.55

3 ARTIFICIAL NEURAL NETWORKS

Artificial Neural Networks (ANNs) are a computational process that attempts to represent and compute a mapping from multivariate data sets as inputs to another as outputs. A neuron is the smallest part of the neural network. To approximate a multi-variant function of f(x), the ANN is developed in three layers which are inputs, hidden and output layers. The numbers of neurons in input and output layers are the number of input and output variables, respectively, while the number of neurons in hidden layer is normally determined by trial and error. In learning process, an algorithm tries to find the best weight for approximation function of f(x). The Feed Forward Back Propagation (FFBP) algorithm is recommended as a useful method in hydraulic and hydrology problems. This technique is a descent algorithm which tries to minimize the error in different epochs. The weights of network change by the method such that the error decreases along a descent direction. In the descent direction method, two parameters, namely learning rate (LR) and momentum factor (MF) set the weight of network. Architecture of three-layer neural network is shown in Figure 1.

In this study, the collected data were normalized using following equation:

$$X_n = \frac{0.9(X - X_{\min})}{(X_{\max} - X_{\min})} + 0.1 \qquad [1]$$

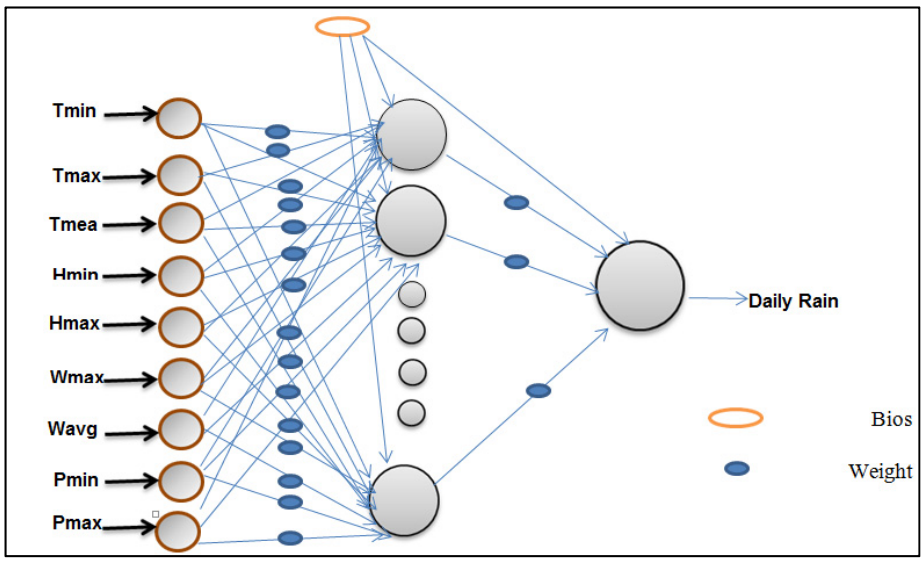

Figure 1. Structure of a three-layer neural network.

Furthermore, three statistical parameters, coefficient of determination (R^2), mean absolute error (MAE) and root mean square error (RMSE), were chosen to evaluate the accuracy of neural network and hybrid neural network - learning automaton (CLA-ANN) as given in the following:

$$R^2 = 1 - \frac{\sum_{i=1}^{p}(O_i - P_i)^2}{\sum_{i=1}^{p}(O_i - \overline{O}_i)^2} \quad [2]$$

$$MAE = \frac{1}{n}\sum_{i=1}^{p}\left|O_i - P_i\right| \quad [3]$$

$$RMSE = \sqrt{\frac{\sum_{i=1}^{p}(O_i - P_i)^2}{n}} \quad [4]$$

where O_i and P_i are observed and simulated values respectively, $\overline{O}$ is the average of observed data and n is the number of samples.

4 CELLULAR AUTOMATON - LEARNING (CLA)

A cellular automaton (CA) is a mathematical model and can be used for computation and systems simulation. It is a discrete model and consists of regular grid of cells. The number of dimension in grid is finite and cells can be one, two or multi-dimensional. In CA, a simple rule is defined for each cell and a set of cells are able to choose neighbourhood. Generally, the rule of cells is fixed and not changed over time. In this method, an initial state is assigned to each cell and a new generation is created based on the state of the cell and its neighbourhood.

Learning automata (LA) is a machine-learning algorithm and able to learn through interaction with its environment. It is designed based on probability distribution and updates its action to improve its own performance over time.

A composition of CA and LA is able to solve the weakness of rule cells. As a result, Cellular Learning Automata (CLA) is recommended as a CA with LA in each cell. The CLA is superior in comparison to CA and LA, because of its ability of learning. However, the LA residing in a particular cell determines its state (action) and the CA operates under its rule. The rule of the CLA and the actions selected by the neighbouring cells determine the reinforcement signal to the LA residing in a cell. The governing equation for CLA with d-dimensional can be expressed as:

$$\text{CLA}=(Z^d, \phi, \text{A}, \text{N}, \text{F}) \quad [5]$$

where Z^d is a lattice of d-tuples of integer number, ϕ is a finite set of states, A is a set of LA assigned to each cell, $N = (\overline{x_1}, \ldots, \overline{x_m})$ is neighborhood vector and it is a finite subset of Z^d, $F: \emptyset^m \rightarrow \beta$ is a rule of the cellular learning automata, where β is the set of values that the reinforcement signal can take.

The CLA is classified into synchronous and asynchronous. In synchronous CLA, all cells are synchronized with a global clock and executed at the same time (Beigy and Meybodi, 2004).

5 RESULTS AND DISCUSSIONS

The total collected data (2249 dataset) were divided randomly into training and testing subsets. Around 80% of the datasets (1806 data sets) were used for training and 20% for testing (443 datasets). To determine the main parameters on rainfall, a sensitivity analysis with thirteen scenarios was performed on collected data. As shown in Table 2, all parameters were used in the first scenario and a parameter has been removed in the next scenarios. The results indicated that the lowest error (MAE=0.0066 and RMSE=0.0811) was obtained from first scenario with nine parameters. Therefore, this scenario was chosen for the next analysis.

Table 2. Sensitivity analysis for different parameters.

order	variables	MAE	RMSE	R^2
1	Tmin, Tmax, Tmean, Hmin, Hmax, Wmax, 'Wavg, Pmin, Pmean	0.0066	0.0811	0.541
2	Tmin, Tmax, Tmean, Hmin, Hmax, Wmax, 'Wavg, Pmin	0.0156	0.125	0.529
3	Tmin, Tmax, Tmean, Hmin, Hmax, Wmax, 'Wavg, Pmean	0.0149	0.122	0.519
4	Tmin, Tmax, Tmean, Hmin, Hmax, Wmax, 'Wavg	0.0173	0.131	0.468
5	Tmin, Tmax, Tmean, Hmin, Hmax, Wmax, Pmean	0.016	0.126	0.517
6	Tmin, Tmax, Tmean, Hmin, Hmax, Wmax, Pmin	0.0163	0.128	0.501
7	Tmin, Tmax, Tmean, Hmin, Hmax, Wmax	0.0191	0.138	0.494
8	Tmin, Tmax, Tmean, Hmin, Hmax, 'Wavg	0.0165	0.128	0.443
9	Tmin, Tmax, Tmean, Hmin, Hmax,	0.0167	0.129	0.375
10	Tmin, Tmax, Tmean, Hmin,	0.017	0.131	0.418
11	Tmin, Tmax, Tmean,	0.0177	0.133	0.292
12	Tmin, Tmax	0.0203	0.142	0.263
13	Tmin	0.0249	0.157	0.0209

5.1 Classification of rainy days using ANN and CLA

In this section, ANNs and CLA were employed for classification of collected datasets into rainy and no-rainy days. Accuracy of these methods was evaluated using statistical parameters. Table 3 shows the CLA (R^2=0.796, MAE=0.166) is able to classify the data with a higher accuracy in comparison with the ANNs (R^2= 0.556 and MAE=0.186). It might be due to the performance of CLA and ANN to present results. In this classification, zero and one were chosen for rainy and no-rainy days, respectively. However, the result of ANNs was zero and one, while the result of CLA was exactly in terms of zero and one. Therefore, classification of CLA is more accurate than ANNs and this method can be used as a robust technique to classify the rainy days.

Table 3. Comparison of CLA and ANN to classify data.

Classification	RMSE	MAE	R^2
ANN	0.431	0.186	0.556
CLA	0.407	0.166	0.796

5.2 Prediction of rainfall

In order to predict daily rainfall, three methods were employed including, ANNs with learning function of LM (Levenberg-Marqwardt), ANNs with learning function of BFGS (Broyden, Fletcher, Goldfarb, Shanno) and hybrid of CLA-ANN. All datasets including rainy and no-rainy days were used for these methods. It should be mentioned that hybrid of CLA-ANN is able to automatically divide datasets into rainy and no-rainy days, while ANNs used all data for prediction of rainfall.

The Feed Forward Back Propagation (FFBP) was developed with two learning functions of LM and BFGS with different number of neurons in hidden layer. As shown in Table 4, the best result was obtained with 9 and 6 neurons in hidden layer for LM and BFGS, respectively. The provided results indicated that performance of LM with R^2=0.839 and RMSE= 0.222 is better than BFGS (R^2=0.698 and RMSE= 0.246). Therefore, for hybrid of ANNs and CLA, the LM was chosen as an activation function.

In next step, to improve accuracy of result, a hybrid of ANNs and CLA was used to prediction of daily rainfall. In this method, high accuracy was obtained for a network with 9 neurons in hidden layer (Table 4).

The results showed that a combination of ANNs and CLA provides better prediction for daily rainfall (with R^2=0.881 and RMSE= 0.202) in comparison with ANNs. As mentioned, in the hybrid of ANN-CLA, the CLA automatically classifies the datasets into rainy and no-rainy days and then, ANNs only used rainy days for prediction of daily rainfall. This procedure increases accuracy of ANNs and provides better prediction.

Table 4. Quality results in the forecast based on ANN and CLA-ANN.

	ANN(BFGS)			*ANN(LM)*			*CLA-ANN(LM)*		
No of Neurons	*RMSE*	*MAE*	R^2	*RMSE*	*MAE*	R^2	RMSE	MAE	R^2
1	0.198	0.039	0.651	0.219	0.048	0.791	0.231	0.054	0.726
2	0.200	0.040	0.654	0.221	0.048	0.783	0.208	0.043	0.798
3	0.220	0.048	0.657	0.234	0.055	0.744	0.211	0.045	0.789
4	0.210	0.044	0.671	0.223	0.051	0.775	0.211	0.045	0.809
5	0.199	0.039	0.678	0.217	0.0472	0.803	0.208	0.0432	0.845
6	**0.246**	**0.060**	**0.698**	0.268	0.0716	0.821	0.207	0.043	0.867
7	0.199	0.039	0.677	0.218	0.0477	0.815	0.209	0.044	0.811
8	0.215	0.046	0.674	0.228	0.052	0.756	0.223	0.049	0.857
9	0.221	0.049	0.681	**0.222**	**0.049**	**0.839**	**0.202**	**0.041**	**0.881**
10	0.211	0.044	0.659	0.232	0.054	0.823	0.216	0.047	0.857

In Table 5, the technique presented in this study is compared with previous study and other methods. The results indicated that the accuracy of ANNs-CLA is higher or comparable with other soft computing models. This technique can be used as a robust tool for prediction of problem related to water science and hydrology problems.

Table 5. A comparison between present and previous research.

Authors	Rainfall prediction technique	Correlation coefficient
Abbot and Marohasy (2014)	ANN	R=0.86
Wu et al. (2015)	RBF	R=0.755
Valverde et al. (2014)	ANN	R=0.719
Babel et al. (2015)	ANN	R=0.61
Sattari et.al. (2014)	MLP artificial neural network	R=0.87
He et al. (2015)	hybrid wavelet and ANN	R=0.47
Present Study	CLA-ANN	R=0.88

6 CONCLUSIONS

Prediction of rainfall is one of the most important parameters in hydrology. In this research, two methods, ANNs and CLA, were employed for classification of rainy and no-rainy days. The results indicated that accuracy of CLA with R^2=0.796 and MAE=0.166 is better than ANNs (R^2=0.566 and MAE=0.186) for classification. In order to predict daily rainfall, three methods were employed including ANNs with learning function of LM, ANNs with learning function of BFGS and hybrid of ANNs-CLA. Although the ANN with learning function of LM predicts the rainfall with high accuracy (R^2=0.839 and RMSE= 0.222), a hybrid of ANNs-CLA provides better results with higher accuracy (R^2 = 0.88 and RMSE= 0.202). The techniques presented in this study can be successfully used as a robust tool for prediction of problem related to water resources, hydrology and hydraulic issues.

ACKNOWLEDGEMENTS

The author would like to thank Estahban Branch, Islamic Azad University, for the financial support.

REFERENCES

Abbot, J. & Marohasy, J. (2014). Input Selection and Optimisation for Monthly Rainfall Forecasting in Queensland, Australia, using Artificial Neural Networks. *Atmospheric Research,* 138, 166-178.

Abhishek, K., Singh, M.P., Ghosh, S. & Anand, A. (2012). Weather Forecasting Model using Artificial Neural Network. *Procedia Technology,* 4, 311-318.

Babel, M.S., Badgujar, G.B. & Shinde, V.R. (2015). Using the Mutual Information Technique to Select Explanatory Variables in Artificial Neural Networks for Rainfall Forecasting. *Meteorological Applications,* 22(3), 610-616.

Beigy, H. & Meybodi, M.R. (2004). A Mathematical Framework For Cellular Learning Automata. *Advances in Complex Systems,* 07(03n04), 295-319.

Chau, K.W. & Wu, C.L. (2010). A Hybrid Model Coupled with Singular Spectrum Analysis for Daily Rainfall Prediction. *Journal of Hydroinformatics,* 12(4), 458-473.

D'ambrosio, D., Di Gregorio, S., Gabriele, S. & Gaudio, R. (2001). A Cellular Automata Model for Soil Erosion by Water. *Physics and Chemistry of the Earth, Part B: Hydrology, Oceans and Atmosphere*, 26(1), 33-39.

El-Shafie, A., Mukhlisin, M., Najah, A.A. & Taha, M.R. (2011). Performance of Artificial Neural Network and Regression Techniques for Rainfall-Runoff Prediction. *International Journal of Physical Sciences*, 6(8), 1997-2003.

El-Shafie, A.H., El-Shafie, A., El Mazoghi, H.G., Shehata, A. & Taha, M.R. (2011). Artificial neural network technique for rainfall forecasting applied to Alexandria, Egypt. *International Journal of Physical Sciences*, *6*(6), 1306-1316.

El-Shafie, A., Noureldin, A., Taha, M., Hussain, A. & Mukhlisin, M. (2012). Dynamic Versus Static Neural Network Model for Rainfall Forecasting at Klang River Basin, Malaysia. Hydrol. *Earth Syst. Sci.,* 16(4), 1151-1169.

Feng, Y., Liu, Y., Tong, X., Liu, M. & Deng, S. (2011). Modeling Dynamic Urban Growth using Cellular Automata and Particle Swarm Optimization Rules. *Landscape and Urban Planning,* 102(3), 188-196.

Folino, G., Mendicino, G., Senatore, A., Spezzano, G. & Straface, S. (2006). A Model Based on Cellular Automata for the Parallel Simulation of 3D Unsaturated Flow. *Parallel Computing,* 32(5–6), 357-376.

Gazzaz, N.M., Yusoff, M.K., Aris, A.Z., Juahir, H. & Ramli, M.F. (2012). Artificial Neural Network Modeling of the Water Quality Index for Kinta River (Malaysia) using Water Quality Variables as Predictors. *Marine Pollution Bulletin,* 64(11), 2409-2420.

Geetha, G. & Selvaraj, R.S. (2011). Prediction of Monthly Rainfall In Chennai Using Back Propagation Neural Network Model. *International Journal of Engineering Science and Technology.* 3(1), 211-213.

Georgakakos, K.P. & Bras, R.L. (1984). A Hydrologically Useful Station Precipitation Model: 1. Formulation. *Water Resources Research,* 20(11), 1585-1596.

Li, W., Cui, L., Zhang, Y., Zhang, M., Zhao, X. & Wang, Y. (2014). Statistical Modeling of Phosphorus Removal in Horizontal Subsurface Constructed Wetland. *Wetlands,* 34(3), 427-437.

Mohammadpour, R., Ab. Ghani, A. & Azamathulla, H.M. (2013). Prediction of Equilibrium Scour Time Around Long Abutments. *Proceedings of the Institution of Civil Engineers: Water Management*, 166(7), 394-401.

Mohammadpour, R., Ghani, A.A. & Azamathulla, H.M. (2013). Estimation of Dimension and Time Variation of Local Scour at short Abutment. *International Journal of River Basin Management,* 11(1), 121-135.

Mohammadpour, R., Ghani, A., Vakili, M. & Sabzevari, T. (2015a). Prediction of temporal scour hazard at bridge abutment. Natural Hazards, 10, 1-21

Mohammadpour, R., Shaharuddin, S., Chang, C.K., Zakaria, N.A., Ab Ghani, A. & Chan, N.W. (2015). Prediction of Water Quality Index in Constructed Wetlands using Support Vector Machine. *Environmental Science and Pollution Research*, 22(8), 6208-6219.

Nasseri, M., Asghari, K. & Abedini, M.J. (2008). Optimized Scenario for Rainfall Forecasting using Genetic Algorithm Coupled with Artificial Neural Network. *Expert Systems with Applications,* 35(3), 1415-1421.

Nizar Ali, C. & Dudul, S.V. (2011). Committee of Artificial Neural Networks for Monthly Rainfall Prediction using Wavelet Transform. Business, Engineering and Industrial Applications (ICBEIA). *International Conference on, 5-7 June 2011,* 125-129.

Olsson, J., Uvo, C.B., Jinno, K., Kawamura, A., Nishiyama, K., Koreeda, N., ... & Morita, O. (2004). Neural Networks for Rainfall Forecasting by Atmospheric Downscaling. *Journal of Hydrologic Engineering*, 9(1), 1-12.

Partal, T. & Cigizoglu, H.K. (2009). Prediction of Daily Precipitation using Wavelet-Neural Networks. *Hydrological sciences journal*, 54(2), 234-246.

Partal, T. & Kişi, Ö. (2007). Wavelet and Neuro-Fuzzy Conjunction Model for Precipitation Forecasting. *Journal of Hydrology*, 342(1), 199-212.

Prasetya, R.B., Fariza, A., Hasim, J.A.N. & Basuki, A. (2015). River Flood Spreading Prediction System using Cellular Automata (Case study Bengawan Solo River). *International Conference on Data and Software Engineering (ICoDSE),* 25-26 Nov. 2015, 201-206.

Ravazzani, G., Rametta, D. & Mancini, M. (2011). Macroscopic Cellular Automata for Groundwater Modelling: A first approach. *Environmental Modelling & Software,* 26(5), 634-643.

Sattari, M.T. & Nahrein, F. (2014). Monthly Maximum Rainfall Prediction Using Artificial Neural Networks and M5 Model Tree. *Iranian of Irrigation & Water Engineering*, 4(14), 83-98.

Song, K., Park, Y.S., Zheng, F. & Kang, H. (2013). The Application of Artificial Neural Network (ANN) Model to the Simulation of Denitrification Rates in Mesocosm-Scale Wetlands. *Ecological Informatics,* 16, 10-16.

Valverde, M.C., Araujo, E. & Velho, H.C. (2014). Neural Network and Fuzzy Logic Statistical Downscaling of Atmospheric Circulation-Type Specific Weather Pattern for Rainfall Forecasting. *Applied Soft Computing*, 22, 681-694.

Wu, J., Long, J. & Liu, M. (2015). Evolving RBF Neural Networks for Rainfall Prediction using Hybrid Particle Swarm Optimization and Genetic Algorithm. *Neurocomputing*, 148, 136-142.

ESTIMATION OF ACTUAL EVAPOTRANSPIRATION USING GIS AND REMOTE SENSING (CASE STUDY: TAPI RIVER CATCHMENT, INDIA)

KALPESH BORSE[1], PRAVEEN RATHOD[2], VIVEK L. MANEKAR[3] & PRASIT G. AGNIHOTRI [4]

[1, 2,3,4] Civil Engineering Department, Sardar Vallabhbhai National Institute of Technology, Surat,
kalpeshborse22@gmail.com; praveenrathodsh03@gmail.com; vlm@ced.svnit.ac.in; pga@ced.svnit.ac.in

ABSTRACT

This study demonstrates the determination of evapotranspiration using Gis and remote sensing. Landsat images of resolution 30m is used in the present study. Gridded Landsat images are available in eleven different bands, all bands are composited and processed for mosaic to form a single image for study area in Arc GIS 10.1. After forming the mosaic, a single image is processed for the study area delineation. After delineating, masking is done to extract the exact study area. Obtained image is then processed for NDVI map in ERDAS Imagine 2014. Once the NDVI map is obtained based on the NDVI value, study area is classified into 5 different classes viz, Water Bodies, Agriculture Land, Built-up Land, Barren Land and Forest. Average value of NDVI is obtained in each classification. Using the NDVI, crop coefficient (Kc) is obtained for every class. In the present study to obtain reference evapotranspiration, Penman-Montieth model was used. From the Kc and Reference evapotranspiration actual evapotranspiration was calculated. Obtained results were validated using the actual ground truth data. It has been found that the results are showing good agreement with the actual result.

Keywords: NDVI; crop coefficient (Kc); evapotranspiration; arc GIS; reference evapotranspiration.

1 INTRODUCTION

In today's scenario, water conservation is very important. Globally, climate is changing and most of the places temperature trend indicates increasing. Everything on this planet needs more water than usual usage if the temperature increases. Crop water requirement differs from crop to crop. Evapotranspiration is an important factor for irrigation management. Therefore, the determination of evapotranspiration is an essential part of irrigation supply. One of the widely-accepted method to determine the evaporation is by multiplying the reference evapotranspiration (Et_0) to the crop coefficient (Kc) (Hunsaker et al., 2003). Food and Agricultural Organization has given crop coefficient values for different crops at different stages. Determination of crop coefficient are given in FAO-56, (Allen et al., 2005). In FAO-56, crop coefficients are intended for use with reference grass (Allen et al. 1998). FAO-56 also mentioned method for predicting Et_0 from Penman– Montieth equation which is based on a hypothetical grass reference of height 0.12 m having an albedo of 0.23 and surface resistance of 70 s m−1 for 24 h time steps (Allen et al., 2005). Standardized equations for computing parameters in the FAO-56 Penman–Montieth equation are given in Allen et al. (1998), Pereira et al. (1996), Smith et al. (1992) and Pereira and Allen (1999). Crop coefficient represents the total effects of major characteristics that distinguish the crop from the reference evapotranspiration Et_0 (Allen, 2000). These characteristics are crop height, albedo of the crop-soil, and crop-soil surface. Detail study of each parameter has been studied by Allen (2000). During the period of crop growing, Kc value increases from minimum to fully developed canopy. Usually, Kc value is a time dependent smooth curve. Once the full canopy is developed, Kc value starts declining and it depends on growth characteristics of the crop and irrigation management (Kamble, 2013). Crop coefficients primarily depend on leaf age, the dynamics of canopies, canopy roughness, light absorption by the canopy, crop physiology and surface wetness (Justice, 2002).

The Normalized Difference Vegetation Index (NDVI) is extensively used for the irrigation scheduling, change detection, land cover characterization, vegetation monitoring, drought detection and Crop yield assessment (Justice, 2002; Kamble and Irmak, 2013; Kamble et al., 2013). NDVI calculates the red and Near Infrared reflectance. Between wavelength of 0.7μm and 1.3μm, green vegetation reflectance will be more so NDVI value varies between -1 to +1; +1 value of NDVI indicates the High Vegetation and -1 value indicates the zero vegetation. Many researchers (Eric et al., 2008; Kamble et al., 2013) have shown that there is strong correlation existed between crop coefficient (Kc) and NDVI. The normalized difference vegetation index can be easily obtained by processing satellite images of at least two bands of Red and NIR bands in ArcGIS. Once the NDVI value is obtained from the satellite images, that value can be correlated with Kc. Once the Kc is obtained indirectly from the NDVI value, actual evapotranspiration can be obtained.

Determination of actual Evapotranspiration from the NDVI dependent Kc value is effective within the crop, vegetative or forest area. However, determination of evaporation from no vegetative places like water

bodies or barren land, the above-mentioned method will not be more effective because reflectance in the Red and Near Infrared range will be almost zero for the water bodies.

The objective of this study is to determine actual evapotranspiration from the green vegetation by using NDVI and Kc models using Gis and remote sensing technique.

2 STUDY AREA DESCRIPTION

Tapti River/ Tapi River is a river flowing through Central India. Tapati, Tapti, Tapee, Tapi are the various names used to denote Tapi River. Also known as, the daughter of Sun God, its basin extends over an area of 65, 145 km sq. In India, Tapi River originates at Multani of Betul District of Madhya Pradesh. The Basin of Tapi River lies in three Indian States, namely, Gujarat, Madhya Pradesh and Maharashtra. Covering an area about 3,837 km^2, 9,804 km^2 and 51,504 km^2 respectively. This study is limited to the Lower Tapi basin as shown in Figure.1 (Most of the area is in Gujarat State of India) and it lies between east longitudes of 72^0 67' and 73^0 41', and between north latitudes of 21^{0}21' and 21^0 66'.

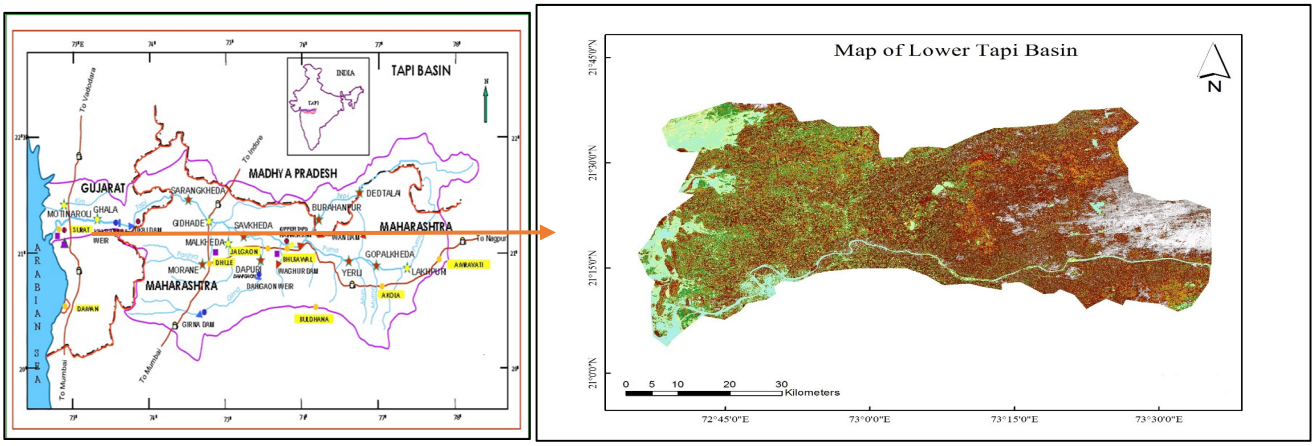

Figure 1. Lower Tapi Basin.

3 DATA COLLECTION

In the present study, climatic data, e.g. Minimum Temperature, Maximum Temperature, Wind Velocity, Relative Humidity, Sunshine Hour Precipitation and Pan Evaporation are procured from the State Water Data Centre (SWDC), Gandhinagar (Gujarat) for the period of 1999 to 2014. Rainfall data are of daily frequency and all other parameters frequencies are twice of daily frequency. A total of four stations data were used which were uniformly distributed over the entire study area. Fifteen years of average climatic data are given in Table 1. For the Generation of NDVI map, Landsat image were used and the resolution of these images is 30m.

Table 1. Average climatically data for the period 1999 - 2014.

Station	Min Temperature (0c)	Max Temperature (0c)	Relative Humidity (%)	Wind Speed (Km/hr.)	Sunshine (min)	Pan Evaporation (mm)	Rainfall (cm)
Amli	20.74	33.20	65.00	4.78	30	2.00	8.96
Chopadvav	22.35	32.45	62.50	9.16	30	3.14	6.37
Kakrapar	22.90	33.20	69.65	0.52	30	2.18	6.35
Ukai	23.19	31.85	65.32	3.10	30	2.20	10.04

4 RESEARCH METHODOLOGY

In the present study, it is mainly focused on the determination of evapotranspiration from satellite images and climatic parameters because these data are easily available and more reliable. Detail flowchart of methodology is shown the in Figure. 2.

4.1 Estimation of Actual Evapotranspiration

Radiance of the reflectance for the crops is good between 0.86μm to 1.24μm so NDVI was calculated between these two bands from the remote sensing data but, at the same time, water bodies have no reflectance in this range, thus evapotranspiration was determined by the NDVI. Before obtaining the NDVI values from the composite raster image of Landsat satellite image, the image had to be classified. In the present study, area image was classified into five different classes namely Forestland, Agricultural Land, Water Bodies, Built-up area and Barren Land. Different classes and their contribution of area are given in the

Table 2. Once the image was classified, NDVI raster can be generated in ArcGIS by image analysis tool. Many researcher (Baburao et al., 2013; Rafin et al., 2008) have provided the relationship between NDVI and Kc. In the present study, regression equation Eq. [1] given by Baburao et al. (2013) was used.

$$Kc = 1.457NDVI - 0.1725 \quad [1]$$

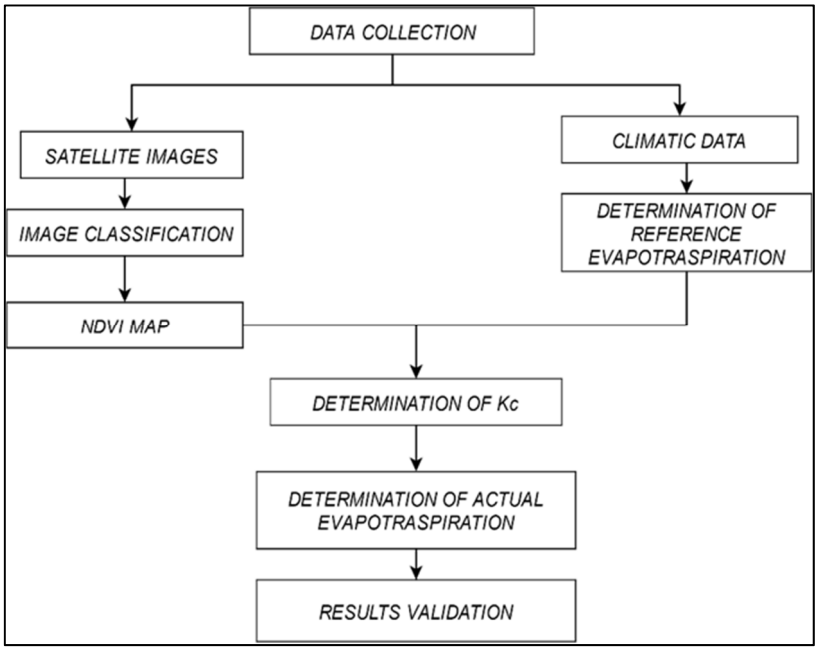

Figure 2. Flow chart of research methodology.

Once the Kc values were obtained for the different NDVI values, reference evapotranspiration was determined from the climatic parameters and by using Et_c/Et_0 relationship with the Kc value, actual evapotranspiration (Etc) was calculated. To convert observed Pan Evaporation into evapotranspiration, relation given by Trezza (2002) was used.

$$E(t) = EP(t)\, x\, tanh[P(t)/EP(t)] \quad [2]$$

where E(t) represents the actual evapotranspiration, EP(t) is the pan evaporation value, P(t) is the rainfall, and tanh is the hyperbolic tangent function. Thus, obtained evapotranspiration was compared with the predicted evapotranspiration. Statistically, Root Mean Square Error (RMSE) was employed to validate the proposed methodology and Normalized Root Mean Square Error should be near or equal to zero for good prediction.

5 RESULTS AND DISCUSSIONS

Landsat images of study area were obtained from the website (https://earthexplorer.usgs.gov/). Landsat satellite images were in eleven different bands, all these bands were composited and made into a single image by mosaic tool in the ArcGIS. Study area was classified into five different classes namely Forest area, Agricultural Land, Water Bodies, Barren land and Built-up area. Image classification was performed by Maximum Likelihood algorithm in the ArcGIS by collecting at least 100 samples in each classes. Result obtained after classification is shown in Table 2. From the table, it can be seen that there is more barren land fallowed by Forest land. Area of all classifications made in the study were estimated based on the pixel counts (Table 2).

5.1 Estimating evapotranspiration for vegetation from the NDVI and Kc model

There is good correlation between Kc with NDVI and Evapotranspiration (Rafn, 2008). There are different values of crop coefficient for different crops given by FAO-56, on the other hand, leaf reflectance is also different for different crops. By using reflectance between Red and NIR, NDVI map was generated in ArcGIS as shown in figure 3. From the NDVI values, Kc values were computed using the regression model given by Baburao et.al (2013) as shown in Eq. (1). Using Etc/Eto=Kc, the actual evapotranspiration (Etc) can be calculated by multiplying Kc to Eto. Eto values were computed using Penman-Montieth Method. However, using satellite images, which has resolution of 30 m, it will be quite difficult to obtain crop coefficient for a particular crops. Hence, in this study, average value of NDVI for particular class was obtained from the satellite image.

Table 2. Classified area of Lower Tapi basin in Km^2.

Class	Pixel Count	Area (Km^2)
Water Bodies	181172	163.0548
Agriculture Land	1735924	1562.3316
Built-up Land	863802	777.4218
Barren Land	1517835	1366.0515
Forest	277817	250.0353

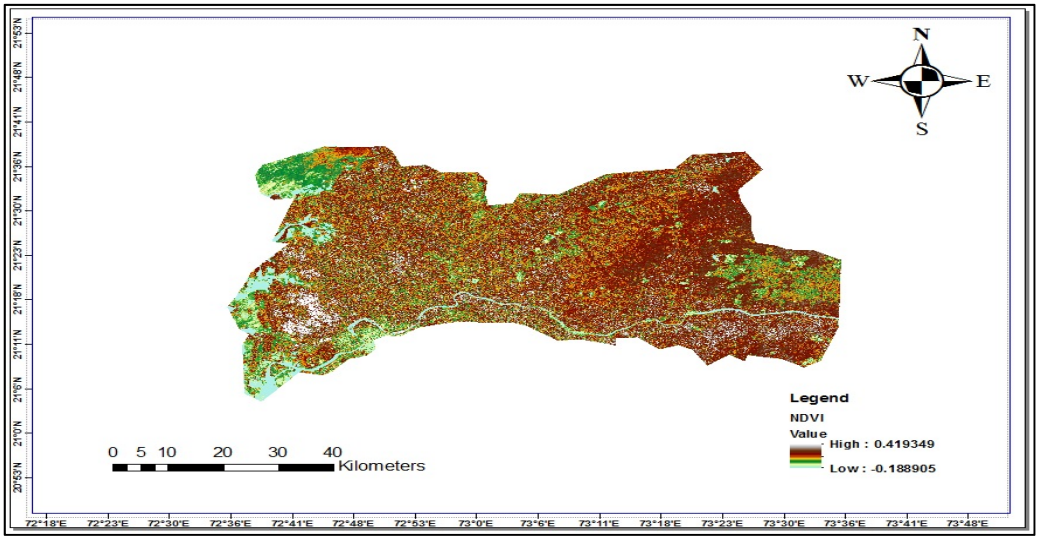

Figure 3. NDVI map for Lower Tapi Basin.

For the predicted evapotranspiration rates during Jan2011-Dec2012, the observed evapotranspiration values are shown in Figure. 4 to Figure.7.

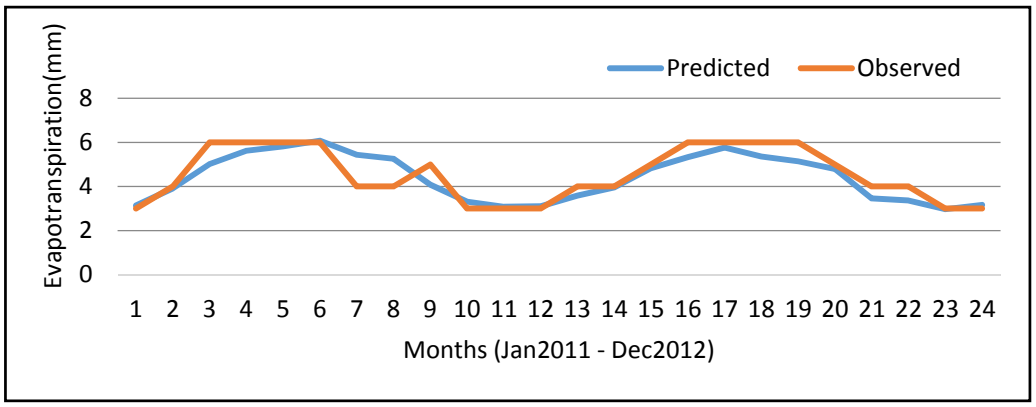

Figure 4. Observed and predicted evaporation for Amli

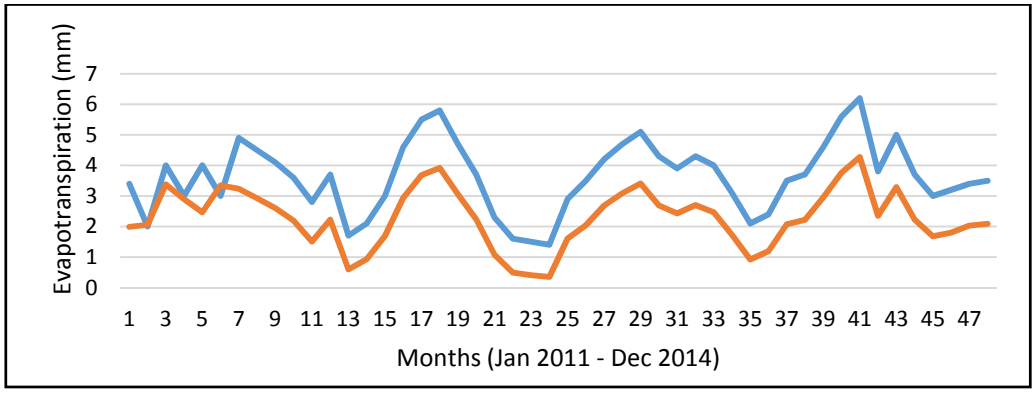

Figure 5. Observed and predicted evaporation for Chopadvav.

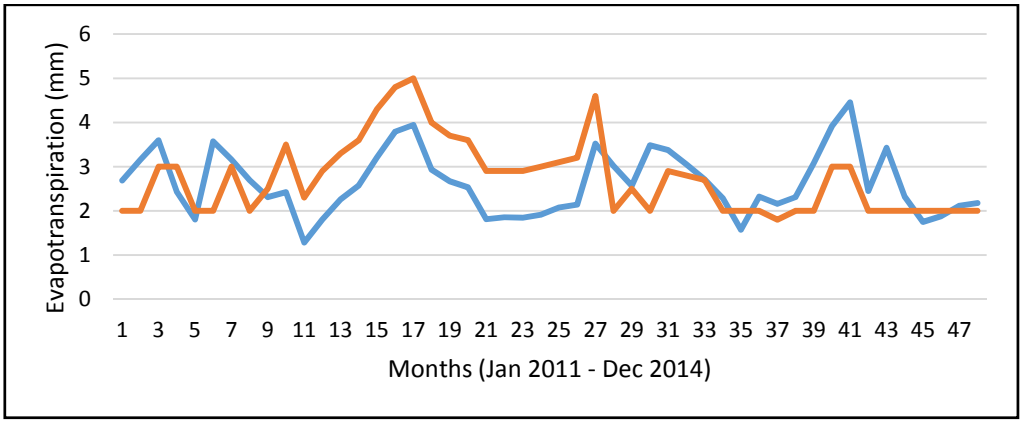

Figure 6. Observed and predicted evaporation for Kakrapar.

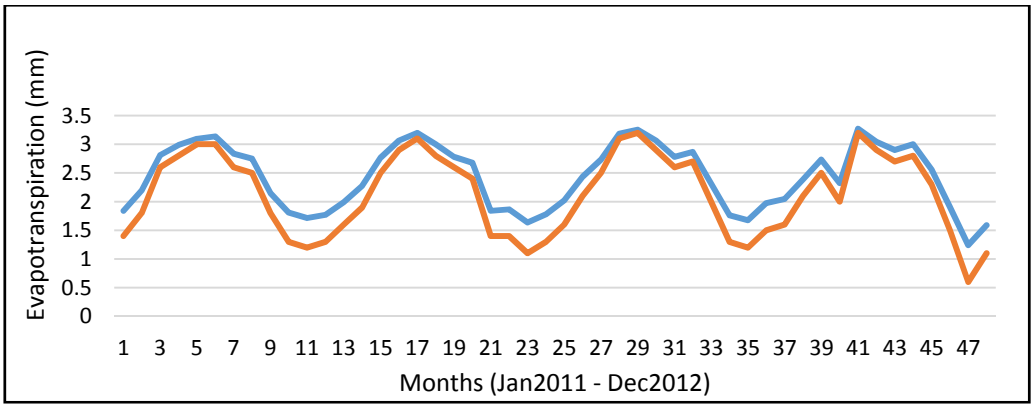

Figure 7. Observed and predicted evaporation for Ukai.

From Figure 4 to Figure 7, one can find that the predicted values are very near to the observed values.

6 CONCLUSIONS

Present study has demonstrated the methodology for estimation of crop coefficient using NDVI values. Evapotranspiration rate were determined using estimated crop coefficient. Comparison of estimated evapotranspiration with the observed evapotranspiration shows good agreement with average RMSE of 0.3 from all stations. It is concluded that the suggested method in the present study is useful for estimating evapotranspiration.

REFERENCES

Allen, R.G. (2000). Using the FAO-56 Dual Crop Coefficient Method over an Irrigated Region as Part of an Evapotranspiration Intercomparison Study. *Journal of Hydrology*, 229(1), 27-41.

Allen, R.G., Pereira, L.S., Smith, M., Raes, D. & Wright, J.L. (2005). FAO-56 Dual Crop Coefficient Method for Estimating Evaporation from Soil and Application Extensions. *Journal of irrigation and drainage engineering*, 131(1), 2-13.

Allen, R.G., Pereira, L.S., Raes, D. & Smith, M. (1998). ETc-single crop coefficient (kc). Crop Evapotranspiration (guidelines for computing crop water requirements). *FAO Irrigation and Drainage Paper*. FAO, 103-134.

Eagleman, J.R. (1967). Pan Evaporation, Potential and Actual Evapotranspiration. *Journal of Applied Meteorology,* 6(3), 482-488.

Gao, Bo-Cai. (1996). NDWI—a Normalized Difference Water Index for Remote Sensing of Vegetation Liquid Water from Space. *Remote Sensing of Environment*, 58(3), 257-266.

Gu, Y., Jesslyn, F.B., James, P.V. & Brian, W. (2007). A Five-Year Analysis of MODIS NDVI and NDWI for Grassland Drought Assessment Over the Central Great Plains of the United States. *Geophysical Research Letters*, 34(6).

Hunsaker, D.J., Paul, J., Pinter, Jr., Edward, M.B. & Bruce, A.K. (2003). Estimating Cotton Evapotranspiration Crop Coefficients with a Multispectral Vegetation Index. *Irrigation Science*, 22(2), 95-104.

Justice, C.O. & Townshend, J.R.G. (2002). Special Issue on the Moderate Resolution Imaging Spectroradiometer (MODIS): A New Generation of Land Surface Monitoring. *Remote Sens. Environ.* 83, 1–2.

Kamble, B. & Irmak, A. (2008). Assimilating Remote Sensing-Based ET into SWAP Model for Improved Estimation of Hydrological Predictions. In *Geoscience and Remote Sensing Symposium, 2008. IGARSS 2008. IEEE International*, 3, III-1036.

Kamble, B., Ayse, K. & Kenneth, H. (2013). Estimating Crop Coefficients using Remote Sensing-Based Vegetation Index. *Remote Sensing*, 5(4), 1588-1602.

Pereira, L.S., Perrier, A., Allen, R.G. & Alves, I. (1996). Evapotranspiration: Review of Concepts and Future Trends. *Journal of Irrigation and Drainage Engineering*, ASCE 25.

Rafn, E.B., Contor, B. & Ames, D.P. (2008). Evaluation of a Method for Estimating Irrigated Crop-Evapotranspiration Coefficients from Remotely Sensed Data in Idaho. *Journal of Irrigation and Drainage Engineering*, 134(6), 722-729.

Snyder, R.L. (1992). Equation for Evaporation Pan to Evapotranspiration Conversions. *Journal of Irrigation and Drainage Engineering*, 118(6), 977-980.

Trezza, R. (2002). Evapotranspiration using a satellite-based surface energy balance with standardized ground control. *PhD dissertation. Logan, Utah, USA: Utah State University.*

